RADIATIVE CAPTURE OF PROTONS AND DEUTERONS INTO ^{3}He

by

Steven Eugene King

Department of Physics
Duke University

Date: _____

Approved:

_____

N. Russell Roberson, Supervisor

_____

_____

_____

_____

A dissertation submitted in partial fulfillment of the requirements for the degree of Doctor of Philosophy in the Department of Physics in the Graduate School of Duke University

1983

Abstract

RADIATIVE CAPTURE OF PROTONS AND DEUTERONS INTO ^{3}He

by

Steven Eugene King

Department of Physics
Duke University

Date: _____

Approved:

_____
N. Russell Roberson, Supervisor

_____

_____

_____

_____

An abstract of a dissertation submitted in partial fulfillment of the requirements for the degree of Doctor of Philosophy in the Department of Physics in the Graduate School of Duke University

1983

RADIATIVE CAPTURE OF PROTONS AND DEUTERONS INTO ^{3}He

by

Steven Eugene King

An investigation of the $^2H(\vec{p},\gamma)^3He$ and $^1H(\vec{d},\gamma)^3He$ reactions has been made to provide precision measurements of angular distributions of both cross section and analyzing power in order to test current models of the three-body system. Angular distributions of cross section for the $^2H(p,\gamma)^3He$ reaction have been measured at proton beam energies of 6.5, 8.0, 11.0, 15.0, and 16.0 MeV at 13 to 17 angles. Angular distributions of analyzing power were also measured at both 8 and 16 MeV for 9 and 13 angles, respectively. The analyzing powers and cross sections were obtained for the $^1H(\vec{d},\gamma)^3He$ reaction at E_p = 1.62 MeV for 5 angles from 50° to 135°. Finally, fore-aft asymmetries were measured in 1 MeV steps between 6 and 16 MeV.

We have used direct capture model calculations to compare with our experimental results. The ^{3}He ground state wave functions were two-body (p+d) projections of three-body wave functions generated from Faddeev-type equations. Distorted waves were used in the continuum p+d channel. The direct radiative capture calculations assumed E1, E2, and E3 multipole transitions.

A comparison of the extracted a_2 coefficients with the calculations indicates a sensitivity to the inclusion of D-state components in the ^{3}He wave function. Theoretical three-body ^{3}He ground state wave functions having D-state probabilities of 5-9% (η = 0.050 to

0.038) are consistent with our data. The transition matrix analysis at 8 and 16 MeV including E1(s=3/2) terms (transitions to the ^{3}He D-state) result in σ(E1;s=3/2) of 0.5 to 5% and σ(E2) of 1 to 3% at 8 MeV in agreement with theoretical predictions. This is contrary to previous analyses which found a somewhat larger σ(E2). The fore-aft asymmetry data is well accounted for by model calculations that consider only E1-E2 interference. Previous measurements of both σ_t and $\sigma(90^o)$ have varied widely. The present results confirm those measurements with large peak cross sections.

The $^1H(\vec{d},\gamma)^3He$ reaction, when analyzed in conjunction with previous $^2H(\vec{p},\gamma)^3He$ data at the same excitation energy, gives σ(M1) of 1-8% with a good indication of M1(s=3/2) transitions.

ACKNOWLEDGEMENTS

I would like to thank my thesis advisor, Dr. Russell Roberson for his interest, advise, and long standing support of my physics education. The interest of, and many enjoyable discussions with Dr. Henry Weller are gratefully acknowledged. In addition, the assistance in data acquisition and comradeship of the rest of the capture group, Drs. Ron Tilley, Mike Wright, and Colleen Fitzpatrick, and George Mitev, Bob August, Doug Wagenaar, and John Riley was most appreciated.

Many other people contributed to the successful completion of this project. The fine craftmanship of Al Lovette, Robert Hogan, and Gene Harris of the Instrument Shop greatly assisted in the hardware development. I am indebted to Mike Bailey for the preparation of the figures in this work, Sidney Edwards for electronic and computer maintenance, Bob Rummel and Paul Carter for technical support, and Wendy Watson for assistance in the final preparation of this work.

Finally, my heartfelt thanks for the long standing support and encouragement of my education by my parents and family.

TABLE OF CONTENTS

List of Figures

List of Tables

1 INTRODUCTION

The three-body problem occupies a special place in nuclear physics, being the simplest testing ground for two-nucleon forces in a many-body system. Over the past few decades experimental research on the two-nucleon system has been extensive. Although quite complex, realistic nucleon-nucleon potentials have been developed which explain the bound state ^{2}H properties and the low-energy two-nucleon reaction data. Models of the two-nucleon interaction based on QCD are now under development. However, before investigating the effects of quark degrees of freedom in nuclear phenomena, the limits of validity of the nucleon and meson descriptions of the nuclear force must first be understood (Gibson, 1983). The presently available nucleon-nucleon potentials can be used to generate "exact" three-body wave functions using the Faddeev formalism. A full three-body treatment of reactions involving the three nucleon system can therefore provide an interesting test of the extent to which the two-nucleon potentials apply to many-body systems.

The radiative capture reaction into ^{3}He (or photonuclear disintegration of ^{3}He) provides an important tool in the study of the three-body system. An important feature of radiative capture is the selectivity of the electromagnetic interaction which favors the lower multipoles (E1, E2, and M1). As a result, the number of transitions that contribute to this reaction are small, simplifying the analysis. If the continuum wave function can be approximated by plane waves (ie. no nuclear interaction between the proton and deuteron in the continuum state), the reaction proceeds solely via the electromagnetic

interaction which is, in principle, well known. In addition, the weakness of the interaction allows the use of perturbation theory. Calculations of radiative capture using the three-body wave functions for the ground state of ^{3}He based on the nucleon-nucleon potentials have been made. However, none of the present calculations have treated the final state consistently. Currently, full three-body calculations with three-body wave functions for both the ^{3}He bound-state and the continuum p-d wave functions are being carried out by Lehman and his co-workers (1983).

The aim of this work is to provide highly accurate angular distributions of cross section and analyzing power at excitation energies in ^{3}He from 9.8 to 16.2 MeV for the ^{2}H($\vec{p}$,γ)^{3}He reaction and at an excitation energy of 6.0 MeV for the ^{1}H($\vec{d}$,γ)^{3}He reaction. It was hoped that these measurements could provide a good test of the wave functions obtained from the full three-body calculations. It was also hoped that information on the small components of the ground state of ^{3}He could be obtained by the direct extraction of the T-matrix elements from the experimental data.

1.1 ^{3}He Wave Functions

Much of the theoretical work on the three-body system has centered on the bound state wave functions of ^{3}H and ^{3}He. In a nuclear system the total angular momentum and its projection, parity, and the isospin projection (ie. charge) are good quantum numbers. The bound state of

^{3}He has a total angular momentum of 1/2 (Li, 1951) and an isospin projection of 1/2. In addition ^{3}He has a binding energy of 7.718 MeV (Mattauch et al., 1965) and a magnetic dipole moment of -2.2128 nuclear magnetons (Lindegren, 1965).

The principle component of the ^{3}He wave function is expected to be the spatially symmetric L=0 state as this has the lowest energy associated with rotational motion. Since the spatial component of the L=0 wave function is symmetric and the total wave function must be antisymmetric under exchange of the spin and space coordinates of the two protons, the proton spins must be antisymmetric. The protons are thus coupled to spin 0 resulting in a total spin of S=1/2 in ^{3}He. The isospin of ^{3}He is 1/2. As justification, assume that ^{3}He and ^{3}H are part of an isospin quartet with T=3/2 (the only other possibility). Under this assumption, bound states of ^{3}n and ^{3}Li would be expected. Since these isotopes are not found, we conclude that ^{3}He and ^{3}H form an isospin doublet with T=1/2. Parity is equivalent to a 180° rotation about an axis passing through center-of-mass and normal to the plane containing the three particles. S-states are invariant under rotation and thus have a positive parity. Therefore, the dominant component of the ground state wave function is $^2S_{1/2^+}(T=1/2)$. Calculations using several realistic nucleon-nucleon potentials give a probability of the S-state, P_S, of 89-91% of the total wave function (Hennell and Delves, 1975). Two other S-states can contribute, one with a purely antisymmetric spatial component and the other with a mixed symmetry (S') component. Calculations of the antisymmetric S-state show a

contribution of only 0.02% to the total wave function (Delves, 1968; Delves et al., 1969). From the realistic model calculations the mixed-symmetry state contribution ranges from 1 to 3% (Sasakawa, Okuno, and Sawada, 1981). The S'-state arises from the differences in the two-nucleon triplet-even and singlet-even central force.

Non-central forces lead to a mixing of orbital angular momentum in the ground state. Tensor forces in particular give a D-state contribution in ^{3}He. Since the S-state does not contribute to the orbital magnetic moment, the presence of a D-state component is indicated by the fact that the ^{3}He magnetic moment is not equal to the magnetic moment of the unpaired neutron. The D-state (L=2) must have quartet spin (2S+1=4) in order to still have a total angular momentum of 1/2, giving $^4D_{1/2}$. The D-state probability is predicted to be 7 to 10% (Sasakawa, Okuno, and Sawada, 1981). Finally, two P-states, $^4P_{1/2}$ and $^2P_{1/2}$, can contribute, but are thought to be unimportant (Derrick, 1960).

At this point it is important to define and examine the relationship between the parameters associated with the components of the ^{3}He wave function. The S, S', and D-state components of the bound state of ^{3}He will be referred to as ψ_S, $\psi_{S'}$, and ψ_D, respectively. The probability of a state, P_L, is defined as:

$$P_L = \int |\psi_L(r)|^2 \, r^2 \, dr. \qquad 1\text{-}1$$

It has been pointed out by Amado (1981) that the quantity P_D for the deuteron is not an experimentally determinable quantity. The D-state

probability depends on the short range properties of the wave function which requires a detailed knowledge of the short range forces. If a full dynamic theory for the nuclear forces existed, the quantity P_D could be calculated directly from the theory. In fact, Friar (1979) has demonstrated that the meson exchange effects can be shifted between the wave functions and current operators using the unitarity transformation in such a way as to make P_D essentially arbitrary. This argument is also true for ^{3}He. As a result, P_D and thus P_S and $P_{S'}$ must be viewed only as calculated parameters of the theory indicative of the strengths of the S, S', and D-state contributions within the context of a given model. For this purpose they are physically intuitive parameters.

So what properties of the ^{3}He wave function can be related to the electromagnetic experiments? For the excitation energies studied in this experiment, the radiative transition strength is determined predominately by the asymptotic part of the ^{3}He wave function. As a result the asymptotic normalizations can be related to experimental observables. The asymptotic normalizations in ^{3}H denoted as C_S^1 and C_D^1 for the S and D-states, respectively, are defined as:

1-2
$$\lim_{\rho\to\infty} u_0(\rho) \to C_S^1 \, e^{-\mu\rho}/\rho$$

and

$$\lim_{\rho\to\infty} u_2(\rho) \to C_D^1 \, (e^{-\mu\rho}/\rho) \left[1 + \frac{3}{\mu\rho} + \frac{3}{\mu^2\rho^2}\right]$$

where ρ is the radial distance between the neutron and deuteron and μ is the wave number (Gibson and Lehman, 1983). For ^{3}He the radial dependence can be written in terms of Whittaker functions to account for

the Coulomb contribution (Friar et al., 1982). The S to D asymptotic normalization ratio is defined as

$$1\text{-}3 \qquad \eta = \frac{C_D^1}{C_S^1}.$$

In addition to the asymptotic normalizations and their ratios, there is a distorted wave parameter, D_2, which is defined as:

$$1\text{-}4 \qquad D_2 = \frac{\int_0^\infty \rho^4 \, d\rho \, u_2(\rho)}{15\int_0^\infty \rho^2 \, d\rho \, u_0(\rho)} \simeq -\frac{C_D^1}{\mu^2 C_S^1}.$$

The approximation is only true if the main contribution to the integrals comes from the region of large ρ in which case the u_L wave functions can be replaced by their asymptotic forms. Gibson and Lehman (1983) have shown that this approximation leads to significant differences for small D-state components in separable potential calculations.

1.2 Review of Theory

The interaction Hamiltonian for the photonuclear disintegration reaction is

$$1\text{-}5 \qquad H' = -\int \vec{J}(\vec{x}) \cdot \vec{A}(\vec{x}) \, d\vec{x}$$

where $\vec{A}(\vec{x})$ is the four-vector potential of the electromagnetic field and $\vec{J}(\vec{x})$ is the four-vector current density of the nucleus determined by the charge, spin, and meson exchange current distributions. The weakness of this force makes the use of perturbation theory a good approximation. The transition matrix elements for the γ-ray induced reaction are given

as

$$1\text{-}6 \qquad T = \langle \varphi_f | H' | \psi_i \rangle$$

where $|\varphi_f\rangle$ is the wave function of the p+d system and $|\psi_i\rangle$ is the bound state of ^{3}He. Although the initial and final states are reversed in the current radiative capture study, historically, photonuclear disintegration has been most frequently studied. In order to avoid confusion, the meaning of the initial and final states will be as defined above throughout this work. Thus, final state interactions are the nuclear force interactions in the p+d state when the proton and deuteron are in the proximity of one another.

The electromagnetic Hamiltonian, H', is usually converted from a current density to a charge density form using Siegert's theorem (Lafferty and Cotanch, 1982). The operator $\vec{J}\cdot\vec{A}$ is changed to $\vec{r}_i\cdot\vec{u}$ in the long wavelength approximation where $\vec{r}_i$ is the coordinate of the ith proton and $\vec{u}$ is the photon polarization vector. The absorbed γ-ray can be denoted by the angular momentum it carries, L. The order of the multipolarity of the radiation is given by 2^L so L = 1, 2, or 3 are dipole, quadrupole, and octupole radiation, respectively. If the parity change of the nucleus is $(-1)^L$ then the transition is electric and if $(-1)^{L+1}$ magnetic. Thus the electromagnetic transitions can be referred to as EL or ML. For example, M1 refers to a magnetic dipole transition.

The previous theoretical calculations of radiative capture into ^{3}He have concentrated on σ_T and $\sigma(90^\circ)$. Several calculations of angular distributions of cross section do exist, but they have been limited to a

direct comparison with the experimental angular distributions themselves. Few theoretical works have calculated the energy dependence of the angular distribution coefficients and when this has been done, it was usually for one or two specific coefficients. No vector analyzing powers have been published (Arriaga and Santos (1983) state that in a paper yet to be published that their calculations show that the vector analyzing powers for the $^{1}H(\vec{d},\gamma)^{3}He$ reaction are essentially zero).

Early angular distribution measurements and calculations concentrated on determining P_D and P_S, through the measurement of the isotropic contribution to the angular distributions of cross section. A finite isotropic angular distribution can result from either M1 transitions to the S'-state of the ^{3}He wave function, transitions to the D-state, or phase differences between transitions of the same multipolarity from continuum states of different J to the S-state. Since most of the early calculations assumed plane wave continuum wave functions, transitions from states differing by only J were equal. Thus, any isotropic angular distribution of cross section was attributable to S' or D states. Bosch et al. (1964) used Gunn-Irving wave functions to calculate the fore-aft asymmetry and the isotropic cross section as a function of energy. Including μ_S and $\mu_{S'}$ in their calculations, a sensitivity to $\mu_{S'}$ was noted. In this comparison with measurements made with proton energies below 3 MeV, $P_{S'}(^{3}He)$ = 7% was found to give the best fit to the data.

Bailey et al. (1967) considered the D-state contribution to the isotropic component of the angular distributions by using a square well

two-body interaction and tensor interaction to construct the wave functions. They found a significant sensitivity to P_D with P_D = 1% giving the best fit to the contemporary experimental results.

Gibson and O'Connell (1970) used a full plane wave form of the electromagnetic interaction rather than the usual multipole expansion. In the ^{3}He bound state, ψ_S was based on a zero-range force between the proton and deuteron. ψ_D was made to fit the ^{3}He rms radius. The continuum wave functions were plane waves. Probabilities of 92, 6, and 2% for P_S, P_D, and $P_{S'}$, respectively, were assumed. Their angular distribution calculated at an excitation energy of 15.3 MeV was in good agreement with the data of Belt et al. (1971). The contribution from D-state and magnetic spin-flip transitions were negligible except at extreme angles. However, they found that the contributions of electric multipoles higher than E2 were significant.

Barbour and Hendry (1972) also calculated an angular distribution to compare to the Belt data. These authors used the Faddeev formalism with separable potentials (Lovelace, 1964) to generate an "exact" three-body ^{3}He wave function (described in chapter 6). Assuming only E1 and E2 transitions, they found good agreement with the E_x = 15.3 MeV data but not with the E_x = 12.1 MeV data. They also note a sensitivity to P_S, with 1.9% giving the best solution. An important feature of this calculation was the inclusion of final state interactions which enhanced the cross section by 25%.

More recently Hendry and Phillips (1973) have performed a similar

three-body calculation with separable potentials which included the effects of tensor forces. Their calculation of the M1 contribution to the reaction show it is significant only below 7.5 MeV excitation energy. On the other hand, almost no sensitivity of the isotropic cross section to P_D was found. This is contrary to previous calculations which did not use three-body wave functions.

In a further refinement Aufleger and Drechsel (1981) used realistic three-body ^{3}He wave functions based on the Reid soft-core potential (Reid, 1968), a plane wave final state, and included E1, E2 and M1 transitions. The final state interactions were neglected, resulting in a cross section 40% lower than the experimental data. Angular distributions were calculated at excitation energies of 10.8 and 15.3 MeV. P_D made an insignificant contribution to the angular distribution in this calculation. The M1 contribution was 1.5% at 10.8 MeV excitation energy.

Most recently, Arriaga and Santos (1983) calculated vector and tensor analyzing powers for the $^1H(\vec{d},\gamma)^3He$ reaction. In their calculation a plane wave expansion of the electromagnetic operator and realistic ^{3}He wave functions were used. The resulting deuteron vector analyzing power was essentially zero. However, the tensor analyzing powers were finite and in particular T_{20} was sensitive to the ratio of the asymptotic normalizations, η. At deuteron energies below 20 MeV the difference in the analyzing powers when the asymptotic form of the ^{3}He wave function was used compared to the use of a realistic wave function was found to be small.

1.3 Review of Experimental Work

Both the experimental studies of radiative capture and photonuclear disintegration have a long history. In this section a brief review of some of the pertinent work (generally $\sigma(\theta)$ and $A(\theta)$) will be discussed. The $^2H(p,\gamma)^3He$ reaction was first measured by Curran and Strothers (1939). Measurements of angular distribution of cross sections were first made by Fowler *et al.* (1949) and Griffiths and Warren (1955). For proton energies below 2 MeV these results exhibited a $\sin^2\theta$ angular dependence with small but finite isotropic cross sections. Measurements of the γ-ray polarization from the capture reaction (Wilkinson, 1952) demonstrated the dominance of the electric dipole radiation. The first photonuclear disintegration experiment on ^3He (Cranberg, 1958) produced angular distribution results. However, the measurements were distorted by the difficulty of separating two-particle break up from the three-particle break up reactions.

Early efforts in the measurement of angular distributions of cross section (Griffiths *et al.*, 1962; and Wolfli *et al.*, 1966) concentrated on the measurement of the isotropic component of the cross section. The goal of these experiments was to determine the small S' and D-state components ground state wave functions.

Fetisov *et al.* (1965) measured angular distributions for the $^3He(\gamma,p)^2H$ reaction from 6 to 170 MeV excitation energy using a cloud chamber. These measurements demonstrated that the angular distributions

were not symmetric about 90°, but had a fore-aft asymmetry which increased with increasing energy. However, the poor statistics and large energy averaging resulted in large errors in determining the angular distribution parameters and made any quantitative analysis difficult.

Belt et al. (1971) measured precision angular distributions for the $^{1}H(d,^{3}He)\gamma$ reaction from 5° to 175° at 12.1 and 15.3 MeV excitation energies by detecting the recoiling ^{3}He's with a spectrometer. The angular distributions were fit using a sine-cosine expansion (see §5.2). The extracted parameters could be used to determine the E1, E2, and M1 transition strengths. The isotropic cross section was found to be about 1% of the total cross section. Also, they found the higher order expansion coefficients deviated from E1-E2 calculations using plane waves for the continuum wave function. The use of realistic continuum wave functions improves the agreement somewhat. The differences in these terms were attributed to the presence of higher order multipole transitions.

Kundu et al. (1971) made extensive angular distribution measurements for excitation energies of 13 to 45 MeV. Their data exhibits a smooth energy dependence and reflects the importance of E2 radiation at high energies. Also, the isotropic cross section which is small at low energies increases above 30 MeV; an effect attributed to the D-state of ^{3}He. Matthews et al. (1974) measured an angular distribution using the $^{2}H(p,^{3}He)\gamma$ reaction at $E_{p} = 16$ MeV and found reasonable agreement with the data of Belt and Kundu.

In the previous capture work on this reaction undertaken at TUNL (Skopik et al., 1979), measurements of $\sigma(\theta)$ and $A(\theta)$ were made at E_x = 8.83, 9.83, and 10.83 MeV. A T-matrix analysis was used to extract individual transition amplitudes from the data. Assuming that only channel spin 1/2 E1 and E2 transitions were important, the E2 cross section was determined at each energy and was found to contribute 12 to 14% to the total cross section. The theoretical values for the $\sigma(E2)$ term range from 1 to 2% of σ_T in this energy region (Aufleger and Drechsel, 1981). In addition a significant difference in the phase between E1 and E2 amplitudes was found ($\simeq 80^{\circ}$) which is contrary to the plane wave assumptions made in many theoretical calculations.

Recent work (Anghinolfi et al., 1983) at slightly higher energies (E_x = 21 - 32 MeV) shows some differences with the measurements of Kundu. Both β (fore-aft asymmetry) and γ terms of the sine-cosine expansion (defined in §5.2) are smaller in the newer measurement indicating less contribution from the higher order multipoles.

Finally Engelbert and Clausnitzer (1981) have measured analyzing powers at E_x = 6 MeV for the $^2H(\vec{p},\gamma)^3He$ reactions. The only nonzero coefficient was b_1. The results of this precise measurement which is just 0.5 MeV above threshold give a strong indication of the presence of M1 radiation (see chapter 7).

1.4 Overview of this Work

In this work the $^{2}H(\vec{p},\gamma)^{3}He$ and $^{1}H(\vec{d},\gamma)^{3}He$ reactions were used to study the three-body problem. The central aims of the present experiment were:

1. To measure precision angular distributions of cross sections and analyzing power as a function of energy, and to use these measurements to determine the major transition amplitudes and phases involved in this reaction.
2. To verify previous measurements of the yield curves of σ_T and σ_{90^o} cross sections.
3. To resolve the difference between the calculated and measured electric quadrapole (E2) cross section.
4. To look for sensitivity to the S' and D-state in the capture reactions. Of special interest is the use of the $(\vec{p},\gamma)$ and $(\vec{d},\gamma)$ reactions at low excitation energies to determine magnetic dipole radiation contributions.
5. To compare the current results to a direct capture calculation using two-body projections of three-body ^{3}He wave functions which included D-state strength.
6. To encourage the development of a full three-body calculation of capture reaction observables.

In chapter 2 the experimental techniques are discussed while chapter 3 provides a description of the data analysis. The cross

section results are given in chapter 4 and the angular distribution results in chapter 5. The $^{2}H(p,\gamma)^{3}He$ data are compared to our direct capture calculations as well as other theoretical work in chapter 6. In chapter 7 the $^{1}H(\vec{d},\gamma)^{3}He$ reaction is discussed. Finally, the conclusions are given in chapter 8.

2 EXPERIMENTAL TECHNIQUES AND EQUIPMENT

2.1 Introduction

The facilities of the Triangle Universities Nuclear Laboratory (TUNL), shown in Figure 2-1, were used in the measurement of the data reported in this thesis. Radiative capture of both polarized and unpolarized protons incident upon deuterium and deuterons upon hydrogen was studied with NaI spectrometers. The development of a long, large-volume gas cell and long tungsten collimators for use with the TUNL NaI spectrometers resulted in an improvement in the count rate and enabled the extension of the excitation energy range in ^{3}He relative to previous measurements (Skopik et al., 1979). These improvements facilitated the measurement of high accuracy angular distributions of cross section and analyzing power for the ^{2}H(p,γ)^{3}He reaction. Deuteron capture on hydrogen posed a special problem in that only one third of the beam energy is available in the center-of-mass which results in relatively low energy γ-rays. The large neutron background induced by the high energy deuteron beam prevented measurements above the deuteron breakup threshold.

2.2 Ion Beams

The unpolarized ion beams were produced in a direct-extraction negative ion source (label Denis II in Figure 2-1). The beams were passed through a horizontal parallel-plate chopper driven at radio

Figure 2-1. Triangle Universities Nuclear Laboratory Cyclo-Graaff facilities.

Cyclo-Graaff Laboratory

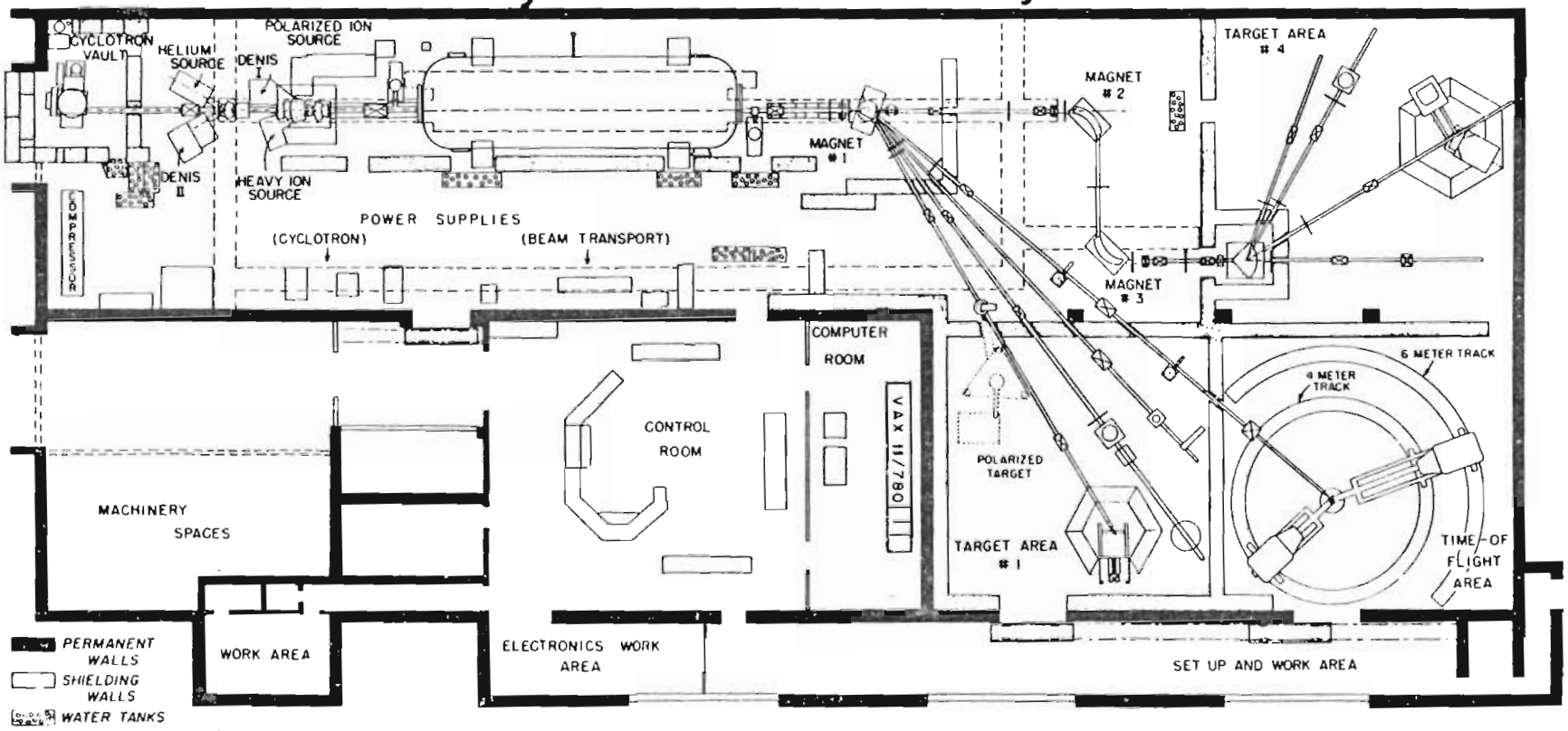

frequencies, a vertical parallel-plate auxiliary pulse chopper which removed the retrace pulse, and a double-gap klystron buncher which provided a 2 nsec beam burst on target with a repetition rate of 2 MHz. The pulsed beam was accelerated with a model FN tandem Van de Graaff. The accelerated beam passed through a pair of 90° magnets and a 30° bending magnet on its way to the gas target in the target area (labeled room #4 in Figure 2-1). A capacitive pick-off tube located in front of the gas target was used to produce a timing pulse for each beam burst. After passing through the gas target (described below) the beam was finally stopped in a tantalum lined Faraday cup located for shielding purposes approximately 2 m beyond the laboratory wall (not shown in Figure 2-1. The integration of beam current from this Faraday cup was used in the calculation of cross sections and relative normalizations. For the unpolarized proton beam typical currents on target were 100 - 300 nA, while for the deuteron beam 50 to 100 nA were used. However, in the deuteron capture measurements at E_d = 1.62 MeV the beam current could not be accurately measured. This was probably the result of an increase in angular dispersion due to scattering in the gas and of the increase in electrons emitted from the exit foil.

The polarized beams were produced by a Lamb-shift polarized ion source (Clegg et al., 1974). Because of a much lower beam intensity compared to the unpolarized source, a different pulsing system is used with the polarized ion source. By applying a 160 V, 2 MHz linear ramp voltage to the anode of the duoplasmatron, the beam is prebunched into 70 nsec burst (Wender et al., 1980). The prebunched beam is then passed

through a two-stage double-drift klystron buncher system to provide a 2-3 nsec beam burst on target. The two stages of the buncher operated at 4 MHz and 8 MHz, respectively. Since the beam pulses are produced entirely by bunchers (ie. no choppers), approximately 6 to 9% of the beam current is outside the main beam burst as measured by the monitor time-of-flight TAC. The data is collected only for the duration of the beam burst, requiring a correction for the beam outside the time window to be made to the integrated beam current. Typical polarized beam currents on target were 60 nA for protons and 15 to 30 nA for deuteron beams. The low beam currents for deuterons resulted from the low transmission efficiency of the tandem Van de Graaff at the low beam energies.

The beam polarization was measured on a beam stop located in front of the target chamber using the quench ratio technique (Trainor et al., 1974) and was typically 0.62 with an uncertainty of ± 0.03. To produce a pure vector-polarized deuteron beam, the spin filter of the polarized ion source selected the state 3 beam (Tonsfeld, 1980) with the magnetic field set so that the tensor polarization was zero. Figure 2-2 shows both vector and tensor deuteron beam polarizations as a function of magnetic field setting in the argon canal region of the source for each magnetic substate. The arrow and the dashed lines indicate the magnetic field used in this experiment for pure vector polarization (zero tensor polarization). At the chosen field setting the vector beam polarization for deuterons, p, is $-2/3 p_z$ giving

$$2\text{-}1 \qquad p = -\frac{2}{3}\left(1 - \frac{i_q}{i_b}\right)$$

Figure 2-2. Deuteron beam polarization for the 3 magnetic substates as a function of magnetic field in the argon canal region (Tonsfeld, 1980). The arrow and dashed lines indicate the field used to obtain a pure vector polarized deuteron beam.

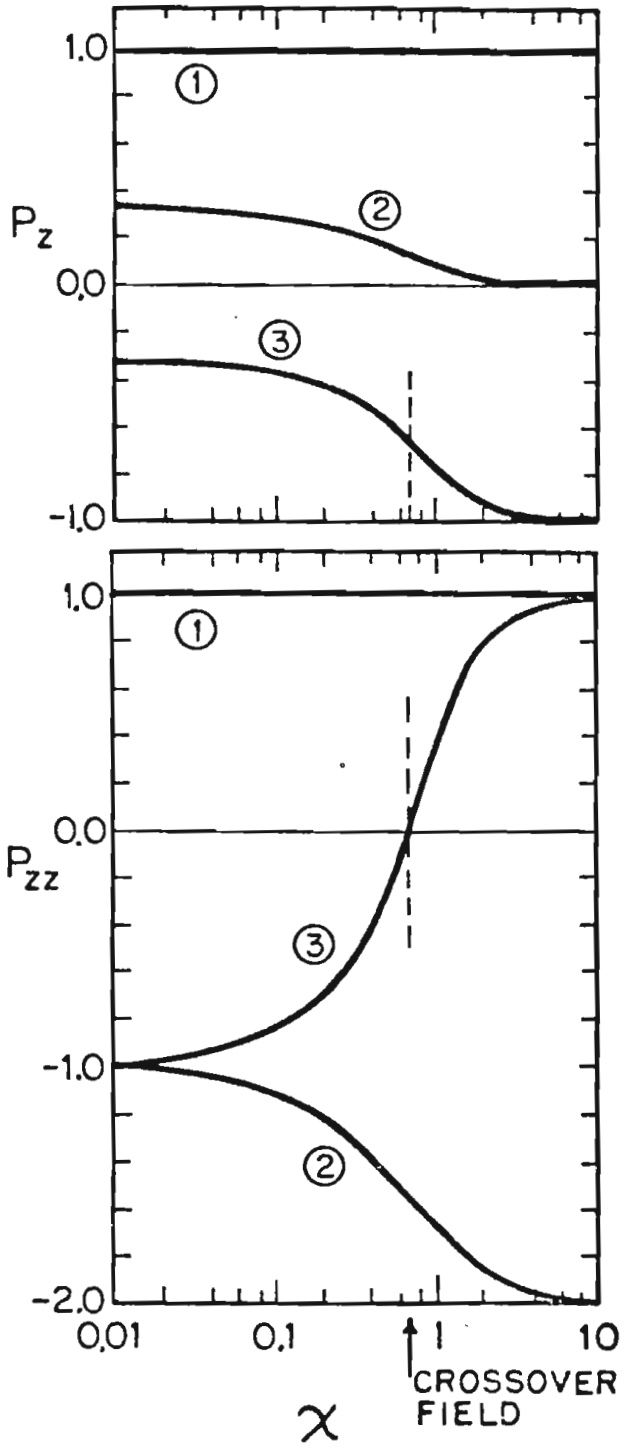
1.0
①
P_z
②
0.0
③
-1.0
1.0
①
0.0
P_{zz}
③
-1.0
②
-2.0
0.01
0.1
1
10
CROSSOVER FIELD
χ

where i_q is the beam current measured during the quenching of the polarized beam magnetic substate and i_b is the unquenched beam current.

2.3 Target System

The use of a gas target system substancially reduced the background in the γ-ray spectra above E_p = 8 MeV compared to the previous solid CD_2 target studies and allowed an increase in the incident beam on target. It also enabled measurements over a much larger energy range than was possible with solid targets since the interfering γ-rays from the $^{12}C(p,\gamma)$ reaction were no longer present. The long gas cell also allows the detectors to be well shielded from the large flux of γ-rays produced at the entrance and exit foils. However, it was found that the deuterium gas itself contributed to the background via neutrons produced from the breakup of the deuterium and from deuteron induced reactions in the chamber walls due to scattered deuterons. The gas cell was kept to the minimum length that would allow sufficient shielding of the detectors from the entrance and exit windows for all detector angles. One of the motivations in the design of a large gas cell was to make deuteron capture measurements at complimentary energies. However, the high energy deuteron beams produced so much neutron induced background in the γ-ray detectors from the deuteron breakup neutrons that no measurements were possible at the appropriate energies. To do these experiments will require a spectrometer for detection and energy analysis of the recoil ^3He ions at small angles. If the beam energy is below the deuteron breakup

threshold, then deuteron capture is possible with the equipment available.

The gas target system is shown in Figure 2-3. It consist of our standard thin-walled brass target chamber with vacuum flanges inserted into both the entrance and the exit beam tubes. The entrance collimator and window flange consisted of a 0.23 cm diameter collimator with a tube for collecting back-scattered electrons, a suppressor ring to keep electrons on the collimator, and an entrance window to the target chamber. The window was a 0.6 μm thick nickel foil mounted on a tantalum disk with a 0.317 cm aperture. The entire assembly was located 2 to 3 cm inside the entrance tube supported by adjustable threaded rods. The exit foil was a 2.5 μm thick, 1.6 cm diameter Havar foil. The length of the gas cell was 23 cm and the chamber itself was 15 cm in diameter. All parts of the set-up exposed to the beam were lined with tantalum to reduce background γ-rays. In addition a Lucite top and bottom were used on the target chamber to minimize the neutron induced background. The target chamber was filled with 34.4 to 83.1 kPa of high purity (>99.99%) deuterium gas for the proton capture experiments. For the deuteron capture experiments at low energies ultra-high purity (>99.998%) hydrogen at a nominal 83.1 kPa was flowed through the chamber at a rate of 60 cc/min in order to minimize target contamination.

For the measurement of the analyzing power at 8.0 MeV a 500 $\mu g/cm^2$ solid CD_2 target was used as in Skopik *et al.* (1979). The low beam intensity from the polarized-ion source resulted in poor timing at this energy precluding the use of the TOF system. Without the timing, the

Figure 2-3. Gas target system showing the collimators, entrance and exit windows, and charged particle monitor.

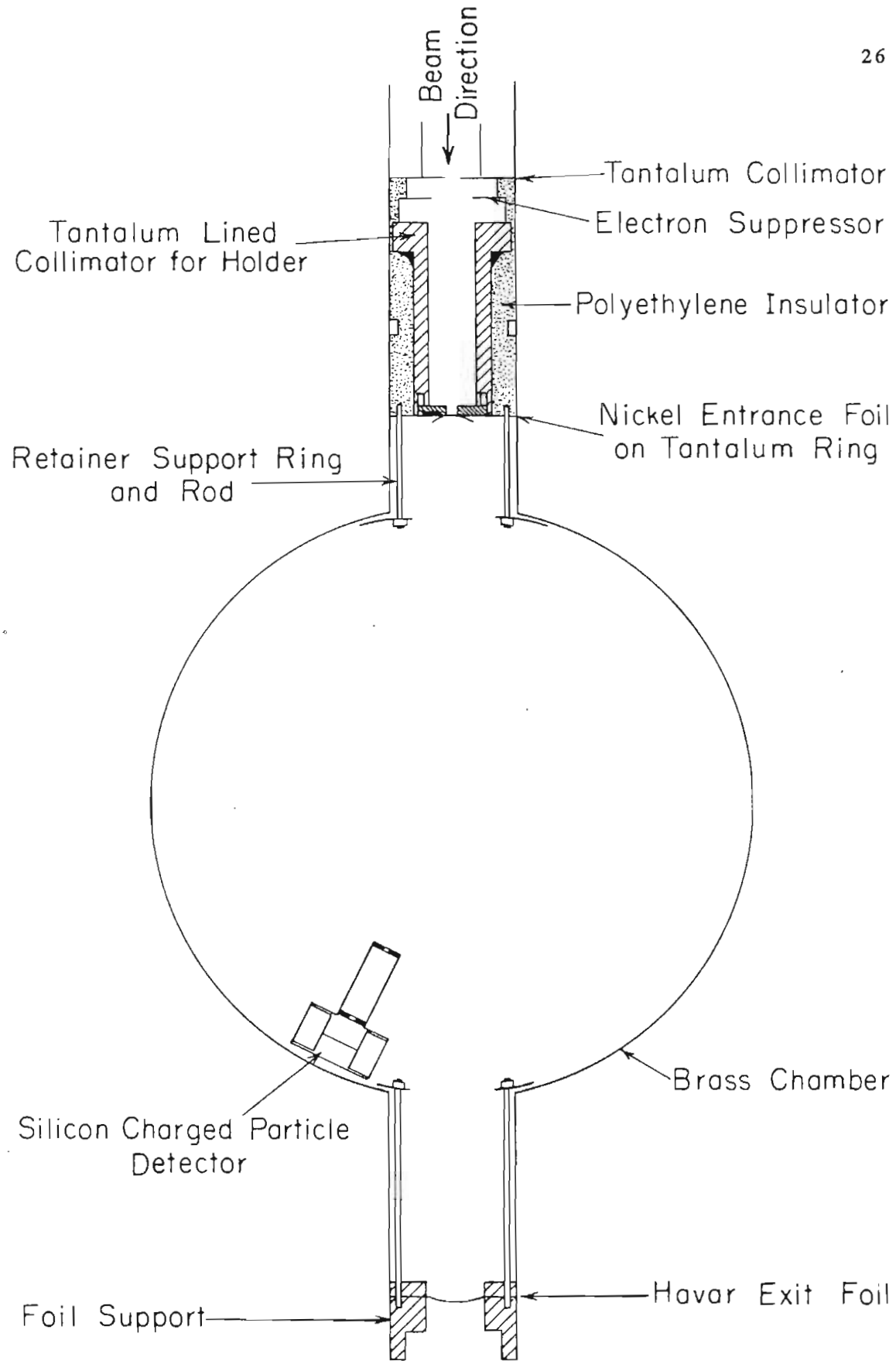
Beam Direction
Tantalum Collimator
Electron Suppressor
Tantalum Lined Collimator for Holder
Polyethylene Insulator
Nickel Entrance Foil on Tantalum Ring
Retainer Support Ring and Rod
Brass Chamber
Silicon Charged Particle Detector
Foil Support
Havar Exit Foil

background using the gas target is too large to extract reliable results at this energy. The backgrounds were measured with a CH_2 target. The background target thickness was normalized to the foreground via the measurement of the $^{12}C(p,p)$ reaction in the monitor detector. However, using pulsed unpolarized beams of higher current, the gas target was used for the cross section angular distribution measurements.

2.4 NaI Detectors

The γ-rays were detected by two 25.4 by 25.4 cm cylindrical NaI(Tl) spectrometers as shown in Figure 2-4. The distance from the center of the target chamber and the back face of the NaI detector was 149.2 cm. The conical lead collimators directly in front of the NaI detectors were designed to illuminated 97% of the back face of the detectors. The collimated detectors each subtended a solid angle of 21.9 msr for a point target at the center of the chamber. For the angular distribution measurements with the gas cell, the target size was defined by sets of vertical tungsten and lead slits. The front tungsten slits were designed to be tangent to a line from the center of the target chamber to the maximum angle subtended by the rear lead collimators. The separation of these front collimators was 1.55 cm at the narrowest point. Lead extentions of the vertical collimator slits, which subtended a cone 10^{o} greater than that of the lead detector collimator, provided additional shielding. Further tungsten, lead, and paraffin shielding was used as needed.

Figure 2-4. NaI detectors, collimators, shielding, and gas target system.

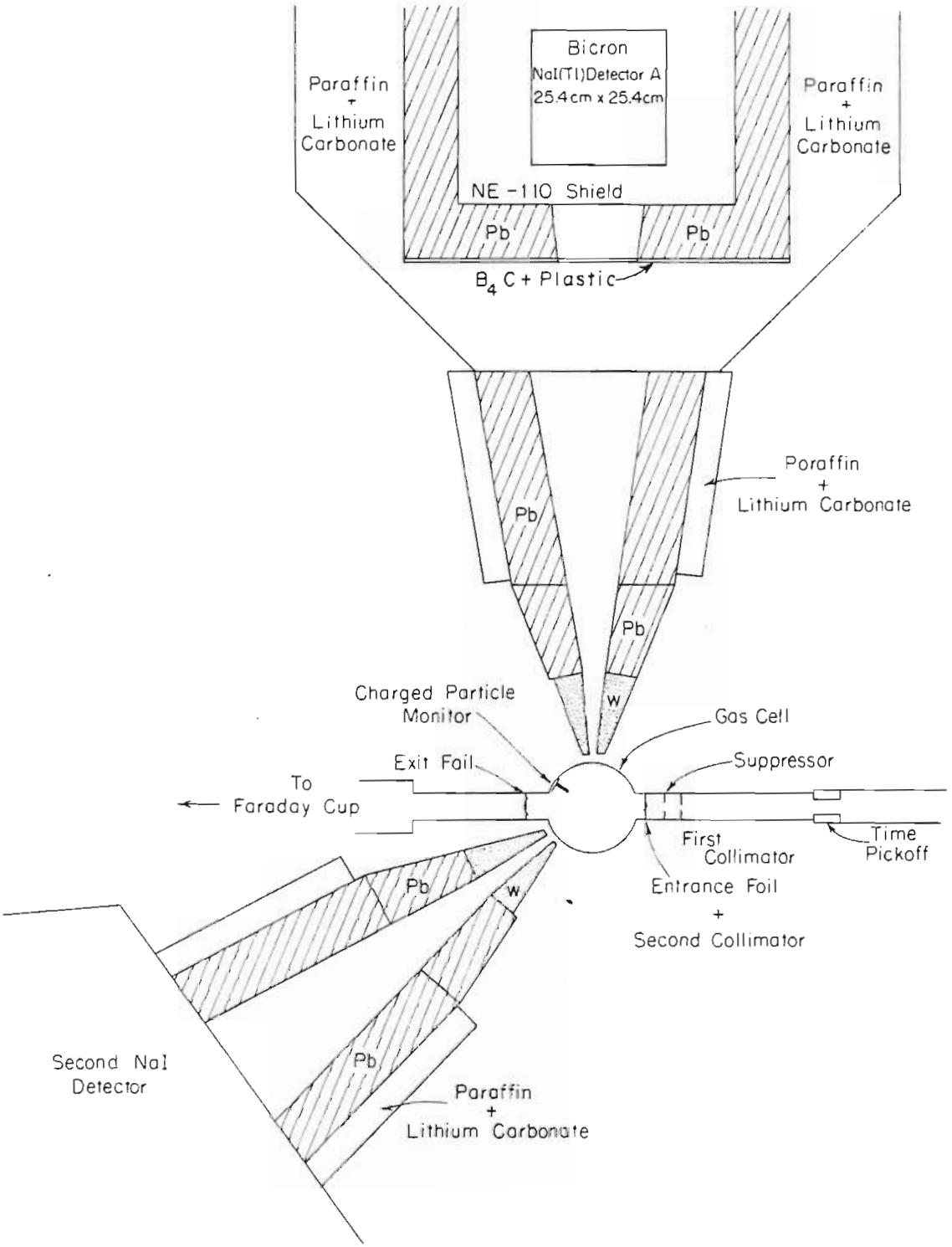
Bicron
NaI(Tl)Detector A
25.4cm x 25.4cm
Paraffin
+
Lithium
Carbonate
Paraffin
+
Lithium
Carbonate
NE-110 Shield
Pb
Pb
B4C + Plastic
Poraffin
+
Lithium Carbonate
Pb
Pb
W
Charged Particle
Monitor
Gas Cell
Exit Foil
Suppressor
To
Faraday Cup
First
Collimator
Time
Pickoff
Entrance Foil
+
Second Collimator
Pb
W
Second NaI
Detector
Pb
Paraffin
+
Lithium Carbonate

Surrounding the NaI crystals, well-shaped NE-110 plastic scintillators (Suffert et al., 1968) provided active anticoincidence shielding. In addition, 10 cm of lead and 20 cm of lithium carbonate doped (50% by weight) paraffin provided passive γ-ray and neutron shielding. Both detectors have a 0.6 cm thick boron plastic sheet between the paraffin and lead on the front face of the detectors. Detector A of Figure 2-4 has additional shielding of 0.15 cm cadmium sheets between the lead and paraffin in the sides, top, and bottom, while detector B is surrounded by additional boron plastic. Both the cadmium and boron plastic shielding serve to attenuate thermal neutrons.

2.5 Monitor Detectors

One or two silicon surface barrier detectors were used to monitor the beam current, and beam position, as well as target contamination. The detectors were placed at 25^{o} relative to the beam direction in the lab and were between 400 to 2000 microns thick. The dimensions of the rectangular collimators were 0.87 by 1.2 mm for the rear collimator and 1.0 by 3.9 mm for the front collimator. The collimators were separated by a distance of 25.6 mm. The small collimators were necessary to limit the count rates in the detectors and minimize finite geometry corrections. For gas target geometry, the expression for the number of counts (Silverstein, 1959) in the detector is given, to first order, by

$$N(\theta,\varphi) = n N_v G_{00} \varepsilon \sigma(\theta,\varphi) \qquad 2\text{-}2$$

where n is the number of incident beam particles, N_v is the atomic volume density of the target, ε is the efficiency of the detector, $\sigma(\theta,\phi)$ is the cross section of the interaction, and G_{00} is a purely geometric factor. For the double vertical slit geometry used in the monitor detectors this factor is

2-3 $$G_{00} = \frac{w_1 \, w_2 \, \ell}{rh \, \sin(\theta)}$$

where w_1 and w_2 are the width of the front and rear collimators respectively, ℓ is the distance between the two collimators, r is the distance from the center of target to the rear collimator, h is the height of the rear collimator, and θ is the angle from the beam axis at which the detector is located. For the present geometry $G_{00} = 1.565 \times 10^{-4}$ cm-sr.

To limit electron damage to the detectors which were located directly in the gas, it was necessary to shield the both the back and front faces of the detectors; the shields on the front faces were 10 micron thick polyethylene foils. It was also necessary to use permanent magnets on the collimator snouts to provide a field of 300 gauss.

2.6 Electronics

The electronics for the NaI spectrometers have three major functions. The first is the processing of the linear γ-ray energy signal. Next time-of-flight timing is used in conjunction with the pulsed beam to reduce cosmic-ray as well as neutron induced background.

Finally, the rejection of coincidence events between NaI and plastic shield scintillators further reduces the cosmic-ray effects as well as counts from Compton scattered γ-rays, bremsstrahlung γ-rays, and pair produced γ-rays that escape from the central crystal. A simplified schematic drawing of the electronics is shown in Figure 2-5. Each function of the electronics will be described in detail below.

Six RCA 8575 phototubes view each NaI detector. The signals from anodes of the gain matched tubes are mixed and then clipped to 350 nsec with a partially terminated clipping line. This signal was fanned-out and sent to both a fast (400 nsec) linear gate and to a TD101 discriminator. The TD101 contains two discriminators; one set low to provide good timing and the other set to provide energy discrimination. The discriminator output is used to trigger a gate generator that opens the fast linear gate for 400 nsec and then blocks all gates for 10 μsecs. These features reduce the pile-up effects of low energy γ-rays. The linear signal was then amplified and sent to an ADC. NaI detectors are occasionally subject to gain shifts, some of which are count rate dependent. To reduce these shifts, a Canberra 2050 analogue-digital gain stabilizer was used in conjunction with a light emitting diode pulser. The LED, located in the center of the rear surface of the NaI crystal, was pulsed at 800 Hz to provide a simulated γ-ray pulse. The gain stabilizer automatically maintained a constant output voltage for this peak. As can be seen in Figure 2-5, these LED pulses were not passed to the ADC's in order to reduce dead-time in the computer system.

The TD101 output was also used as the start-pulse of a

Figure 2-5. NaI and shield scintillator electronics.

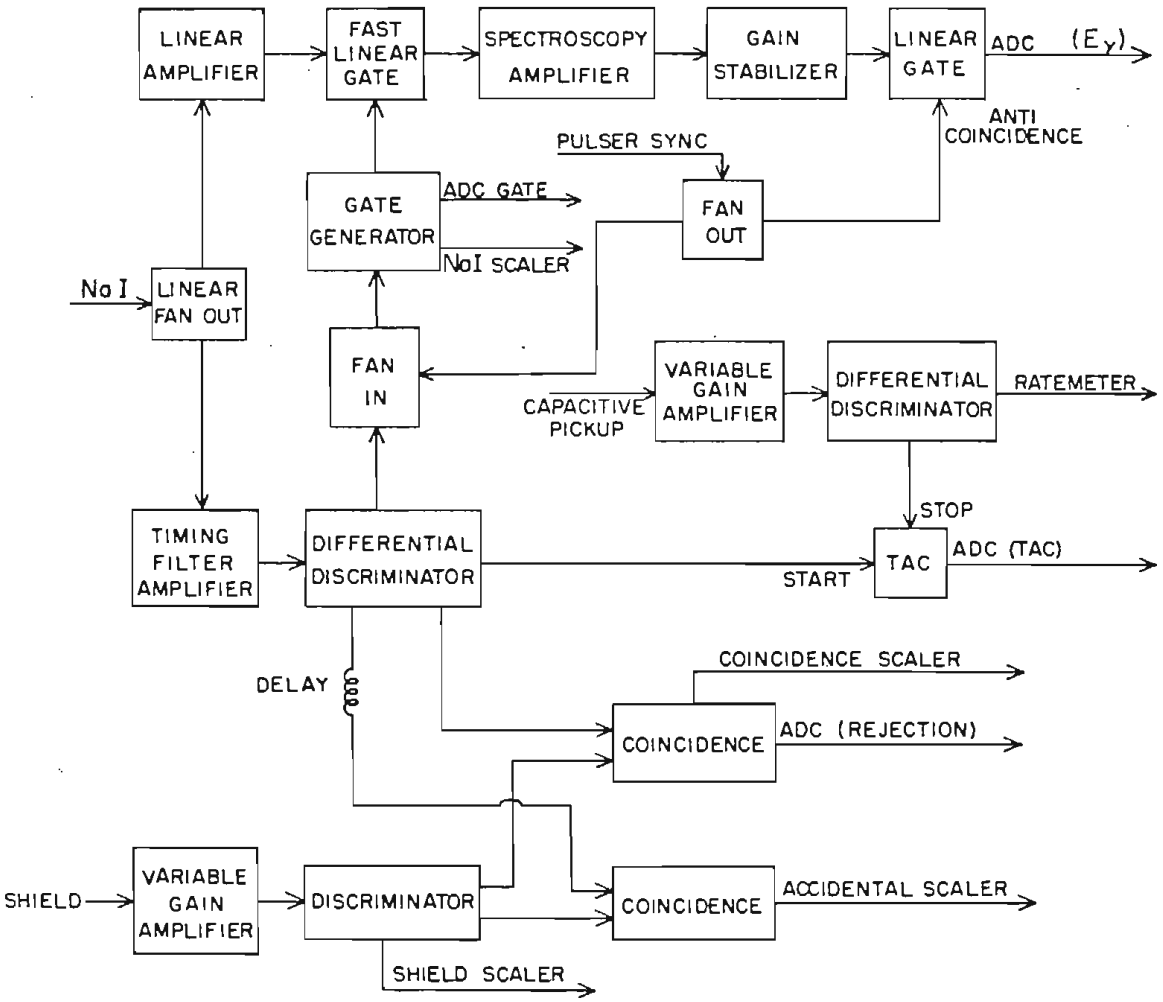
LINEAR AMPLIFIER
FAST LINEAR GATE
SPECTROSCOPY AMPLIFIER
GAIN STABILIZER
LINEAR GATE
ADC (Ey)
ANTI COINCIDENCE
PULSER SYNC
GATE GENERATOR
ADC GATE
NoI SCALER
FAN OUT
NoI
LINEAR FAN OUT
FAN IN
CAPACITIVE PICKUP
VARIABLE GAIN AMPLIFIER
DIFFERENTIAL DISCRIMINATOR
RATEMETER
STOP
TIMING FILTER AMPLIFIER
DIFFERENTIAL DISCRIMINATOR
START
TAC
ADC (TAC)
DELAY
COINCIDENCE SCALER
COINCIDENCE
ADC (REJECTION)
SHIELD
VARIABLE GAIN AMPLIFIER
DISCRIMINATOR
COINCIDENCE
ACCIDENTAL SCALER
SHIELD SCALER

time-to-analogue converter (TAC) while the stop was provided by the time pick-off signal. The analog signal that represents the time difference between the NaI signal and the pick-off signal is then sent to an ADC in coincidence with the E_γ signal. Only those events with the proper time signature are selected. This allows the elimination of those events corresponding to fast-neutron capture in the NaI crystal as well as a reduction of the time uncorrelated events.

After being processed by fast discriminators, the NaI and shield pulses were sent to a coincidence module. Coincident events are those that occur in both detectors within an overlap time of 60 nsec. The output of the coincidence module provides a logic pulse (R2) which is used to route the coincident events into different spectra in the computer. Besides rejecting over 99% of the cosmic rays, the coincidence requirement improves the full energy peak resolution by eliminating many of the events in which a low energy γ-ray escapes from the central crystal. True events are routed to the coincident spectra if an accidental coincidence occurs. The rate of accidental coincidences depends on the count rate in both the shield and NaI detectors. A second coincidence circuit in which the shield pulse is delayed by 330 nsec is used to measure the occurrence of random coincidences between the NaI and shield scintillators and provides a measure of the accidental coincidence rate. During the present experiment the accidental coincident rate ranged from 1 to 10%.

The monitor electronics are shown in Figure 2-6. The Ortec 142A preamp furnished both energy and timing signals. The energy signal is

Figure 2-6. Monitor Electronics.

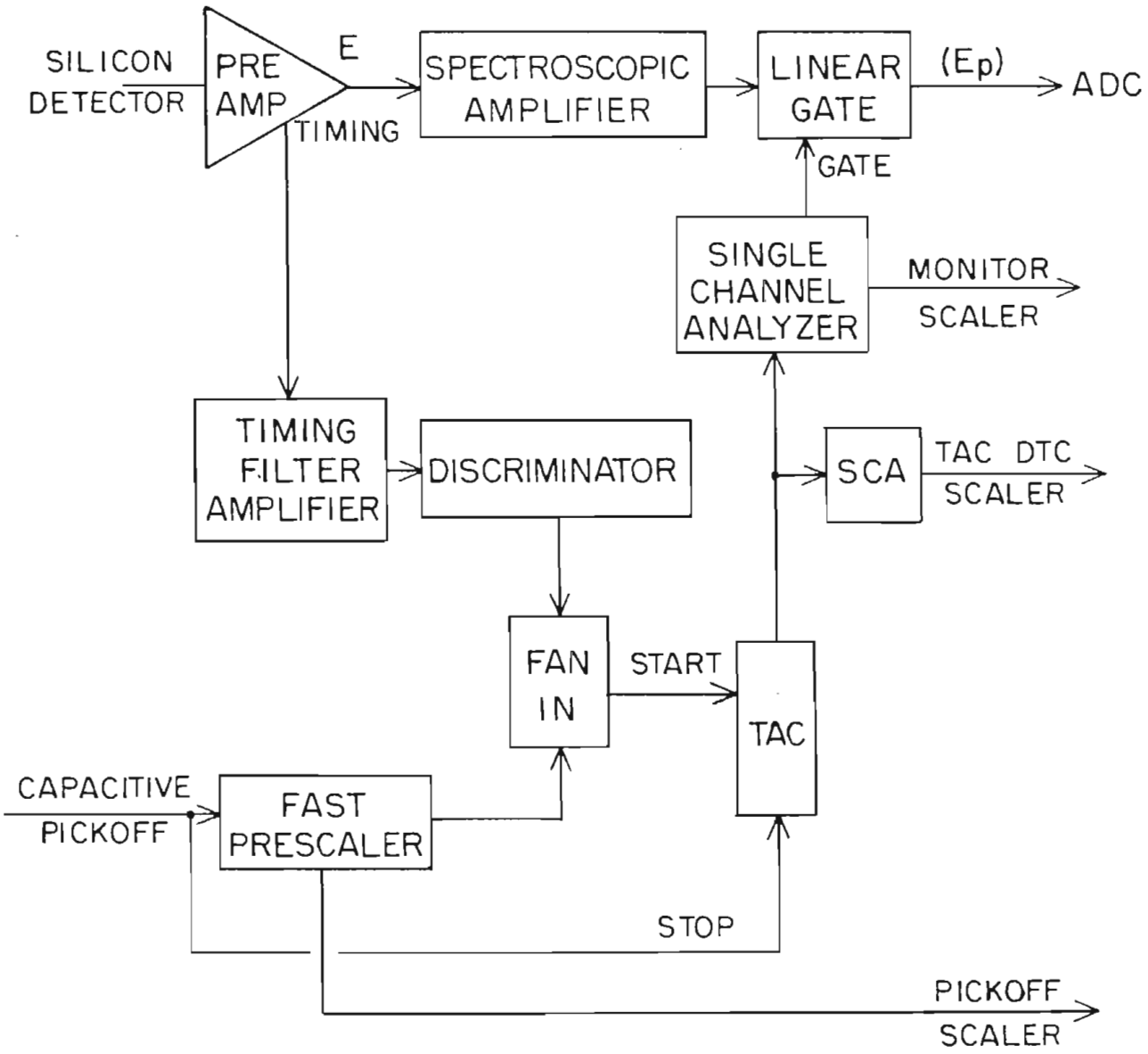
SILICON DETECTOR
PRE AMP
E
TIMING
SPECTROSCOPIC AMPLIFIER
LINEAR GATE
(Ep)
ADC
GATE
SINGLE CHANNEL ANALYZER
MONITOR SCALER
TIMING FILTER AMPLIFIER
DISCRIMINATOR
SCA
TAC DTC SCALER
FAN IN
START
TAC
CAPACITIVE PICKOFF
FAST PRESCALER
STOP
PICKOFF SCALER

amplified, gated, and input to an ADC. The timing signal is also processed and provides the start pulse for a time-of-flight TAC. The gating condition for the energy signal was that the event occur within a time window of approximately 15 nsec surrounding the TAC peak corresponding to the beam burst. The TAC also contributes to the electronic dead time. To measure this contribution, a prescaled (factor of 10^5) pick-off signal was fanned into the start of the TAC. Since the pick-off signal is also the TAC stop signal, a single channel analyzer window can be set on the corresponding TAC output peak. By counting both the number of pick-offs as well as the number that pass through the TAC, the dead time correction can be made. This correction, generally less than 1%, is in addition to the usual ADC and computer dead time correction.

2.7 Data Acquisition

A Digital Equipment Corporation VAX 11/780 computer is used at TUNL for all data acquisition. A block diagram of the hardware configuration is shown in Figure 2-7. The data acquisition system, XSYS, is described in detail in Gould _et al._, King _et al._, Roberson and Edwards, Holzsweig and Poore (1981), and the TUNL XSYS Reference Manual (1982). A brief description of the system including work done by the author follows. The ADC's, scalers, and output devices are located in or connected to a standard CAMAC crate. The crate controller is connected to a BiRa Corp. MBD-11 microprogrammed branch driver. The MBD uses a general reentrant program to pass information between the CAMAC

Figure 2-7. TUNL VAX 11/780 computer system.

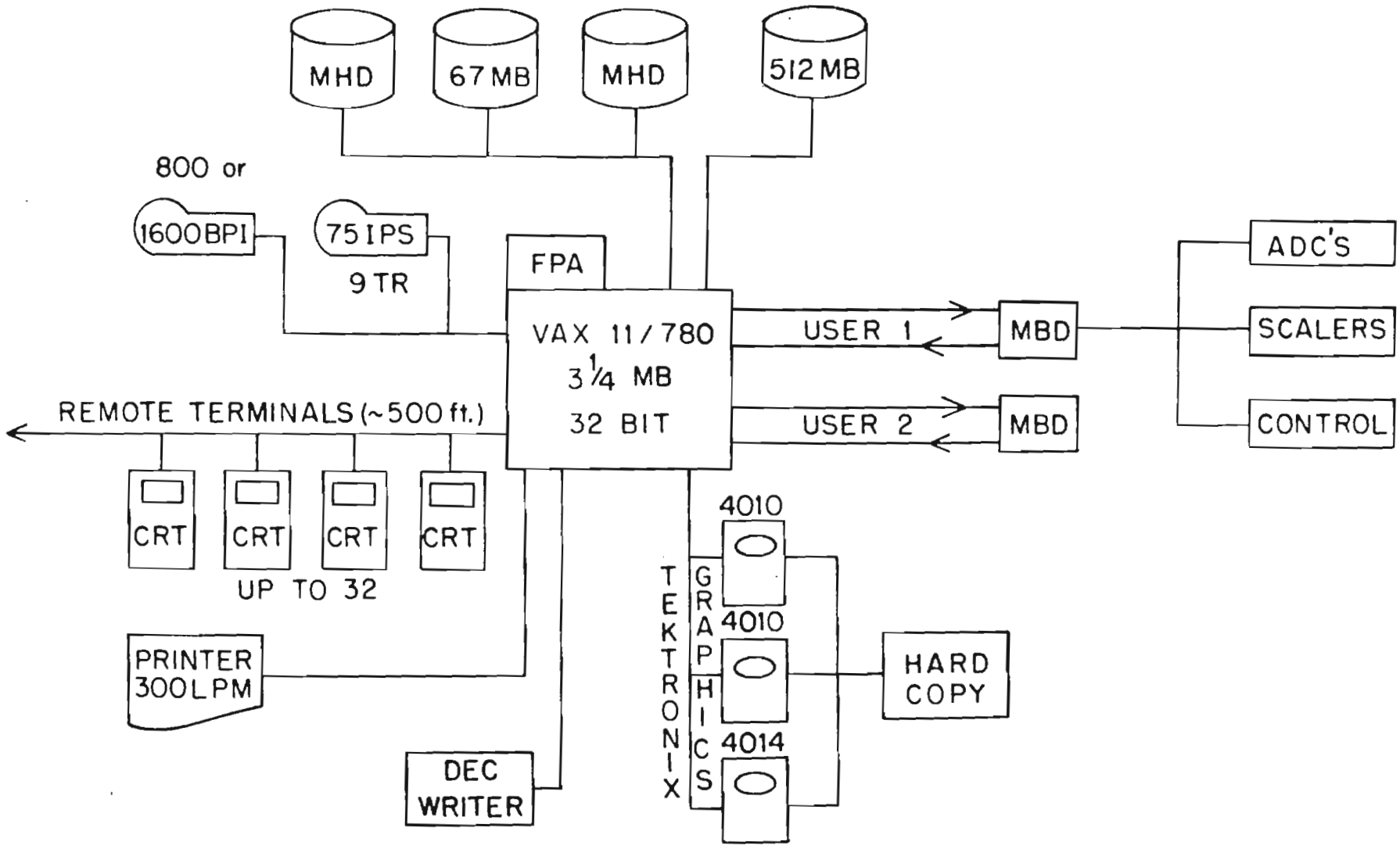
MHD
67 MB
MHD
512 MB
800 or
1600 BPI
75 IPS
9 TR
FPA
VAX 11/780
3 1/4 MB
32 BIT
USER 1
USER 2
MBD
MBD
ADC'S
SCALERS
CONTROL
REMOTE TERMINALS (~500 ft.)
CRT
CRT
CRT
CRT
UP TO 32
PRINTER
300 LPM
DEC
WRITER
TEKTRONIX
GRAPHICS
4010
4010
4014
HARD
COPY

crate and the VAX via the UNIBUS. The MBD uses DMA data transfer to a dual channel buffer in the VAX. A subprocess, X_SORT, processes the data when a buffer is filled. A routine written in a specialized event analysis language, EVAL, is used by X_SORT to efficiently sort the data into spectra. All data and control information is contained in global memory sections so that all data acquisition commands have access to the needed information. The modularity of the system provides easy upgrading and little interference between programs. The data spectra are displayed on a Tektronix 4010 graphics terminal.

The data acquisition program, CAP, used in this work is given in Appendix A. For each NaI detector a linear γ-ray signal, a time-of-flight TAC signal, and a NaI-shield coincidence logic signal where sent to the computer. The coincidence signal (R2) is a logic signal used to route coincident events into so-called rejection spectra. The signals from the two NaI systems were digitized by two LeCroy 2295A 12-input ADC modules. The two charged particle monitor energy spectra were also accumulated. In addition four logic signals for each detector were input to the Kinetic Systems 3610 scalers: NaI counts, shield counts, coincidence counts, and accidental coincidence counts. Additional scalers were used to count beam current integrator pulses, time pulses, beam pick-off pulses, and monitor counts. Dead times for the ADC's and associated electronics were calculated by comparing the number of NaI scaler counts to the number of NaI events stored by the computer. Typically, the dead time corrections to the data were 0.2 to 2%. Scalers and derived quantities such as accidental coincidence rates

were displayed and monitored during the experiments. Spectra were accumulated online in partial runs of 1 to 3 hours duration in order to monitor the quality of the data. At the end of each run, the spectra were stored on magnetic tape for later analysis.

Data from the ADC's associated with each NaI detector were sorted into 13 spectra. The total γ-ray energy spectrum was accumulated along with six conditional energy spectra. The raw time-of-flight TAC spectrum was accumulated along with three γ-ray energy gated TAC spectra. The selection of an energy gate surrounding the γ-ray energy of interest greatly reduced the time uncorrelated events in the TAC spectrum allowing proper selection of the prompt γ-ray TAC peak for sorting the γ-ray energy spectra. An example of an energy gated TAC spectrum with a gate set on the γ-rays of interest is shown in Figure 2-8.

The logic signal, R2, which indicates a coincidence between the NaI detector and the shield, was digitized by the appropriate 12-input ADC. This produced a spectrum containing two peaks: one peak in channel zero indicating an event in the NaI but not in the shield and one peak at some high channel indicating the a coincidence between the shield and NaI detectors.

The conditions for sorting the energy spectra were two-fold. The sorting conditions were gates set in the time-of-flight spectra and in the R2 coincidence logic spectrum. First, the data were sorted according to whether or not the R2 coincidence signal was present. If

Figure 2-8. Typical background subtracted γ-ray energy and energy gated time-of-flight (TOF) spectra at E_p = 15 MeV and $\theta_{lab} = 90^o$ for the $^2H(p,\gamma)^3He$ reaction. The peak is summed over a region starting 1.5 peak widths below the centroid and ending 1.1 peak widths above the centroid as shown by the brackets. In the TOF spectrum the window set for the γ-rays of interest is shown.

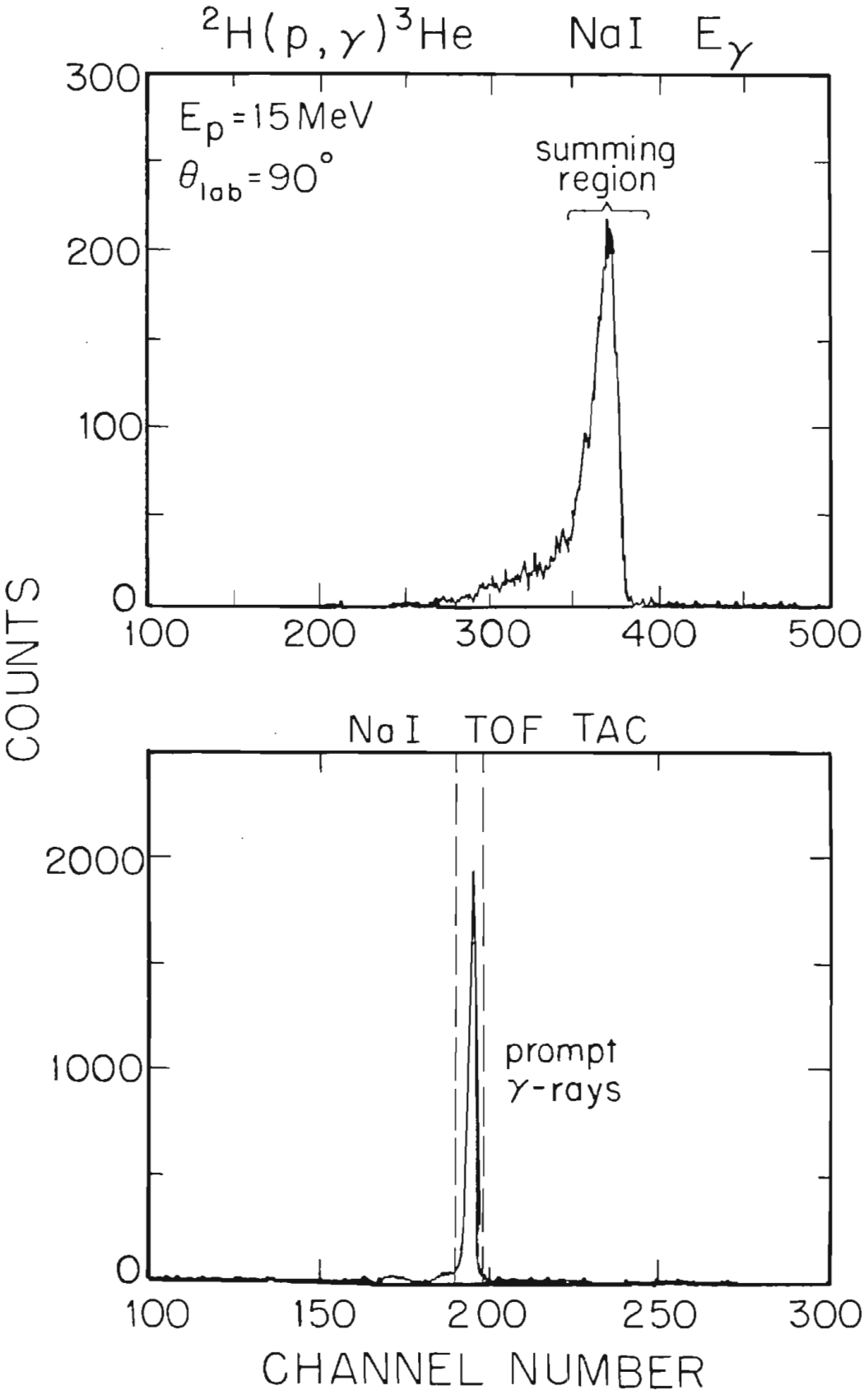
$^2H(p,\gamma)^3He$ NaI E_γ
E_p = 15 MeV
θ_{lab} = 90°
summing region
300
200
100
0
100
200
300
400
500
COUNTS
NaI TOF TAC
2000
1000
0
prompt
γ-rays
100
150
200
250
300
CHANNEL NUMBER

R2 was present, the γ-ray events stored in the "rejected" spectra; if R2 was not present, the events were stored in the "accepted" spectra. In addition three gates were set in the time-of-flight TAC spectrum; below the prompt γ-ray peak, surrounding the peak, and above the peak. Figure 2-8 gives a typical sorted γ-ray energy spectrum for events that are in the prompt γ-ray TAC peak and are not in coincidence with the shield. The figure has already had background subtracted as will be discussed in chapter 3.

3 Data Analysis

3.1 Preliminary Analysis

The offline analysis of data used XSYS commands, a peak fitting program MULFIT (Appendix B), and a variety of routines based on a common data base structure. The data analysis used the offline version of CAP, the data acquisition and analysis package, to initialize spectra, scalers, and gates. The spectra and scalers were read from tape, stored, accumulated, and displayed using XSYS. Through the selection of points via the curser on the Tektronix storage scope, the initial guess of position and width of the peak or peaks to be fit as well as the fitting region were chosen. A MULFIT input file was generated from these interactive selections and a standard file containing the other parameters necessary for fitting the peak.

The data must be corrected for losses from electronic and computer dead time, from the rejection of γ-rays in accidental coincidence with the shield, and from missed pick-off pulse signals (a problem at low beam currents). The correction factors were calculated and supplied to MULFIT in order to properly propagate the errors in the corrected data. The monitor spectra were summed after background subtraction and corrected for dead time losses. The monitor sums were used as a check of the BCI normalization, as well as for an alternative method for determining absolute cross section.

The background in the γ-ray spectrum varied greatly depending on

the reaction, (p,γ) or (d,γ), the beam energy, and the angular position of the detector. As a result, the subtraction of background required several methods. For the $^{2}H(p,\gamma)^{3}He$ reaction background measurements were made by plugging the collimators with 15 cm of lead. This method was preferred over target-out background measurements which clearly did not account for all the background in the spectrum. The measured background ranged from 3 to 20% of the total counts with the large backgrounds occurring at low energies and at extreme angles where the cross section was small. Even after subtracting the counts measured with the lead plug in place, there was still an additional small flat background in the region of the peak. This background was determined by fitting a flat line to the data in a energy region just above the γ-ray peak. The fitting region was usually 4 to 5 peak widths. This background represented an additional subtraction of 0.01% to 5% of the total counts. The net result shown in Figure 2-8 corresponds well to our standard γ-ray line shape with little or no evidence of additional background.

For deuteron capture, the measurements of background were more difficult because the magnitude of the background, uncertainties in normalization of runs to the monitors, and lack of beam current integration. The background was subtracted by using TOF TAC windows set on the flat region of the timing spectrum both above and below the γ-ray peak. This provided a good measure of the background for the the deuteron capture reaction as most of the background is uncorrelated with time. In addition better statistical measurements of background, and

the ability to measure the background simultaneously with the data under identical beam conditions make this a more reliable measurement. If any of the background is time correlated, it will not be measured by this technique. Checks of the background using the lead plug technique gave similar results with much poorer statistical accuracy and gave no indication of time-correlated background. The measured background ranged from 20% to 50% of the total counts.

3.2 MULFIT

The fitting of data was performed by a code called MULFIT the source and documentation for which are given in Appendix B. The data were fit with an empirically determined γ-ray response function (Turner, 1978) by varying the peak width (FWHM), centroid, and height to minimize χ^2. The empirical line shape was determined by fitting a spectrum obtained with the $^3H(p,\gamma)^4He$ reaction at E_p = 5 MeV. The fitting program subtracts the backgrounds discussed above, and corrects for dead time in the ADC and electronics, accidental rejections, and missing pick-off signals. The widths of the fitted peaks, from the initial fit, were plotted as a function of γ-ray energy. A smooth curve was then fitted to these widths to obtain the experimental energy dependence. Subsequently, the peaks were refit using the proper energy dependent width as a constraint. This procedure improved the systematic behavior of the fits. The fitted line shapes were integrated for a range that extended from 1.5 widths below the centroid to 1.1 widths above the centroid (see Figure 2-8). Also the data was summed for the same

region. All results given in this work use the summed data. The fitted areas were also used in the analysis to verify the consistency of the results.

3.3 Final Analysis

The results of MULFIT, both the integrated peak areas and summed areas were tabulated using a data base system developed by Wright (1983) and the author of this thesis. This data base system and the programs associated with it allowed the convenient manipulation and plotting of all information. The utilities available permit the calculation of fore-aft asymmetries, plotting of angular distributions, input generation for angular distribution and polarization fitting codes, normalizations, sorting, and finite geometry corrections. The tabulated results were normalized, when possible, to both monitor sums and beam current integration as a consistency check.

3.4 Finite Geometry Correction Method

A major problem with the use of a gas cell as target has been the necessity to correct for finite geometry effects. This is of particular importance for the present geometry in which the target thickness doubles when the detector is rotated from 90° to 30°. In order to analyze the angular distributions it is necessary to correct the data for the variations resulting from the changing target thickness. The center of target beam energy was used for all calculations. The

variations of energy loss in the target as a function of angle were neglected. The maximum energy loss over the effective target length was 30 keV at 8 MeV and at 83.1 kPa pressure resulted in insignificant changes in the angular distribution or cross section. The effective target thickness is required in order to calculate absolute cross sections. To first order the target thickness varies as $1/\sin(\theta)$. For the accuracy desired in the present experiment, a more definitive result is necessary.

To calculate the angular geometric correction factor and target thickness, a Monte Carlo code, SOLAC, was written. The effects that were considered were the finite size and position of the beam in the gas, the finite size of the detector, the shape and position of the collimators, and the attenuation of γ-rays through the edges of the collimators.

The differential γ-ray count rate into a detector at angle θ_d with respect to the beam axis is

$$3\text{-}1 \qquad dg = \sigma_{p,\gamma}(\theta_\gamma)\ l_1^{-2}\ F_p\ N_D\ \varepsilon_d(E_\gamma)\ C_1\ dA_b\ dl_b\ dA_d$$

$$C_1 = e^{-\mu\tau}$$

where $\sigma_{p,\gamma}(\theta_\gamma)$ is the capture cross section of interest for the angle θ_γ which is the angle between the initial particle direction and the outgoing γ-ray, l_1 is the distance from the capture reaction to the differential element dA_d on rear face of the NaI crystal, F_p is the number of protons incident on the target, N_D is the number density of

deuterium atoms in the target gas cell, $\varepsilon_d(E_\gamma)$ is the efficiency of the NaI detector for γ-ray energy E_γ, dA_b is the differential cross sectional area of the beam, dl_b is the differential element along the beam axis, and dA_d is a differential surface element on the rear face of the NaI detector. C_1, the collimator transmission probability, is 1.0 if the γ-ray does not penetrate the collimator and is the probability of transmission if the γ-ray path passes through a collimator. In the calculation of C_1 the thickness of collimator penetrated by a particular γ-ray is labeled by τ and μ is the γ-ray attenuation coefficient (Storm and Israel, 1970). The count rate in the detector is the integral over the detector area and the beam, gas intersection volume.

The detector was modeled as a disk perpendicular to the line from the center of the target to the center of the detector. The target itself was a cylinder the length of the gas cell whose diameter has been based on an optical measurement of the beam spot on a quartz viewing crystal at the center of the target chamber. The trajectory of all beam particles was assumed to be parallel to the beam axis. The first collimators were modeled as a set of planar wedges and the second detector collimator is a conic section with a vertex at the target center and illuminating 97% of the rear face of the NaI detector. To numerically calculate this 5-fold integral, a point can be randomly selected in the gas target and the second point on the rear face of the detector. The differential γ-ray count rate given by Equation 3-1 can then be calculated and the process was repeated for another set of randomly chosen points.

In this work, the correction factor must account for the finite geometry of the target and detectors as well as the variation of the target thickness as a function of detector angle. The correction for the finite geometry effects for a detector at angle θ_d is derived from Equation 3-1 and is given as:

$$3\text{-}2 \qquad C'(\theta_d) = \frac{\sigma_p(\theta_d)N_c(\theta_d)}{l_p^2} \left[\sum_{i=1}^{N} \frac{\sigma_i(\theta')\ C_i}{l^2(\theta')_i} \right]^{-1}$$

$$N_c(\theta_d) = \sum_{i=1}^{N} C_i$$

where σ_p is the best guess of the point geometry cross section, l_p is the distance from the center-of-target to the center-of-detector, C_i is the transmission probability for a given γ-ray trajectory, $N_c(\theta_d)$ is the number of histories, N, weighted by the transmission probability of each γ-ray. The summation is over sets of randomly chosen points in the detector and target. For each pair of randomly chosen points, σ_i is the best guess cross section cross section at θ', l_i is the distance from the reaction point to the detection point, and θ' is the angle of the γ-ray from the beam axis. To correct for the variation of target thickness as a function of angle, the correction factor is multiplied by the ratio of the number of γ-rays seen by the detector at the angle θ_d, $N_c(\theta_d)$, to the number of γ-rays seen by the detector at 90°, $N_c(90^\circ)$. The total correction factor is then given by

$$3\text{-}3 \qquad C(\theta_d) = \frac{\sigma_p(\theta_d)N_c(90^\circ)}{l_p^2} \left[\sum_{i=1}^{N} \frac{\sigma_i(\theta')\ C_i}{l^2(\theta')_i} \right]^{-1}.$$

Since σ_p (and σ_i) is unknown, the calculation of the correction factor

is an iterative procedure with the resulting corrected cross section for one calculation providing the best guess for the next iteration. The correction factor calculated in this manner is then used to normalized the data to the target thickness seen at 90^{o}.

The absolute cross sections derived from this experiment depend on the effective target thickness which in turn depends on the geometry of the target and collimators. The Monte Carlo code integrates over the full length of the gas target. The target thickness is calculated for the detector at 90^{o} as

$$T_D = N_D \, l_2 \sum_{i=1}^{N} C_i / N \qquad 3\text{-}4$$

where l_2 is the length of the gas cell along the beam axis, N_D is the density of the deuterium gas, and the C_i's are again the transmission probabilities.

An additional effect not considered in the finite geometry calculation but of potential importance is the small angle scattering of γ-rays from the collimators into the detector. For the energy region considered four interactions of γ-rays with matter are of importance. They are pair production, Raleigh scattering, Compton scattering, and photoelectron emission. Both Raleigh and Compton scattering contribute to the scattering of high energy γ-rays off of the collimators and into the detector. Raleigh scattering has a very small cross section and an upper limit on the probability of a γ-ray scattering into the the detector is 10^{-6}. Incoherent or Compton scattering for small angles is much more significant. A more extensive calculation to estimate an

upper limit on the contribution of scattered γ-rays was undertaken. Only scattered γ-rays with less than 350 keV energy loss were considered to be in the capture peak, requiring a scattering angle of less than 3.5^{o}. The results indicate an upper limit of 0.5% contribution to the count rate. The angular dependence of this effect is much smaller and thus was neglected. The systematic error for the absolute cross sections includes this factor.

3.5 Finite Geometry Correction Results

The Monte Carlo calculation was performed for each energy at which an angular distribution was measured. The typical number of iterations required for convergence of the calculated correction factor was 80,000. Although the calculation of the correction factor was in principle iterative, only one iteration beyond the first order correction of $\sin(\theta)$ was necessary for convergence of the correction factor. As seen in Figure 3-1, the calculated correction factor was within 2% of the first order correction of $\sin(\theta)$ within the angular range of 30^{o} to 150^{o}. The resulting target thickness, as well as the attenuation coefficients used are given in Table 3-1. The γ-rays that pass through the collimators increase the target thickness by 10 to 15% compared to the thickness calculated assuming the collimators were completely opaque.

To further investigate the possible errors in the calculation resulting from the finite geometry correction, calculations were made in

Figure 3-1. The SOLAC generated angular distribution correction factor (solid line) and the first order correction factor approximation of $\sin(\theta)$ (dashed line).

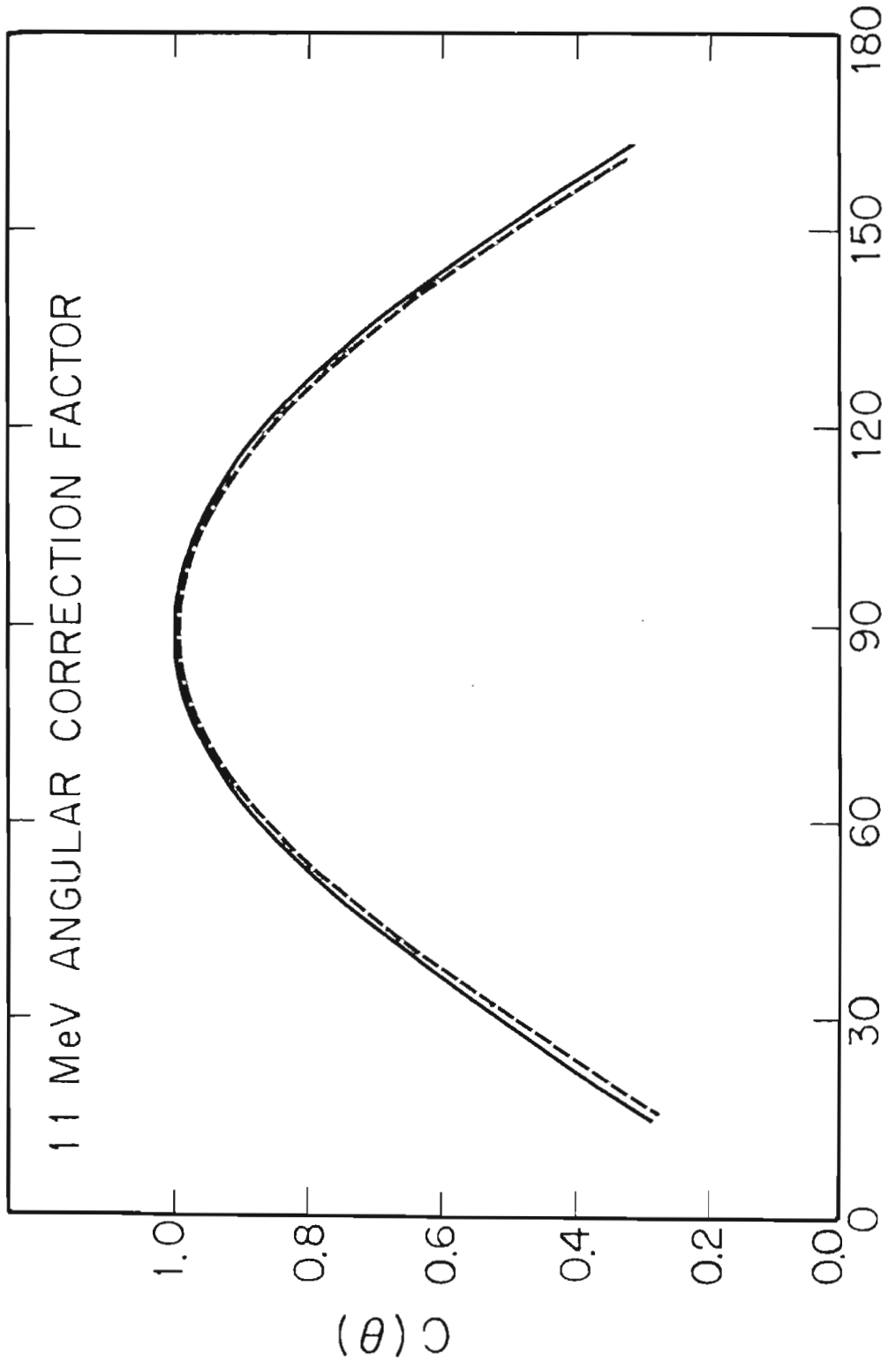
11 MeV ANGULAR CORRECTION FACTOR
C (θ)
1.0
0.8
0.6
0.4
0.2
0.0
0
30
60
90
120
150
180
ANGLE (deg)

Table 3-1. Absolute cross section information. The γ-ray attenuation coefficient, τ, the effective target thickness, T_D, for 34.4 kPa and 90^o detector angle, and the energy dependent NaI detector efficiency, ε_d for the right detector (see Figure 2-4) are given.

E_p (MeV)	τ (cm^{-1})	T_D ($\mu g/cm^2$)	ε_d (%)
6.5	0.756	108.1	24.5
8.0	0.774	107.8	24.8
10.93	0.811	106.5	25.2
14.96	0.854	105.0	25.3
15.94	0.870	104.8	25.3

which the beam position was moved from the center of the rotation of the detector, the collimators were shifted off center, the radial position of the collimators was changed, and the attenuation coefficient varied. All perturbations within the possible ranges of experimental error had insignificant effects on the calculated correction factors.

4 Absolute Cross Sections

4.1 Overview

The measurements and calculations of σ_T and $\sigma(90^o)$ yield curves for the reaction $^2H(p,\gamma)^3He$ (Q = 5.49 MeV) have been quite extensive, extending over a period of more than 20 years. While the primary results of this work involved the measurements of angular distributions of cross section and analyzing power, the confirmation of previous absolute cross sections lends credence to the present measurements since the absolute cross sections are much more sensitive to the possible errors in the calculation of target thickness and finite geometry corrections than the angular distribution results.

Although many measurements of σ_T and $\sigma(90^o)$ exist, there are still some areas of controversy. First, a 40% difference exist between the peak total cross section reported by Wolfli *et al.* (1966) and the previous TUNL work (Skopik, 1979). Also, the only complete overlap between the peak cross section energy region and the high energy tail of the total cross section is the early work of Fetisov (1964). However, the statistical errors in Fetisov's data are large (~15%). The $\sigma(90^o)$ yield curve also has a peak cross section uncertainty with two large groups of data with either 110 to 120 μb/sr or 85 to 95 μb/sr cross section. Another check of these cross sections would be beneficial.

4.2 Measurement of Cross Section

Equation 3-1 gives the differential γ-ray count rate in the detector. After calculating the integral over the finite geometry we find the differential cross section at a detector angle θ_d is

$$4\text{-}1 \qquad \frac{d\sigma}{d\Omega}(\theta_d) = \frac{N_\gamma(\theta_d)}{F_p \; T_D(\theta_d) \; (\Omega_d \varepsilon_d)}$$

$$T_D(\theta_d) = T_D(90^\circ)/C(\theta_d)$$

where $N_\gamma(\theta)$ is the number of γ-rays detected, $T_D(\theta_d)$ is the effective target thickness for the detector at an angle θ_d, Ω_d is the detector solid angle, and ε_d is the energy dependent NaI detector efficiency. Both $T_D(90^\circ)$, the effective target thickness, and $C(\theta_d)$ the angular finite geometry correction factor, are calculated by the Monte Carlo program described in chapter 3. F_p, the number of protons incident on the target, is determined from the beam current integration (BCI). The determination of $(\Omega_d \varepsilon_d)$ will be discussed in the next section.

The beam current integration and target thickness were checked by using a solid state charged particle detector to measure elastic scattering at $\theta_{LAB} = 25^\circ$. The capture cross section can be normalized to the $^2H(p,p)$ cross section which is known to approximately 1 to 3% in this energy region. The cross sections of Kocher and Clegg (1966), van Oers et al. (1960), Kikuchi et al. (1960), and Caldweld et al. (1955) were interpolated at the energies used in the radiative capture experiment. The NaI detector views a different target than the solid

state detectors so the normalization to the monitor is not independent of the target thickness determination of the finite geometry Monte Carlo calculation. The angular distribution coefficients and fore-aft asymmetries extracted using monitor normalizations were essentially the same as those extracted using BCI normalizations. The total cross sections based on the monitor normalizations are discussed in §4-5.

4.3 Efficiency

The measurement of absolute cross section required the knowledge of the detector efficiency. Since new NaI collimators were in use in this experiment, the change in geometry was expected to result in a somewhat different efficiency. The technique for determining $\Omega_d \varepsilon_d$ has been described previously (Weller and Roberson, 1980). Measurements of a thick target yield curve were made over the resonance at E_p = 14.24 MeV in the reaction $^{12}C(p,\gamma)^{13}N$. The γ-ray yield for this resonance has been measured as $6.83 \pm 0.22 \times 10^{-9}$ γ-rays/proton (Marrs et al., 1975). This gives an absolute calibration at a γ-ray energy of 15.1 MeV.

Our yield curve measurements with a 2.0 mg/cm^2 ^{12}C target are given in Figure 4-1. The γ-ray peak was fitted and summed over the same energy region and with the same procedure as the reaction of interest. The weighted average of the measurements at a beam energy of 14.27 and 14.28 MeV were used for the on resonance counts, while a linear least squares fit to the yield above and below the resonance gave the off resonance yield. The difference between on and off resonance counts is

Figure 4-1. Thick target yield curves for the NaI detector efficiency measurements using the E_p = 14.26 MeV resonance in the reaction $^{12}C(p,\gamma)^{13}N$.

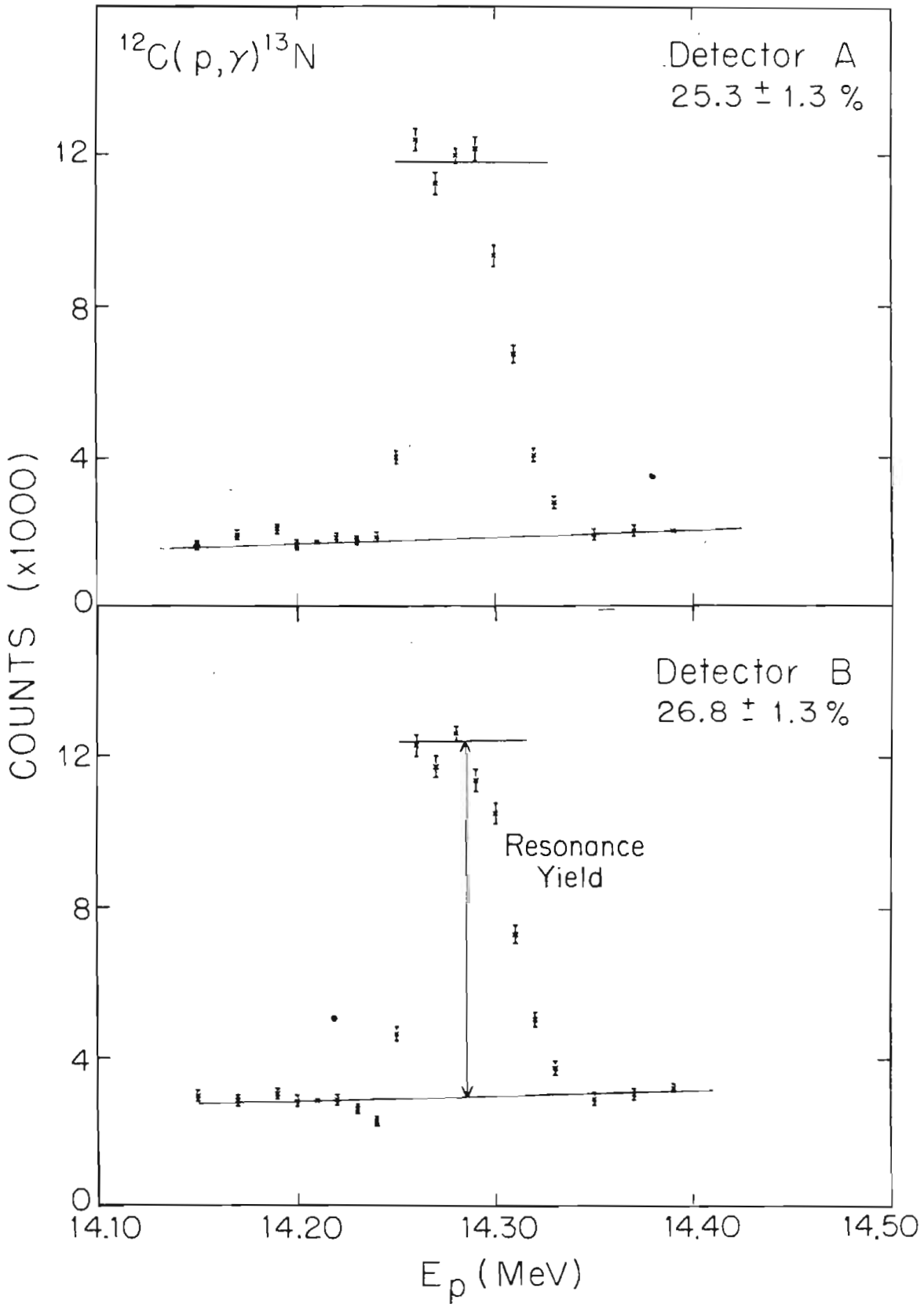
$^{12}C(p,\gamma)^{13}N$
Detector A
25.3 ± 1.3 %
Detector B
26.8 ± 1.3 %
Resonance
Yield
COUNTS (x1000)
0
4
8
12
14.10
14.20
14.30
14.40
14.50
E_p (MeV)

the yield for the resonance and gives an efficiency, ε_d at E_x = 15.1 MeV of 0.253 $\pm$ 0.013 for the right detector and 0.268 $\pm$ 0.013 for the left detector (see Figure 2-4). These efficiencies assume a detector solid angle of 21.9 msr based on the lead collimator size. The efficiency measurements were made with the same experimental set-up as used for the gas target measurements. Thus, any contribution of small angle (γ,γ) scattering off of the collimators is included, to first order, in the efficiency at this energy. The error in the efficiency quoted here actually includes the error in the solid angle but since our measurement determines the product of solid angle and efficiency and the errors can not be separated, we have assumed that the solid angle has no error and that the fractional error in $\Omega_d\varepsilon_d$ is included in ε_d above.

The extrapolation of the efficiency to other energies depends on the energy dependence of the γ-ray attenuation in paraffin and plastic, the fraction of the total response in the peak region as well as energy dependence of the fraction of the full energy spectrum rejected by the shield electronics. The fraction of the total response in the peak region has been shown to be constant (Hayward, 1979) in this energy region. Measurements of the shield rejection ratio and attenuation provide the energy dependence of ε_d. Fortunately, the rejection ratio decreases as a function of increasing energy and the attenuation decreases. For this work the maximum correction factor relative to the efficiency measurement at the calibration point of 15.1 MeV is 3%. Included in Table 3-1 are the detector efficiencies, ε_d, for the right detector (Detector A in Figure 2-4) at the energies used to measure

absolute cross section. The left detector efficiency has the same energy dependence.

4.4 Errors

At the energies of E_p = 6.5 and 8.0 MeV, there was considerable error in the beam current integration due to beam dispersion and electron emission from the exit foil. To measure the BCI error, a 500 $\mu g/cm^2$ solid carbon target was placed in the center of the target chamber. The counts in a charged particle detector located at an angle of 160^o were monitored for the reaction $^{12}C(p,p)$ with deuterium gas and entrance and exit foils in the chamber and then with both gas and foils removed. The correction for the decrease in the beam current integration may be obtained by taking the ratio of the counts. The correction factor measured at 8 MeV to the BCI was 1.17 $\pm$ 0.03 with the error including both statistical error as well as an estimate of the systematic monitor errors.

The absolute cross section is subject to systematic errors in addition to the usual statistical errors. The systematic errors include uncertainties in beam current integration, detector efficiency measurement errors, fitting errors, uncertainty in target thickness, in finite geometry correction factors, and in the subtraction of backgrounds. A tabulation of the errors is given in Table 4-1. The range of errors given for some effects represents the variations with the experimental conditions. The overall uncertainty in the cross

Table 4-1. Absolute Cross Section Error Analysis. Factors contributing to the overall error using BCI normalization.

Source of Error	Error(%)
BCI Error	4
BCI Correction at 6.5 and 8 MeV	3
BCI Correction at 16 MeV	3
Efficiency	5-6
Statistical Uncertainty	1-3
Background Uncertainty	2-6
Fitting error	2
Target Thickness	6
Miscellaneous	2
Overall error	10-12

section when the data is normalized to the BCI is no more than 12%. The additional errors in 6.5, 8.0, and 16 MeV are too small to change the overall error.

The monitor normalized cross sections do not include beam current integration errors. However, additional errors in the interpolated elastic scattering cross section, the detector solid angles, the collimator sizes and positions, statistics, background uncertainties, summing regions, and beam position must be considered. The collimators were measured with an optical micrometer. The error in the solid angle of the detector is approximately 3%. Small changes in beam position coupled with the narrow geometry and short radial distance to the monitor detectors results in an average fluctuation of almost 2% in the monitor count rate with occasional fluctuations of up to 6%. The relative uncertainty between the BCI and monitor normalizations is 6 to 8%.

4.5 Total Cross Section

The total cross section, $\sigma_T(p,\gamma)$ was determined by the angular integration of the fit to the angular distributions measured at proton beam energies of 6.5, 8.0, 11.0, 15.0, and 16.0 MeV. The BCI normalized total cross sections are given in Table 4-2 as well as the $\sigma_T(\gamma,p)$ cross sections which were calculated from $\sigma_T(p,\gamma)$ using the principle of detailed balanced (Hayward, 1970). Figure 4-2 gives the (γ,p) cross sections for the present data along with the results of Griffiths

Table 4-2. Absolute cross sections for $^{2}H(p,\gamma)^{3}He$ reaction in terms of both radiative capture cross sections and photonuclear cross sections. The results are normalized to the BCI and show statistical errors only.

E_p (MeV)	$\sigma_{90}(p,\gamma)$ μb/sr	$\sigma_{90}(\gamma,p)$ μb/sr	$\sigma_T(p,\gamma)$ μb	$\sigma_T(\gamma,p)$ mb
6.5	1.46 ± .02	123. ± 2.4	12.6 ± .09	1.06 ± .01
8.0	1.44 ± .03	123. ± 1.5	12.2 ± .09	1.04 ± .02
10.93	1.32 ± .03	111. ± 1.3	12.0 ± .20	1.01 ± .02
14.96	1.25 ± .03	98. ± 1.2	10.7 ± .20	0.84 ± .02
15.94	1.13 ± .03	86. ± 1.2	9.7 ± .10	0.75 ± .01

Figure 4-2. Total cross sections for the $^{2}H(p,\gamma)^{3}He$ reaction. The cross section is expressed using the principle of detail balance in terms the $^{3}He(\gamma,p)^{2}H$ reaction. The error bars for the present data as well as for most of the other works include statistical errors only. The present data is given in tabular form in Table 4-2.

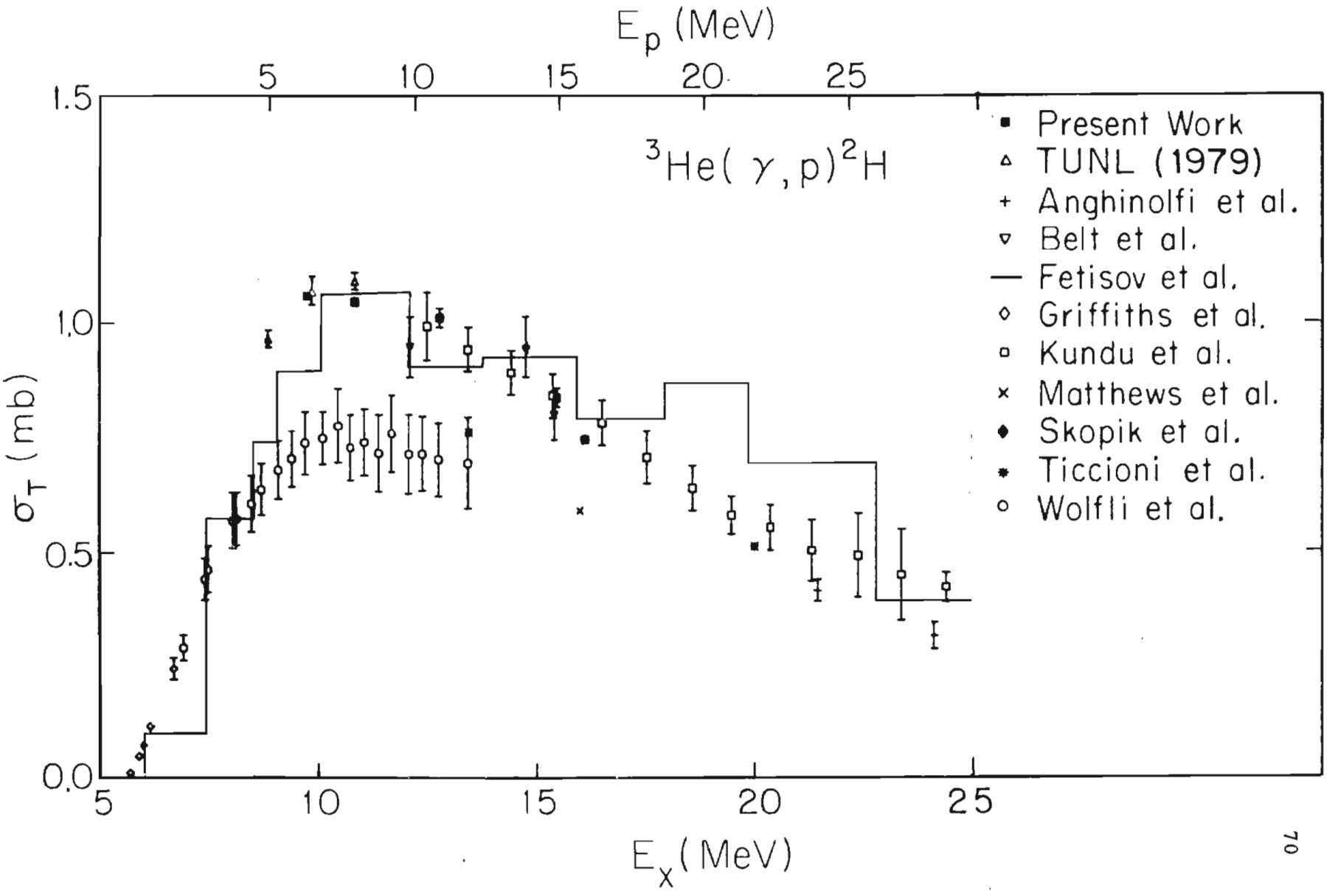
E_p (MeV)
5
10
15
20
25
1.5
1.0
0.5
0.0
σ_T (mb)
$^3He(\gamma,p)^2H$
Present Work
TUNL (1979)
Anghinolfi et al.
Belt et al.
Fetisov et al.
Griffiths et al.
Kundu et al.
Matthews et al.
Skopik et al.
Ticcioni et al.
Wolfli et al.
E_x (MeV)

et al. (1962), Fetisov et al. (1965), Wolfli et al. (1966), Belt et al. (1971), Kundu et al. (1971), Ticcioni et al. (1973), Matthews et al. (1974), Skopik et al. (1979), Skopik et al. (1983), and Anghinolfi et al. (1983). The error bars on the present work are statistical only.

There is a substantial discrepancy between the data of Wolfli and the present results, the previous TUNL data (Skopik et al., 1979), and the cloud chamber data of Fetisov. Wolfli used a 7.5 by 7.5 cm NaI detector, and the discrepancy may have resulted from insufficient knowledge of the detector efficiency. Our new data ties in very well with the higher energy results adding support to the larger values. The low total cross sections of Ticcioni at 12.5 Mev excitation energy and of Matthews at 16 MeV results from low values of 90^{o} cross sections. The present measurement of total cross section exhibit a smooth energy dependent behavior with no evidence of structure. A check of the cross section measurements at 11 and 15 MeV using monitor normalizations agreed well considering the relative error between BCI and monitor normalizations. The 16 MeV polarized beam measurements have a 8% difference in cross section between the two normalization procedures with the monitor normalization cross section being the largest. Additional uncertainties in timing as a result of using a polarized beam and early problems in this work of the emission of electrons from the exit foil affecting the BCI probably account for the difference. At 6.5 and 8.0 MeV the monitor solid state detectors were not used because of the deterioration that the detectors had previously experienced in the

gas target.

4.6 90^{o} Cross Section

In Figure 4-3 the present BCI normalized 90^{o} cross section data are shown along with the radiative capture results of Belt *et al.* (1971), Chang *et al.* (1974), Halbert *et al.* (1972), Matthews *et al.* (1974), Skopik *et al.* (1979), and Anghinolfi *et al.* (1983). These data are plotted as $\sigma(\gamma,p)$ for ease of comparison with photonuclear disintegration data. Table 4-2 gives the 90^{o} cross sections expressed both as (γ,p) cross sections and as (p,γ) cross sections. The results of the present work gives a slightly larger cross section than obtained by most other capture experiments. The present results are in good agreement with the earlier TUNL measurements. Not shown are the yield curves of Chang *et al.* (1972) and von Woude *et al.* (1971) which exhibit resonant behavior not observed in any subsequent work. In addition, the cross section of Matthews is ~20% too low. Halbert's $\sigma(90^{o})$ yield curve gives an indication of structure near 15 MeV excitation energy. The present measurement at 15 MeV agrees with the peak of this structure, but without more data the structure can not be confirmed.

The radiative capture measurements of the present work and the previous TUNL work are compared to the large quantity of photonuclear data in Figure 4-4. The 90^{o} yield curve data falls into three groups. First, the low cross section group has a peak cross of approximately 85

Figure 4-3. $^{2}H(p,\gamma)^{3}He$ radiative capture differential cross sections at $\theta_{cm} = 90^{\circ}$ expressed in terms of the (γ,p) reaction. The present data is given in tabular form in Table 4-2.

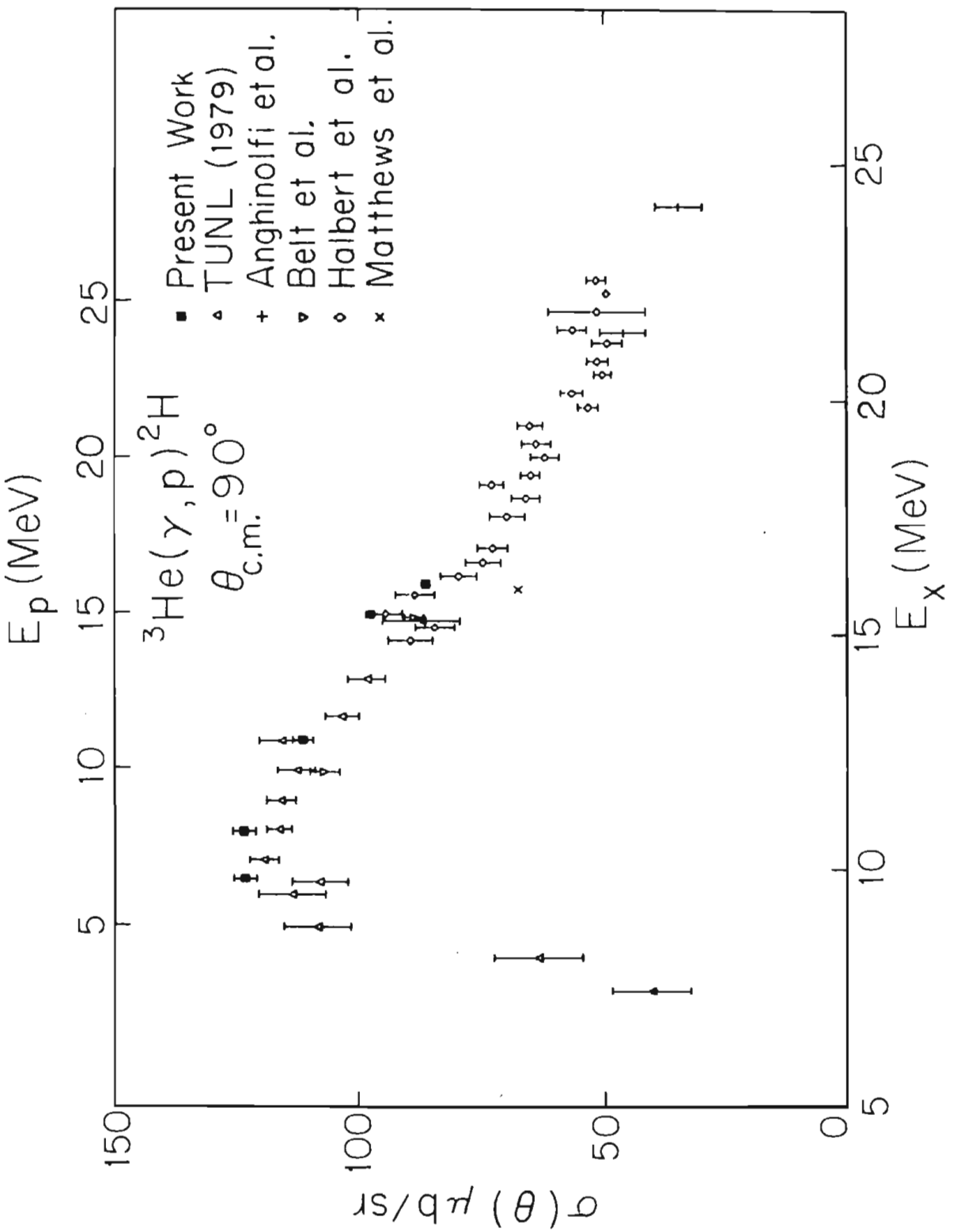
$^3He(\gamma,p)^2H$
$\theta_{c.m.}=90^\circ$
Present Work
TUNL (1979)
Anghinolfi et al.
Belt et al.
Holbert et al.
Matthews et al.
E_p (MeV)
E_x (MeV)
$\sigma(\theta)$ μb/sr
0
50
100
150
5
10
15
20
25

Figure 4-4. The 90^{o} differential cross sections for the $^{3}He(\gamma,p)^{2}H$ reaction. Also shown are the radiative capture results of the present work and of Skopik *et al.* (1979).

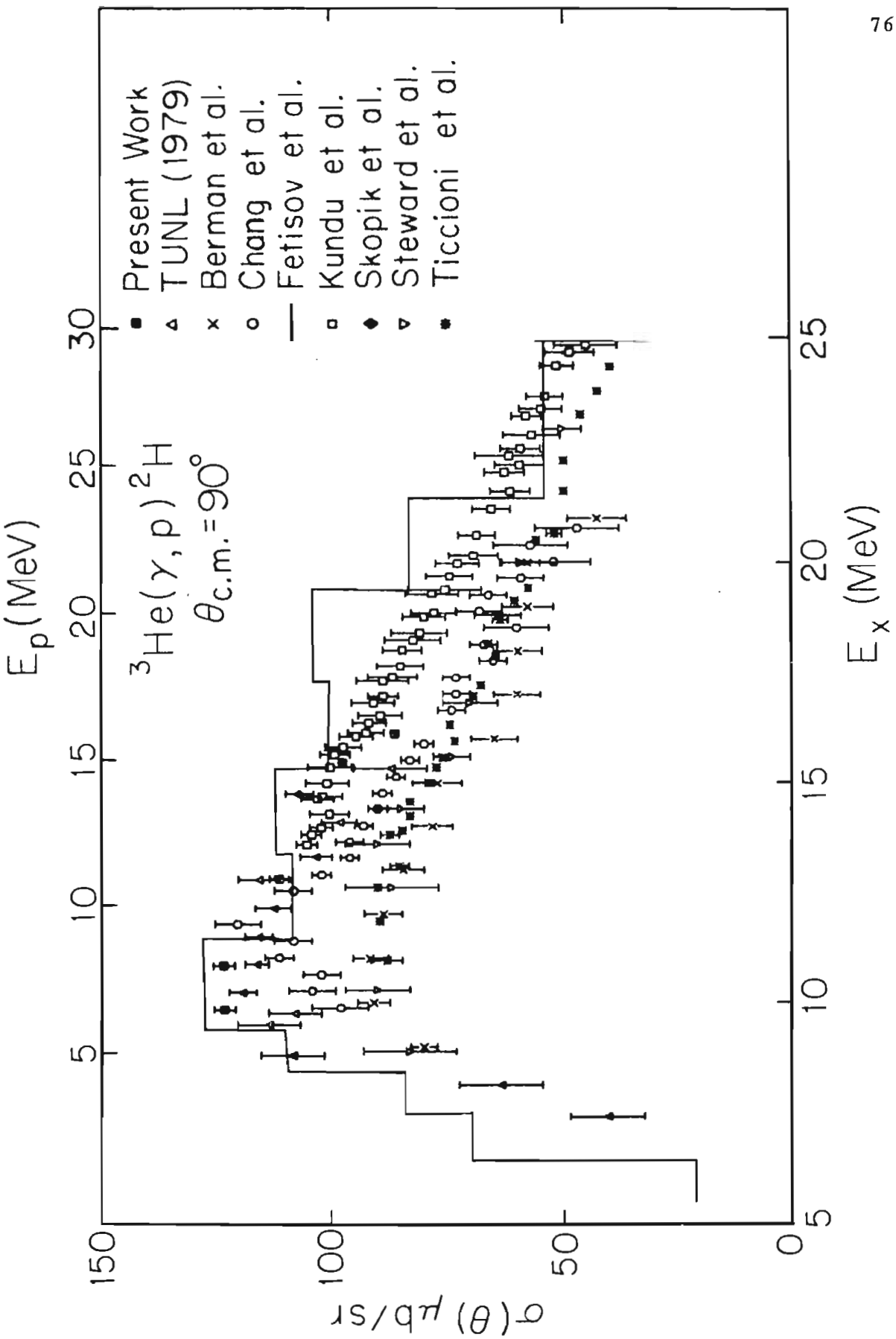
Present Work
TUNL (1979)
Berman et al.
Chang et al.
Fetisov et al.
Kundu et al.
Skopik et al.
Steward et al.
Ticcioni et al.
$^3He(\gamma,p)^2H$
$\theta_{c.m.}=90°$
E_p (MeV)
E_x (MeV)
$\sigma(\theta)$ μb/sr
0
50
100
150
5
10
15
20
25
30

to 95 μb/sr (Berman et al., 1964; Steward et al., 1965; Matthews et al., 1974; and Ticcioni et al., 1973). Next, the group of experiments with high cross sections gives a peak cross section of about 120 μb/sr (Fetisov et al., 1964; Kundu et al., 1973; and Skopik et al., 1983). Both groups of experiments have yield curves with the same energy dependence and differ by only a normalization factor. Finally, one photodisintegration experiment (Chang et al., 1974) has a different energy dependence with a high peak cross section but which eventually (>15 MeV) converges with the low cross section data.

The capture experiments above 15 MeV of Halbert et al. (1972), Anghinolfi et al. (1983), and Belt et al. (1971) support the low cross section group of photonuclear experiments. The present data at 6.5, 8.0, and 11.0 MeV confirm the high peak cross section of about 120 μb/sr, but the results at 15 and 16 MeV are slightly below the high cross section data as seen in Figure 4-4. However, as stated before the present data is above the rest of the capture data which converge with the low cross section high energy tail results. Further work is clearly needed above 15 MeV excitation energy. Chang et al. (1974) have a rather sharp peak cross section at E_x = 12.0 MeV while most of the other data including the current results have a broad peak between 10 and 12 MeV.

5 Angular Distributions for the $^2H(p,\gamma)^3He$ Reaction

5.1 Introduction

The measurement of angular distributions of cross section and analyzing power provides a powerful tool for studying the radiative capture process. Within the context of a model, information on both the bound state and continuum wave functions coupled in this reaction as well as the interaction between these states can be obtained. The angular distribution results also allow the extraction of the partial cross sections of the electromagnetic multipolarities of the interaction. If sufficient information is available, the magnitude and phases of the transition matrix amplitudes can be extracted.

In the following chapter, the formalism and measurements of angular distributions of cross section and analyzing power will be discussed. The fore-aft asymmetry measurements will also be presented. Finally, the transition matrix element analysis of the polarized data will be looked at in detail. The interpretation and implications of these results will be discussed in chapter 6.

5.2 Angular Distribution Formalism

The angular distribution of cross section can be expanded as

$$\sigma(\theta) = A_0 \left[1 + \sum_{k=1}^{k_{max}} a_k P_k(\cos\theta)\right] \qquad 5\text{-}1$$

where A_0 and a_k are fitted coefficients and $P_k(\cos\theta)$ are the Legendre polynomials. The angular distributions measured in this work were fit with this expansion using a χ^2-minimization criterion. The maximum value of k_{max} that was statistically justified was 4.

Earlier works in the three-body problems have expanded the unpolarized angular distributions in terms of the sine and cosine functions (Eichmann, 1963) as follows:

$$\sigma(\theta) = B\,(\,\alpha + \sin^2\theta + \beta\sin^2\theta\cos\theta + \gamma\sin^2\theta\cos^2\theta + \varepsilon\cos\theta) \qquad 5\text{-}2$$

or some subset of the terms in this equation. The conversion between the Legendre polynomials and the sine, cosine expansion of the angular distribution is given in Table 5-1. The equation in this form gives some useful information. The isotropic term, α, is a measure of the M1 transitions, transitions to the D-state of ^{3}He, and $\Delta S=1$ (spin-flip transitions). Most expansions have neglected ε thus requiring $a_1 = -a_3$. When sufficient information was given, previous angular distribution measurements were refitted using Eqn. 5-1 in order to obtain the a_k's and associated errors. If the angular distribution was not available the sine-cosine coefficients were converted to a_k's. However, for this latter case the error propogation is incorrect because the error matrix is not known. This leads, in general, to an over estimate of the error.

The expression for analyzing power for a vector polarized beam is

$$A(\theta) = \frac{(N_+ - N_-)}{P(N_+ + N_-)} \qquad 5\text{-}3$$

where $N_+(N_-)$ are the number of counts with the spin up (down) defined

Table 5-1. Relationship between the Legendre polynomial and Sin(θ), Cos(θ) expansions of the unpolarized cross sections.

$A_0 = B[\alpha + 0.667 + 0.133\ \gamma]$
$a_1A_0 = B[\varepsilon + 0.4\ \beta]$
$a_2A_0 = B[-0.667 + 0.0953\ \gamma]$
$a_3A_0 = B[-0.4\ \beta]$
$a_4A_0 = B[-0.2286\ \gamma]$

according to the Madison Convention (H.H. Barschall and W. Haeberli, 1970) and P is the vector beam polarization. The analyzing power can be rewritten for the two detectors as

$$5\text{-}4 \qquad A(\theta) = \frac{1}{P}\,\frac{r-1}{r+1}$$

$$r^2 = \frac{L_+ R_-}{L_- R_+}$$

where $L_+(L_-)$ are the number of counts in the left detector for spin up (down) measurements and $R_+(R_-)$ are the number of counts in the right detector (Detector A in Figure 2-4). This equation eliminates the need for normalizations resulting from differences in the detector efficiencies as well as normalizations between runs. Fluctuations in BCI and various other systematic errors are canceled, to first order, when this ratio method is used.

The angular distributions of the product of cross section and analyzing power were expanded according to

$$5\text{-}5 \qquad \frac{A(\theta)\ \sigma(\theta)}{A_0} = \sum_{k=1}^{k_{max}} b_k\ P_k^1(\cos\theta)$$

where the b_k are the coefficients fitted to the data and the $P_k^1(\cos\theta)$ are the associated Legendre polynomials of the first kind. As in the case of the unpolarized cross sections, the expansions were performed up to $k_{max}=4$.

5.3 Angular Distributions of Cross Section

Measurements of angular distributions of cross sections at the

nominal proton beam energies of 6.5, 8.0, 11.0, 15.0, and 16.0 MeV have been made over angular ranges of 30^{o} to 150^{o} at 13 to 17 angles. The angular distributions were corrected for finite geometry effects as described in §3.5. The angular distribution data with statistical errors is presented in tabular form in Table 5-2. Figure 5-1 gives the unpolarized angular distributions as well as the Legendre polynomials fits. The deduced a_k coefficients are given in Table 5-3. The angular distribution at 6.5 MeV was constrained to be zero at 0^{o} in order to prevent the cross section from being negative at small angles. The only coefficient significantly effected was a_4. At all energies the angular distribution is chiefly characterized by a $\sin^2\theta$ dependence which results from the dominance of the E1 cross section (Wilkinson, 1952). The angular distributions become more forward peaked as a function of increasing proton energy indicating the increased presence of non-E1 radiation.

At 15 MeV we have combined our results with those of Belt et al. (1971) and Skopik et al. (1983) as shown in Figure 5-2. Although the absolute cross sections of the two capture experiments agreed within error (~10%), the electrodisintegration results (Skopik et al., 1983) were about 20% higher. This cross section difference is partially the result of a 0.5 MeV excitation energy difference. The three sets of data were fit separately to determine the A_0 coefficient. These coefficients were then used to normalize and combine the three data sets. The solid line shown in Figure 5-2 is a fit to the combined data and corresponds to the a_k coefficients given in the figure. The

Table 5-2. Observed cross section and analyzing power angular distributions for the $^{2}H(\vec{p},\gamma)^{3}He$ reaction at proton energies of 6.5, 8.0, 11.0, 15.0, and 16.0 MeV. The uncertainties represent one standard deviation of the statistical error.

E_p	θ_{cm}	$\sigma(\theta)/A_0$	$A(\theta)\sigma(\theta)/A_0$
6.5	31.1	0.54 ± 0.02	
	41.5	0.86 ± 0.02	
	46.6	1.04 ± 0.02	
	51.7	1.16 ± 0.03	
	62.0	1.41 ± 0.03	
	72.1	1.53 ± 0.04	
	82.2	1.52 ± 0.03	
	92.2	1.41 ± 0.02	
	112.0	1.16 ± 0.03	
	121.9	0.82 ± 0.03	
	131.7	0.65 ± 0.02	
	141.4	0.45 ± 0.02	
	151.1	0.26 ± 0.01	
8.0	31.3	0.59 ± 0.01	
	41.6	0.89 ± 0.02	0.016 ± 0.045
	51.9	1.19 ± 0.03	0.096 ± 0.051
	62.2	1.42 ± 0.03	0.069 ± 0.055

Table 5-2. Continued

E_p	θ_{cm}	$\sigma(\theta)/A_0$	$A(\theta)\sigma(\theta)/A_0$
	72.4	1.49 ± 0.04	
	77.4	1.51 ± 0.06	0.085 ± 0.079
	82.5	1.48 ± 0.03	
	92.5	1.47 ± 0.03	0.056 ± 0.050
	102.4	1.24 ± 0.05	
	107.4	1.14 ± 0.05	0.033 ± 0.069
	112.3	1.12 ± 0.04	
	117.2	0.97 ± 0.03	
	121.1	0.75 ± 0.03	0.021 ± 0.043
	131.9	0.60 ± 0.02	0.045 ± 0.035
	141.6	0.40 ± 0.02	-0.043 ± 0.039
	151.2	0.27 ± 0.01	
10.93	31.5	0.66 ± 0.03	
	36.7	0.72 ± 0.05	
	41.9	0.91 ± 0.04	
	52.3	1.26 ± 0.05	
	54.4	1.34 ± 0.04	
	62.6	1.41 ± 0.06	
	72.8	1.50 ± 0.03	
	82.9	1.45 ± 0.04	

Table 5-2. Continued

E_p	θ_{cm}	$\sigma(\theta)/A_0$	$A(\theta)\sigma(\theta)/A_0$
	92.9	1.41 ± 0.04	
	102.9	1.28 ± 0.05	
	112.7	1.09 ± 0.04	
	122.5	0.79 ± 0.03	
	125.2	0.75 ± 0.03	
	132.2	0.61 ± 0.02	
	141.8	0.43 ± 0.02	
	146.6	0.32 ± 0.02	
	151.4	0.26 ± 0.01	
14.96	31.7	0.63 ± 0.03	
	42.2	0.95 ± 0.02	
	52.7	1.24 ± 0.04	
	54.8	1.28 ± 0.03	
	63.0	1.38 ± 0.03	
	73.2	1.49 ± 0.03	
	83.4	1.54 ± 0.07	
	93.4	1.43 ± 0.04	
	102.8	1.21 ± 0.06	
	111.2	1.07 ± 0.05	
	122.9	0.72 ± 0.05	

Table 5-2. Continued

E_p	θ_{cm}	$\sigma(\theta)/A_0$	$A(\theta)\sigma(\theta)/A_0$
	125.6	0.71 ± 0.03	
	132.6	0.62 ± 0.04	
	142.1	0.45 ± 0.02	
	151.7	0.27 ± 0.02	
15.94	31.8	0.68 ± 0.02	
	42.3	0.92 ± 0.02	0.047 ± 0.028
	52.7	1.25 ± 0.04	0.008 ± 0.049
	63.1	1.39 ± 0.05	0.068 ± 0.061
	73.3	1.57 ± 0.05	0.055 ± 0.068
	83.5	1.46 ± 0.05	0.082 ± 0.069
	93.5	1.40 ± 0.04	-0.019 ± 0.059
	103.5	1.23 ± 0.04	
	113.3	0.97 ± 0.03	-0.020 ± 0.046
	123.0	0.79 ± 0.03	
	132.6	0.53 ± 0.02	-0.005 ± 0.047
	142.2	0.40 ± 0.02	-0.013 ± 0.021
	153.1	0.25 ± 0.01	

Figure 5-1. Angular distributions of cross section for the $^{2}H(p,\gamma)^{3}He$ reaction at various energies. The data is shown with statistical errors. The curves are fits to the data using Legendre polynomial expansions through k=4. The data is given in Table 5-2. The fitted coefficients are given in Table 5-3.

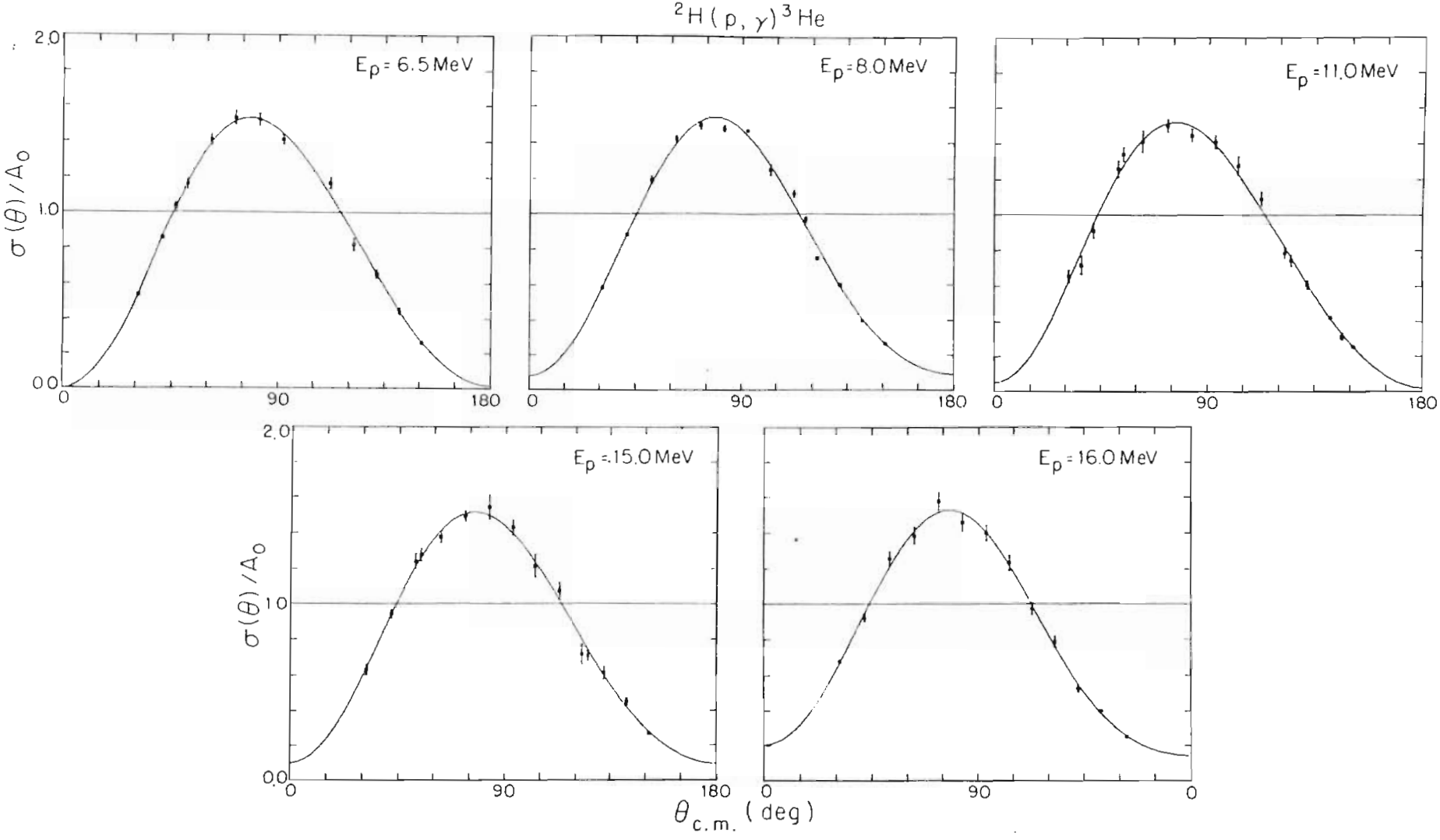
$^2H(p,\gamma)^3He$
E_p = 6.5 MeV
E_p = 8.0 MeV
E_p = 11.0 MeV
E_p = 15.0 MeV
E_p = 16.0 MeV
$\sigma(\theta)/A_0$
2.0
1.0
0.0
0
90
180
$\theta_{c.m.}$ (deg)

Table 5-3. Coefficients and standard deviations from fits of Legendre polynomials to cross section data and associated Legendre polynomials to analyzing power times cross section. The χ^2 per degree of freedom is given for both the cross section and analyzing power.

E_p (MeV)	Legendre Coefficients		χ^2
6.5	a_1	0.222 ± 0.008	1.47
	a_2	-0.961 ± 0.010	
	a_3	-0.230 ± 0.018	
	a_4	-0.034 ± 0.019	
8.0	a_1	0.256 ± 0.014	1.78
	a_2	-0.933 ± 0.021	
	a_3	-0.261 ± 0.037	
	a_4	0.017 ± 0.046	
	b_1	0.057 ± 0.022	0.62
	b_2	0.018 ± 0.012	
	b_3	-0.016 ± 0.013	
	b_4	-0.012 ± 0.014	

Table 5-3. Continued

E_p (MeV)	Legendre Coefficients		χ^2
10.93	a_1	0.278 ± 0.012	1.23
	a_2	-0.907 ± 0.023	
	a_3	-0.264 ± 0.031	
	a_4	-0.058 ± 0.034	
14.96	a_1	0.266 ± 0.013	0.98
	a_2	-0.889 ± 0.022	
	a_3	-0.268 ± 0.030	
	a_4	-0.021 ± 0.037	
15.94	a_1	0.294 ± 0.009	1.16
	a_2	-0.869 ± 0.015	
	a_3	-0.269 ± 0.026	
	a_4	0.040 ± 0.030	
	b_1	0.028 ± 0.012	0.70
	b_2	0.018 ± 0.006	
	b_3	0.003 ± 0.005	
	b_4	-0.001 ± 0.004	

Figure 5-2. Angular distributions of cross section at a proton beam energy of 15 MeV from the present work, Skopik et al. (1983), and Belt et al. (1971) are shown along with statistical errors. The solid curve is the Legendre polynomial fit to the data with the coefficients given in the figure. The dashed curve is the theoretical prediction by Aufleger and Drechsel (1981) which will be discussed in chapter 6.

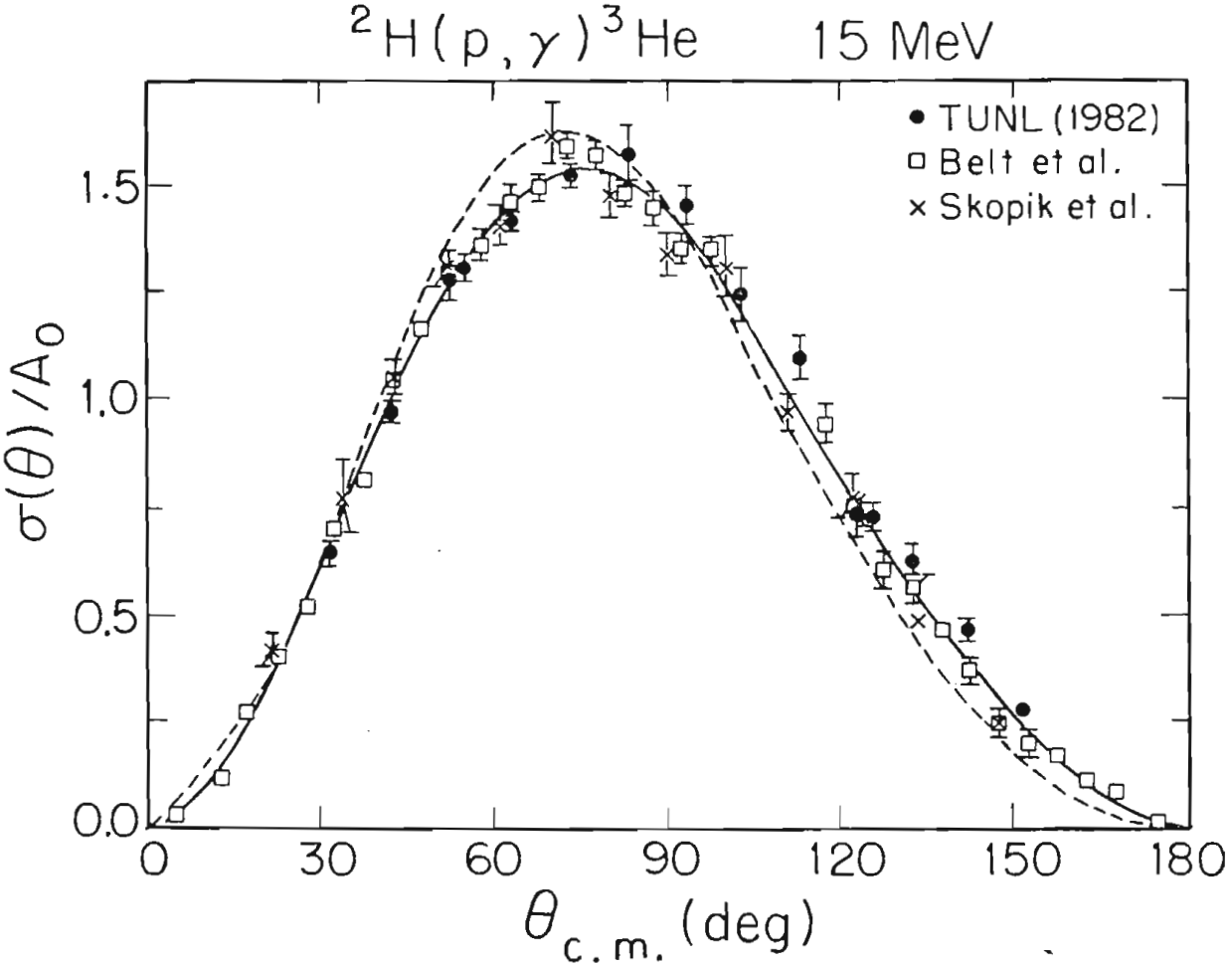

a_1	0.321 ± 0.006	a_3	-0.317 ± 0.007
a_2	-0.904 ± 0.007	a_4	-0.085 ± 0.008

agreement between the measurements is excellent. It is important to realize that these measurements were made by three totally different experimental techniques. Belt detected recoil ^{3}He nuclei from deuteron capture on hydrogen, Skopik used the ^{3}He(e,d)e'p reaction and detected the outgoing deuterons, while in the present experiment we measured proton capture and detected the outgoing γ-rays. The dashed line is a theoretical calculation by Aufleger and Drechsel (1981) and will be discussed in §6.3.

5.4 Fore-Aft Asymmetries

Because of the predominance of the E1 cross section in the ^{2}H(p,γ)^{3}He reaction, the extraction of other multipolarities is more difficult. One technique that is useful for studying non-E1 radiation is the measurement of fore-aft asymmetries. Only interference terms between transition amplitudes of different polarity contribute significantly to the fore-aft asymmetry. For example E1-E2 and E1-M1 interference could lead to finite fore-aft asymmetries. The fore-aft asymmetry is defined by

$$a_s = \frac{N_f - N_a}{N_f + N_a} \qquad 5\text{-}6$$

where N_f and N_a are the number of γ-rays measured at the zeros of the Legendre polynomial P_2, the angles 54.7° and 125.3° in the center of mass, respectively. The fore-aft asymmetries were measured by placing one NaI detector at approximately 55° and one at 125° and then swapping the angular positions and repeating the measurement. The expression

used to determine the fore-aft asymmetry for this two detector measurement is analogous to the two-detector analyzing power equation and is given by

$$5\text{-}7 \qquad a_s = \frac{r - 1}{r + 1},$$

$$r^2 = \frac{L_f R_f}{L_a R_a}$$

in which L and R are the number of counts for the left and right detectors as previously defined. This results in the cancellation, to first order, of several experimental uncertainties. First, errors in beam current integration or gas pressure effect both the forward and aft measurements equally. In addition this form of the equation eliminates the need for normalization between runs and for the difference in detector efficiencies.

In terms of the Legendre polynomial expansion of the cross section, the fore-aft asymmetry is defined as

$$5\text{-}8 \qquad a_s = \frac{0.5773a_1 - 0.3849a_3}{1 - 0.392a_4}.$$

The fore-aft asymmetries were measured in proton beam energy steps of approximately 1 MeV between 6 and 16 MeV. The results are given in both Table 5-4 and Figure 5-3. Agreement between the present data and previous experiments is reasonably good. There is rather little energy variation of the present results above 10 MeV as compared to the data of Kundu (1971). An extension of the present energy dependence would tend to support the asymmetry measurements of Anghinolfi et al. (1982) which lie below those of Kundu. Both of these higher energy measurements have

Table 5-4. Fore-aft asymmetries measured using the two detector method with their statistical errors. The measurement method is discussed in §5-4.

E_p (MeV)	Fore-aft Asymmetries
5.86	0.153 ± 0.019
6.37	0.188 ± 0.009
6.88	0.201 ± 0.017
8.0	0.234 ± 0.009
8.94	0.286 ± 0.007
9.94	0.290 ± 0.009
10.44	0.262 ± 0.030
10.93	0.320 ± 0.009
11.95	0.273 ± 0.023
12.95	0.260 ± 0.026
13.96	0.283 ± 0.025
14.96	0.292 ± 0.020
15.94	0.274 ± 0.008

R = .4

R = .5

Eθ
10 12.2

Figure 5-3. Fore-aft asymmetry measurements for the $^{2}H(p,\gamma)^{3}He$ reaction as a function of energy. The results of the present work are shown with the results of Anghinolfi *et al.* (1982), Belt *et al.* (1971), Kundu *et al.* (1972), Skopik *et al.* (1979), Skopik *et al.* (1983), and Wolfli *et al.* (1966). The fore-aft asymmetries from the present work are tabulated in Table 5-4.

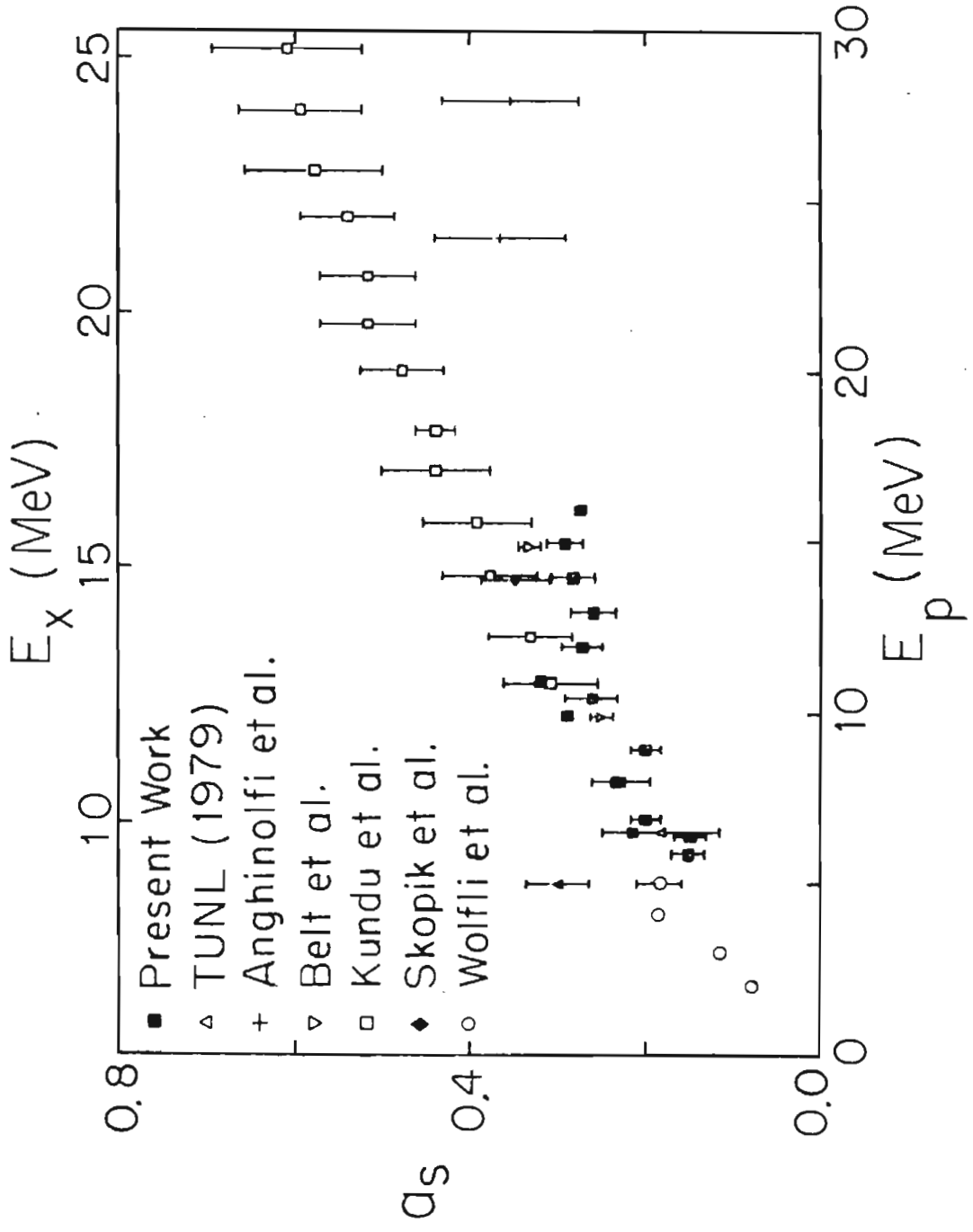
■ Present Work
△ TUNL (1979)
+ Anghinolfi et al.
▽ Belt et al.
□ Kundu et al.
◆ Skopik et al.
○ Wolfli et al.
E_x (MeV)
E_p (MeV)
a_s
0.8
0.4
0.0
0
10
15
20
25
30

substantial errors and clearly more work is needed to establish the fore-aft asymmetries in the energy region above 16 MeV excitation energy.

5.5 Angular Distribution of Analyzing Power

Angular distributions of analyzing power were measured at E_p = 8.0 MeV with 9 angles and at 16 MeV with 13 angles. The 8 MeV analyzing power angular distribution measurements were made with a solid CD_2 target for the experimental reasons discussed in Chapter 2. The analyzing power data is presented in Table 5-2 along with the the cross section information. The product of analyzing power and cross section are shown in Figure 5-4 along with fits based on the associated Legendre polynomial expansion given in Eqn. 5-5. The coefficients are given in Table 5-3. The analyzing powers were generally small. The only terms in the angular distribution expansion that were significantly nonzero were the b_1 coefficients at both energies and the b_2 coefficient at 16 MeV.

5.6 Transition Matrix Analysis

5.6.1 Introduction

The angular distributions of cross section and analyzing power can provide further information on the reaction via the extraction of

Figure 5-4. Angular distributions of the product of analyzing power and cross section for the $^{2}H(\vec{p},\gamma)^{3}He$ reaction at 8 MeV and 16 MeV proton energies including statistical errors. The curves are fits to the data using an expansion in terms of the associated Legendre polynomials through k=4. The fitted coefficients are given in Table 5-3.

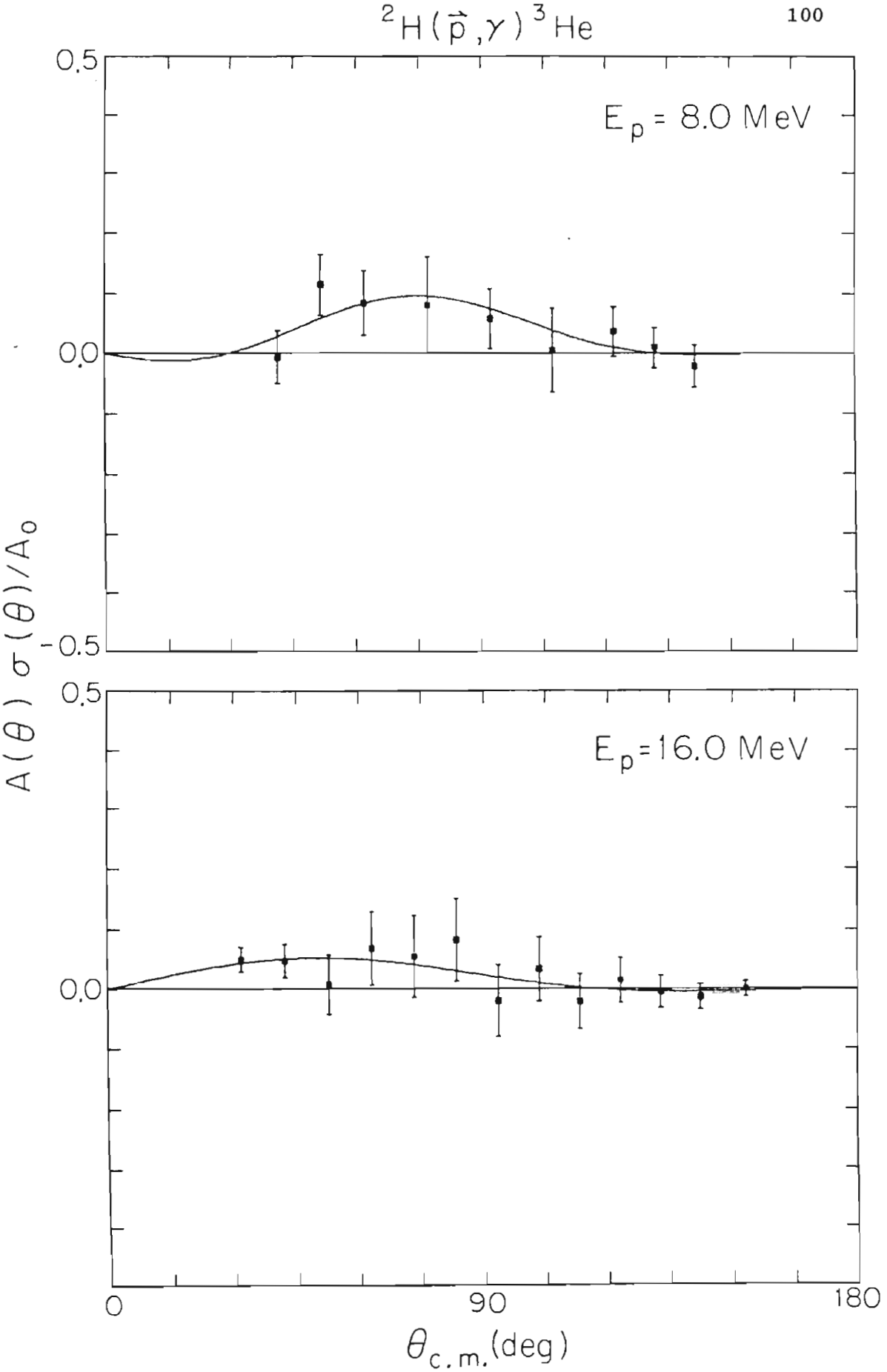
$^2H(\vec{p},\gamma)^3He$
E_p = 8.0 MeV
E_p = 16.0 MeV
0.5
0.0
-0.5
0
90
180
$A(\theta)\ \sigma(\theta)/A_0$
$\theta_{c.m.}$(deg)

transition matrix elements (Seyler and Weller, 1979). This analysis not only provides the partial cross sections of the different multipolarities but can, in some cases, provide a model independent determination of the amplitude and phases for individual channels. Unfortunately, in the case of the $^{2}H(p,\gamma)^{3}He$ reaction, the number of transition amplitudes and phases is so large (16 amplitudes and 15 relative phases for E1, E2, and M1 transitions only) that a completely model independent analysis is not possible.

In order to effectively discuss the analysis and results, the notation and some basic reaction formalism must be given. The channel spin coupling scheme was chosen for this analysis. The angular momenta for the a(x,L)c reaction are

$\vec{a}$ - total angular momentum of the target

$\vec{l}$ - orbital momentum of the incoming particle

$\vec{x}$ - spin of the incident particle

$\vec{s}$ - channel spin of the reaction

$\vec{L}$ - multipolarity of the γ-ray

$\vec{c}$ - spin of the residual nucleus

$\vec{J}$ - total angular momentum of the system

where

$$\vec{x} + \vec{a} = \vec{s}$$

$$\vec{l} + \vec{s} = \vec{J}$$

and $$\vec{L} + \vec{c} = \vec{J}.$$

The reduced transition matrix element is denoted as:

5-9 $$T = \langle pL(c)J\pi \,||\, R \,||\, l(xa)sJ\pi \rangle.$$

Where π is the total parity, p is the mode (1 electric, 0 magnetic) of the γ-ray, and R is the electromagnetic operator for the transition. The complex T-matrix element can be represented by a real amplitude and phase. These amplitudes can be labeled by the quantum numbers ℓ, s, and the γ-ray multipolarity. In the present work, the notation, $^{2s+1}\ell_J \exp(i\varphi_{(2s+1)\ell})$ is used to denote the transition matrix element.

5.6.2 E1-E2 Analysis

For the $^2H(\vec{p},\gamma)^3He$ reaction we have $\vec{x} = 1/2$, $\vec{a} = 1$, and $\vec{c} = 1/2$. The two possible channel spins ($\vec{s}$) are 1/2 (doublet terms) and 3/2 (quartet terms). Figure 5-5 is a schematic representation of the reaction channels with all transition amplitudes of M1, E1, and E2 multipolarities considered. Only the E1(s=1/2), E2(s=1/2), and E1(s=3/2) transitions will be considered here. The predominate bound state wave function in ^{3}He is ^{2}S with an admixture of ^{4}D (see §1.2). Spin-flip transitions, in which $\Delta S \neq 0$ going from the p+d continuum to the ^{3}He bound state, are insignificant. The reason is the electric transition operator (given in Eqn. 6-1) does not couple states of different spin. The only spin-flip strength results from final state interactions in the continuum. This too is weak as a result of the small $\ell \cdot s$ potential. As a result, the E1(s=1/2) transition is $^2p \rightarrow {}^2S$ and the E1(s=3/2) transition is $^4p \rightarrow {}^4D$. The E2(s=1/2) terms ($^2d \rightarrow {}^2S$) are indicated by the presence of a nonzero a_3 in the angular distribution (M1 amplitudes do not contribute to the a_3 coefficient if only E1, E2, and M1 transitions are considered). For the low energy

Figure 5-5. Schematic representation of radiative capture transitions in the ℓ, s coupling scheme for the E1, E2, and M1 transitions in the $^{2}H(p,\gamma)^{3}He$ reaction.

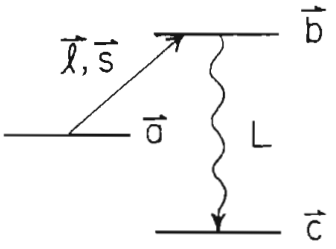

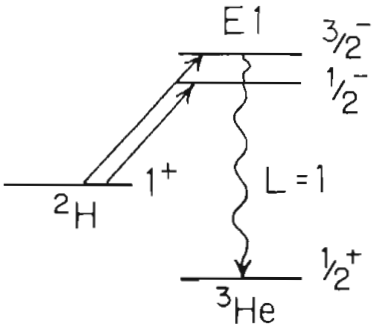

ℓ	s	j	amp
1	$1/2$	$1/2$	$^2p_{1/2}$
1	$1/2$	$3/2$	$^2p_{3/2}$
1	$3/2$	$1/2$	$^4p_{1/2}$
1	$3/2$	$3/2$	$^4p_{3/2}$
3	$3/2$	$3/2$	$^4f_{3/2}$

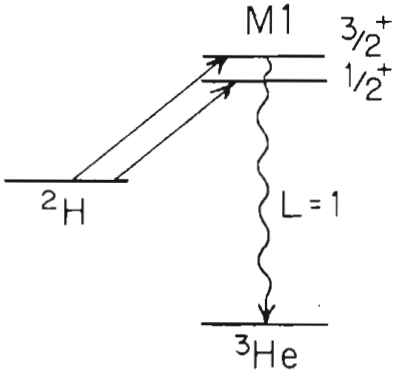

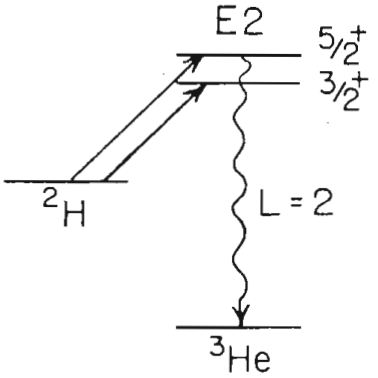

ℓ	s	j	amp
0	$1/2$	$1/2$	$^2s_{1/2}$
0	$3/2$	$3/2$	$^4s_{3/2}$
2	$1/2$	$3/2$	$^2d_{3/2}$
2	$3/2$	$1/2$	$^4d_{1/2}$
2	$3/2$	$3/2$	$^4d_{3/2}$

ℓ	s	j	amp
0	$3/2$	$3/2$	$^4s_{3/2}$
2	$1/2$	$3/2$	$^2d_{3/2}$
2	$1/2$	$5/2$	$^2d_{5/2}$
2	$3/2$	$3/2$	$^4d_{3/2}$
2	$3/2$	$5/2$	$^4d_{5/2}$
4	$3/2$	$5/2$	$^4g_{5/2}$

$^1H(\vec{d},\gamma)^3He$ reaction the s-wave M1 transitions will also be considered (see chapter 7). For the current calculations the following transition amplitudes are included

5-10 E1: $^2p_{1/2}$, $^2p_{3/2}$, $^4p_{1/2}$, $^4p_{3/2}$

E2: $^2d_{3/2}$, $^2d_{5/2}$.

The E1, $^4f_{5/2}$ and the E2, $^4g_{7/2}$ and $^4s_{3/2}$ terms are neglected on the basis of direct capture calculations given in Chapter 6 and angular momentum barrier considerations. The E2(s=3/2) transitions are also neglected based on the direct capture model calculations because of their expected small amplitudes. In addition the M1 transitions shown in Figure 5-5 are not included since as pointed out by Schiff (1937) for a pure symmetric S ground state, the M1 transitions are expected to be quite small due to orthogonality of the initial and final states. M1 strength can only arise from transitions to the D and S'-states of ^3He. Since these states represent a small component of the total wave function, the M1 strength is expected to be small. The M1 contribution to the angular distribution is mainly isotropic. Hendry and Phillip (1973) have shown that the M1 contribution in this energy region is extremely small. Thus, as a first approximation, the M1 transitions will be neglected.

Even considering only 4 E1 amplitudes and 2 E2 amplitudes, there are eleven unknowns and only 9 equations from the 4 a_k's, 4 b_k's and the normalization equation. One further assumption is necessary to analyze the data. The phases and amplitudes of the transitions are assumed to

be independent of the total angular momentum of the channel, J. The validity of this assumption is the result of the weakness of the spin-orbit interaction in this channel. As a result, 3 amplitudes remain from the combination of the 6 amplitudes listed in Equation 5-10: ^2p, ^4p and ^2d with two relative phases.

With this limited set of amplitudes, the expression for the a_k and b_k coefficients in terms of the transition amplitudes are

5-11
$$1.0 = 6(^2p)^2 + 6(^4p)^2 + 10(^2d)^2 \quad \text{Normalization}$$
$$a_1 = 20.78\ ^2p^2d \cos(\phi_{2_d} - \phi_{2_p})$$
$$a_2 = -6.0\ (^2p)^2 + 7.14\ (^2d)^2 + 2.87\ (^4p)^2$$
$$a_3 = -20.78\ ^2p^2d \cos(\phi_{2_d} - \phi_{2_p})$$
$$a_4 = -17.14\ (^2d)^2$$
$$b_1 = -6.798\ ^4p^2d \sin(\phi_{4_p} - \phi_{2_d})$$
$$b_2 = 2.046\ ^2p^4p \sin(\phi_{4_p} - \phi_{2_p})$$
$$b_3 = -4.524\ ^4p^2d \sin(\phi_{4_p} - \phi_{2_d})$$
$$b_4 = 0.0$$

Inspection of the equations for a_k's and b_k's reveals that the a_2 coefficient will be -1 if the cross section is pure E1(s=1/2). Both the E1(s=3/2) and the E2 transitions reduce the magnitude of a_2. In particular, under the assumptions given above any isotropic cross section, which can be written as (see Table 5-1)

5-12
$$a = A_0\ [1 + a_2 + a_4],$$

is solely the result of the ^4p transition. The a_k coefficients do not

have any channel spin interference terms. In addition, $a_1 = -a_3$. For the b_k's the phase and amplitude restrictions result in the elimination of many terms since $\sin(0^\circ)=0$. The sole remaining contribution to the b_k's are channel spin interference terms. The experimental values of the b_1 coefficients suggest the presence of a small M1 transition amplitude since $b_1 \neq 0$, while $b_3 \simeq 0$. Large phase differences for transitions of the same ℓ but different J could also explain this effect. However, as previously stated transitions that differ only by J are expected to have similar amplitudes and phases. Since the M1 contribution is not in the current analysis, the T-matrix analysis was repeated neglecting b_1 in order to determine the sensitivity of the solutions to this term. No significant changes in the results were noted.

The cross section and analyzing power data were fit with the transition amplitude directly rather than the fitting of a_k and b_k coefficients. This allowed for the correct propogation of the full error matrix. The results for the amplitudes and phases are given in Table 5-5. The errors and χ^2 of the amplitudes and phases reflects a renormalization of the errors in the cross section angular distribution data by χ taken from the cross section angular distribution fits. Examination of the table shows there are two solutions at each energy with the same amplitudes but different phases. The E1(s=3/2) cross section increases between 8 and 16 MeV while the E2 cross section increases slightly. The E1(s=3/2) phases do not change with energy. One solution gives 14 to 17° and the other 163 to 165°. The E2 phase is

Table 5-5. T-Matrix solutions of the amplitudes and phases from the fit to the data using E1(s=1/2), E1(s=3/2), and E2(s=1/2) terms.

E_p (MeV)	$\sigma(^2p)$ (%)	$\sigma(^4p)$ (%)	$\varphi_{4_p}-\varphi_{2_p}$ (^{o})	$\sigma(^2d)$ (%)	$\varphi_{2_d}-\varphi_{2_p}$ (^{o})	χ^2
8.0	95.7 ±1.9	3.1 ±1.4	17 ±13	1.2 ±0.6	-26 ±29	1.0
8.0	95.7 ±1.9	3.1 ±1.4	163 ±13	1.2 ±0.6	26 ±20	1.0
15.94	92.1 ±1.2	6.5 ±0.8	14 ±12	1.3 ±0.1	-2 ±26	1.0
15.94	92.1 ±1.2	6.5 ±0.8	165 ±12	1.3 ±0.1	3 ±26	1.0

either 26^{o} or -26^{o} at 8 MeV and near 0^{o} at 16 MeV with substantial errors.

The χ^2 as a function of σ(E1; s=3/2) and σ(E2; s=1/2) was mapped from 0 to 10% for E1 and 0 to 8% for E2 in 0.5% steps. The phases at each grid point were searched to produce a minimum χ^2. The χ^2 contour plot for E_p = 8 MeV is given in Figure 5-6 and for E_p = 16 MeV in Figure 5-7. The 8.0 MeV plot gives a σ(E2) in the range of 1 to 3% while the range of solutions is somewhat broader for σ(E1; s=3/2)) giving 0.5 to 5%. In the 16 MeV plot the solution is even broader with the σ(E2; s=1/2) in the range of 1 to 5% and the σ(E1; s=3/2) in the range of 2 to 8%.

Previous analyses (Skopik et al., 1979) of the transition amplitudes only included σ(E1; s=1/2) and σ(E2; s=1/2) terms. This resulted in large E2 cross sections contrary to theoretical calculations (Aufleger and Drechsel, 1981). If only s=1/2 terms are included in the analysis the restrictions on phase and amplitudes for transition matrix elements of different total momentum can be removed. In order to achieve the same quality fit to the data, the terms with the same ℓ and s but different J exhibit large differences in the amplitudes and phases. This is contrary to the expectation of a small spin-orbit interaction in this reaction. If the phases and amplitudes are restricted with the same phase assumptions as used in the current analysis, the E1(s=1/2)-E2(s=1/2) analysis can no longer fit the present data, especially a_2 and b_1. The inclusion of the σ(E1;s=3/2) amplitude in the analysis results in an E2 cross section which is only a few

Figure 5-6. Contours of reduced χ^2 as a function of E1(s=3/2) and E2(s=1/2) cross section for the polarized angular distribution measurement at E_p = 8 MeV. The two relative phases were searched at each grid point to yield the minimum χ^2. The minimum χ^2 is also given as the $\times$ in the plot.

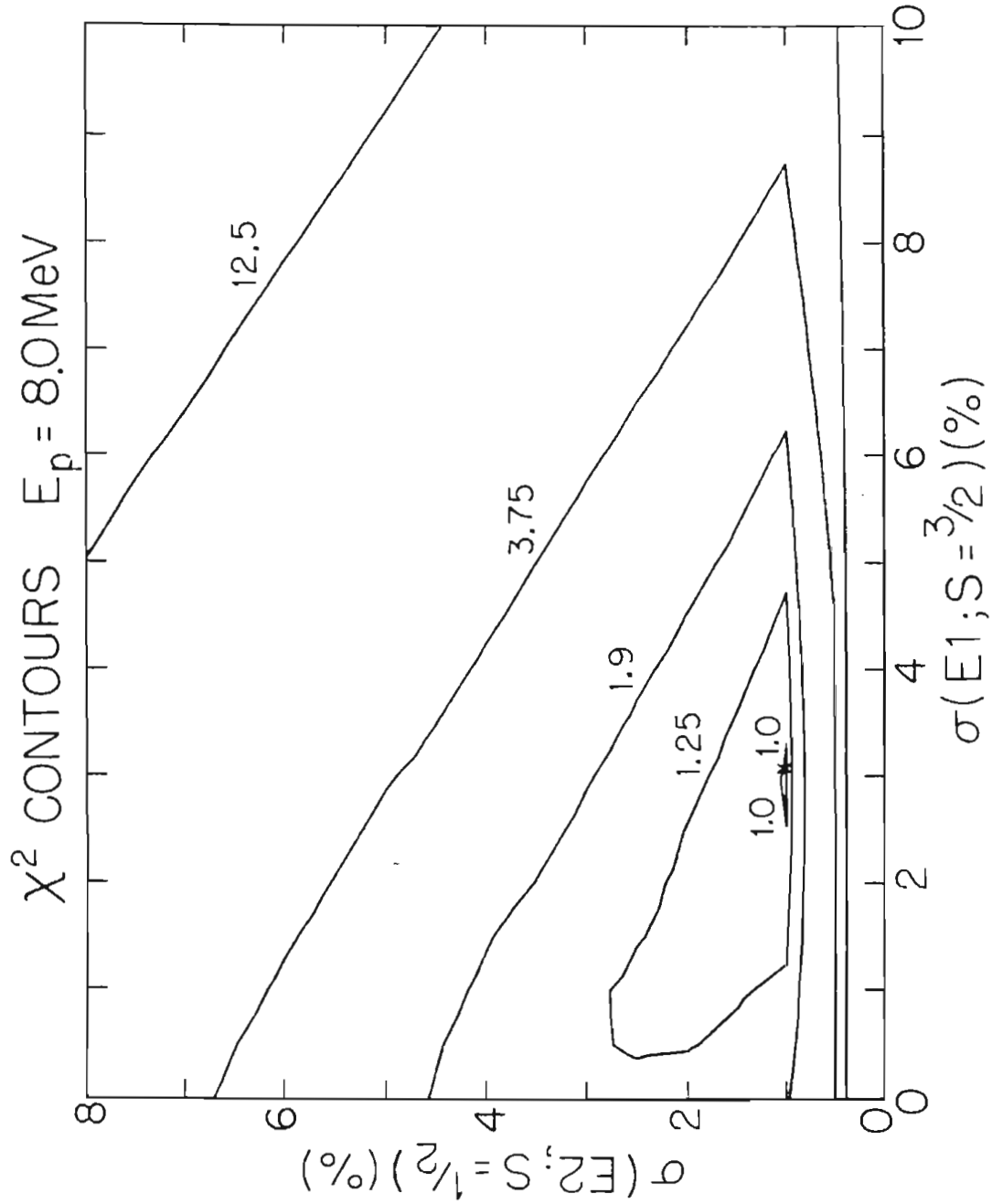
χ^2 CONTOURS E_p = 8.0 MeV
12.5
3.75
1.9
1.25
1.0
1.0
$\sigma(E1;S=3/2)$ (%)
$\sigma(E2;S=1/2)$ (%)
0
2
4
6
8
10

Figure 5-7. Contours of reduced χ^2 for E_p = 16 MeV with the same conditions as in Figure 5-6.

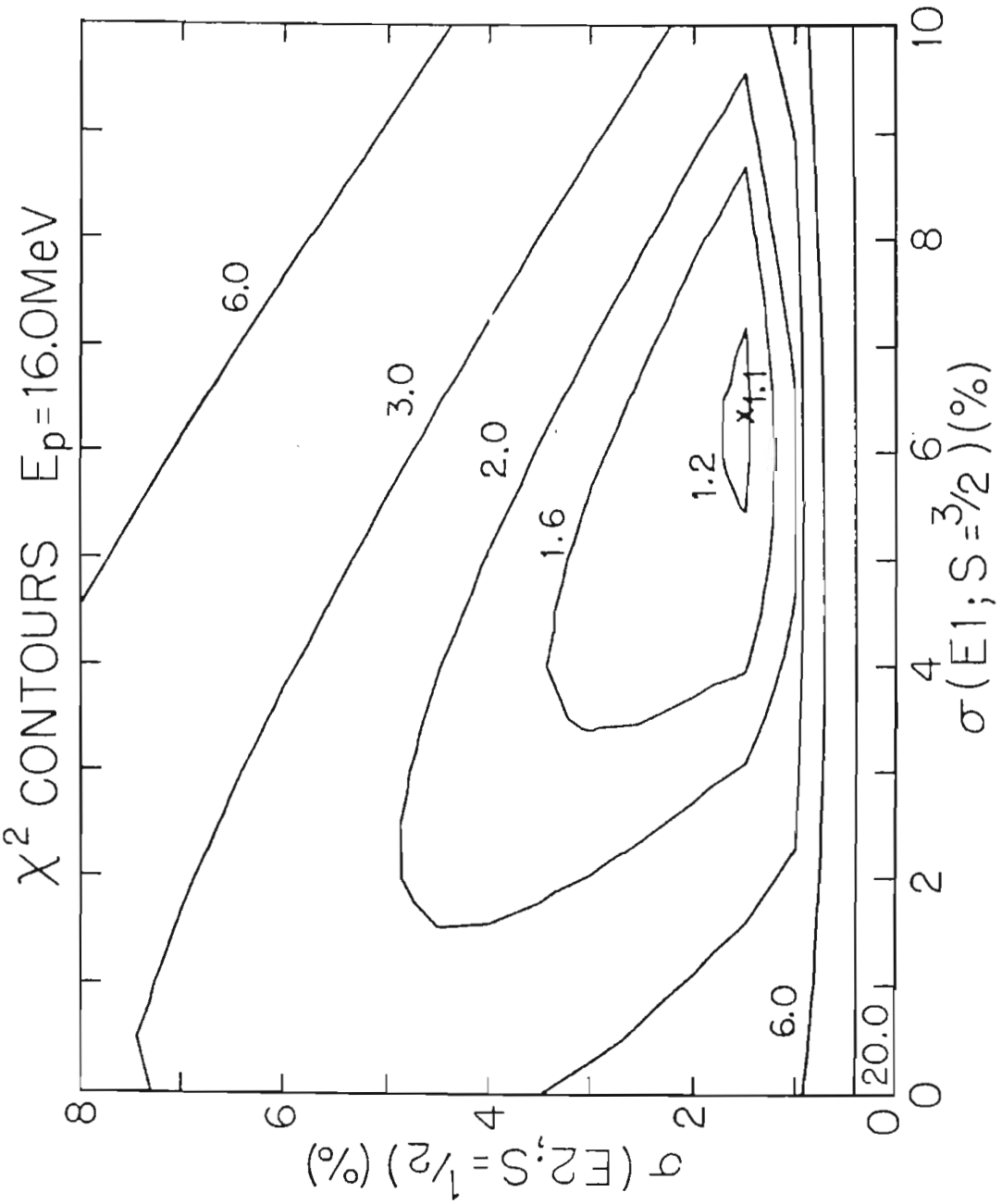
χ² CONTOURS Ep=16.0MeV
6.0
3.0
2.0
1.6
1.2
x1.1
6.0
20.0
σ(E1; S=3/2) (%)
q (E2; S=1/2) (%)
0
2
4
6
8
10

percent of the total cross section. This is within the range of theoretical values for the E2 cross section (Aufleger and Drechsel, 1981).

Considering the number of assumptions required to perform the T-matrix analysis, the question arises as to the validity of the results just discussed. The question is whether the inclusion of other small T-matrix elements or the removal of the phase assumptions will change the partial cross sections reported here. To study this problem, the T-matrix analysis procedure was repeated with the addition of other amplitudes and/or phases. First, the assumption that the phase and amplitudes of the transitions are independent of the total angular momentum was dropped for E1(s=1/2) transitions and then for E2(s=1/2) transitions. Other analyses included the separate addition of amplitudes and phases corresponding to M1, E2(s=3/2), and E3(s=1/2) transitions. In almost all cases the solutions of the analyses with additional terms gave partial cross sections for E1(s=1/2), E2(s=1/2), and E1(s=3/2) within the ranges reported above.

In general, the inclusion of additional amplitudes and phases were not statistically significant except for the inclusion of M1 transitions. Several analyses with one or more individual M1 transitions amplitudes indicates 0.1 to 1.0% M1 cross section reduces the E1(s=3/2) amplitude to the lower part of the range given in the χ^2 contour plots. The magnitudes of the b_1 coefficients are better accounted for with the inclusion of this term. Thus, while no definitive results can be given for these additional terms, their

inclusion appears to only slightly affect the original analysis. Measurement of pure tensor and pure vector polarized deuteron capture (King et al., 1983) at the same excitation energy will further restrict the T-matrix analysis and allow a better determination of the s=3/2 transitions.

6 Comparison of Theoretical and Experimental Results

6.1 Introduction

In this chapter the direct capture calculations of the $^{2}H(p,\gamma)^{3}He$ reaction will be described in detail. Since a complete three-body calculation of the $^{2}H(p,\gamma)^{3}He$ capture reaction is not yet available, we have performed an effective two-body direct model calculation using the best available wave functions for the continuum state and the ^{3}He bound state. The results of this model and the theoretical works of Barbour and Phillips (1970), Gibson and Lehman (1975), and Aufleger and Drechsel (1981) will be compared to the 90^{o} and total cross section yield curves. Also, the coefficients extracted from the angular distributions of cross section and analyzing power will be compared to the direct capture calculations. Of particular interest is the sensitivity of the a_2 coefficient to the D-state components in ^{3}He. Finally, a comparison will be made between the theoretical results and the E1(s=1/2), E2(s=1/2), and E1(s=3/2) cross sections and phases extracted at E_p = 8 MeV and 16 MeV.

6.2 Direct Capture Formalism

In direct capture the incoming particle undergoes a radiative transition from the continuum scattering state to a single-particle state in the final nucleus (Rolfs, 1973). More detailed descriptions of the direct capture model are given elsewhere (Brown, 1964; Clement

et al., 1965; and Weller and Roberson, 1980). The radial component of the electric transition matrix elements are written, in the long wavelength approximation, as

$$6\text{-}1 \qquad T^L_{\ell j} \propto (C^2 S_{\ell j})^{1/2} \langle u_{\ell',j'}(r) | q_{eff} r^L | \varphi_{\ell,j} \rangle$$

where $|u_{\ell',j'}(r)\rangle$ represents the final state wave function, $|\varphi_{\ell,j}\rangle$ is the incident continuum wave function with orbital and total angular momentum ℓ and j, respectively. $C^2 S_{\ell j}$ is the spectroscopic factor associated with the final state.

The electromagnetic transition operator is $q_{eff} r^L$, where L is the multipolarity of the interaction and q_{eff} is the kinematic effective charge. The effective charge is a scaling factor in the computation of cross sections. For electric multipoles of order L, the effective charge can be written as (Buck and Pilt, 1977):

$$6\text{-}2 \qquad q^L_{eff} = \frac{(A_2^L Z_1 + (-)^L Z_2 A_1^L)}{(A_1 + A_2)^L}$$

in which the subscripts 1 and 2 refer to the projectile and the target, respectively. For the $^2H(p,\gamma)^3He$ reaction the E1, E2 and E3 effective charges are 0.333, 0.555, and 0.259, respectively. The use of the long wavelength approximation has been shown to be valid in the energy region of this experiment and introduces less than 0.6% effects in the a_k coefficients when compared with the "exact" form of the operator obtained using Siegert's theorem (Lafferty and Cotanch, 1982). However, above E_x = 25 MeV this approximation leads to substantial error. Terms corresponding to E1, E2, E3, and M1 capture were included in the present

calculation. The $^4d_{5/2}$ transition to the D-state in ^{3}He is the only M1 contribution in this calculation and has a negligible effect. This model is not expected to correctly treat the M1 contribution (Lehman, 1983) since the deuteron is treated as a point nucleus. As a result, the mixed symmetry S'-state from which most of the M1 contribution arises (Aufleger and Drechsel, 1981) is not properly included for the M1 calculation. The calculations are performed using the direct capture code HIKARI (Kitazawa, 1980). In the spectator model assumed in this calculation the transition amplitudes going to single-particle states of different total momentum do not interfere (Weller and Roberson, 1980). As a result, the calculation is performed by separately calculating the cross section and angular distribution coefficients for the S and D-state wave functions of ^{3}He. The cross sections were then added together, and the a_k's and b_k's are combined weighted by the A_0's from the separate calculations.

6.2.1 Bound State of ^{3}He

In the direct-capture model the bound state wave function is treated as a single particle wave function of the captured particle with a point particle core. Clearly this does not properly describe the ^{3}He ground state. On the other hand, Gibson and O'Connell (1970) have shown that calculations using phenomenological bound state wave functions with the correct asymptotic normalizations and using plane waves in the incident channel can adequately describe the cross section and the angular distribution data of Belt et al. (1972).

We have used a two-body projection of the three-body wave function of the ^{3}He ground state in this work. Gibson and Lehman (1982) have generated momentum space three-body ^{3}He ground-state wave functions from Faddeev-type equations and using $^1S_0$ and $^3S_1$-$^3D_1$ separable interactions. These interactions were determined by the scattering lengths and effective charges for the singlet and triplet channels, the deuteron binding energy, quadrupole moment, and the deuteron D-state probability. The wave functions are actually calculated for ^{3}H rather than ^{3}He, but the Coulomb interaction is known to have an insignificant effect on the bound-state wave function, changing only the binding energy (Friar et al., 1982).

The two-body (n+d) wave functions needed for the present calculation were projected out of the three-body wave functions by Lehman (1983) who evaluated the overlap integral between the three-body triton wave function and the product of the deuteron wave function plus a neutron. The resulting momentum-space wave functions were then Fourier transformed using a product integration technique for Bessel functions (Lehman, Parke, and Maximon, 1981) to obtain configuration space wave functions. The S-state component of the two-body wave function includes both S and S' components of the three-body wave function. The D-state contribution enters the Gibson-Lehman calculation in the form of the D-state probability in the deuteron. The ^{3}He wave functions were obtained for deuteron D-state probabilities, $P_D(d)$, of 0, 4, and 7%. Table 6-1 gives the S-state and D-state probabilities of both the three-body ^{3}He wave function and the (p+d) two-body wave

Table 6-1. Calculated parameters of the S-state and D-state in both the three-body and projected two-body wave functions of ^{3}He for different values of $P_D(d)$. The table includes the probabilities of the wave function components as well as asymptotic parameters (defined in §1.2).

$P_D(d)$	0%	4%	7%
$P_S(^3He)$(%)	98.26	93.16	89.08
$P_{S'}(^3He)$(%)	1.74	1.74	1.74
$P_D(^3He)$(%)	0.0	5.08	9.12
P_S(n+d)(%)	43.0	43.1	43.2
P_D(n+d)(%)	0.0	0.51	0.65
P_S(n+d)(rel. %)	100.0	98.8	98.5
P_D(n+d)(rel. %)	0.0	1.2	1.5
C'_S	1.92	1.84	1.788
C'_D	0.0	0.0924	0.0685
η	0.0	0.050	0.0383
D_2	0.0	-0.236	-0.224

functions. The two-body wave function probabilities are given both as a percentage of the total wave function and as relative percentage in which the sum of the projected components is 100%. Also include in the table are the asymptotic normalizations defined in §1.2, the asymptotic normalization ratio, and the asymptotic distorted wave parameter, D_2. For comparison, the value of D_2 for ^{3}H extracted from $(\vec{d},t)$ reactions quoted in Knutson, Colby, and Bieszk (1979) is -0.275 fm^2. For ^{3}He the experimental value of D_2 ranges from -0.22 to -0.37 fm^2 (Knutson, Colby, and Hichwa, 1981; Brandan and Haeberli, 1977; Roman et al., 1977). The S-state asymptotic normalization is in good agreement with the experimental value of 1.82 ± 0.05 (Platter et al., 1977) for the wave functions with 4 to 7% $P_D(d)$. Figure 6-1 gives the radial components, $u_S(r)$ and $u_D(r)$, of the three wave functions with $P_D(d)$ of 0, 4, and 7%. The n+d two-body wave functions are $u_L(r) = r\psi_L(r)$ where the normalization is defined by:

$$\sum_L \int u_L^* \, u_L \, dr = 1. \qquad 6\text{-}3$$

The coordinate r is the separation between the single proton and the center-of-mass of the deuteron like pair in the ^{3}He nucleus. The $u_D(r)$ radial functions for $P_D(d) = 4$ and 7% are very similar. However, the S-state radial function, $u_S(r)$ has a significant increase in magnitude at larger radii with increasing D-state probability.

6.2.2 Incident Continuum Wave Function

The continuum wave function that is used to describe the incident

Figure 6-1. The two-body bound-state radial wave functions, $u_L(r)$, of ^{3}He projected from the three-body wave functions of Gibson and Lehman (1983). Both the S-state and D-state wave functions are given with the assumption of 0, 4, and 7% deuteron D-state in the calculations of three-body wave functions.

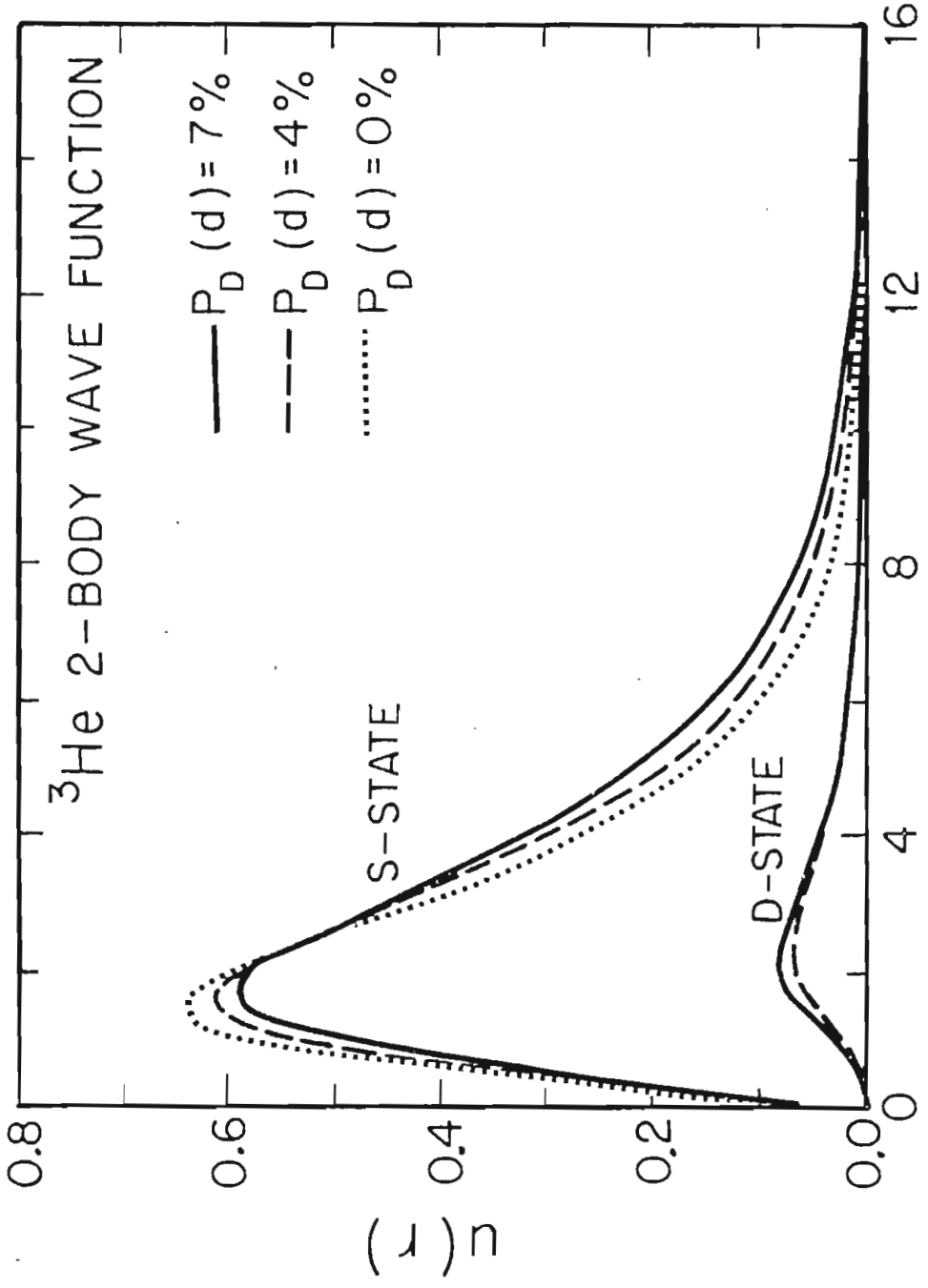
^{3}He 2-BODY WAVE FUNCTION
P_D (d) = 7%
P_D (d) = 4%
P_D (d) = 0%
S-STATE
D-STATE
u(r)
RADIUS (fm)
0.0
0.2
0.4
0.6
0.8
0
4
8
12
16

need at 12 fm

proton-deuteron channel was obtained from optical model potentials which were extracted from elastic scattering of protons (neutrons) from deuterons. Two optical model parameter sets were used. Those of Guss (1982) were obtained from 14 MeV $^2H(\vec{n},n)^2H$ scattering with the energy dependence based on global parameters for light ion scattering. The Coulomb term, added for the present case, did not change the wave functions significantly. The parameters of DeVries, Perrenoud, and Slaus (1972) were obtained by fitting E_p = 17 to 46.3 MeV angular distributions for the $^2H(p,p)^2H$ reaction. Neither optical model parameter set is based on elastic scattering of protons from deuterons in the energy region of the current measurements. The optical model potential is defined as

$$V(r) = -V_0 f(a_0,r_0,r) + i\,4\,a_d W_d \frac{d}{dr} f(a_d,r_d,r) + \left[\frac{h}{m_\pi c}\right]^2 V_{so} \frac{1}{r}\frac{d}{dr} f(a_{so},r_{so},r)\,\vec{L}\cdot\vec{S} + V_c(r_c) \qquad 6\text{-}4$$

$$f(a_k,r_k,r) = \left[1 + \exp(r - r_k A^{1/3}/a_k)\right]^{-1}$$

where V_0 is the central potential, W_d the imaginary potential, V_{so} the spin-orbit potential, and V_c the Coulomb potential for a uniform charged sphere. The central potential has a Woods-Saxon form factor, while both W_d and V_{so} have surface peaked form factors. Both sets of optical model parameters are given in Table 6-2.

Table 6-2. Optical model parameters used in the generation of the continuum wave function are taken from Guss (1982) and DeVries et al. (1972).

Parameter	Guss	DeVries
V_0 (MeV)	90.075 - 0.4871 E_p	76.9 - 0.55 E_p
r_0 (fm)	1.153	1.00
a_0 (fm)	0.454	0.402
W_d (MeV)	6.547 - 0.1005 E_p (E_p>10)	2.49 - 0.03 E_p
	4.500 + 0.1005 E_p (E_p<10)	
r_d (fm)	1.104	1.74
a_d (fm)	0.691	0.378
V_{so} (MeV)	2.408 - 0.0331 E_p	-
r_{so} (fm)	1.049	
a_{so} (fm)	1.119	
r_c (fm)	1.3	1.3

6.3 Other Theoretical Work

A great deal of theoretical effort has gone into the calculation of photonuclear reactions in the mass three system. Primarily, the calculations have been concerned with the total and 90^{o} cross sections. While several authors have calculated angular distributions for a direct comparison with experimental results no calculations of the energy dependence of the angular distribution coefficients, a_k and b_k, have yet been published.

Three of the more recent calculations will be compared to our experimental cross sections: Aufleger and Drechsel (1981), Gibson and Lehman (1975), and Barbour and Phillips (1970). Within the context of their model, Barbour and Phillips (1970) performed an "exact" three-body calculation which used separable s-wave spin-dependent charge-independent interactions that were determined from experimental two-nucleon effective range parameters. Their calculations demonstrated the importance of treating the continuum p+d state exactly. The inclusion of final state interactions produces a 25% larger total cross section than a calculation neglecting these effects. The inclusion of the mixed-symmetry S' component as well as the D-state component was found to have little effect (<10%) on the cross sections. The only electromagnetic multipole included was the dominant E1 interaction.

Gibson and Lehman (1975) also performed an "exact" calculation using separable $^1S_0$ and $^3S_1$-$^3D_1$ interactions which were determined from

the two-nucleon effective ranges and scattering lengths as well as the deuteron binding energy. Again only E1 transitions were considered. The 90° yield curve for their calculation is much different from the calculation of Barbour and Phillips even though they used essentially the same formalism. They attribute the lower peak cross section to differences in the ground state wave function. In particular, Barbour and Phillips used spectator functions in the generation of the bound state that had a greater trinucleon charge radius than the Gibson and Lehman wave functions. Barbour and Phillips wave functions for ^{3}He have an rms charge radius of 1.87 fm and C_S^1 of 1.81 fm while Gibson and Lehman have a charge radius of 1.77 fm and C_S^1 of 1.54 fm. The experimentally determined charge radius is 1.87 $\pm$ 0.05 fm (Collard et al., 1965) and C_S^1 is 1.82 $\pm$ 0.05 fm (Platter et al., 1977). Finally, they determined the main contribution to the final state interaction results from the off-shell singlet rescattering. This corresponds to the absorption of an E1 photon then an immediate disintegration into an intermediate state composed of a singlet correlated pair plus nucleon which then rescatters into the deuteron plus a on-shell proton state.

The calculations of Aufleger and Drechsel (1981) (see §1.2) used realistic bound-state wave functions obtained with the Reid soft-core potential but neglected final-state interactions. These calculations have substantially lower cross sections. Included in the calculation are E1, E2, and M1 transitions. They find a smooth energy dependence with little D-state effect unlike the significant D-state related structure in the cross section given by Craver et al. (1977). The

difference is attributed by Aufleger and Drechsel to numerical problems in the previous calculation. In addition they present a normalized angular distribution at E_x = 15.3 MeV which is shown in Figure 5-2. The agreement with the experimental angular distribution is generally good, but the a_1 coefficient is significantly greater than the experimental value. The large a_1 may indicate the calculated M1 cross section is too large.

Other works in which an angular distribution is calculated are given in §1.2. The calculations of Gibson and O'Connell, 1970 used plane waves in the final state and S, S' and D-states in ^{3}He that were based on a proton bound to a deuteron by a zero range force that correctly described the asymptotic behavior and binding energies of the ^{3}He bound state and were the eigenfunctions of the same Hamiltonian. The wave functions are fit to the experimental asymptotic normalizations. The electromagnetic operator was treated as a full plane wave form and not the usual multipole expansion. These calculations give little contribution from spin-flip or D-state transitions. The agreement with the angular distribution of Belt et al. (1971) at 15.3 MeV excitation energy is better than that based on the calculations of Aufleger and Drechsel (1981) (shown in Figure 5-2).

6.4 Total and 90^o Cross Sections

Both the σ_T and $\sigma(90^o)$ cross sections are very sensitive to the wave functions and model parameters in the direct capture calculations.

The spectroscopic factor assuming the captured proton is in a single particle state is three. The spectroscopic factor was weighted by the portion of the total ^{3}He wave function in the p+d projected component from the Faddeev-type wave functions given in Table 6-1. Figure 6-2 shows the total cross section with the direct capture calculations using the continuum wave functions generated by the optical model derived by Guss (1982). Calculations using three bound state wave functions are shown in the figure. They included either 0, 4, or 7% deuteron D-state probability, $P_D(d)$, assumed in the calculation of the ^{3}He wave function. The calculated cross sections are smaller than experimental results. However, with $P_D(d)$ of 7% the calculated cross section is within 10% of the peak experimental value. The change in cross section with the inclusion of D-state in the ^{3}He wave function is not the direct result of the D-state transitions but is the effect of the radial increase of the S-state component of ^{3}He as can be seen in Figure 6-1. The peak cross section of the calculation is 2 MeV lower in excitation energy than the experimental peak.

The difference in magnitude of the direct capture calculation compared to the experimental data is not of great concern since this is highly dependent on the spectroscopic factor and effective charge. Dynamic and many-body contributions to the effective charge could significantly effect the calculations. Clear evidence of the inadequacies of the effective charge in this model is found in the study of the complimentary ^{2}H(n,γ)^{3}He reaction (Mitev et al., 1982). The fore-aft asymmetry measurements were expected to be 1/5 the ^{2}H(p,γ)^{3}He

Figure 6-2. Total cross sections for the $^{2}H(p,\gamma)^{3}He$ reaction expressed in terms of the (γ,p) cross sections using the principle of detailed balance. The dotted, dashed, and solid lines are direct capture calculations described in the text with 0, 4, and 7% $P_D(d)$ assumed in the calculation of the ^{3}He bound state, respectively. The calculations include E1, E2 and E3 multipolarities. These calculations use the optical model parameters of Guss (1982) to generate the continuum wave function. The symbols for the data are the same as used in Figure 4-2.

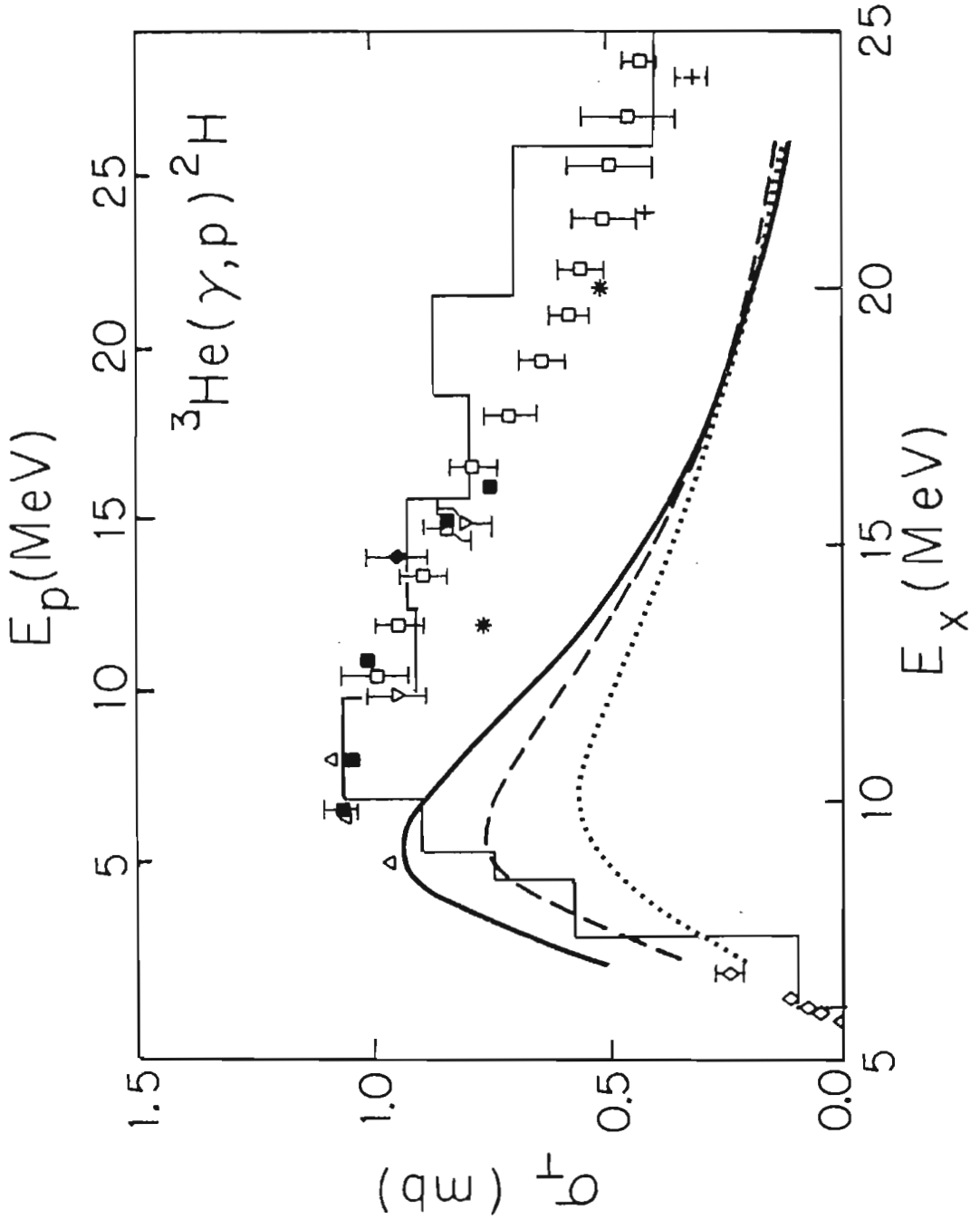
$^3He(\gamma,p)^2H$
E_p(MeV)
E_x(MeV)
σ_T (mb)
1.5
1.0
0.5
0.0
5
10
15
20
25

reaction results due to the 1/5 reduction in the $\sigma(E2)$ kinematic effective charge compared to (p,γ). Contrary to the reduction predicted in the direct capture calculation, the (p,γ) and (n,γ) asymmetries are essentially equal. In addition, small changes in the optical model parameters can make substantial effects in the cross sections. The direct calculations using wave functions generated from DeVries et al. (1972) optical model parameters have a peak energy in agreement with the experimental data. In addition the energy dependence of the calculation is similar to the experimental results, but still have a 20% lower cross section than our data. In the energy region (E_p>17 MeV) where the optical model parameters from DeVries were fit to elastic data the fit was generally better than the calculations using the optical model parameters of Guss.

The $\sigma(90^o)$ calculations exhibit behavior which is similar to that of the calculated total cross sections. Figure 6-3 compares the calculations using the optical model parameter set from Guss (1982) with the experimental results. The calculations using the Guss parameters predicted a D-state contribution to the 90^o cross section of about 0.35 μb/sr at an excitation energy of 11 MeV, a value too small to be observed in A_0. This result is similar to that of Aufleger and Drechsel (1981) but quite different from that of Craver et al. (1977) (which gave 8 μb/sr). Again, the energy dependence of the calculations using the DeVries optical model parameters follows the experimental data more closely than calculations using the Guss parameters. This is seen in Figure 6-4.

Figure 6-3. Differential cross sections at $\theta_{cm} = 90^{o}$ for (p,γ) measurements. The cross sections are expressed in terms of the (γ,p) cross sections. The dotted line is a direct capture calculation with a bound state of ^{3}He generated using a $P_D(d)$ of 0%, the dashed line using 4% $P_D(d)$, and the solid line using 7% $P_D(d)$. Again the optical model parameters of Guss are used. The symbols for the data are given in Figure 4-3.

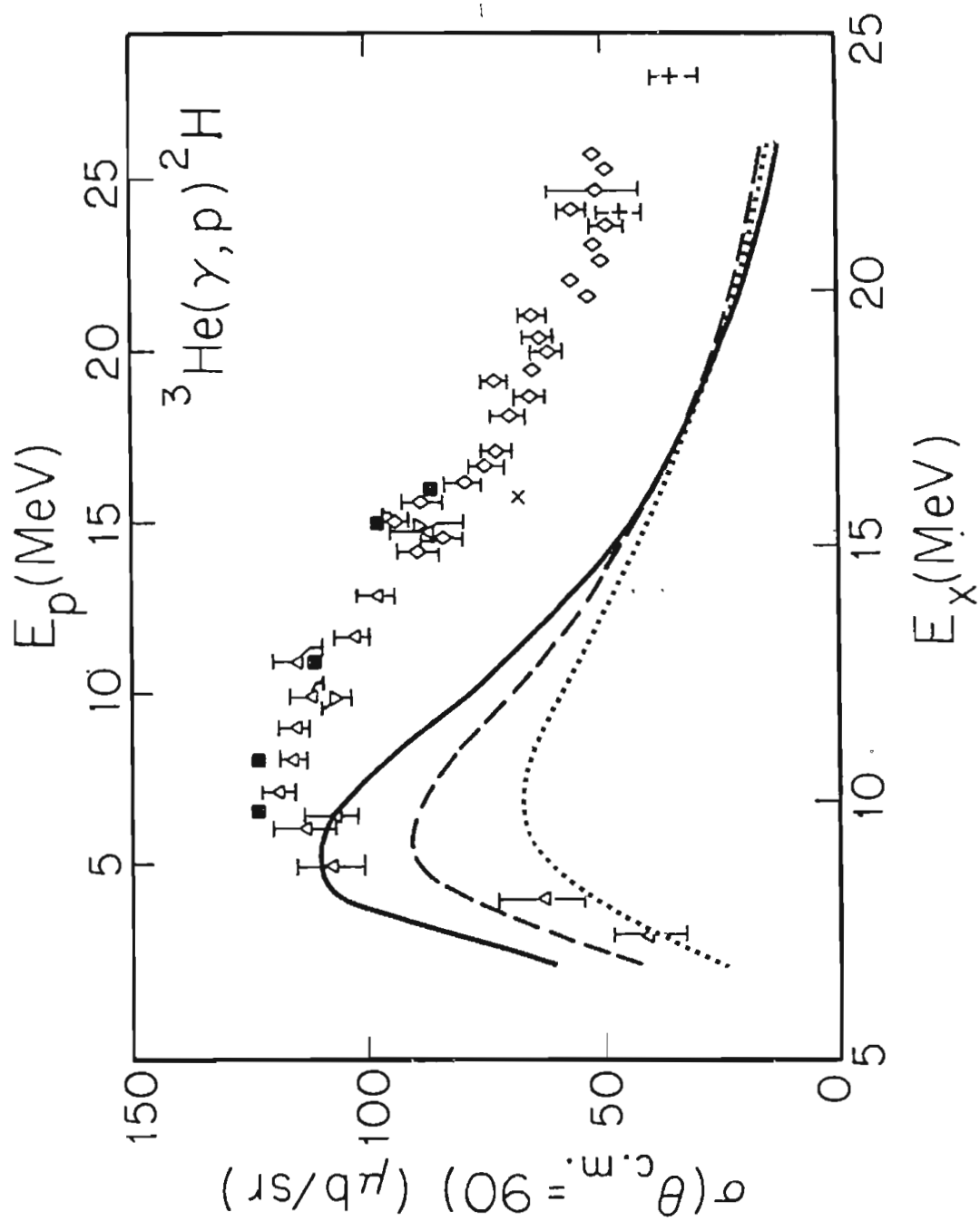
$^3He(\gamma,p)^2H$
E_p(MeV)
E_x(MeV)
$\sigma(\theta_{c.m.}=90)$ (μb/sr)
0
50
100
150
5
10
15
20
25

Figure 6-4. The 90° yield curve data given in Figure 6-3 with the calculations using the optical model of DeVries et al. (1972) to generate the continuum wave function. The symbols and curves are of the same notation as in Figure 6-3.

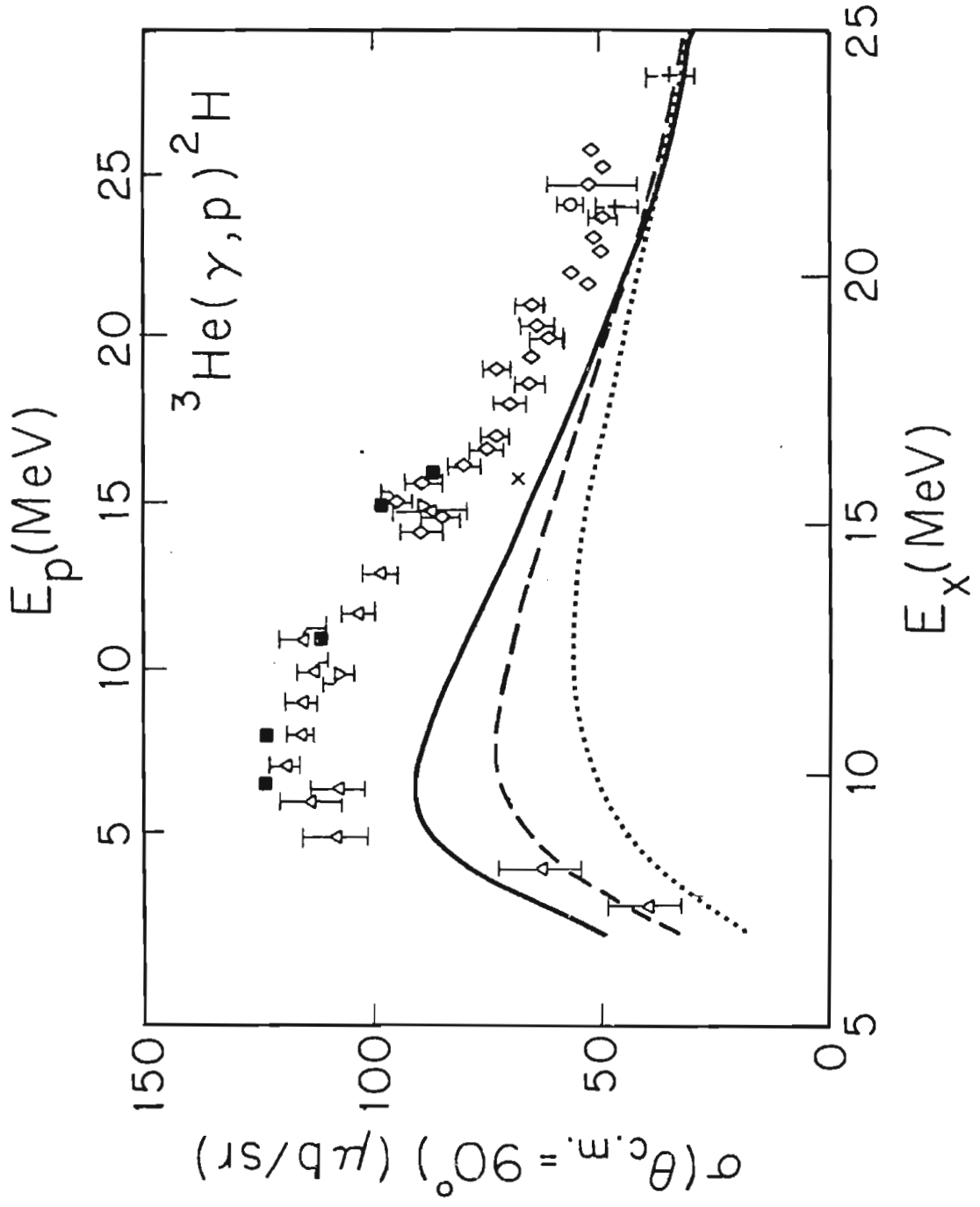
$^3He(\gamma,p)^2H$
E_p(MeV)
E_x(MeV)
$\sigma(\theta_{c.m.}=90^\circ)$ (μb/sr)
0
50
100
150
5
10
15
20
25

For comparison Figure 6-5 gives the 90^{o} yield curve calculations from Barbour and Phillips (1970), Gibson and Lehman (1975) and Aufleger and Drechsel (1981). Barbour and Phillips have achieved good agreement with the cross section by explicitly including final-state interactions which enhance the cross section by 20-25%, Gibson and Lehman's "exact" treatment of the separable S--wave potential for E1 transitions is only about 20% smaller than the peak experimental cross section. The lower peak cross section results from Gibson and Lehman's use of bound-state spectator functions that have smaller trinucleon charge radii. Finally the calculation using realistic bound state wave functions (Aufleger and Drechsel, 1981) with E1, E2, and M1 transitions is 40% lower than our experimental results. The lower cross sections is, in part, the result of neglect of the final state interactions in this calculation.

6.5 Angular Distributions

In Figure 6-6 the angular distribution coefficients of cross section and analyzing power are given for the present work as well as those from Belt *et al.* (1971), Skopik *et al.* (1979), Skopik *et al.* (1983), Matthews *et al.* (1974), and Engelbert and Clausnitzer (1981). The results are generally consistent except for the a_2 and a_4 coefficients from the previous TUNL data (Skopik *et al.*, 1979). The discrepancy in these measurements is probably due to uncorrected background effects resulting from the use of a CD_2 target. Included in the figure are three calculations. The dashed curve is a direct capture

Figure 6-5. The 90^{o} yield curve data with the theoretical calculations of Barbour and Phillips (1970) (solid line), Gibson and Lehman (1975) (dotted line), and Aufleger and Drechsel (1981) (dashed line). The symbols are of the same notation as Figure 6-3.

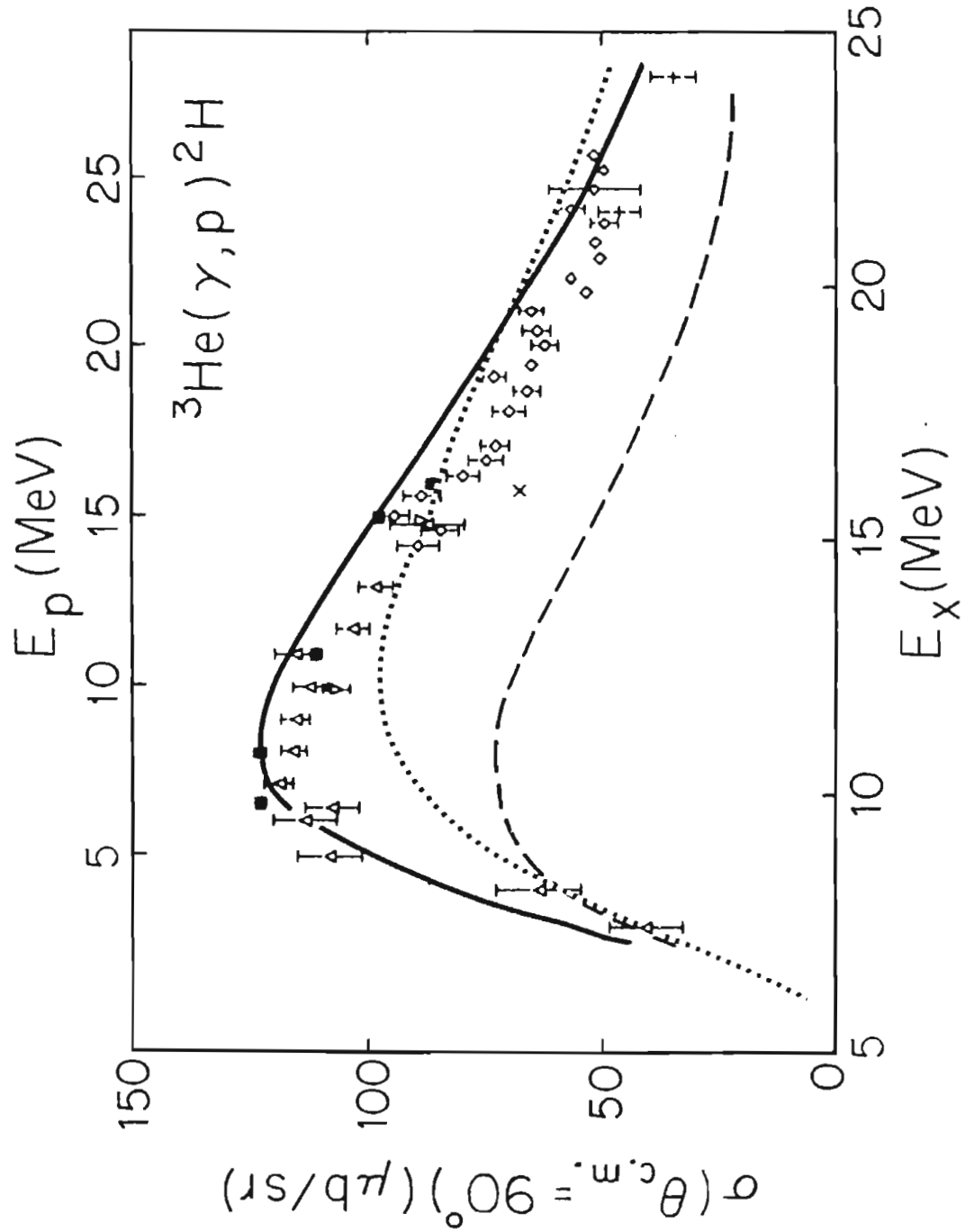
$^3He(\gamma,p)^2H$
E_p (MeV)
E_x (MeV)
$\sigma(\theta_{c.m.}=90^\circ)$ (μb/sr)
150
100
50
0
5
10
15
20
25

Figure 6-6. The angular distribution coefficients for cross section and analyzing power in the $^{2}H(p,\gamma)^{3}He$ reaction and the direct model calculations using the Guss parameters. The dashed curve is the 0% $P_D(d)$ calculation and the solid curve is a calculation using 7% $P_D(d)$. The dot-dashed curve is a calculation with 7% $P_D(d)$ and with the $\sigma(E1)$ renormalized to fit the total cross section data. The identification of the data is as follows:

- ■ Present Results
- ○ Present Results (constrained)
- △ TUNL (1979)
- ▽ Belt et al.
- ◆ Skopik et al.
- × Mathews et al.
- ✱ Engelbert et al.

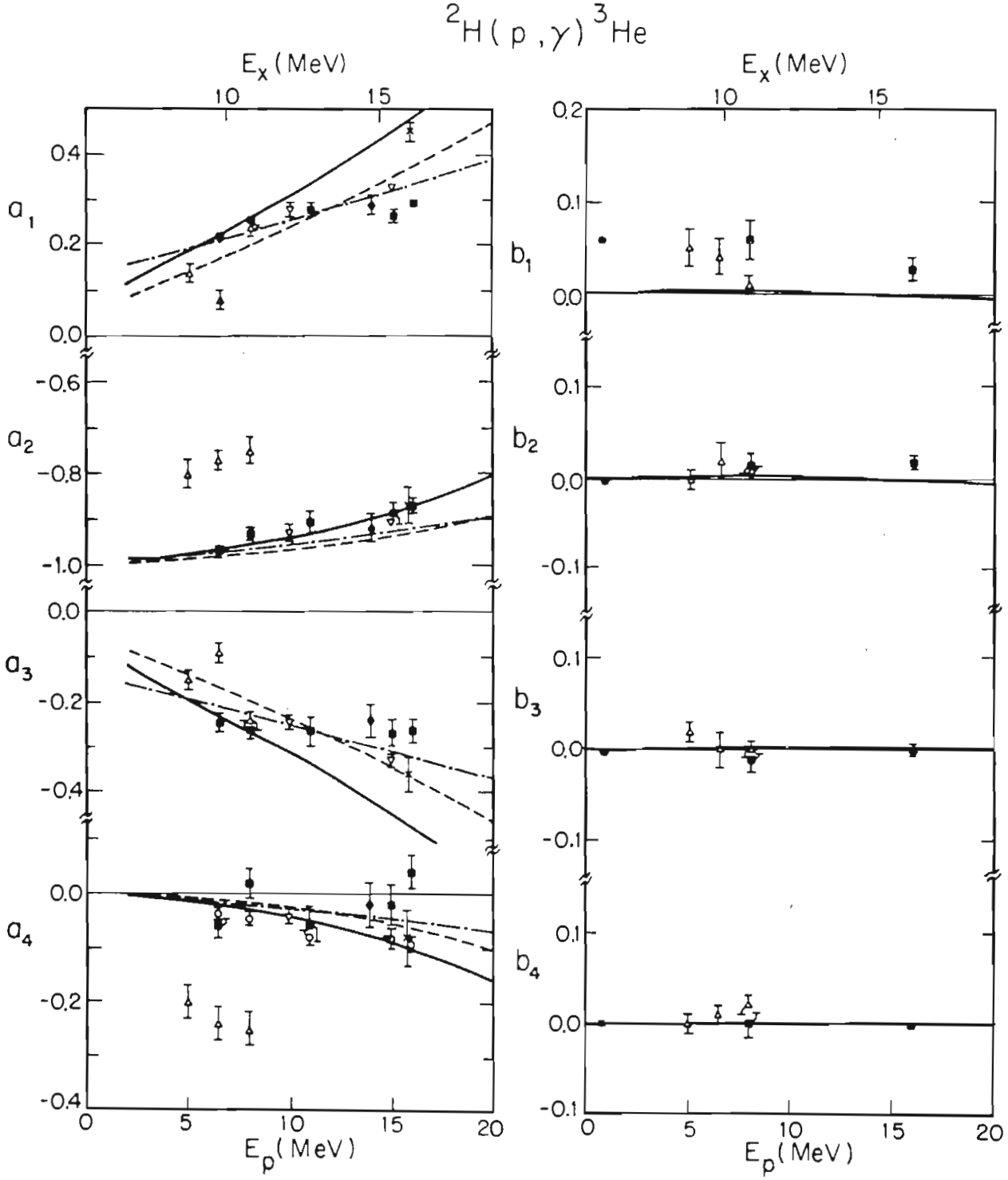
$^2H(p,\gamma)^3He$
E_x (MeV)
E_x (MeV)
a_1
a_2
a_3
a_4
b_1
b_2
b_3
b_4
E_p (MeV)
E_p (MeV)

calculation using the Guss parameters with 0% $P_D(d)$ in the bound state calculation of ^3He and the solid curve with 7% $P_D(d)$.

All of the a_k coefficients show a sensitivity to the inclusion of the D-state into ^3He. An examination of the origins of this sensitivity shows that only the a_2 coefficient is effected by transitions to the D-state component of the ground state in ^3He. For the other coefficients, the changes are due primarily to an enhancement of the E2 cross section which resulted from the change in the radial dependence of $u_S(r)$ (see Figure 6-1). In examining the coefficients we find the 0% $P_D(d)$ a_1 calculation is in better agreement with the data than the 7% $P_D(d)$ solution. On the other hand, the experimental a_3 coefficient shows little energy dependence unlike any of the calculations.

The a_4 coefficients which are due to E2 or higher multipolarities, tend to be small and difficult to measure. As seen in Figure 6-6, the experimental a_4 coefficients from the present work show fluctuations comparable with the statistical errors. Another manifestation of this same effect can be observed in Figure 5-1 which shows the angular distributions of cross section. There it is seen that the angular range of 30° to 150° is insufficient to fix the cross sections near 0° and 180°. The angular distributions measured by Belt et al. (1971) (see Figure 5-2) over a more extensive angular range demonstrate that the cross sections near 0° and 180° are, in fact, quite small. Using this information, the present angular distributions were refitted with the constraints that the cross sections were near zero at the end points. The only statistically significant changes was in the a_4 coefficients.

The constrained a_4 coefficients are shown as open circles in Figure 6-6 and show a more systematic energy dependence in agreement with the other experimental results.

One of the primary results of this experiment is the discovery of the sensitivity of the a_2 coefficients to the D-state in ^{3}He. As seen in equation 5-11 a pure s=1/2 E1 transition would give -1 for a_2. As E2 and E1(s=3/2) transition strength enter the calculations, the value of a_2 is reduced. In Figure 6-7 three calculation of a_2 using ^{3}He wave functions which assumed $P_D(d)$ of 0, 4, and 7% are given. The agreement with the experimental results is good for the generally accepted range of $P_D(d)$ of 4 to 7%. This represents 5 to 9% D-state probability in the three-body ^{3}He wave function. Use of the optical model wave functions increases the D-state effect on a_2 by a factor of 3 compared to direct calculations using plane waves. Plane waves have been used in the calculations of Aufleger and Drechsel (1981) and Craver et al. (1977).

It is clearly evident that the direct model calculations do not correctly predict the magnitude and energy dependence of the total and 90° cross sections, nor the energy dependence of the a_1 and a_3 coefficients. To investigate the causes of this energy dependence problem, the E1 effective charge was renormalized in order to fit the experimental total cross sections. This renormalization was carried out in approximately 1 MeV steps from E_x = 2 to 20 MeV. These renormalized direct capture calculations give good agreement with the 90° cross sections. The resulting a_k coefficients are given as the dot-dashed line in Figure 6-6. The energy dependence of a_1, a_3, and a_4 using 7%

Figure 6-7. The a_2 angular distribution coefficients are shown as a function of proton bombarding and excitation energies. Data from the present work, Skopik et al. (1983), Belt et al. (1971), and Matthews et al. (1974) are shown with statistical error bars. The curves are the results of the direct capture calculations including E1, E2, and E3 radiation and using Lehman and Gibson's ^{3}He wave functions as described in the text. Curves 1, 2, and 3 assume 7, 4, and 0% deuteron D-state probability respectively in the calculation of the ^{3}He bound state.

$P_D(d)$ is now in much better agreement with the data. Although the agreement with the experimental a_2 coefficients is somewhat worse, the 0% $P_D(d)$ solution also shifts by a similar amount. The inclusion of D-state in the calculation still makes a significant improvement in comparison with the a_2 coefficients extracted from the data. The discrepancy in the energy dependence of the angular distribution coefficients is primarily due to insufficient $\sigma(E1)$ in the direct model calculation. The direct E2 cross section appears to be correctly described in the model.

The E3 contribution to the direct capture calculation of the angular distribution is small but finite. Even though it represents only a 10^{-5} part of the total cross section, the E1-E3 interference effects on both a_2 and a_4 are significant. The effect on a_2 is a decrease of 0.01 to 0.02 in the energy region studied and a_4 is enhanced by approximately 0.01.

The fore-aft asymmetries are shown in Figure 6-8 again with 0 and 7% D-state calculations. The calculations bracket the experimental results. The energy dependence of the fore-aft asymmetries is better accounted for in the renormalized direct model calculations (dot-dashed line).

The plots of the cross section weighted analyzing powers show that b_2, b_3, and b_4 are, within error, essentially zero. The b_1 coefficient while quite small shows a distinct trend of increasing with decreasing beam energy. This energy dependence is characteristic of the M1

Figure 6-8. The fore-aft asymmetries given in Figure 5-3 with the direct calculations described in the text. The calculation represented by the dashed line assumed 0% deuteron D-state probability while the solid line curve assumed 7% $P_D(d)$ in the calculation of the ^{3}He bound state. As in Figure 6-6 the dot-dashed curve results from a renormalization of $\sigma(E1)$. The optical model parameters of Guss (1982) were used.

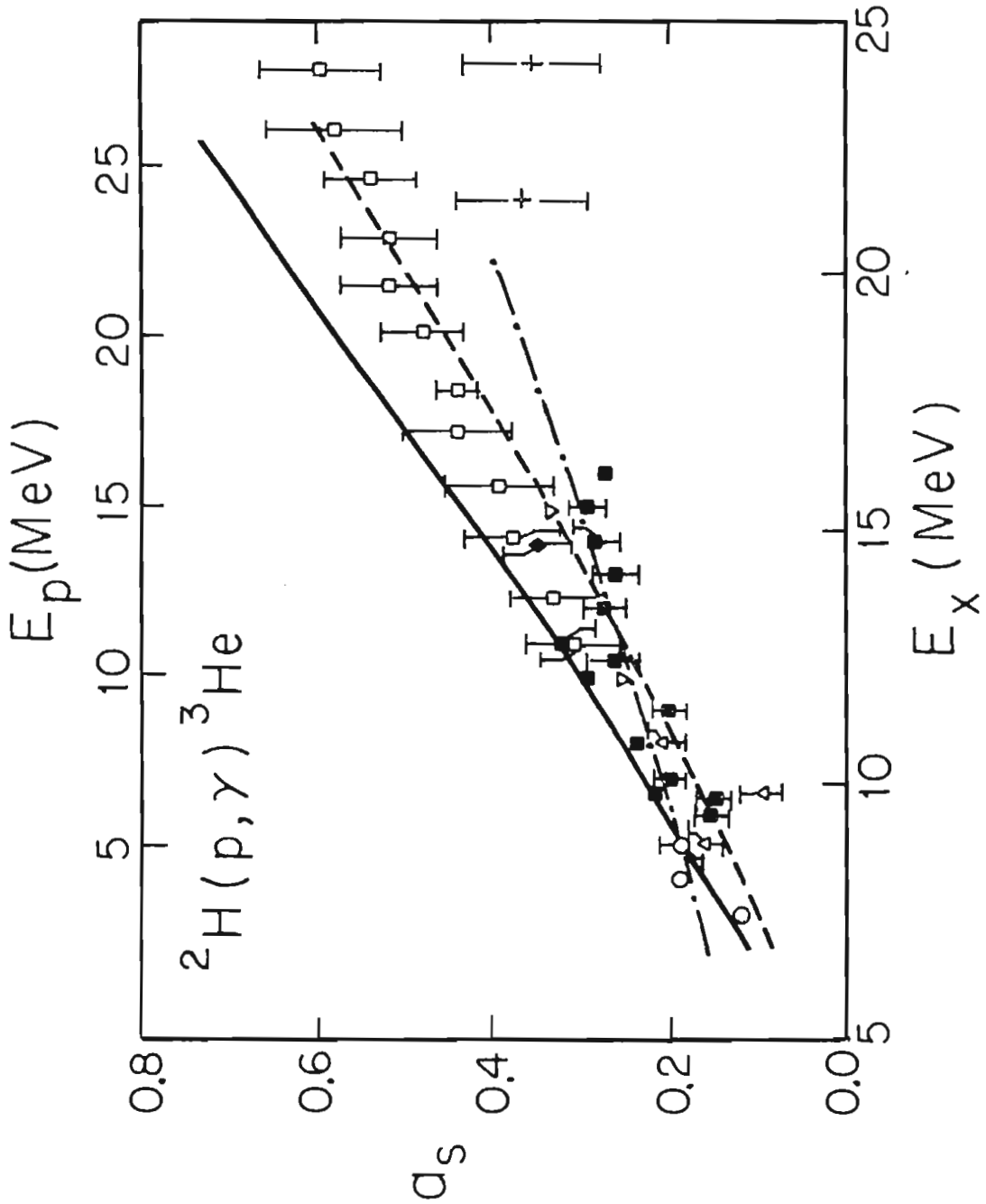
E_p(MeV)
E_x (MeV)
a_s
$^2H(p,\gamma)^3He$
5
10
15
20
25
0.0
0.2
0.4
0.6
0.8

multipole a few hundred keV excitation energy above threshold and may be an indication of M1 strength in the $^{2}H(p,\gamma)^{3}He$ reaction. Further evidence of M1 radiation is obtained from the low energy deuteron capture as discussed in the chapter 7. The direct capture calculations give essentially zero for all of the b_k's. However, a proper treatment of the M1 strength may account for the finite b_1 coefficients.

6.6 Partial Cross Sections

In §5.6 the partial cross sections for E1, E2, and E1(s=3/2) were extracted from the polarized angular distributions. Table 6-3 contains the direct capture prediction of these partial cross sections for comparison to the data (see Table 5-5). The cross sections are given for $P_D(d)$ of 0, 4, and 7% in the ^{3}He calculations. All phases are expressed relative to the E1(s=1/2) transitions.

The differences in the direct model calculations of cross section and phases using a $P_D(d)$ of 4 or 7% are not distinguishable by the current experimental results. At 8 MeV for both calculations, the quartet spin E1 strength was a factor of four smaller than that of the T-matrix analysis, 0.7% compared to 3.1%. The E2 cross section was in good agreement with the data. Two phase solutions were found in the T-matrix analysis at both energies. Solution 1 of Table 5-5 agrees quite well with the direct model calculations of the E1(s=3/2) phase but not with the E2 relative phase. On the other hand, solution 2 agrees with the calculated E2 phase but not with the E1(s=3/2) phase. At

Table 6-3. Partial cross sections from the direct capture calculations for E_p = 8 MeV and 16 MeV. All cross sections are given as a percentage of the total cross section and all phases are given relative to the E1(s=1/2) transitions.

E_p (MeV)	8.0			16.0		
P_D(d) (%)	0	4	7	0	4	7
σ(E1; s=1/2)	99.3	98.3	98.2	97.2	94.8	93.9
σ(E2; s=1/2)	0.65	0.9	1.1	2.8	3.5	4.4
φ_{E2} (^{o})	23	22	20	30	28	28
σ(E3; s=1/2)	0.001	0.001	0.001	0.004	0.005	0.008
φ_{E3} (^{o})	23	23	24	32	31	31
σ(E1; s=3/2)	0.0	0.74	0.66	0.0	1.4	1.5
$\varphi_{E1'}$ (^{o})	-	26	29	-	28	28
σ(M1; s=3/2)	0.0	0.02	0.02	0.0	0.16	0.18
φ_{M1} (^{o})	-	4	4	-	4	4

16 MeV the direct model calculation cross section is again four times smaller than the extracted $\sigma(E1;s=3/2)$ and the extracted $\sigma(E2)$ is also smaller than the calculated cross section. Solution 1 again agrees with the E1(s=3/2) phase but the E2 phase now differs by $\sim 30^{o}$ for both solutions It is worth noting that the phases extracted in the T-matrix analysis have fairly large errors. The calculated cross sections are within the range of solutions found in the analysis in the mapping of χ^2 solutions versus $\sigma(E2)$ and $\sigma(E1;s=3/2)$ (see Figures 5-6 and 5-7).

7 DEUTERON CAPTURE BY PROTONS AT E_x = 6 MeV in ^{3}He

7.1 Overview

Use of the $^1H(\vec{d},\gamma)^3He$ reaction to compliment the $^2H(\vec{p},\gamma)^3He$ reaction enables a more thorough analysis of the transition matrix elements that contribute to this reaction. Although the angular distributions are identical for both reactions (except for an inversion in the center-of-mass of $\theta_d = 180^o - \theta_p$), the vector analyzing powers change as a result of spin 1 for the deuterons in contrast to the spin 1/2 protons. In addition, with a deuteron beam, one can also measure tensor analyzing powers. As will be seen in this chapter, the additional information provides a sensitive tool for determining the s=3/2 quartet channel spin transitions as well as the M1 partial cross section. The measurement of a vector polarized angular distribution at E_x = 6 MeV in ^{3}He will be presented along with the complimentary vector polarized proton capture of Engelbert and Clausnitzer (1981). These data should be sensitive to small M1 admixtures of the order of a few percent. A full three-body calculation which is not available at this time could be compared directly with these observables. Alternatively, one could hope to extract an M1 strength directly from the data using the T-matrix formalism as described in chapter 5. Unfortunately, due to the large number of possible contributing amplitudes, a completely model independent extraction of the M1 strength is not possible. We have, instead, attempted to estimate the M1 strength by performing an analysis based on what we believe are a reasonable set of simplifying

assumptions.

The magnetic dipole transition operator is given as:

$$7\text{-}1 \qquad \mu = \frac{1}{2}(\mu_p + \mu_n) \sum_{k=1}^{3} \sigma^{(k)} + \frac{1}{2}(\mu_p - \mu_n) \sum_{k=1}^{3} \tau_3^{(k)} \sigma^{(k)}$$

where $\sigma^{(k)}$, and $\tau_3^{(k)}$ are the spin and isospin for the three particles, respectively, μ is the individual nucleon magnetic moment. The symmetric S-state is an eigenstate of the magnetic dipole transition operator. Since the operator does not change the spin in the transition, the continuum state must have the same spin and isospin as the S-state and is therefore orthogonal to it. The M1 transition to the pure symmetric S-state is therefore expected to be small due to the orthogonality. The mixed-symmetry, S'-state and the D-state admixtures in the ground state of ^{3}He are known to be important in thermal n-d capture (M1). Furthermore, meson-exchange corrections have been shown to be essential in order to calculate the thermal n-d capture cross section (Hadjimichael, 1973; Torre and Gouland, 1983). Since M1 strength at threshold is so sensitive to meson-exchange effects and the details of the three-body wave function, M1 strength above threshold may also reflect details of these quantities. The cross section just above threshold is expected to be a mixture of M1 and E1 radiation. Therefore, the analyzing powers which arise from interference effects should be sensitive to the presence of these two radiations.

7.2 Measurements and Results for the $^1H(\vec{d},\gamma)^3He$ Reaction

To study M1 and s=3/2 amplitudes, the transition matrix analysis requires the combined data of angular distributions of proton analyzing power, deuteron vector analyzing power, and cross section. Our measurements at a center-of-target beam energy of 1.62 MeV (E_x = 6.0 MeV) were made to take advantage of the high precision measurements of the $^2H(\vec{p},\gamma)^3He$ reaction at E_p = 0.77 MeV (Engelbert and Clausnitzer, 1981). Using a vector polarized deuteron beam, analyzing powers were obtained at five angles between 50^o and 135^o relative to the beam axis. The experimental apparatus is identical to the $^2H(p,\gamma)^3He$ measurements. The gas target arrangement used here gave an energy spread of less than 200 keV for the events observed at the extreme angles where the target thickness is greatest. The deuteron analyzing powers were measured using the two detector technique described in §5.2.

The $^2H(\vec{p},\gamma)^3He$ data reported in King et al. (1983) was measured at the University of Giessen. Analyzing powers were obtained at 13 angles over the range of 10^o to 150^o with a mean statistical error of 10^{-2}. The target consisted of a 20 Torr gas cell which was 2 cm long. The energy spread in the gas was 80 keV.

In the case of the $^2H(p,\gamma)^3He$ reaction the unpolarized differential cross section is given by Eqn. 5-1 while the analyzing powers were expanded in terms of the associated Legendre polynomials using Eqn. 5-5. In the case of the $^1H(d,\gamma)^3He$ reaction, we must

consider the cross section for a reaction initiated by vector polarized particles having spin 1. This cross section can be written as

$$7\text{-}2 \qquad \sigma_d(\theta,\phi) = \sigma_d(\theta)\left[1 + \frac{3}{2}\, p\, A_d(\theta)\right].$$

In this case we make the same expansion for the unpolarized cross section in terms of Legendre polynomials

$$7\text{-}3 \qquad \sigma_d(\theta) = A_0\left[1 + \sum a_k P_k(\cos\theta)\right].$$

The deuteron analyzing power $A_d(\theta)$ is given by

$$7\text{-}4 \qquad A_d(\theta) = \frac{2}{3}\,\frac{1}{P}\,\frac{N_+ - N_-}{N_+ + N_-},$$

where $N_+(N_-)$ are the number of counts observed when the beam is spin up(down) and P is the beam polarization. This is the same as before except for the 2/3 factor. The product of the (unpolarized) cross section and the deuteron analyzing power $A_d(\theta)$ can now be expanded in terms of associated Legendre polynomials as:

$$7\text{-}5 \qquad \frac{3}{2}\,\sigma_d(\theta)\,A_d(\theta) = A_0\left[\sum b_k\, P_k^1(\cos\theta)\right].$$

The unpolarized cross section data used in the present analysis of both the $^1H(\vec{d},\gamma)^3He$ and $^2H(\vec{p},\gamma)^3He$ data were obtained using the $^1H(d,\gamma)^3He$ reaction at E_d = 1.62 MeV (TUNL data). These data were fitted to an expansion in terms of Legendre polynomials following Eqn. 5-1. However, since previous work had more accurately evaluated the isotropic component (assuming no fore-aft asymmetry) (Griffiths et al., 1962) and the fore-aft asymmetry (Wolfli et al., 1966) in this

cross section the expansion was performed subject to the constraints:

7-6 $$0.5774a_1 - 0.3849a_3 = 0.051 \pm 0.005$$

and

$$-1.04a_2 - 1.017a_4 = 1.0.$$

The angular distribution data and the fit obtained using this procedure are shown in Figure 7-1 as a function of $\theta_\gamma(cm)(p,\gamma)$. The cross section data is also given in Table 7-1 and the extracted a_k coefficients are presented in Table 7-2.

The product functions $A(\theta)\sigma(\theta)$ for both the proton and deuteron case were fit to an expansion using Eqn. 5-5 and Eqn. 7-5, respectively, as shown in Figure 7-1. The analyzing power data are given in Table 7-1 and the b_k parameters are given in Table 7-2. In the center-of-mass, the transformation of angles between the (p,γ) and (d,γ) reaction is

7-7 $$\theta_\gamma(cm)(p,\gamma) = 180^\circ - \theta_\gamma(cm)(d,\gamma).$$

In terms of the a_k coefficients, this transformation is the equivalent to changing the signs of a_1 and a_3 going from the (p,γ) to the (d,γ) case. For the b_k coefficients, the signs of b_2 and b_4 change. All angular distribution and analyzing power results are expressed in terms of $\theta_\gamma(p,\gamma)$.

The relationship between the b_k coefficients obtained in the $^2H(\vec{p},\gamma)^3He$ reaction and those obtained in the $^1H(\vec{d},\gamma)^3He$ reaction when both are measured at the same excitation energy makes a comparison of the two particularly sensitive to the presence of s=3/2 transitions.

Figure 7-1. Cross section and analyzing power measurements at E_x = 6 MeV; (a) Cross section data from the $^1H(d,\gamma)^3He$ plus Legendre polynomial fit including constraints (see text), (b) Analyzing powers time cross sections from the $^2H(\vec{p},\gamma)^3He$ reaction (Engelbert and Clausnitzer, 1983) plus fit, (c) same as (b) except for the $^1H(\vec{d},\gamma)^3He$ reaction. The γ-ray angles are expressed relative to the proton. Error bars represent statistical uncertainties only. The data is also given in Table 7-1.

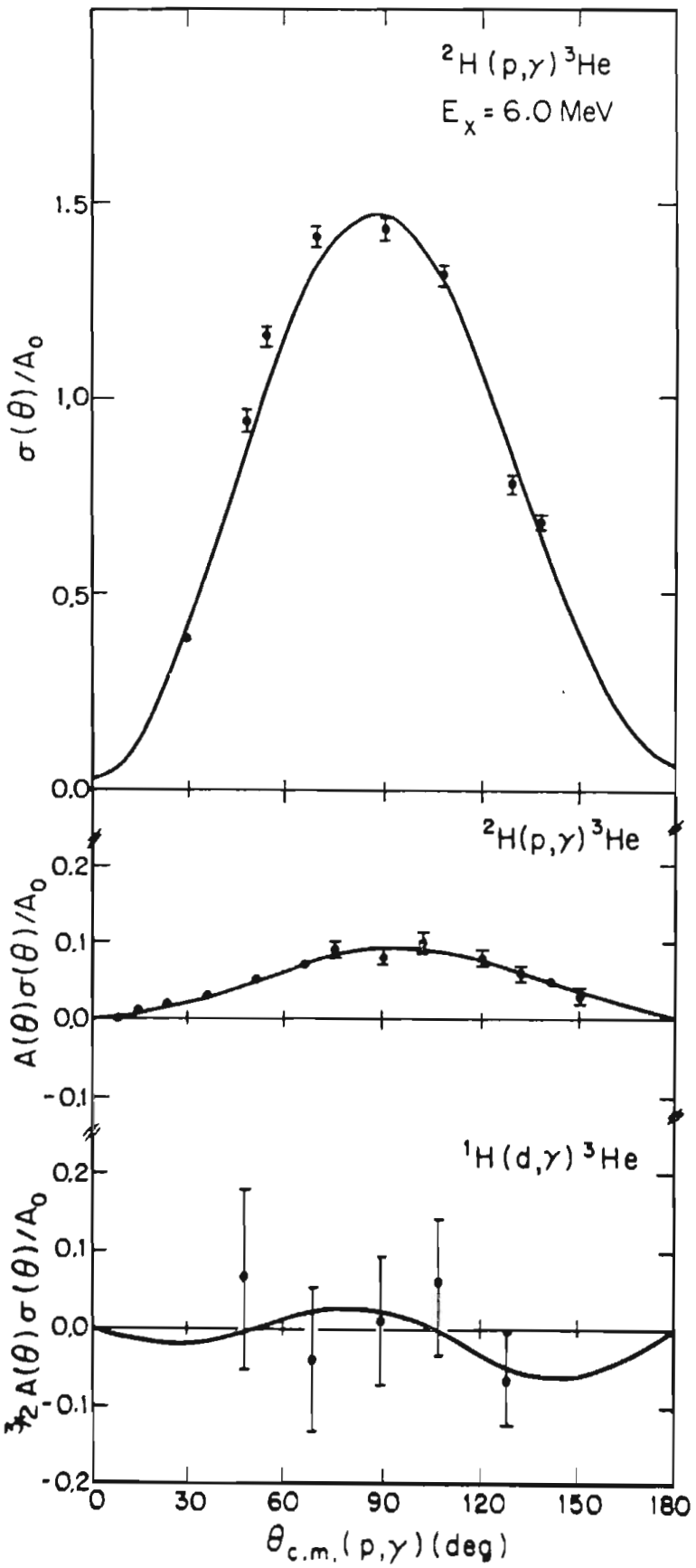
$^2H(p,\gamma)^3He$
$E_x = 6.0$ MeV
$\sigma(\theta)/A_0$
1.5
1.0
0.5
0.0
$^2H(p,\gamma)^3He$
$A(\theta)\sigma(\theta)/A_0$
0.2
0.1
0.0
-0.1
$^1H(d,\gamma)^3He$
$\frac{3}{2}A(\theta)\sigma(\theta)/A_0$
0.2
0.1
0.0
-0.1
-0.2
0
30
60
90
120
150
180
$\theta_{c.m.}(p,\gamma)$ (deg)

Table 7-1. Cross sections and analyzing powers for the $^{1}H(\vec{d},\gamma)^{3}He$ reaction at 6.0 MeV excitation energy. The γ-ray angles quoted are with respect to the proton in the center-of-mass frame. The uncertainties represent one standard deviation of the statistical error.

E_d	θ_{cm}	$\sigma(\theta)/A_0$	$\frac{3}{2}A_d(\theta)\sigma(\theta)/A_0$
1.62	29.2	0.37 ± 0.02	
	48.8	0.93 ± 0.03	0.070 ± 0.120
	53.7	1.15 ± 0.03	
	68.5	1.41 ± 0.02	-0.043 ± 0.097
	90.0	1.43 ± 0.02	0.010 ± 0.083
	108.5	1.31 ± 0.02	0.058 ± 0.089
	128.8	0.77 ± 0.02	-0.069 ± 0.060
	139.0	0.67 ± 0.02	

Table 7-2. Coefficients of the Legendre polynomial fits to the angular distribution data of cross section and analyzing power for the $^{2}H(\vec{p},\gamma)^{3}He$ (Engelbert and Clausnitzer, 1981) and $^{1}H(\vec{d},\gamma)^{3}He$ reactions at E_x = 6 MeV. The expansions are in terms of the γ-ray angles relative to the proton in the center-of-mass.

Reaction	Coefficient	
(d,γ)	a_1	0.041 ± 0.02
	a_2	-0.961 ± 0.02
	a_3	-0.072 ± 0.02
	a_4	0.00 ± 0.04
(d,γ)	b_1	-0.006 ± 0.045
	b_2	0.018 ± 0.037
	b_3	-0.018 ± 0.036
(p,γ)	b_1	0.081 ± 0.007
	b_2	-0.005 ± 0.006
	b_3	-0.006 ± 0.006
	b_4	-0.001 ± 0.006

This can be seen as follows. The b_k's can be written in terms of sums of products of transition amplitudes (T)(T'). If we start with the expression for the b_k coefficients in channel spin representation (ℓ,s coupling) as given by Eqn. 21 of Seyler and Weller (1979), then the ratio of the b_k's for $^1H(d,\gamma)^3He$ to those for $^2H(p,\gamma)^3He$ is:

$$7\text{-}8 \qquad \frac{b_k(d,\gamma)}{b_k(p,\gamma)} = \frac{\sqrt{3/2}\ W(1s1s';\tfrac{1}{2}1)(-1)^{\frac{1}{2}-1}}{\sqrt{2/3}\ W(\tfrac{1}{2}s\tfrac{1}{2}s';11)(-1)^{1-\frac{1}{2}}}.$$

This ratio can be explicitly evaluated for three possible types of terms which can appear in the expansion of the b_k's:

1. $s = s' = 1/2$ (pure doublet terms)

$$7\text{-}9 \qquad \frac{b_k(d,\gamma)}{b_k(p,\gamma)} = -3.0$$

2. $s = 1/2$, $s' = 3/2$; or $s=3/2$, $s' = 1/2$ (doublet-quartet terms)

$$7\text{-}10 \qquad \frac{b_k(d,\gamma)}{b_k(p,\gamma)} = \frac{3}{4}, \text{ and}$$

3. $s = s' = 3/2$ (pure quartet-quartet terms)

$$7\text{-}11 \qquad \frac{b_k(d,\gamma)}{b_k(p,\gamma)} = \frac{3}{2}.$$

Hence, if the reaction proceeds via pure s=1/2 T-matrix elements, then the b_k's obtained in the $(\vec{d},\gamma)$ experiment should be a factor of -3 times the b_k's obtained in the $(\vec{p},\gamma)$ experiment. Any s=3/2 strength would cause this ratio to deviate from the factor of -3. Measurements of both sets of b_k's is therefore a sensitive means of investigating the presence of s=3/2 strength in these reactions. Note that the observables $\sigma(\theta)$ and $A(\theta)$ must be plotted against the same center-of-mass angle variable for these comparisons to be valid.

Using the definitions for analyzing power given in Eqn. 5-5 for proton capture and Eqn. 7-5 for deuteron capture, we see that

$$7\text{-}12 \qquad \frac{3}{2}\frac{A_d(\theta)}{A_p(\theta)} = \frac{\sum b_k(d,\gamma)\ P_k^1}{\sum b_k(p,\gamma)\ P_k^1}.$$

So, for example, for $s=s'=\frac{1}{2}$:

$$7\text{-}13 \qquad \frac{A_d(\theta)}{A_p(\theta)} = -2.$$

The measured analyzing powers for both the reactions plotted as a function of the proton center-of-mass angle in Figure 7-2. The analyzing power expected in the $(\vec{d},\gamma)$ case based on that observed in the $(\vec{p},\gamma)$ data with the assumption of only doublet ($s=s'=1/2$) terms is also shown as the solid line. The results clearly indicated the presence of $s=3/2$ strength.

The data of Figure 7-2 establish the presence of $s=3/2$ strength in the two-body photodisintegration of ^{3}He at E_x = 6 MeV. Furthermore, since the b_1 coefficient (see Table 7-2) observed in the $(\vec{p},\gamma)$ data is non-zero, the presence of non-E1 radiation is also established by these data. The two most likely candidates for this radiation are E2 and M1 radiation.

7.3 T-Matrix Analysis

In order to investigate the $s=3/2$ transition strength as well as the E2 and M1 contributions more fully, we have attempted to fit the data to the various E1, E2, and M1 amplitudes involved in the reaction.

Figure 7-2. The analyzing powers measured in the $^{2}H(\vec{p},\gamma)^{3}He$ (triangles) and $^{1}H(\vec{d},\gamma)^{3}He$ reactions ($\times$'s) are given as a function of $\theta_{cm}(p,\gamma)$. The solid curve is the predicted $^{1}H(\vec{d},\gamma)^{3}He$ analyzing power based on the observed $^{2}H(\vec{p},\gamma)^{3}He$ data and the assumption of doublet (s=1/2) terms only.

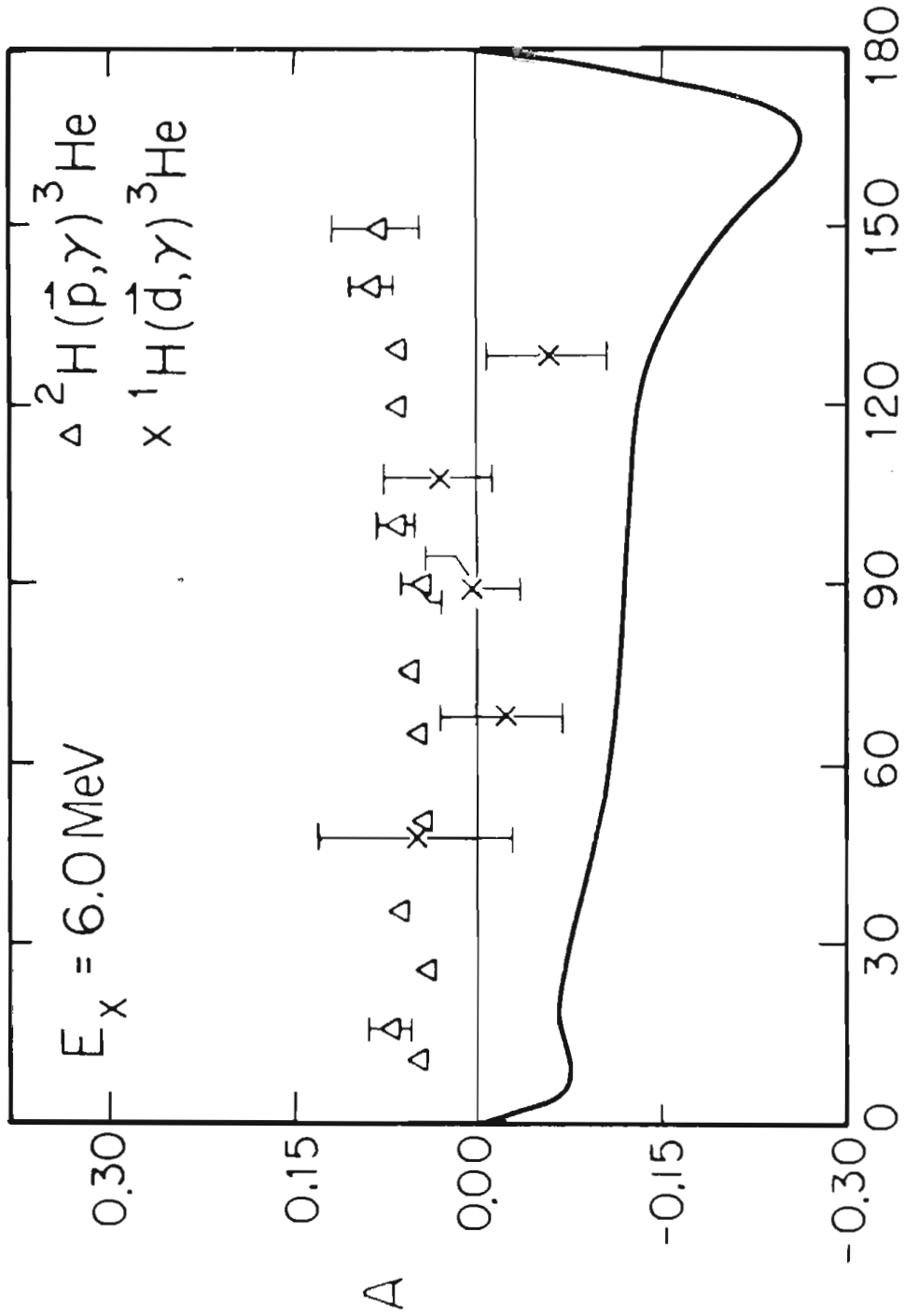
E_x = 6.0 MeV
$\Delta\ ^2H(\vec{p},\gamma)^3He$
$\times\ ^1H(\vec{d},\gamma)^3He$
A
0.30
0.15
0.00
-0.15
-0.30
0
30
60
90
120
150
180
$\theta_{c.m.}$ (deg)

If we consider only E1, E2, and M1 transition matrix elements, there are 16 amplitudes and 15 relative phases in this problem. This number of unknowns prohibits a model independent analysis. However, we observe the following:

1. There is s=3/2 strength present in this reaction.
2. The b_1 is the only non-zero analyzing power coefficient in the experiment.
3. The present calculations based on Faddeev generated ^{3}He wave functions generally account for the observed a_1, a_2, a_3, and a_4 coefficients of the angular distributions. These calculations contain s=1/2 and s=3/2 E1, E2, and E3 radiation, the s=3/2 strength being almost entirely the result of D-state presence in the ground state of ^{3}He. This model calculation predicts b_1 to be essentially zero in both the $(\vec{p},\gamma)$ and $(\vec{d},\gamma)$ reactions.
4. The T-matrix analysis of previous $(\vec{p},\gamma)$ work (Skopik et al., 1979) at higher energies and the current direct model calculation indicated that the amplitudes and phases of T-matrix elements having only a different $\vec{J}$-value were equal.

An analysis of the present data was performed based on these observations, and guided by our model calculations. The following assumptions formed the basis of our analysis:

1. E1 strength results from p-wave capture, E2 strength from d-wave capture, and M1 strength from s-wave capture only.
2. The phases of the various transition amplitudes depend only upon the ℓ-value of the incoming partial wave.

3. Spin-orbit effects are small so that E1 and E2 amplitudes are independent of J.

4. The relative s=3/2-to-s=1/2 strength in the E1 and E2 terms is given by the direct capture model calculations.

The first assumption is justified by angular momentum considerations as a result of the low (0.5 Mev in center-of-mass) beam energy. The f and g partial waves should not contribute significantly. This is born out by the direct capture calculations at this energy. Assumptions two and three follow from the direct calculations indicating phase differences are only a few degrees for T-matrix elements from states differing only by J. Finally, in the E1 and E2 transitions, the s=3/2 contributions primarily result from transitions to the ^{3}He D-state which are included in the direct capture calculation.

The data at E_x = 6 MeV for the angular distribution of the cross section along with the $\vec{p}$ on d and the $\vec{d}$ on p analyzing powers (see Figure 7-1) were fitted to equations containing four amplitudes and two relative phases. The reduction to this number of amplitudes and phases followed from the above assumptions. The amplitudes used consisted of one E1 amplitude, p, (with a 0.28% s=3/2 admixture), one E2 amplitude, d, (containing a 0.08% s=3/2 admixture) and two M1 s-wave amplitudes corresponding to s=1/2, ^{2}s, and s=3/2, ^{4}s. In addition, there were two relative phases amongst these three multipoles. The T-matrix expansion of the angular distribution coefficients for cross section is given as:

7-14 $\quad 1.0 = 6\ p^2 + 10\ d^2 + 2\ {}^2s^2 + 4\ {}^4s^2$ Normalization

$$a_1 = -0.619\ {}^4s\ p\ \cos(\varphi_s-\varphi_p) + 20.81\ p\ d\ \cos(\varphi_d-\varphi_p)$$

$$a_2 = -5.992\ p^2 + 7.145\ d^2 - 0.573\ {}^4s\ d\ \cos(\varphi_s-\varphi_d)$$

$$a_3 = -20.773\ p\ d\ \cos(\varphi_d-\varphi_p)$$

$$a_4 = -17.133\ d^2,$$

for $(\vec{p},\gamma)$ analyzing power

$$b_1 = -1.94\ {}^2s\ p\ \sin(\varphi_s-\varphi_p) - 7.72\ {}^4s\ p\ \sin(\varphi_s-\varphi_p) - 0.477\ p\ d\ \sin(\varphi_d-\varphi_p)$$

$$b_2 = -0.560\ p^2 + 0.374\ d^2 - 1.904\ {}^2s\ d\ \sin(\varphi_s-\varphi_d) - 7.61\ {}^4s\ d\ \sin(\varphi_s-\varphi_d)$$

$$b_3 = -0.087\ p\ d\ \sin(\varphi_d-\varphi_p)$$

$$b_4 = -1.083\ d^2,$$

and for $(\vec{d},\gamma)$ analyzing power

$$b_1 = 6.043\ {}^2s\ p\ \sin(\varphi_s-\varphi_p) - 5.58\ {}^4s\ p\ \sin(\varphi_s-\varphi_p) - 0.358\ p\ d\ \sin(\varphi_d-\varphi_p)$$

$$b_2 = 2.08\ p^2 - 1.79\ d^2 + 5.77\ {}^2s\ d\ \sin(\varphi_s-\varphi_d) - 5.640\ {}^4s\ d\ \sin(\varphi_s-\varphi_d)$$

$$b_3 = -0.066\ p\ d\ \sin(\varphi_d-\varphi_p)$$

$$b_4 = 3.460\ d^2.$$

These equations are based on the assumptions given above and include the s=3/2-to-s=1/2 cross section ratio for E1 and E2 transitions based on the direct capture calculations. The inclusion of M1 strength was found to be necessary in order to fit the data. An F-test for the inclusion of the M1 term gives a 99% confidence limit on the need for this parameter. The fit generated an M1 cross section which is shown as a function of χ^2 in Figure 7-3. The M1 absolute cross sections shown in

Figure 7-3. The deduced M1 cross section as a function of reduced χ^2 obtained under the assumptions given in the text. The 90% confidence limit gives an M1 contribution of 1 to 8% the to the total cross section.

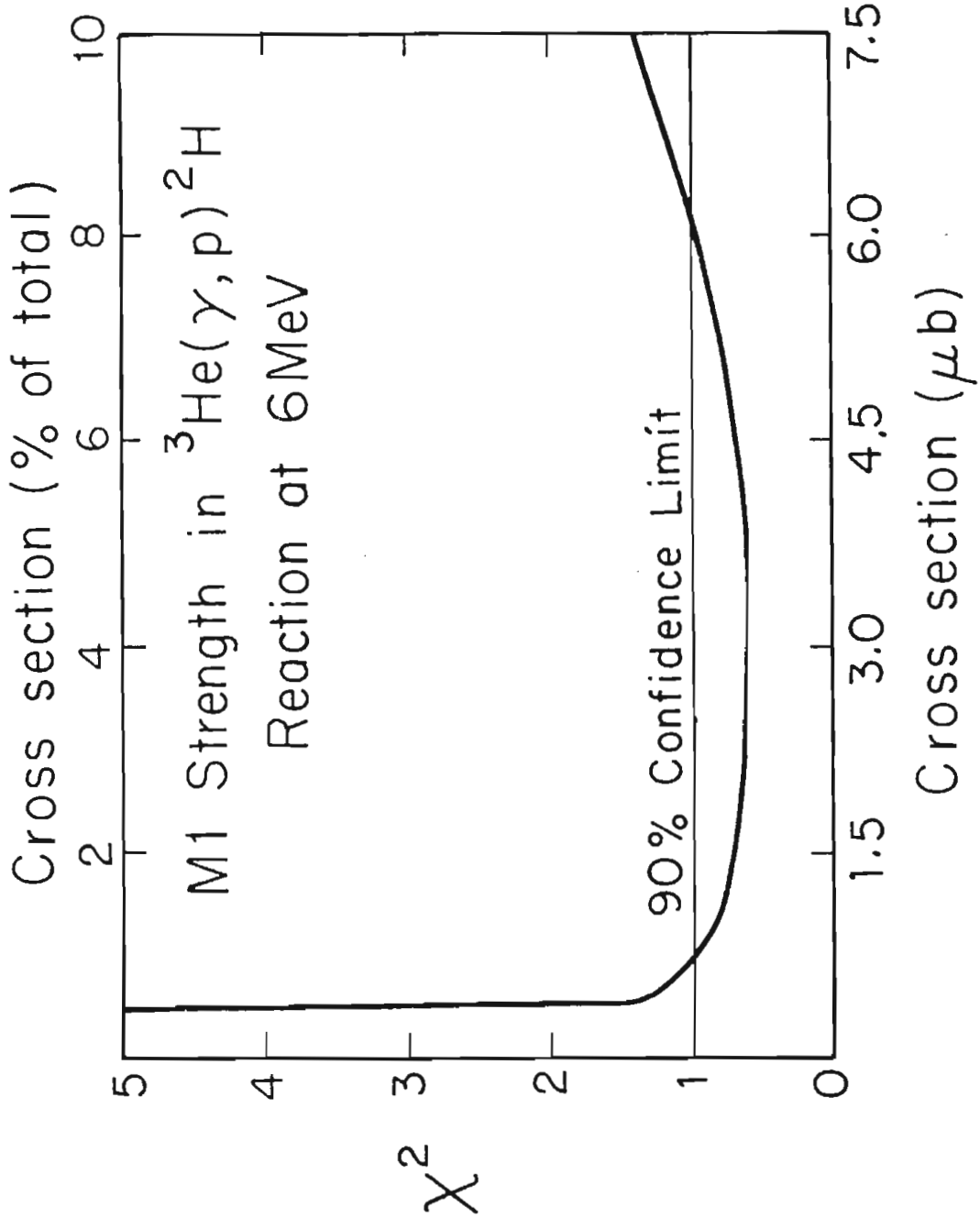
Cross section (% of total)
2
4
6
8
10
M1 Strength in ^{3}He(γ,p)^{2}H
Reaction at 6MeV
90% Confidence Limit
χ^2
5
4
3
2
1
0
1.5
3.0
4.5
6.0
7.5
Cross section (μb)

this figure were obtained from the percentage strength using the cross sections of Griffiths et al. (1962). The results of Figure 7-3 indicate that, under our assumptions, an M1 component constituting 1 to 8% of the total cross section can give rise to the observed differences between the $\vec{p}$ on d and the $\vec{d}$ on p vector analyzing powers. Table 7-3 gives the relative cross sections and phases extracted from the analysis described above. The minimum M1 strength is predominately S=3/2. The E2 cross section is small, 0.1 to 0.6%. The phase for E2 is generally consistent with the phases found at higher energies.

7.4 Conclusions

The calculations of Aufleger and Drechsel (1981) have shown that, after subtracting spurious components which result from orthogonality problems, the M1 strength at E_x = 10.8 MeV in ^{3}He is reduced from 15 to 1.5%. This amount of M1 strength is similar to that deduced in the present analysis for E_x = 6 MeV. However, a full three body calculation which computes directly the present experimental observables (ie. cross sections and analyzing powers) is needed to properly evaluate these results. Nevertheless, we can conclude at this time that:

1. There is s=3/2 capture strength present in the two-body capture channel of ^{3}He at E_x = 6.0 MeV, and
2. A 1 to 8% M1 admixture has been shown to be a sufficient, but not a necessary condition for explaining the present observables.

To further investigate the s=3/2 transitions, the tensor analyzing

Table 7-3. Summary of T-Matrix cross sections and phases for the E1, E2, and M1 analysis. The ranges given are within the 90% confidence limit for the χ^2 for an analysis of the $^2H(\vec{p},\gamma)^3He$ and the $^1H(\vec{d},\gamma)^3He$ reactions at E_x = 6.0 MeV. The phases are relative to the E1 amplitude.

σ(E1)	92.8- 98.3%
σ(E2)	0.1 - 0.6%
ϑ(E2)	36^o - 53^o
σ(M1;^{2}S)	0.0 - 2.5%
σ(M1;^{4}S)	0.4 - 6.5%
σ(M1)	1.0 - 8.0%
ϑ(M1)	11^o - 19^o

powers needs to be measured. Since any finite tensor analyzing power requires the presence of s=3/2 transitions, this should be a particularly sensitive measurement. In addition, inclusion of the tensor analyzing powers in the T-Matrix expansion will allow the number of model dependent assumptions to be reduced.

8 Summary of Conclusions

The following are a summary of the results of our study of the $^{2}H(\vec{p},\gamma)^{3}He$ and $^{1}H(\vec{d},\gamma)^{3}He$ reactions:

1. The measurement of 90^{o} and total cross sections at the proton beam energies of 6.5, 8, 11, 15, and 16 MeV resulted in the confirmation of the high values for the peak cross sections. Calculations by Barbour and Phillips (1970) using the Faddeev-type ^{3}He wave functions based on separable S-wave potential for the E1 multipole and including final state interactions give the best agreement with both total and 90^{o} cross sections.

2. Direct radiative capture calculations assuming E1, E2, and E3 radiation were performed using S and D-state two-body projections of Faddeev generated three-body ^{3}He wave functions and distorted wave continuum wave functions. Comparison of these calculations with experimental σ_{T} and $\sigma(90^{o})$ reveals substantial differences. The calculated cross sections are quite sensitive to the choice of continuum wave functions, indicating the importance of final state interactions.

3. Angular distributions of cross section were measured between 6.5 and 16 MeV. The 15 MeV data is in excellent agreement with angular distributions of Belt et al. (1971) and Skopik et al. (1983). At 8 and 16 MeV angular distributions of analyzing power were also measured. At these energies it was possible, after making a few assumptions based on the direct capture model, to extract the transition amplitudes. The analysis which included ^{2}p, ^{4}p, and ^{2}d T-matrix elements resulted in 0.5

to 5% $\sigma(E1;s=3/2)$ and 1 to 3% $\sigma(E2)$ for 8 MeV and 2 to 8% $\sigma(E1;s=3/2)$ and 1 to 5% $\sigma(E2)$ for 16 MeV. The direct calculation of $\sigma(E1;s=3/2)$ which primarily resulted from transitions to the D-state of ^{3}He is within the range of values obtained from the T-Matrix analysis.

4. The direct capture calculation indicates a sensitivity of the a_2 angular distribution coefficient to the inclusion of the D-state, ψ_D, in the ^{3}He wave function. The calculations indicated that a $P_D(^3He)$ of 5 to 9% would agree with the present data. This corresponds to an S to D asymptotic ratio, η, of 0.0385 to 0.05. The energy dependence of the direct capture calculations for a_1, a_3, and fore-aft asymmetry is greater than the experimental measurements. However, if the calculated $\sigma(E1)$ is renormalized to the total cross section, the calculations using $P_D(d) = 7\%$ give good agreement with the observed energy dependence of $\sigma(90^o)$, a_1, and a_3. Although the a_2 fit from this renormalized calculation is somewhat worse, the inclusion of ψ_D in ^{3}He significantly improves the results. The fore-aft asymmetries measured in approximately 1 MeV steps from 6 to 16 MeV are in good agreement with the renormalized calculations. Since this is a measure of the E1-E2 interference, the calculated quadrupole strength appears to be correct.

5. The controversy over the E2 cross sections between experiments and theory has been resolved with the conclusion that the experimental E2 cross sections of the previous TUNL work (Skopik *et al.*, 1979) were nearly an order of magnitude too large. The current cross sections based on the T-Matrix analysis of the data are in good agreement with theoretical results.

6. The presence of M1 strength in the cross section is indicated by the non-zero b_1 coefficients which vary inversely with energy. The direct capture calculations which do not include M1 transitions give essentially zero for all b_k's. The investigation of M1 transitions was furthered by using both vector polarized proton and deuteron beams at E_x = 6 MeV. A T-Matrix analysis of both sets of analyzing powers as well as the angular distribution of cross section give a 1 to 8% M1 contribution to the cross section within a 90% confidence limit. In addition, the combination of $(\vec{d},\gamma)$ and $(\vec{p},\gamma)$ measurements is especially sensitive to the channel spins of the transitions. The results support the presence of significant and perhaps predominate s=3/2 M1 strength.

In conclusion, contributions from both M1 and E1(s=3/2) transitions have been extracted from the present data. These small transition strengths are good probes of both the S' and D-state components of the ^{3}He wave function. In order to further interpret the present results, a full three-body calculation with a proper treatment of both the bound state and continuum wave functions and including at least E1, E2, E3, and M1 transitions to S, S' and D-states of ^{3}He is needed. Further experimental measurements of tensor analyzing powers for the $(\vec{d},\gamma)$ reaction will enable a better determination of the transition amplitudes that contribute to this reaction, especially the s=3/2 transitions.

9 REFERENCES

R.D. Amado

Comm. Nucl. Part. Phys. 10 (1981) 131

M. Anghinolfi, et al.

(to be published)

A. Arriaga and F.D. Santos

"^{3}He D-State Effects in the $^1H(\vec{d},\gamma)^3He$ Reaction" (to be published)

S. Aufleger and D. Drechsel

Nucl. Phys. A364 (1981) 81

G.M. Bailey, G.M. Griffiths, and T.W. Donnelly

Phys. Lett. 24B (1967) 222

I.M. Barbour and J.E. Hendry

Phys. Lett. 38B (1972) 151

I.M. Barbour and A.C. Phillips

Phys. Rev. C 1 (1970) 165

H.H. Barschall and W. Haeberli, eds.

Polarization Phenomena in Nuclear Reactions, Proc. of the Third Inter. Symp., Madison, WI, 1970

B.D. Belt

Univ. of Tennesse, unpublished thesis, 1970

B.D. Belt, C.R. Bingham, M.L. Halbert, and A. van der Woude

Phys. Rev. Lett. 24 (1971) 1120

B.L. Berman, L.J. Koester, Jr., and J.H. Smith

Phys. Rev. 133 (1964) B117

Philip R. Bevington

Data Reduction and Error Analysis for the Physical Sciences

McGraw-Hill, New York, 1969

R. Bosch, J. Lang, R. Muller, and W. Wolfli

Phys. Lett. 15 (1965) 243

M.E. Brandan and W. Haeberli

Nucl. Phys. A287 (1977) 213

G.E. Brown

Nucl. Phys. 57 (1964) 339

B. Buck and A.A. Pilt

Nucl. Phys. A280 (1977) 133

D.O. Caldweld and J.R. Richardson

Phys. Rev. 98 (1955) 28

C.C. Chang, E.M. Diener, and E. Ventura

Phys. Rev. Lett. 29 (1972) 307

C.C. Chang, W.R. Dodge, and J.J. Murphy II

Phys. Rev. C 9 (1974) 1300

T.B. Clegg, G.A. Bissenger, W. Haeberli, and P.A. Owen

"Lamb-Shift Polarized Ion Sources for Tandem Accelerators at Wisconsin and Triangle Universities Nuclear Laboratory" in Barschall and Haeberli (1970), p. 835

C.F. Clement, A.M. Lane, and J.A. Rook

Nucl. Phys. 66 (1965) 273 and 293

H. Collard et al.

Phys. Rev. 138 (1965) B57

L. Cranberg

Bull. Am. Phys. Soc. 3 (1958) 173

B.A. Craver, Y.E. Kim, and A. Tubis

Nucl. Phys. A276 (1977) 237

S.C. Curran and J. Strothers

Proc. Roy. Soc. A 172 (1939) 72

L.M. Delves

"The Three-Body Problem" in Few Body Problems, Light Nuclei, and Nuclear Interactions, edited by Guy Paic and Ivo Slaus (Gordon and Breach, Science Publishers, New York, 1968), p. 153-247.

L.M. Delves, J.M. Blatt, I. Pask, and B. Davies

Phys. Lett. 28B (1969) 472

L.M. Delves and A.C. Phillips

Rev. Mod. Phys. 41 (1969) 497

G. H. Derrick

Nucl. Phys. 16 (1960) 405

R.M. DeVries, J.L. Perrenoud, and Ivo Slaus

Nucl. Phys. A188 (1972) 449

A.E.L. Duperink et al.

Phys. Lett. 63B (1976) 261

U. Eichmann

Z. Phys. 175 (1963) 115

H.P. Engelbert and G. Clausnitzer

Unpublished thesis, University of Giessen, West Germany, 1981 and private communication

V.N. Fetisov, A.N. Gorubnov, and A.T. Varfolomeev

Nucl. Phys. 71 (1965) 305

W.A. Fowler, C.C. Laurter, and A.V. Tollestres

Phys. Rev. 76 (1949) 1767

J.L. Friar

Phys. Rev. C 20 (1979) 325

J.L. Friar, B.F. Gibson, D.R. Lehman, G.L. Payne

Phys. Rev. C 25 (1982) 1616

B.F. Gibson

"Electromagnetic and Weak Interactions in Few-Nucleon Systems" (to be published in the Proc. of 10th Inter. Conf. on Few Body Problems in Physics), Kalsruhe, Germany, 1983

B.F. Gibson and D.R. Lehman

Phys. Rev. C 11 (1975) 29

B.F. Gibson and D.R. Lehman

Bull. Am. Phys. Soc. 27 (1982) 569 and "Structure of the $^3H \rightarrow n + d(d^*)$ vertexes", (to be published).

B.F. Gibson and J.S. O'Connell

Phys. Lett. 32B (1970) 331 and private communication in Belt (1970)

C.R. Gould, L.G. Holzsweig, S.E. King, Y.C. Lau, R.V. Poore, N.R. Roberson, and S.A. Wender

IEEE Trans. on Nucl. Sci. NS-28 , No. 5 (1981) 3708

G.M. Griffiths and J.B. Warren

Proc. Phys. Soc. A68 (1955) 781

G.M. Griffiths, E.A. Larson, and L.P. Robertson

Can. Jou. Phys. 40 (1962) 402

P. Guss

Duke Univ., private communication, 1982

E. Hadjimichael

Phys. Rev. Lett. 31 (1973) 183

M.L. Halbert, P. Paul, K.A. Snover, and E.K. Waburton

in Proceeding of the International Conference on Few Particle Problems in the Nuclear Interaction, Los Alamos, 1972, I. Slaus, S.A. Moszkowski, R.P. Haddock, and W.T.H. van Oers eds., (North-Holland, Amsterdam, 1972) 531

E. Hayward

Photonuclear Reactions, U.S. Natl. Bur. Stand. Monograph No. 118 Washington, DC, 1970

E. Hayward, W.R. Dodge, and B.H. Patrick

Nucl. Instr. and Meth. 159 (1979) 289

M.A. Hennell and L.M. Delves

Nucl. Phys. A246 (1975) 490

J.A. Hendry and A.C. Phillips

Nucl. Phys. A211 (1973) 533

L.G. Holzsweig and R.V. Poore

IEEE Trans. on Nucl. Sci. NS-28 , No. 5 (1981) 3815

D.J. Hughes and J.A. Harvey, editors

Neutron Cross Sections, 2nd Edition, (USAEC Washington, DC, 1955)

E. Jans et al.

Phys. Rev. Lett. 49 (1982) 974

S. Kikuchi, et al.

Jou. Phys. Soc. Jap. 15 (1960) 9

S.E. King, et al.

"Vector Analyzing Powers of $^{2}H(p,\gamma)^{3}He$ and $^{1}H(d,\gamma)^{3}He$ Reactions at E_x=6 MeV" (to be published, 1983)

S.E. King, Y.C. Lau, and C.R. Gould

IEEE Trans. on Nucl. Sci. NS-28 , No. 5 (1981) 3822

S.E. King, N.R. Roberson, H.R. Weller, and D.R. Tilley

Phys. Rev. Lett. 51 (1983) 877

H. Kitazawa

Tokyo Institute of Technology, private communication, 1980

L.D. Knutson, et al.

Phys. Rev. Lett. 35 (1975) 1570

L.D. Knutson, P.C. Colby, and J.A. Bieszk

Phys. Lett. 85B (1979) 209

L.D. Knutson, P.C. Colby, and B.P. Hichwa

Phys. Rev. C 24 (1981) 411

D.C. Kocher and T.B. Clegg

Nucl. Phys. A132 (1969) 455

I.V. Kozlowsky et al.

Nucl. Phys. A368 (1981) 493

S.K. Kundu, Y.M. Shim, and G.D. Wait

Nucl. Phys. A171 (1971) 384 and unpublished thesis, 1972.

J.M. Lafferty, Jr. and S.R. Cotanch

Nucl. Phys. A373 (1982) 363

D.R. Lehman

George Washington Univ., private communication, 1983

D.R. Lehman, W.C. Parke, and L.C. Maximon

J. Math. Phys. 22 (1981) 1399

C.W. Li

Phys. Rev. 83 (1951) 512

I. Lindegren

"Table of Nuclear spins and Moments" Appendix 4 of Alpha, Beta, and Gamma-ray Spectroscopy (K. Siegbahn, ed., North Holland, Amsterdam, 1965)

C. Lovelace

Phys. Rev. 135 (1964) B1225, and refs. therein

R.E. Marrs, E.G. Adelberger, K.A. Snover, and M.D. Cooper

Phys. Rev. Lett. 35 (1975) 202

J.H.E. Mattauch, W. Thiele, and A.H. Wapstra

Nucl. Phys. 67 (1965) 1

J.L. Matthews, et al.

Nucl. Phys. A223 (1974) 221

G. Mitev, et al.

Bull. Am. Phys. Soc. 27 (1982) 701 and private communication.

A.C. Phillips

Nucl. Phys. A184 (1972) 337

G.R. Plattner, M. Bornand, and R.D. Viollier

Phys. Rev. Lett. 39 (1977) 127

R.V. Reid

Ann. Phys. 50 (1968) 411

N.R. Roberson and S.E. Edwards

IEEE Trans. on Nucl. Sci. NS-28 , No. 5 (1981) 3834

C. Rolfs

Nucl. Phys. A217 (1973) 29

S. Roman, et al.

Nucl. Phys. A289 (1977) 269

T. Sasakawa, H. Okuno, and T. Sawada

Phys. Rev. C 23 (1981) 905

L.I. Schiff

Phys. Rev. 52 (1937) 242

R.G. Seyler and H.R. Weller

Phys. Rev. C 20 (1979) 453

E. A. Silverstein

Nucl. Instr. Meth. 4 (1959) 53

D.M. Skopik

Univ. Saskatchewan, private communication, 1983

D.M. Skopik et al.

Phys. Rev. C 28 (1983) 52

D.M. Skopik, H.R. Weller, N.R. Roberson, and S.A. Wender

Phys. Rev. C 19 (1979) 601

J.R. Stewart, R.C. Morrison, and J.S. O'Connell

Phys. Rev. 138 (1965) B372

E. Storm and H.I. Israel

Nucl. Data Tab. A7 (1970) 565

M. Suffert, W. Feldman, J. Mahieux, and S.S. Hanna

Nucl. Instr. Meth. 63 (1968) 1

G. Ticcioni, S.N. Gardiner, J.L. Matthews, and R.O. Owens

Phys. Lett. 46B (1973) 369

S. Tonsfeld

Unpublished thesis, University of North Carolina, Chapel Hill, 1980

J. Torre and B. Gouland

"Meson Exchange Currents and Radiative Thermal Neutron Capture by Deuterons", (to be published, 1983)

T.A. Trainor, T.B. Clegg, and P.W. Lisowski

Nucl. Phys. A220 (1974) 533

Triangle Universities Nuclear Laboratory

XSYS Reference Manual

Duke University, Durham, NC (1982)

James David Turner

unpublished Ph.D. Dissertation, Duke University, 1978

A. van der Woude, M.L. Halbert, C.R. Bingham, and B.D. Belt

Phys. Rev. Lett. 26 (1971) 909

W.T.H. van Oers and K.W. Brockman, Jr.

Nucl. Phys. 21 (1960) 189

M. Verde

"The Three Body Problem in Nuclear Physics", Hanbuch der Physik,

Bd. 39, S. Flugge, ed. (Springer-Verlag, Berlin, 1957) p. 144

H.R. Weller and N.R. Roberson

Rev. Mod. Phys. 52 4 (1980) 699

H.R. Weller and N.R. Roberson

IEEE Trans. Nucl. Sci. NS-28 2 (1981) 1268

S.A. Wender, C.E. Floyd, T.B. Clegg, and W.R. Wylie

Nucl. Inst. Meth. 174 (1980) 341

D. H. Wilkinson

Phil. Mag. 43 (1952) 659

W. Wolfli, R. Bosch, J. Lang, R. Muller, and P. Marmier

Phys. Lett. 22 (1966) 75

M. Wright

Duke University, private communication, 1982

A Radiative Capture Data Acquisition Package

A.1 Overview

CAP, the radiative capture data acquisition code consist of a group of VAX DCL command files, XSYS commands, FORTRAN programs, EVAL programs, and information files. In this appendix the major procedures for data acquisition will be explained, the data area structure listed, scaler and ADC hardware information given, and the source codes of major components of the system listed. The experimenter may refer to the XSYS Reference Manual (1983) for general information on the system.

CAP was written to process events from one or two NaI detectors each with energy, TOF, and NaI-shield coincidence signals, one or two single parameter monitor events, and the 6 to 14 scalers associated with the experiment. In order to monitor the spectrum quality a measurement usually consisted of several one to two hour runs. After each run the spectra were stored on disk and tape and most of the data areas and scalers cleared. However, the conditional E_γ spectra used in the final analysis were also stored in accumulated spectra as given in Table A-3. For polarized data the partial runs with a beam polarization of spin up are alternated with spin down in order to reduce systematic errors. The Spin Up (Down) data is stored in data areas 1-49(51-95). With unpolarized data, the spectra used for the spin down data in polarized measurements were used for target out or background measurements.

Table A-1 gives the ADC hardware information for both NaI and

monitor detectors including the MBD I/O channel number, the CAMAC slot of the module and the subaddress of the ADC. The hardware locations of the scaler signals are given in Table A-2. The data area or spectrum definitions are all given in Table A-3.

To start up the program, the user must login to an ONLINE account, copy DRA2:[WELLER.CAP]*.* *.*, execute @CAP and answer the questions to determine the experimental configuration.

A.2 Hardware and Data Structures

Table A-1. ADC Hardware Information.

DETECTOR	SIGNAL	MBD CHANNEL	SLOT NO.	SUBADDRESS
Right NaI	Eγ	5	7	10
	TAC	5	7	11
	R2	5	7	12
Left NaI	Eγ	6	8	10
	TAC	6	8	11
	R2	6	8	12
RIGHT(0^{o})	MONITOR	0	1	0
LEFT (side)	MONITOR	1	3	0
QUENCH ADC		N/A	2	0

TABLE A-2. Scaler Definitions

NAME	CAMAC SLOT	ADDRESS
Right NaI	17	2
Right Shield	17	3
Right Coincidence (R_2)	17	4
Right Accidental	17	5
Left NaI	18	2
Left Shield	18	3
Left Coincidence (R_2)	18	4
Left Accidental	18	5
BCI	17	1
Time	18	1
Preset	16	1
Right (0^o) Monitor	17	6
Left(side) Monitor	18	6
Pickoffs	15	1

TABLE A-3. Data Area structure. For unpolarized beams the + spin state data areas become the unpolarized foreground, while the - spin state data areas are for background measurements.

Spectrum	Right Det - 1		Left Det - 2	
	+,(-)			
E_γ	1(51)		4(54)	
TOF	2(52)		5(55)	
R2	3(53)		6(56)	
ENERGY GATED TACS				
E Gate 1	20(70)		40(90)	
E Gate 2	21(71)		41(91)	
E Gate 3	22(72)		42(92)	
E_γ	ACCEPT	REJECT	ACCEPT	REJECT
TAC Gate 1	10(60)	13(63)	30(80)	33(83)
TAC Gate 2	11(61)	14(64)	31(81)	34(84)
Accumulated Gate 2	16(66)		36(86)	
TAC Gate 3	12(62)	15(65)	32(82)	35(85)
Miscellaneous				
MONITORS				
1 Right, 0^o	7(57)			
2 Left, Side	8(58)			
Scratch areas	96-99			

A.3 Command Procedures

The following commands are used in the data acquisition program CAP. They are a combination of command files written to execute XSYS and DCL commands.

ADD N1,N2,N3. - Add data areas N1 and N2 putting the result in N3. N1 or N2 may be negative to subtract data areas.

AIR IN - Put in beam(air) stop

AIR OUT - Take out beam stop

ALLOCATE MTA0: - Assigns tape unit MTA0: to user

@BACKUP MTAX: - Backup data and information files to tape unit X in the same order as dumped. Note all CAPTXXXX.DAT AND XSAVXXXX.DATA files are copied.

BEGIN COMMANDS

BE - Begin unpolarized run or begin a polarized run in the same spin state as the previous run. This command increments the run number, clears scalers and event counters, and starts run.

BE C - Same as BE except all non-accumulated data areas cleared. For polarized runs BE C clears both spin states.

BE C A - Same as BE C except all data areas cleared.

BU(BD) - Begin run with spin state set up (down).

BD C(BU C) - Begin run with spin state set up(down). Clears non-accumulated up(down) data areas.

BU C A(BD C A) - Begin in spin state up (down). Clear all

up and down data areas.

BI(BO) - Same as d) thru f) except for Target in(out).

@BOX - Creation of BOX subprocess and setting of BOX flags.

BOX G 996 - Restore box information from data area 996. Useful procedure for recovering messages.

BOX M N1 C1 - Put message C1 in box number N1.

@CAP - Initialization procedure.

CL N1,N2 - Clears data areas N1 thru N2.

CL N1 - Clears data area N1.

CL ALL - Clears all data areas.

DISMOUNT MTA0: - Dismounts and rewinds tape on unit zero.

DISP - Start Display program on Tektronix terminal.

DU - Dump the data to disk and tape, sum gates, accumulate scalers, print sums, scalers, and dead time corrections.

GATE SET N1, N2, N3, N4 - Set gate N2 of data area N1 to the range of channels N3 to N4.

HA - Halts data acquisition.

MOUNT MTA0: DTXXXX - Mount tape number XXXX on unit MTA0:.

QR - Make a beam polarization measurement by measuring the ratio of quenched beam to unquenched beam on the beam stop via computer control. Gives both incremental and accumulated polarization.

RD DA CAPTXXXX ALL - Read back all data areas of run XXXX from disk. Use TA for reading from tape.

RD DA CAPTXXXX DIF N2,N2 - Read data area N1 from disk into data area N2 from run XXXX.

REST DA - Restores all XSCOM, gates, scalers, etc. to their values at the end of the run given as the current run number.

RN - Display run number.

RN I - Increment run number.

RN N1 - Change run number to N1.

RN D - Decrement run number

SCAL PRES N1 - Change preset scaler to N1 either before or during run.

SCAL SE SCA2 - Create scaler and preset subprocess for two NaI detectors.

ST - Starts data after a HA.

ST CONT N1 - Restart a run with a new accumulation of the preset scaler value to N1.

ST NEW - Start a new run, clear event counters, and reload preset scaler.

@TAPE - To mount a new tape. Must DISMOUNT old tape and have new tape in position and online. Answer questions. This command should only be used with one tape at a time, i.e., it will not work for two tapes.

TRAN N2 N2 - Transfer data in data area N1 to N2

A.4 File Listing

The major elements of CAP, the radiative capture group data acquisition code are given in this appendix. The following routines are listed.

CAP.COM	INITIALIZATION PROCEDURE
TAPE.COM	TAPE MOUNTING PROCEDURE
BOX.COM	BOX DISPLAY INITIALIZATION PROCEDURE
BOXUSR.FOR	SUBROUTINE USED IN BOX
XBOXFLAG.FOR	SUBROUTINE USED TO INITIALIZE BOX FLAGS
BEGIN.COM	COMMAND TO BEGIN DATA ACQUISITION
DMP.COM	COMMAND TO DUMP THE DATA AT THE END OF A RUN
PCP1.EVL	RIGHT DETECTOR SORTING PROGRAM
PCP1.DAP	RIGHT DETECTOR INITIALIZATION INFORMATION FILE
PMON.EVL	MONITOR DATA SORTING PROGRAM
PMON.DAP	MONITOR INITIALIZATION INFORMATION FILE
SCA2.DAP	SCALER SUBPROCESS INFORMATION FILE

```
$!            Initialization command file
$!
$!      CAP
$!
$!      CAPTURE DATA ACQUISITION PACKAGE INITIALIZATION COMMAND FILE
$!
$!      WRITTEN BY STEVEN KING and Michael Wright
$!
$!      Written  3/22/81
$!      Last Modified 9/28/82
$!
$!      CAP IS THE COMMAND FILE TO SETUP THE RADIATIVE CAPTURE STANDARD
$!      DATA ACQUISITION PROGRAM FOR ONE OR TWO DETECTORS WITH POLARIZED
$!      OR UNPOLARIZED BEAM.
$!      THIS FILE (OPTIONALLY) PERFORMS THE FOLLOWING:
$!              1) LOADS MSD
$!              2) MOUNTS TAPE
$!              3) ALLOCATES MEMORY
$!              4) INSTALLS GATES
$!              5) CREATES THE ADC SUBPROCESSES
$!              6) SETS UP SCALERS, PRESET SCALER, AND SCALER DISPLAY
$!              7) DEFINE SYMBOLS FOR COM FILES
$!              8) LIST SETUP INFO
$!
$WRITE SYS$OUTPUT "YOU HAVE NOW ENTERED THE FANTASY WORLD OF RADIATIVE CAPTURE
$!
$!      SEE IF ONLINE OR OFFLINE ACCOUNT IS RUNNING THE FILE
$!
$ ONLINE := "N"
$ IF "''F$USER()'" .EQS. "[20,1]" THEN $ ONLINE := "Y"
$ IF "''F$USER()'" .EQS. "[21,1]" THEN $ ONLINE := "Y"
$!
$!      LOAD MSD PROGRAM
$!
$ IF ONLINE .EQS. "Y" THEN $ PUT
$!
$!      RUN TAPE SETUP COMMAND FILE
$!
$ @TAPE
$!
$!      DEALLOCATE ALL DATA AREAS
$!
$ IF P1 .NES. "RECAP" THEN $ DMEM ALL
$!
$!      SET RUN NUMBER
$!
$ OLDRUN == 1
$ IF ONLINE .EQS. "Y" THEN $ INQUIRE/GLOBAL OLDRUN "$_INITIAL RUN NUMBER "
$ OLDRUN == OLDRUN - 1
$ RN 'OLDRUN'
$ DUMPED := "Y"
$!
$!      TYPE IN TITLE
$!
$ IF ONLINE .EQS. "Y" THEN $ INQUIRE TITLE "$_EXPERIMENT TITLE"
$ TI 'TITLE'
$ IF ONLINE .EQS. "N" THEN $ GOTO ALLOC
$ BEAM := ""
$ STATE := ""
$ INQUIRE/GLOBAL BEAM  "$_BEAM (P, N, OR D) "
$!
$!      ALLOCATE DATA AREAS ACCORDING TO THE EXPERIMENT
$!
$ ALLOC:
$ UP := ""
$ DOWN := ""
$ INQUIRE/GLOBAL POLARIZE "$_POLarized or UNPOLarized"
$ IF POLARIZE .EQS. "POL" THEN $ GOTO ISPOL
$  REALPOL := "N"
$  INQUIRE INOUT "$_IN/OUT SPECTRA? (Y OR N)"
$  IF INOUT .EQS. "N" THEN $ GOTO PCONT
$   POLARIZE := "POL"
$   UP := "I"
$   DOWN := "O"
$   GOTO PCONT
$  ISPOL:
$   REALPOL := "Y"
$   UP := "U"
$   DOWN := "D"
$ IF ONLINE .EQS. "N" THEN $ GOTO PCONT
$ INQUIRE/GLOBAL STATE "$_SPIN STATE (1,2,3) "
$  PCONT:
$ INQUIRE/GLOBAL DETECTORS "$_1 DETECTOR OR 2"
$ INQUIRE/GLOBAL MONITORS  "$_HOW MANY MONITORS? (0,1,2)"
$ SCAT := "N"
$ BOXES := "N"
$  IF ONLINE .EQS. "Y" THEN $ INQUIRE/GLOBAL SCAT  "$_SCALER PROCESS? (Y OR N)"
$  IF ONLINE .EQS. "Y" THEN $ INQUIRE/GLOBAL BOXES "$_BOX DISPLAY? (Y OR N)"
$  INQUIRE/GLOBAL PICKOFF  "$_PICKOFF SCALER? (Y OR N)"
$  INQUIRE/GLOBAL BUFFERED "$_BUFFERED STORAGE? (Y OR N)"
$!
$ SCAL NEW
$  IF P1 .EQS. "RECAP" THEN $ GOTO SETUP_PROCS
$ GATE NEW
$!
$ ANEW   1 512 I*4 1D ENERGY1'UP'  NONESS
$ ANEW   2 512 I*4 1D TAC1'UP'     NONESS
$ ANEW   3 512 I*4 1D ROUT1'UP'    NONESS
$ ANEW  10 512 I*4 1D EBLAC'UP'    NONESS
$ ANEW  11 512 I*4 1D EINAC'UP'    NONESS
$ ANEW  12 512 I*4 1D EABAC'UP'    NONESS
$ ANEW  13 512 I*4 1D EBLRJ'UP'    NONESS
$ ANEW  14 512 I*4 1D EINRJ'UP'    NONESS
$ ANEW  15 512 I*4 1D EABRJ'UP'    NONESS
$ ANEW  16 512 I*4 1D E1ACC'UP'    NONESS
$ ANEW  17 512 I*4 1D T1O1'UP'     NONESS
$ ANEW  18 512 I*4 1D T1O2'UP'     NONESS
$ ANEW  19 512 I*4 1D E1CHTH       NONESS
$ ANEW  20 512 I*4 1D E1CRTH       NONESS
$ GATE  1  2
$ GATE  2  2
$ GATE  10 2
$ GATE  11 2
$ GATE  12 2
$ GATE  13 2
$ GATE  14 2
$ GATE  15 2
$ GATE  16 4  11
$ GATE  17 2
$ GATE  18 4  8888
$ GATE  19 2
$ GATE  20 4
$ GATE  21 4
$ GATE  22 4
$ GATE  23 4
$ GATE  SET 2 2   1 512 NONESS
$ GATE  SET 3 1 100 500 NONESS
$ IF MONITORS .EQ. 0 THEN $ GOTO NOMON1
$  ANEW  7 1024 I*4 1D MONITOR'UP'  NONESS
$  GATE  7 2
$ IF MONITORS .EQ. 1 THEN $ GOTO NOMON1
$  ANEW  8 1024 I*4 1D SIDEMON'UP'  NONESS
$  GATE  8 2
$ NOMON1:
$!
$ IF DETECTORS .EQ. 1 THEN $ GOTO POLAR
$!
$ ANEW   4 512 I*4 1D ENERGY2'UP'  NONESS
$ ANEW   5 512 I*4 1D TAC2'UP'     NONESS
$ ANEW   6 512 I*4 1D ROUT2'UP'    NONESS
$ ANEW  30 512 I*4 1D EBLAC'UP'    NONESS
$ ANEW  31 512 I*4 1D EINAC'UP'    NONESS
$ ANEW  32 512 I*4 1D EABAC'UP'    NONESS
$ ANEW  33 512 I*4 1D EBLRJ'UP'    NONESS
$ ANEW  34 512 I*4 1D EINRJ'UP'    NONESS
$ ANEW  35 512 I*4 1D EABRJ'UP'    NONESS
$ ANEW  36 512 I*4 1D E2ACC'UP'    NONESS
$ ANEW  37 512 I*4 1D T1O3'UP'     NONESS
$ ANEW  38 512 I*4 1D T2O3'UP'     NONESS
$ GATE  4  2
$ GATE  5  2
$ GATE  30 2
$ GATE  31 2
$ GATE  32 2
$ GATE  33 2
$ GATE  34 2
$ GATE  35 2
$ GATE  36 4  31
$ GATE  37 2
$ GATE  38 4   5
```

```
$ GATE 42 5  5
$ GATE BRT 5 2    1 512 NOMEBB
$ GATE BRT 6 1 100 500 NOMEBB
$!
$ POLAR:
$!
$ IF POLARIZE .EQS. "UNPOL" THEN $ GOTO LASTAMEM
$!
$ AMEM 51 512 I*4 1D ENERGY1'DOWN' NOMEBB
$ AMEM 52 512 I*4 1D TAC1'DOWN'    NOMEBB
$ AMEM 53 512 I*4 1D ROUT1'DOWN'   NOMEBB
$ AMEM 60 512 I*4 1D EELAC1'DOWN'  NOMEBB
$ AMEM 61 512 I*4 1D EINAC1'DOWN'
$ AMEM 62 512 I*4 1D EABAC1'DOWN'  NOMEBB
$ AMEM 63 512 I*4 1D EELRJC1'DOWN'
$ AMEM 64 512 I*4 1D EINRJC1'DOWN'
$ AMEM 65 512 I*4 1D EABRJC1'DOWN'
$ AMEM 66 512 I*4 1D T2ACC'DOWN'
$ AMEM 70 512 I*4 1D T101'DOWN'    NOMEBB
$ AMEM 71 512 I*4 1D T301'DOWN'    NOMEBB
$ AMEM 72 512 I*4 1D T301'DOWN'    NOMEBB
$ GATE 51 3  1
$ GATE 52 5  9
$ GATE 53 1 13
$ GATE 60 4 10
$ GATE 61 4 11
$ GATE 62 3 12
$ GATE 63 3 13
$ GATE 64 3 14
$ GATE 65 3 15
$ GATE 66 4 11
$ GATE 70 5  2
$ GATE 71 5  3
$ GATE 72 5  4
$ IF ONLINE .EQS. "Y" THEN $GOTO MONIT
$ AMEM 111 512 R*4 1D R1'UP' NOMEBB
$ AMEM 131 512 R*4 1D R2'UP' NOMEBB
$ AMEM 161 512 R*4 1D R1'DOWN' NOMEBB
$ AMEM 181 512 R*4 1D R2'DOWN' NOMEBB
$ GATE 111 3
$ GATE 131 3
$ GATE 161 3
$ GATE 181 3
$ MONIT:
$ IF MONITORS .EQ. 0 THEN $ GOTO NOMON2
$  AMEM 37 1024 I*4 1D MONITOR'DOWN' NOMEBB
$  GATE 37 2 7
$ IF MONITORS .EQ. 1 THEN $ GOTO NOMON2
$  AMEM 38 1024 I*4 1D SIDEMON'DOWN' NOMEBB
$  GATE 38 2 8
$ NOMON2:
$!
$ IF DETECTORS .EQ. 1 THEN $ GOTO LASTAMEM
$!
$ AMEM 54 512 I*4 1D ENERGY2'DOWN' NOMEBB
$ AMEM 55 512 I*4 1D TAC2'DOWN'    NOMEBB
$ AMEM 56 512 I*4 1D ROUT2'DOWN'   NOMEBB
$ AMEM 80 512 I*4 1D EELAC2'DOWN'  NOMEBB
$ AMEM 81 512 I*4 1D EINAC2'DOWN'
$ AMEM 82 512 I*4 1D EABAC2'DOWN'  NOMEBB
$ AMEM 83 512 I*4 1D EELRJC2'DOWN'
$ AMEM 84 512 I*4 1D EINRJC2'DOWN'
$ AMEM 85 512 I*4 1D EABRJC2'DOWN'
$ AMEM 86 512 I*4 1D T2ACC'DOWN'
$ AMEM 90 512 I*4 1D T102'DOWN'    NOMEBB
$ AMEM 91 512 I*4 1D T302'DOWN'    NOMEBB
$ AMEM 92 512 I*4 1D T302'DOWN'    NOMEBB
$ GATE 54 3  4
$ GATE 55 5  5
$ GATE 56 1  6
$ GATE 80 4 30
$ GATE 81 4 31
$ GATE 82 3 32
$ GATE 83 3 33
$ GATE 84 3 34
$ GATE 85 3 35
$ GATE 86 4 31
$ GATE 90 5  5
$ GATE 91 5  5
$ GATE 92 5  5
$!
$       ALLOCATE CONTROL TYPE DATA AREAS
$!
$ LASTAMEM:
```

```
$ AMEM 998  20 R*4 PROT_DTC-DEF  NOMEBB
$ AMEM 997 128 I*4 1D SCALERB    NOMEBB
$ AMEM 996 256 I*4 1D BOXSAVE    NOMEBB
$ AMEM 995 512 I*4 1D GATESAVE   NOMEBB
$ AMEM 555 812 R*4 1D FITSPEC    NOMEBB
$!
$       SET UP ADC SUBPROCESSES
$!
$ SETUP_PROCS:
$ IF ONLINE .EQS. "N" THEN $ GOTO SETUP_SCALERS
$ IF POLARIZE .EQS. "UNPOL" THEN $ GOTO UNPOLSET
$  EVOP BE PCP1
$   IF MONITORS .GE. 1 THEN $ EVOP BE PMON
$   IF MONITORS .EQ. 2 THEN $ EVOP BE PMN2
$   IF DETECTORS .EQ. 2 THEN $ EVOP BE PCP2
$  GOTO SETUP_SCALERS
$ UNPOLSET:
$  EVOP BE CAP1
$   IF MONITORS .GE. 1 THEN $ EVOP BE MONT
$   IF MONITORS .EQ. 2 THEN $ EVOP BE MON2
$   IF DETECTORS .EQ. 2 THEN $ EVOP BE CAP2
$!
$       SETUP SCALERS AND PRESET TASK
$!
$ SETUP_SCALERS:
$  @SCALDEF
$   IF SCAT .NES. "Y" THEN $ GOTO SETUP_BOXUSR
$   IF DETECTORS .EQ. 1 THEN $ SCAL BE SCA1
$   IF DETECTORS .EQ. 2 THEN $ SCAL BE SCA2
$!
$       SET UP BOXUSR
$!
$ SETUP_BOXUSR:
$ IF BOXES .NES. "Y" THEN $ GOTO SETUP_DTCDEF
$  BOXLINK
$  @BOX
$!
$       DEFINE SCLBUFF DEADTIME HEADERS
$!
$ SETUP_DTCDEF:
$ NUM = 'DETECTORS' + 'MONITORS'
$ DETDTC := ""
$ IF DETECTORS .EQ. 2 THEN $ DETDTC := "6 8"
$ MONDTC := ""
$ IF MONITORS .GE. 1 THEN $ MONDTC := "0 4"
$ IF MONITORS .EQ. 2 THEN $ MONDTC := "/'MONDTC' 1 13"
$ SCLBUFF DEF 'NUM' 5 2 'DETDTC' 'MONDTC'
$!
$       OFFLINE SETUP IS NOW FINISHED
$!
$ IF ONLINE .EQS. "N" THEN $ EXIT
$!
$       DEFINE BUFFERED STORAGE DEVICE NAMES
$!
$ IF BUFFERED .NES. "Y" THEN $ GOTO SYMBOLS
$  TAPE USE 5 XSYSDAT
$   IF DETECTORS .EQ. 2 THEN $ TAPE USE 6 XSYSDAT
$  SUFOPEN := "N"
$!
$       DEFINE SYMBOLS
$!
$ SYMBOLS:
$ DU*M   :== @DMP.COM
$ BE*GIN :== @BEGIN.COM
$ BU*P   :== @BEGIN.COM UP
$ BD*OWN :== @BEGIN.COM DOWN
$ BI*N   :== @BEGIN.COM UP
$ BO*UT  :== @BEGIN.COM DOWN
$ AIR    :== @AIR.COM
$ QR     :== @OLDQUENCH.COM
$!
$       CLEAN SLATE APPROACH
$!
$ CL ALL
$ SCLBUFF CLR ALL
$ SPINSTATE := 1    !  1=UP, 2=DOWN  (OR  IN/OUT)
$ IF POLARIZE .NES. "POL" THEN $ GOTO NOP
$   IF REALPOL .EQS. "N"  THEN $ GOTO NOP
$    POL NEW
$    AIR OUT
$!   SET PIB TO SPIN UP
$!   OUTPUT 1 14 0 16 8
$    ENABLE QUENCH RATIO ADC
$    CNAF 1 5 0 24
```

```
$!  UNQUENCH SOURCE
$   OUTPUT 1 14 0 16 3
$   NOP
$!
$       START LIST FILE
$!
$ LIST NEW
$ LIST DOUB
$!
$       LIST EVERYTHING ON TERMINAL
$!
$ LMEM
$ DATE LIST
$ SCAL LIST
$ TI
$ RN
$ SHOW TIME
$ WRITE SYS$OUTPUT "GOOD LUCK - SEX"
```

Tape Initialization Command File

```
$! TAPE.COM
$! WRITTEN 3/22/81
$! LAST MODIFIED 4/2/82
$!
$       TAPE SETUP COMMAND FILE
$!
$ INQUIRE/GLOBAL USETAPE "$ SET UP TAPE? (Y OR N)"
$ IF USETAPE .NES. "Y" THEN $ EXIT
$  INQUIRE UNIT  "$ DATA TAPE UNIT? (MTA0: OR MTA1:)"
$  INQUIRE LABEL "$ DATA TAPE LABEL? (DTnnnn)"
$  ALLOCATE 'UNIT' TA
$  INQUIRE INIT "$ INITIALIZE TAPE? (Y OR N)"
$  IF INIT .NES. "Y" THEN $ GOTO MNT
$   INQUIRE REALLY "$ DO YOU REALLY WANT TO?  ANY OLD DATA WILL BE LOST"
$   IF REALLY .NES. "Y" THEN $ GOTO MNT
$    INQUIRE DENS "$ TAPE DENSITY? (800 SURPLUS, 1600 GOOD)"
$    INITIALIZE/DENSITY='DENS' 'UNIT' 'LABEL'
$!
$MNT:
$ MOUNT /DATA_CHECK=WRITE 'UNIT' 'LABEL' TA
```

Box Display Initialization Command File

```
$  BOX U
$  BOX F 2 'DETECTORS'
$  BOX F 3 'MONITORS'
$  BOX F 4 'REALPOL'
$  BOX F 5 I 00
$  BOX F 7 'BEAM'
$  BOX F 8 'STATE'
$  BOX F I 00
```

Box Display Subroutine

```
      SUBROUTINE BOXUSR
C
C  MOST VARIABLES ARE NAMED WITH THE FOLLOWING PATTERN:
C
C                   t_c_name_I
C
C  WHERE
C  t    = TYPE       A=REAL, I=INTEGER, C=CHARACTER
C  c    = CATEGORY,  O=OLD, N=NEW, D=DIFFERENCE
C  name = SCALER NAME
C  I    = LOOP       NUMBER OF DISPLAY LOOP
C
C**** MAP TO XSCOM
C
      INCLUDE 'XSYSDIR:XSCOM.FOR/NOLIST'
C
      CHARACTER*8  BXLABEL(36),BXCHAR(36)
      CHARACTER*32 BXMESS(10)
      CHARACTER*4  BXFLAG(32)
      COMMON       /BOXSAVE/BXLABEL,BXCHAR,BXMESS,BXFLAG
      REAL*4       RFLAG(32),X
      INTEGER*4    IFLAG(32)
      LOGICAL*4    LFLAG(32)
      BYTE         BFLAG(128)
      EQUIVALENCE  (BXFLAG(1),BFLAG(1)),(RFLAG(1),BFLAG(1))
      EQUIVALENCE  (IFLAG(1),BFLAG(1)),(LFLAG(1),BFLAG(1))
      CHARACTER*8  C_TIME,C_R_ACC1,C_R_ACC2,C_R_TOTACC1,C_R_TOTACC2
      CHARACTER*2  C_HOUR,C_MIN,C_SEC
      CHARACTER*32 AYMESS
C
C**** SAVE VARIABLES BETWEEN SUBROUTINE CALLS
C
      SAVE I_O_NAI1,I_O_NAI2,I_O_PHLD1,I_O_PHLD2,
     | I_O_NAI1_2,I_O_NAI2_2,I_O_PHLD1_2,I_O_PHLD2_2,
     | A_O_ACC1,A_O_ACC2,A_O_COIN1,A_O_COIN2,A_O_ACC1_2,A_O_ACC2_2,
     | I_O_TIME,I_O_TIME_1,I_O_TIME_2,I_O_PRESET,
     | LOOP_1,LOOP_2,I_O_SEC
      LOGICAL FIRST/.TRUE./
C
C**** PERFORM INITIAL LABELING AFTER THE FLAGS HAVE BEEN SET.
C
      IF (FIRST) THEN
       IF (BXFLAG(1).EQ.'    ') RETURN
       CALL BOXLABEL( 9,'REM TIME')
       CALL BOXLABEL(10,'LIVETIME')
       IF ((IFLAG(3).GE.1).CALL BOXLABEL(20,'DTC ONON')
       IF ((IFLAG(3).GE.2) CALL BOXLABEL(18,'DTC ONON')
       CALL BOXLABEL(13,'RUN  NUM')
       CALL BOXLABEL(28,'INT PRES')
C
       CALL BOXLABEL( 1,'ACC1  CR')
       CALL BOXLABEL(21,'NaI1  CR')
       CALL BOXLABEL(22,'PHLD1 CR')
       CALL BOXLABEL(23,'TACC1 CR')
       CALL BOXLABEL(34,'DTC DET1')
       CALL BOXLABEL(35,'RELV TM1')
       CALL BOXLABEL(24,'T RELV 1')
       CALL BOXLABEL(27,'EVACTR 1')
C
       IF (IFLAG(2).EQ.2) THEN
        CALL BOXLABEL( 2,'ACC2  CR')
        CALL BOXLABEL(29,'NaI2  CR')
        CALL BOXLABEL(30,'PHLD2 CR')
        CALL BOXLABEL(31,'TACC2 CR')
        CALL BOXLABEL(32,'DTC DET2')
        CALL BOXLABEL(33,'RELV TM2')
        CALL BOXLABEL(34,'T RELV 2')
        CALL BOXLABEL(33,'EVACTR 2')
       ENDIF
       FIRST = .FALSE.
      ENDIF
C
C**** UPDATE EVAL EVENT COUNTERS
C
      IEVACTR6 = EVACTR(6)
      IEVACTR7 = EVACTR(7)
      CALL BOXINTEG(27,IEVACTR6)
      IF (IFLAG(2).EQ.2) CALL BOXINTEG(35,IEVACTR7)
C
C**** DISPLAY TIME IN HOURS, MINUTES, AND SECONDS
C
      I_N_TIME = SCLREAD(7)
      IHOUR = I_N_TIME/36000
      CALL OTSCVT_I_TI(IHOUR,C_HOUR,%VAL(1))
      MIN = (I_N_TIME-(IHOUR*36000))/600
      CALL OTSCVT_I_TI(MIN,C_MIN,%VAL(2))
      ISEC = (I_N_TIME-(IHOUR*36000)-(MIN*600))/10
      CALL OTSCVT_I_TI(ISEC,C_SEC,%VAL(2))
      C_TIME = C_HOUR//':'//C_MIN//':'//C_SEC
      CALL BOXCHAR(10,C_TIME)
C
C**** DISPLAY PROJECTED TIME UNTIL COMPLETION OF RUN
C
      I_N_PRESET = SCLREAD(12)
      A_N_PRESET = I_N_PRESET
      A_D_PRESET = I_N_PRESET-I_O_PRESET
      A_D_TIME   = I_N_TIME-I_O_TIME
      I_O_TIME   = I_N_TIME
      I_O_PRESET = I_N_PRESET
      IF (A_D_PRESET.EQ.0) GOTO 100
      CALL LIBSINT_OVER(0)
      I_RTIME = -A_N_PRESET*(A_D_TIME/A_D_PRESET)
      CALL LIBSINT_OVER(1)
      IHOUR = I_RTIME/36000
      CALL OTSCVT_I_TI(IHOUR,C_HOUR,%VAL(1))
      MIN = (I_RTIME-(IHOUR*36000))/600
```

```
      CALL OTS@CVT_L_TI(MIN,C_MIN,%VAL(2))
      ISEC = (I_RTTME-(IHOUR*3600)-(MIN*600))/10
      CALL OTS@CVT_L_TI(ISEC,C_SEC,%VAL(2))
      C_TIME = C_HOUR//':'//C_MIN//':'//C_SEC
      CALL BOXCHAR(9,C_TIME)
C
C**** CHECK FOR NEW RUN
C
  100 IF (BCLREAD(1).LT.I_O_BCI) THEN
       I_O_BCI = 0
       LOOP_1 = 0
       LOOP_2 = 0
       I_O_NAI1   = 0
       I_O_BHLD1  = 0
       I_O_NAI2   = 0
       I_O_BHLD2  = 0
       A_O_ACC1   = 0
       A_O_COIN1  = 0
       A_O_ACC2   = 0
       A_O_COIN2  = 0
       I_O_TIME_1   = 0
       I_O_NAI1_2   = 0
       I_O_BHLD1_2  = 0
       I_O_NAI2_2   = 0
       I_O_BHLD2_2  = 0
       A_O_ACC1_2   = 0
       A_O_ACC2_2   = 0
       I_O_TIME_2   = 0
       CALL BOXREAL(1,0)
       CALL BOXINTEG(21,0)
       CALL BOXINTEG(22,0)
       CALL BOXREAL(23,0)
       CALL BOXINTEG(25,0)
       CALL BOXINTEG(26,0)
       IF (IFLAG(2).EQ.2) THEN
        CALL BOXREAL(2,0)
        CALL BOXINTEG(29,0)
        CALL BOXINTEG(33,0)
        CALL BOXREAL(31,0)
        CALL BOXINTEG(33,0)
        CALL BOXINTEG(34,0)
       ENDIF
       IF (BXFLAG(4).EQ.'Y    ') THEN
        AY=0.
        AYERR=1.
        ENCODE(32,1000,AYMESS) AY,AYERR
        CALL BOXMESS(2,AYMESS)
        ARU=0.
        ALU=0.
        ARD=0.
        ALD=0.
        IARU=ARU
        IARD=ARD
        IALU=ALU
        IALD=ALD
        ENCODE(32,2000,AYMESS)IARU,IALU,IARD,IALD
        CALL BOXMESS(4,AYMESS)
       ENDIF
      ELSE
       I_O_BCI = BCLREAD(1)
      ENDIF
C
C**** INCREMENT AND CHECK LOOP COUNTER
C
      LOOP_1 = LOOP_1+1
      IF (LOOP_1.LE.5) RETURN
      LOOP_1 = 0
C
C**** GET COINCIDENCE COUNTS
C
      A_N_ACC1   = BCLREAD(3)
      A_N_COIN1  = BCLREAD(4)
      A_N_ACC2   = BCLREAD(11)
      A_N_COIN2  = BCLREAD(10)
      A_D_ACC1   = A_N_ACC1 -A_O_ACC1
      A_D_COIN1  = A_N_COIN1-A_O_COIN1
      A_D_ACC2   = A_N_ACC2 -A_O_ACC2
      A_D_COIN2  = A_N_COIN2-A_O_COIN2
      A_O_ACC1   = A_N_ACC1
      A_O_COIN1  = A_N_COIN1
      A_O_ACC2   = A_N_ACC2
      A_O_COIN2  = A_N_COIN2
C
C**** CALCULATE AND DISPLAY ACCIDENTAL RATES
C
      IF (A_D_COIN1.EQ.0..OR.A_D_COIN2.EQ.0.
     1 .OR.A_N_COIN1.EQ.0..OR.A_N_COIN2.EQ.0.) GOTO 300
      A_R_ACC1 = (A_D_ACC1/A_D_COIN1)*100.
      A_R_ACC2 = (A_D_ACC2/A_D_COIN2)*100.
      CALL FOR@CVT_D_TF(A_R_ACC1,C_R_ACC1,%VAL(1))
      CALL FOR@CVT_D_TF(A_R_ACC2,C_R_ACC2,%VAL(1))
      DO 200 I=1,6
       C_R_ACC1(I:I) = C_R_ACC1(I+2:I+2)
  200 C_R_ACC2(I:I) = C_R_ACC2(I+8:I+8)
      C_R_ACC1(7:7) = ' '
      C_R_ACC2(7:7) = ' '
      C_R_ACC1(8:8) = '%'
      C_R_ACC2(8:8) = '%'
      CALL BOXCHAR(1,C_R_ACC1)
      IF (IFLAG(2).EQ.2) CALL BOXCHAR(2,C_R_ACC2)
      A_R_TOTACC1 = (A_N_ACC1/A_N_COIN1)*100.
      A_R_TOTACC2 = (A_N_ACC2/A_N_COIN2)*100.
C
      CALL FOR@CVT_D_TF(A_R_TOTACC1,C_R_TOTACC1,%VAL(2))
      CALL FOR@CVT_D_TF(A_R_TOTACC2,C_R_TOTACC2,%VAL(2))
      CALL BOXCHAR(7,C_R_TOTACC1)
      IF (IFLAG(2).EQ.2) CALL BOXCHAR(31,C_R_TOTACC2)
C
C**** DO SLOWEST UPDATE LOOP
C
  300 LOOP_2 = LOOP_2+1
      IF (LOOP_2.LE.6) GOTO 400
      LOOP_2 = 0
C
C**** GET NUMBER OF DETECTOR COUNTS
C
      I_N_NAI1   = BCLREAD(2)
      I_N_BHLD1  = BCLREAD(5)
      I_N_NAI2   = BCLREAD(8)
      I_N_BHLD2  = BCLREAD(9)
      I_D_NAI1   = I_N_NAI1  -I_O_NAI1
      I_D_BHLD1  = I_N_BHLD1 -I_O_BHLD1
      I_D_NAI2   = I_N_NAI2  -I_O_NAI2
      I_D_BHLD2  = I_N_BHLD2 -I_O_BHLD2
      A_O_NAI1   = I_O_NAI1
      A_O_BHLD1  = I_O_BHLD1
      A_O_NAI2   = I_O_NAI2
      A_O_BHLD2  = I_O_BHLD2
      I_O_NAI1   = I_N_NAI1
      I_O_BHLD1  = I_N_BHLD1
      I_O_NAI2   = I_N_NAI2
      I_O_BHLD2  = I_N_BHLD2
C
      I_D_TIME_1 = I_N_TIME-I_O_TIME_1
      A_D_TIME_1 = I_D_TIME_1
      I_O_TIME_1 = I_N_TIME
C
C**** CALCULATE AND DISPLAY DETECTOR COUNT RATES
C
      IF (I_D_TIME_1.EQ.0) GOTO 400
      I_R_NAI1   = (A_D_NAI1*10.)/I_D_TIME_1
      I_R_BHLD1  = (A_D_BHLD1*10000.)/I_D_TIME_1
      I_R_NAI2   = (A_D_NAI2*10.)/I_D_TIME_1
      I_R_BHLD2  = (A_D_BHLD2*10000.)/I_D_TIME_1
      CALL BOXINTEG(21,I_R_NAI1)
      CALL BOXINTEG(22,I_R_BHLD1)
      IF (IFLAG(2).EQ.2) THEN
       CALL BOXINTEG(29,I_R_NAI2)
       CALL BOXINTEG(30,I_R_BHLD2)
      ENDIF
      IF ((BXFLAG(6)(1:2).EQ.'ON'.OR.BXFLAG(6)(1:2).EQ.'on').AND.
     . (I_R_NAI1.EQ.0.OR.I_R_BHLD1.EQ.0.OR.(IFLAG(2).EQ.2.AND.
     . (I_R_NAI2.EQ.0.OR.I_R_BHLD2.EQ.0)))) THEN
       CALL BLAST('Warning: A scaler has quit counting!')
       CALL STOP(MODCHAN)
      ENDIF
C
C**** CALCULATE AND DISPLAY RESOLVING TIMES
C
  400 A_D_NAI1_2  = I_N_NAI1 -I_O_NAI1_2
      A_D_BHLD1_2 = I_N_BHLD1-I_O_BHLD1_2
      A_D_NAI2_2  = I_N_NAI2 -I_O_NAI2_2
      A_D_BHLD2_2 = I_N_BHLD2-I_O_BHLD2_2
      A_N_NAI1    = I_N_NAI1
      A_N_BHLD1   = I_N_BHLD1
      A_N_NAI2    = I_N_NAI2
      A_N_BHLD2   = I_N_BHLD2
      I_O_NAI1_2  = I_N_NAI1
```

```
      I_O_SHLD1_2 = I_N_SHLD1
      I_O_NAI2_2 = I_N_NAI2
      I_O_SHLD2_2 = I_N_SHLD2
      A_O_ACC1_2 = A_N_ACC1-A_O_ACC1_3
      A_O_ACC2_2 = A_N_ACC2-A_O_ACC2_3
      A_O_ACC1_3 = A_N_ACC1
      A_O_ACC2_3 = A_N_ACC2
      A_N_TIME = I_N_TIME
      A_O_TIME_2 = I_N_TIME-I_O_TIME_2
      I_O_TIME_2 = I_N_TIME
      DEN1 = A_O_NAI1_2*A_O_SHLD1_2
      DEN2 = A_O_NAI2_2*A_O_SHLD2_2
      DEN3 = A_N_NAI1*A_N_SHLD1
      DEN4 = A_N_NAI2*A_N_SHLD2
      IF (DEN1.EQ.0..OR.DEN3.EQ.0.
     1  OR.DEN2.EQ.0..OR.DEN4.EQ.0.) GOTO 500
      !RESTIM1 = (A_O_ACC1_2*A_O_TIME_2*1.E3)/DEN1
      !RESTIM2 = (A_O_ACC2_2*A_O_TIME_2*1.E3)/DEN2
      !TOTRT1 = (A_N_ACC1*A_N_TIME*1.E3)/DEN3
      !TOTRT2 = (A_N_ACC2*A_N_TIME*1.E3)/DEN4
      CALL BOXINTEG(23,!RESTIM1)
      CALL BOXINTEG(24,!TOTRT1)
      IF (IFLAG(2).EQ.2) THEN
       CALL BOXINTEG(33,!RESTIM2)
       CALL BOXINTEG(34,!TOTRT2)
      ENDIF
C
C**** DISPLAY ANALYZING POWER
C
  500 IF (BXFLAG(4).EQ.'Y   ') THEN
       CALL SHORTSUM(14,1,ARU)
       CALL SHORTSUM(34,1,ALU)
       CALL SHORTSUM(44,1,ARD)
       CALL SHORTSUM(84,1,ALD)
C
C*****  CALCULATE BEAM POLARIZATION
C
       QR=POL_BEAM
       IF (QR.EQ.0.) QR = .43
       IF (BXFLAG(7).EQ.'N   ') THEN
         P= 94/(.12+(1./QR))
       ELSE
         IF((BXFLAG(7).EQ.'P   ').OR.(BXFLAG(7).EQ.'D   ')) THEN
           IF(IFLAG(8).EQ.3) THEN
             P= -.6447*QR
           ELSE
             P = QR
           ENDIF
         ELSE
           CALL BLAST('WARNING: BEAM FLAG IS INCORRECT')
           P=QR
         ENDIF
       ENDIF
       !ARU=ARU
       !ARD=ARD
       !ALU=ALU
       !ALD=ALD
       ENCODE(32,2000,AYMESS) !ARU, !ALU, !ARD, !ALD
 2000  FORMAT ('Q+: ',I4,' N+: ',I4,' D-: ',I4,' N-: ',I4)
       CALL BOXMESS(4,AYMESS)
       IF (ARU.EQ.0.0.AND.ALU.EQ.0.0.AND.ARD.EQ.0.0.AND.ALD.EQ.0.0) THEN
        AY=0.
        AYERR=1
       ELSEIF (ARU.EQ.0.0.AND.ALU.EQ.0.0) THEN
        X=ARD-RFLAG(5)*ALD
        Y=ARD+RFLAG(5)*ALD
        AY=(1./P)*(X/Y)
        AYERR=(1./P)*SQRT(((1.-(X/Y))*SQRT(ARD))**2+
                          ((1.-(X/Y))*SQRT(ALD)*RFLAG(5))**2)/Y
       ELSEIF (ARD.EQ.0.0.AND.ALD.EQ.0.0) THEN
        X=ALU-RFLAG(5)*ARU
        Y=ALU+RFLAG(5)*ARU
        AY=(1./P)*(X/Y)
        AYERR=(1./P)*SQRT(((1.-(X/Y))*SQRT(ARU))**2+
                          ((1.-(X/Y))*SQRT(ALU)*RFLAG(5))**2)/Y
       ELSE
        IF (ARU.EQ.0.) ARU=.1
        IF (ALU.EQ.0.) ALU=.1
        IF (ARD.EQ.0.) ARD=.1
        IF (ALD.EQ.0.) ALD=.1
        R=SQRT((ALU*ARD)/(ALD*ARU))
        AY=(1./P)*((R-1.)/(R+1.))
        SUM=(1./ALU)+(1./ARD)+(1./ALD)+(1./ARU)
        AYERR=(1./P)*((R/((R+1.)*(R+1.)))*SQRT(SUM))
       ENDIF
       ENCODE(32,1000,AYMESS) AY,AYERR
 1000  FORMAT(' Total Ay = ',F6.3,' +/-',F6.3)
       CALL BOXMESS(2,AYMESS)
      ENDIF
C
C**** DISPLAY DEAD TIME CORRECTIONS
C
  600 IF (IFLAG(3).GE.1) CALL BOXREAL(20,DTC(1))
      IF (IFLAG(3).GE.2) CALL BOXREAL(16,DTC(2))
      CALL BOXREAL(24,DTC(4))
      IF (IFLAG(2).EQ.2) CALL BOXREAL(32,DTC(7))
C
C**** DRAW MISC VALUES ON SCREEN
C
      CALL BOXINTEG(12,X_RUN)
      CALL BOXINTEG(28,PRESET)
C
C**** FINISHED
C
      RETURN
      END
```

Box Flag Initialization Routine

```
C XBFLAG
C Michael Wright
C March 1982
C
C Set flags in XSCOM for use by BOXUSR
C
C NOTE: This program is not strictly XSYS compatible since it uses
C X_FLAGS in an unauthorized manner.
C
      INCLUDE 'XSYSDIR:XSCOM.FOR/NOLIST'
      INCLUDE 'XSYSDIR:XERRDEF.FOR/NOLIST'
      LOGICAL*1 L_FLAGS(32),FLAG
      EQUIVALENCE (L_FLAGS,X_FLAGS)
C
C**** MAP X_SCOM GLOBAL SECTION
C
      CALL MGBLSC(XLOC(X_BUF),40,'XSCOM',0,0,X_ERR)
      IF (X_ERR.GT.1) CALL XBPERR(%VAL(X_ERR),'BFLAG',X_MERR)
C
C**** GET ARGUMENTS
C
      CALL PARSE
C
C**** SET THE APPROPRIATE FLAG
C
      IF (X_I1.EQ.'T ') THEN
       FLAG = .TRUE.
      ELSEIF (X_I1.EQ.'F ') THEN
       FLAG = .FALSE.
      ELSE
       CALL XERROR(XERR_CMNDERR,'BFLAG',0)
      ENDIF
      IF (X_N1.LE.21.OR.X_N1.GT.32)
       CALL XERROR(XERR_CMNDERR,'BFLAG',0)
      L_FLAGS(X_N1) = FLAG
C
C**** FINISHED
C
      CALL EXIT
      END
```

Air Stop Control Command File

```
$!            AIR.COM
$!
$!    THIS COMMAND FILE IS USED TO TAKE THE AIR STOP IN OR OUT
$!
$ IF P1 .EQS. "IN" THEN $ OUTPUT 1 14 1 16 2
$ IF P1 .EQS. "OUT" THEN $ OUTPUT 1 14 0 16 2
```

Beam Polarization Quench Ratio Measurement

```
$ !      OLDQUENCH.COM
```

```
$!
$!      THIS COMMAND FILE IS USED TO TAKE A QUENCH
$!      RATIO USING THE OLD PIB COMPUTER LINK.
$!
$ POL ADC 5 0 0 14 1 500 2 3 20.  'ENGY'
```

Scaler Definition Command File

```
$!  SCALDEF.COM
$!  APRIL 1982
$!
$!  THIS COMMAND FILE DEFINES THE SCALERS USED BY THE CAPTURE
$!  GROUP DATA ACQUISITION SYSTEM.  IT IS CALLED INITIALLY BY CAP.COM
$!  AND MAY BE CALLED BY HAND LATER IN THE RUN IF THE SCALERS NEED TO
$!  BE CHANGED.
$!
$   SHEAD  := ""
$   SBOX   := ""
$   PHEAD  := ""
$   PBOX   := ""
$   IF DETECTORS .EQ. 1 THEN GOTO SCAL1
$
$   SCAL HEAD 1 BCI  NaI1 SHLD1 COIN1 ACC1 MONITOR
$   SCAL BOX  1  4     5     6     7    8     19
$   SCAL HEAD 2 TIME NaI2 SHLD2 COIN2 ACC2 PRESET
$   SCAL BOX  2  11    13    14    15   16    3
$   SCAL NUMB 1 17 1 2 3 4 5 6 KB3610
$   SCAL NUMB 1 18 1 2 3 4 5   KB3610
$   SCAL NUMB 1 16 1 REGISTER
$   IF MONITORS .NE. 2 THEN $ GOTO NOSIDE
$    SHEAD  = $IDEMON
$    SBOX   = 17
$    SCAL NUMB 1 18 6 KB3610
$    NOSIDE:
$   IF PICKOFF .NES. "Y" THEN GOTO NOPICK
$    PHEAD  = PICKOFFS
$    PBOX   = 34
$    SCAL NUMB 1 15 1 KB3610
$    NOPICK:
$   SCAL HEAD 3 'SHEAD' 'PHEAD'
$   SCAL BOX  3 'SBOX'  'PBOX'
$   EXIT
$
$  SCAL1:
$   SCAL HEAD 1 BCI NaI1 SHLD1 COIN1 ACC1 MONITOR
$   SCAL BOX  1  4     5     6     7    8     19
$   SCAL HEAD 2 TIME PRESET
$   SCAL BOX  2  11    3
$   SCAL NUMB 1 17 1 2 3 4 5 6 KB3610
$   SCAL NUMB 1 18 1 KB3610
$   SCAL NUMB 1 16 1 REGISTER
$   IF MONITORS .NE. 2 THEN $ GOTO NOSIDE2
$    SHEAD  = $IDEMON
$    SBOX   = 17
$    SCAL NUMB 1 18 2 KB3610
$    NOSIDE2:
$   IF PICKOFF .NES. "Y" THEN GOTO NOPICK2
$    PHEAD  = PICKOFFS
$    PBOX   = 34
$    SCAL NUMB 1 18 2 KB3610
$    NOPICK2:
$    SCAL HEAD 2 TIME PRESET 'SHEAD' 'PHEAD'
$    SCAL BOX  2 11    3     'SBOX'  'PBOX'
```

Begin Command File

```
$!  BEGIN.COM
$!  WRITTEN FALL 1981
$!  LAST MODIFIED 5/9/83
$!
$!      BEGIN RUN WITH CLEAR OPTION FOR ONE OR TWO DETECTORS,
$!      POLARIZED OR UNPOLARIZED
$!
$!      WRITTEN BY STEVEN KING AND MICHAEL WRIGHT
$!
$!      CHECK FOR POLARIZED SPIN STATES
$!
$ IF P1  EQS. "UP"   THEN $ GOTO SPINUP
$ IF P1  EQS. "DOWN" THEN $ GOTO SPINDOWN
$!
$!      BEGIN UNPOLARIZED RUN FOR 1 OR 2 DETECTORS
$!      CLEAR MOST DATA AREAS IF P1 = "C"
$!      CLEAR EVERYTHING IF P2 = "A"
$!
$ IF P1       NES. "C" THEN $ GOTO SCAL
$ IF DUMPED  EQS. "Y" THEN $ GOTO CLEAROK
$  INQUIRE CLEARQ "$ RUN NOT DUMPED, IS CLEAR OK (Y OR N)"
$  IF CLEARQ .NES. "Y" THEN $ EXIT
$  CLEAROK:
$!
$!      CLEAR EVERYTHING
$!
$ IF P2 .NES. "A" THEN GOTO UNCLEAR
$  CL ALL
$  SCAL CLEAR ALL
$  SCLBUFF CLR ALL
$  IF REALPOL .EQS. "Y" THEN $ POL NEW
$  GOTO START
$!
$!      CLEAR ALL NONACCUMULATED DATA AREAS
$!
$ UNCLEAR:
$ CL   1,15  NOMESS
$ CL  19,35  NOMESS
$ CL  39,45  NOMESS
$ CL  47,85  NOMESS
$ CL  89,115 NOMESS
$ CL 119,135 NOMESS
$ CL 139,165 NOMESS
$ CL 169,185 NOMESS
$ CL 189,199
$!
$!      CLEAR ALL SCALERS
$!
$ SCAL:
$  SCAL CLEAR ALL
$  GOTO START
$!
$!      BEGIN UP (+) SPIN STATE RUN
$!      CLEAR DOWN SPIN STATE DATA AREAS IF P2 = "C"
$!      CLEAR EVERYTHING IF P3 = "A"
$!
$ SPINUP:
$ IF P2       NES. "C" THEN $ GOTO SUCLEAROK
$ IF DUMPED  EQS. "Y" THEN $ GOTO SUCLEAROK
$  INQUIRE CLEARQ "$ RUN NOT DUMPED, IS CLEAR OK (Y OR N)"
$  IF CLEARQ .NES. "Y" THEN $ EXIT
$  SUCLEAROK:
$
$ SPINSTATE == 1
$ IF REALPOL .EQS. "N" THEN $ GOTO NOTREALUP
$  OUTPUT 1 14 0 16 8
$  WAIT 00:00:05
$  NOTREALUP:
$!
$ IF P3 .NES. "C" THEN $ GOTO SUBCAL
$ IF P3 .NES. "A" THEN GOTO SUCLEAR
$  CL ALL
$  SCLBUFF CLR ALL
$  IF REALPOL .EQS. "Y" THEN $ POL NEW
$  GOTO SUBCAL
$!
$!      CLEAR SPIN UP NONACCUMULATED DATA AREAS
$!
$ SUCLEAR:
$ CL   1,15  NOMESS
$ CL  19,35  NOMESS
$ CL  39,49  NOMESS
$ CL 101,115 NOMESS
$ CL 119,135 NOMESS
$ CL 139,149
$!
$!      CLEAR SCALERS AND SET EVOP VARIABLES
$!
$ SUBCAL:
$ SCAL CLEAR ALL
$ IF MONITORS .GE. 1 THEN $ EVOP VARSET SPIN 0 1
$ IF MONITORS .EQ. 2 THEN $ EVOP VARSET SPIN 1 1
$ IF DETECTORS .EQS. "1" THEN $ GOTO SU1S
$  EVOP VARSET SPIN 5 1
$  EVOP VARSET SPIN 6 1
```

```
 GOTO START
BU18:
 EVOP VARSET SPIN 5 1
 GOTO START

      BEGIN DOWN (-) SPIN STATE RUN
      CLEAR DOWN SPIN STATE DATA AREAS IF P2 = "C"
      CLEAR EVERYTHING IF P3 = "A"
      SET SPIN DIRECTION TO DOWN

SPINDOWN:
IF P2  .NES. "C" THEN $ GOTO $DCLEAROK
IF DUMPED .EQS. "Y" THEN $ GOTO $DCLEAROK
 INQUIRE CLEARQ "$ RUN NOT DUMPED, IS CLEAR OK (Y OR N)"
 IF CLEARQ .NES. "Y" THEN $ EXIT
 $DCLEAROK:

SPINSTATE == 2
IF REALPOL .EQS. "N" THEN $ GOTO NOTREALDOWN
 OUTPUT 1 14 1 14 8
 WAIT 00:00.08
 NOTREALDOWN:

IF P2 .NES. "C" THEN $ GOTO $DSCAL
IF P3 .NES. "A" THEN GOTO $DCLEAR
 CL ALL
 SCAL CLEAR ALL
 SCLBUFF CLR ALL
 IF REALPOL .EQS. "Y" THEN $ POL NEW
 GOTO $DSCAL

      CLEAR SPIN DOWN NONACCUMULATED DATA AREAS

$DCLEAR:
CL  51,65  NOMESS
CL  69,85  NOMESS
CL  89,99  NOMESS
CL 151,165 NOMESS
CL 169,185 NOMESS
CL 189,199

      CLEAR SCALERS AND SET EVOP VARIABLES

$DSCAL:
SCAL CLEAR ALL
IF MONITORS .GE. 1 THEN $ EVOP VARSET SPIN 0 0
IF MONITORS .EQ. 2 THEN $ EVOP VARSET SPIN 1 0
IF DETECTORS .EQS. "1" THEN $ GOTO $D1S
 EVOP VARSET SPIN 5 0
 EVOP VARSET SPIN 6 0
 GOTO START
$D1S:
 EVOP VARSET SPIN 5 0
 GOTO START

      INCREMENT RUN NUMBER AND START

START:
 RN I

      PROCESS BUFFERED TAPE

 IF BUFFERED .NES. "Y" THEN $ GOTO NOBUFF
  IF P1 .EQS. "USE" THEN $ GOTO NOBUFF
  IF P2 .EQS. "USE" THEN $ GOTO NOBUFF
  IF P3 .EQS. "USE" THEN $ GOTO NOBUFF
  IF P4 .EQS. "USE" THEN $ GOTO NOBUFF
      VERIFY RUN NUMBER (FOR BUFFERED FILE NAME)
   NEWRUN = F$LOGICAL("XRUN")
   OLDRUN1 = OLDRUN + 1
   IF NEWRUN .EQ. OLDRUN1 THEN $ GOTO RNOK
   INQUIRE RUNQ "$ IS RUN NUMBER ''NEWRUN' OK (Y OR N)"
   IF RUNQ .EQS. "Y" THEN $ GOTO RNOK
   INQUIRE RUNQ "$_DESIRED RUN NUMBER"
   RN 'RUNQ'
   RNOK:
  IF BUFOPEN .EQS. "N" THEN $ GOTO NOTOPEN
   TAPE CLOSE 5
   IF DETECTORS .EQ. 2 THEN $ TAPE CLOSE 6
   DELETE * EVN;*
   NOTOPEN:
  TAPE OPEN 5 'INITSIZE'
  IF DETECTORS .EQ. 2 THEN $ TAPE OPEN 6 'INITSIZE'
  BUFOPEN := "Y"
  GOTO FINALLY
  NOBUFF:
  BUFOPEN := "N"

FINALLY:
 START NEW
 TI
 DUMPED := "N"
```

Dump Command File

```
! DMP.COM
! WRITTEN FALL 1981
! LAST MODIFIED 10/21/82
!
! THIS COMMAND FILE DUMPS THE DATA AND XSCOM TO TAPE AND DISK AND
! PRINTS RANDOM INFORMATION ON THE CONSOLE
!
      VERIFY RUN NUMBER
!
NEWRUN = F$LOGICAL("XRUN")
OLDRUN1 = OLDRUN + 1
IF NEWRUN .EQ. OLDRUN1 THEN $ GOTO RNOK
INQUIRE RUNQ "$ IS RUN NUMBER ''NEWRUN' OK (Y OR N)"
IF RUNQ .EQS. "Y" THEN $ GOTO RNOK
INQUIRE RUNQ "$_DESIRED RUN NUMBER"
RN 'RUNQ'
NEWRUN = RUNQ
RNOK:
OLDRUN == NEWRUN

TI
RN
!
      CHECK SECOND DUMP OPTION
!
IF P1 .EQS. "ONLY" THEN GOTO WRITE
!
      READ SCALERS AND DEADTIMES
!
SCAL READ ALL
LIST HEAD
LIST SING
LIST SCAL LAST ALL NOMESS
 EVOP DTC
LIST DTC NOMESS
!
      TRANSFER OLD SCALERS TO OLDSCALER BUFFER AND TO DATA AREA 997
!
SCLBUFF ADD 'SPINSTATE'
SCAL SAVE 3
SCLBUFF SAVE 997
LIST SCLBUFF 'SPINSTATE' NOMESS
IF POLARIZE .EQS. "POL" THEN $ LIST POL NOMESS
!
      SAVE SCALER DISPLAY BOXES
!
IF BOXES .EQS. "Y" THEN $ BOX P
IF BOXES .EQS. "Y" THEN $ BOX U 996
!
      SAVE GATES
!
GATE SAVE 995
LIST GATE HEAD
!
      SUM PEAKS
!
IF POLARIZE .EQS. "UNPOL" THEN $ GOTO UNPOL
IF SPINSTATE .EQ. 1 THEN $ GOTO UNPOL
 LIST GATE 61 ! ! NOMESS
 LIST GATE 64 ! ! NOMESS
 SUM 61 0 ! ! SHORT
 SUM 64 0 ! ! SHORT
 IF DETECTORS .EQ. 2 THEN $ SUM 81 0 ! ! SHORT
 IF DETECTORS .EQ. 2 THEN $ SUM 84 0 ! ! SHORT
 IF MONITORS .GE. 1 THEN $ SUM 57 0 ! ! SHORT
 IF MONITORS .EQ. 2 THEN $ SUM 58 0 ! ! SHORT
 IF DETECTORS .EQ. 2 THEN $ LIST GATE 81 1 NOMESS
```

```
$  IF DETECTOR$ .EQ. 2 THEN $ LIST GATE 34  1 NOMESS
$  IF MONITOR$  .EQ. 1 THEN $ LIST GATE 37  1 NOMESS
$  IF MONITOR$  .EQ. 2 THEN $ LIST GATE 38  1 NOMESS
$  LIST DOUB
$  GOTO CLOSE
$ UNPOL:
$  LIST GATE 11  1 NOMESS
$  LIST GATE 14  1 NOMESS
$  SUM 11 0 1 1 SHORT
$  SUM 14 0 1 1 SHORT
$  IF DETECTOR$ .EQ. 2 THEN $ LIST GATE 31  1 NOMESS
$  IF DETECTOR$ .EQ. 2 THEN $ LIST GATE 34  1 NOMESS
$  IF MONITOR$  .EQ. 1 THEN $ LIST GATE 7   1 NOMESS
$  IF MONITOR$  .EQ. 2 THEN $ LIST GATE 8   1 NOMESS
$  IF DETECTOR$ .EQ. 2 THEN $ SUM 31 0 1 1 SHORT
$  IF DETECTOR$ .EQ. 2 THEN $ SUM 34 0 1 1 SHORT
$  IF MONITOR$  .EQ. 1 THEN $ SUM  7 0 1 1 SHORT
$  IF MONITOR$  .EQ. 2 THEN $ SUM  8 0 1 1 SHORT
$  LIST DOUB
$!
$!       CLOSE BUFFERED DATA FILES
$!
$ CLOSE:
$ IF BUFFERED .EQS. "N" THEN $ GOTO WRITE
$  IF BUFOPEN .EQS. "N" THEN $ GOTO WRITE
$   TAPE CLOSE 5
$    IF DETECTOR$ .EQ. 2 THEN $ TAPE CLOSE 6
$!
$!       WRITE DATA AND XSCOM TO DISK
$!
$ WRITE:
$ WRT DA CAPT ALL
$ SAVE DA
$!
$!       WRITE DATA AND XSCOM TO TAPE
$!
$ IF USETAPE .EQS. "N" THEN $ GOTO NOTAPE
$  IF BUFFERED .EQS. "N" THEN $ GOTO NOBUFF
$   IF BUFOPEN .EQS. "N" THEN $ GOTO NOBUFF
$    ON ERROR THEN $ CONTINUE
$    COPY XXXX'NEWRUN'.EVN TA:
$    DELETE XXXX'NEWRUN'.EVN;*
$    BUFOPEN == "N"
$    NOBUFF:
$  WRT TA CAPT ALL
$  SAVE TA
$!
$ NOTAPE:
$ DUMPED == "Y"
$!
$!       FITTING OF POLARIZED OR UNPOLARIZED DATA
$!
$ IF P1 .EQS. "" THEN GOTO JUMP
$ IF P1 .EQS. "ONLY" THEN GOTO JUMP
$!
$!       GO TO THE FITTING COMMAND FILE DUFIT
$!
$ @sral:[doug.onefitlduf1t.com 'p1' 'p2' 'p3' 'p4' 'p5'
$ JUMP:
$ EXIT
```

EVAL Sorting Routine for the Old Detector with polarized beam

```
C
C       POLCAP1 - DATA SORTING FOR DETECTOR 1
C
C       WRITTEN BY STEVEN KING
C
C       3/15/81
C
C               SORTING PROGRAM IS DESIGNED TO SORT ENERGY DATA ACCORDING
C               TO A ROUTER AND A GATE SET ON THE TAC.  THE TAC MAY
C               BE SORTED USING GATES ON THE ENERGY SPECTRA.
C               DATA ARE SORTED INTO + SPECTRA IF THE VARIABLE SPIN IS 1 OR
C               - SPECTRA IF SPIN IS 0.
C
C               DATA AREA DEFINITIONS
C
SPEC ENU 1
SPEC TACU 2
SPEC RTU 3
SPEC E1AU 10
SPEC E2AU 11
SPEC E3AU 12
SPEC E1RU 13
SPEC E2RU 14
SPEC E3RU 15
SPEC TACU 16
SPEC T1U 20
SPEC T2U 21
SPEC T3U 22
SPEC ENDN 23
SPEC TACD 24
SPEC RTD 53
SPEC E1AD 40
SPEC E2AD 41
SPEC E3AD 42
SPEC E1RD 43
SPEC E2RD 44
SPEC E3RD 45
SPEC TACD 46
SPEC T1D 70
SPEC T2D 71
SPEC T3D 72
C
C                       EVENT DEFINITIONS
C
FORMAT E 1 11 3
FORMAT T 2 11 3
FORMAT R 3 11 3
C
C                       GATE DEFINITIONS
C
GATE EN1 1 1
GATE EN2 1 2
GATE EN3 1 3
GATE TM1 2 1
GATE TM2 2 2
GATE TM3 2 3
GATE REJ 3 1
C
C                       SPIN VARIABLE
C
VARIABLE SPIN 1
C
C                       3 PARAMETER EVENT (NaI, TAC, & ROUTER)
C
DATA EVSIZE=3
C
C                       DETERMINE SPIN STATE
C
IF SPIN EQ 1
C
C                       SORT SINGLES SPIN UP
C
        SET X=E
        TINC ENU
C
        SET Y=T
        TINC TACU
C
        SET Z=R
        TINC RTU
C
C                       SORT TAC USING 3 ENERGY GATES
C
      IF REJ
      ELSE
        IF X EN1
                TINC Y T1U
        ENDIF
        IF X EN2
                TINC Y T2U
        ENDIF
        IF X EN3
                TINC Y T3U
        ENDIF
      ENDIF
C
C                       SORT ENERGY ACCORDING TO ROUTING
C
        IF Z=REJ
C
C                       SORT REJECTS USING THE 3 TAC WINDOWS
```

```
C
                IF Y TH1
                        TINC X E1RU
                ENDIF
                IF Y TH2
                        TINC X E2RU
                ENDIF
                IF Y TH3
                        TINC X E3RU
                ENDIF
        ELSE
C
CCC                     SORT ACCEPTS USING THE 3 TAC WINDOWS
C
                IF Y TH1
                        TINC X E1AU
                ENDIF
                IF Y TH2
                        TINC X E2AU
                        TINC X EACU
                ENDIF
                IF Y TH3
                        TINC X E3AU
                ENDIF
        ENDIF
ELSE
CCC
CCC                     SORT SINGLES SPIN DOWN
C
        GET X=E
        TINC ENDN
C
        GET Y=T
        TINC TACD
C
        GET Z=R
        TINC RTD
CCC
CCC                     SORT TAC USING 3 ENERGY GATES
C
      IF REJ
      ELSE
        IF X EN1
                TINC Y T1D
        ENDIF
        IF X EN2
                TINC Y T2D
        ENDIF
        IF X EN3
                TINC Y T3D
        ENDIF
      ENDIF
CCC
CCC                     SORT ENERGY ACCORDING TO ROUTING
CCC
        IF Z=REJ
CCC
CCC                     SORT REJECTS USING THE 3 TAC WINDOWS
CCC
                IF Y TH1
                        TINC X E1RD
                ENDIF
                IF Y TH2
                        TINC X E2RD
                ENDIF
                IF Y TH3
                        TINC X E3RD
                ENDIF
        ELSE
CCC
CCC                     SORT ACCEPTS USING THE 3 TAC WINDOWS
CCC
                IF Y TH1
                        TINC X E1AD
                ENDIF
                IF Y TH2
                        TINC X E2AD
                        TINC X EACD
                ENDIF
                IF Y TH3
                        TINC X E3AD
                ENDIF
        ENDIF
ENDIF
```

```
END

        Information File for the Initialization of the Right Detector
        Subprocess

PCP1                    !DATA INFO FILE FOR CAP1   STEVEN KING
9                       !MBD CHANNEL NUMBER
201                     !CHANNEL BUFFER SIZE
INIT
1 20 9 26               !dataway clear
1 28 8 26               !DATAWAY INIT
1 7 9  26               !ENABLE AND CLEAR ADC
1 7 9  9
1 7 10 26
1 7 10 9
1 7 11 26
1 7 11 9
1 30 10 26              !ENABLE CRATE
LAM
1 7 9  0                !READ ADC AND CLEAR AT END
1 7 10 0
1 7 11 2
END
```

```
                EVAL Program for Sorting Monitor Data

C
C               PMON - A POLARIZED MONITOR SORTING PROGRAM
C
C               WRITTEN BY STEVEN KING
C
C               DATE:  3/16/81
C
C                       MONT IS A SORTING PROGRAM TO SORT A SINGLE SPECTRUM
C                       INTO TWO  DATA AREAS ACCORDING TO THE BEAM SPIN STATE.
C
C                       DEFINE SPECTRUM
C
SPEC MONU 7
SPEC MOND 57
C
C                       DEFINE EVENT
C
FORMAT F1 I 10 1
C
C                       SPIN VARIABLE DEFINITION
C
VARIABLE SPIN=1
C
C                       DEFINE EVENT SIZE
C
DATA EVSIZ=1
C
C                       SORT MONITOR DATA
C
C
C                       DETERMINE SPIN STATE
C
IF SPIN EQ 1
        GET F1
        INC MONU
ELSE
        GET F1
        INC MOND
ENDIF
END
```

```
                Initialization Information File for Monitor

PMON
0
1024
INIT
1 1 0 26
LAM
1 1 0 0
END
```

Scaler Initialization Information File

```
4                !MBD CHANNEL NUMBER   WRITTEN BY STEVEN KING
2                !SCALER TASK TIMER INCREMENT
PRESET
12               !PRESET SCALER
50000            !INIT PRESET VALUE
3                !NO. OF PRESET FUNCTIONS
14               !PRESET FUNCTIONS TO LOAD PRESET
9
25
DTC
0                !DTC FOR CHANNELS 0, 5, 6, & 1 USING SCALERS 6, 2, 8, & 13
6
5
2
6
8
1
13
END
```

B MULFIT Peak Fitting Program

The source program for the peak fitting program, MULFIT, is given in this appendix along with the support documentation, MULFIT.HLP. This program was written by the author of this thesis as a general data analysis program for the radiative capture group.

********** MULFIT **********

MULFIT

STEVEN E KING
September 10, 1981

Mulfit is a fitting routine designed to fit one to ten peaks to a standard line shape. It is possible through the use of pgen and parset to set a number of constraints for these peaks. The line shapes used were empirically determined from the T(P,GAMMA) reaction at 8.0 MeV for both high and low rejection.

The form of the line shape is :

H*EXP(d1 + d2*X + d3*X**2 + d4*X**3) X<XO

H*EXP(d5 + d6*X + d7*X**2 + d8*X**3) X>=XO

X = (X(DATA) - CENTROID)/B + STANDARD CENTROID

B = (FULL WIDTH, HALF MAXIMUM) * PROPORTION FACTOR

An optional line shape is to use a linear tail which goes from zero energy to 4 widths below the centroid of the peak. This line shape is in better agreement with Hayward's full energy gamma-ray spectrum but requires more CPU time and is not important unless the tail subtraction is important.

The three parameters to be fit are the height, width, and peak position(centroid). These three parameters are scaled to fit the standard line shape used by using 3 scaling factors: HFAC for height, WFAC for width, and STCEN the standard centroid. In order to implement a new standard shape these three factors must be changed in block data along with the exponential d coefficients.

An important special option is the ability to convolute the gamma response function with a peak width. In order to do so ILOR must be given. Also, penetrabilities are required in channel steps. The level width and step size for integration must be given.

A lower level discriminator option is available to ignore channels with counts <= a cut off parameter given in the input. Other options include summing of regions, ignoring a region imbedded in the fitting region in the fitting procedure, a more detailed output, smoothing of data, and tektronics display.

There are three background options. One is a constant background implemented by setting NBACK to one. This requires an addition parameter which is the background counts per channel. Place the additional parameter at the end of the parameter cards. If NBACK is two, then the program expects the user to supply the background as data for the same channels as the data. IDUMP is a flag that allows the data and the fit to be placed in a disk file for subsequent plotting. The file assigned to unit 10 will contain a spectrum of the fit in integer format.

By using the flag ICORM, it is possible to subtract a constant background that is determined by fitting a given region from the data before fitting the peaks. This is useful for cosmic ray subtraction.

It is recommended that ACRACY, ACRACY1, NTRY, and the separation of PMIN and PMAX be kept as small as possible to insure true minimums and error. However too small a ACRCY1 or DELTAI may result in no convergence. the error for parameters is calculated by a matrix method. However the error on areas is just the statistical error of sum.

The NCI and BACKSCI parameters are used to normalize the background to the data. The DATACOR AND BACKCOR correction factors multiply the data and background respectively and can be used for any and all normalizations. The background errors are propagated and added in quadrature to the error in the area assuming statistical error and taking all normalizations into account.

For a detailed description of how to setup an input file, see the input parameter list. At the end of this document is a sample input.

****

SUBROUTINES:

YFIT
CALCULATES FUNCTION Y(X) FOR A PEAK
PARAMETERS: NO. PEAK, STARTING FROM HIGH ENERGY, AND X

PGEN
GENERATES THE PARAMETERS P

PARSET
SETUP OF PARAMETERS IN PROPER FUNCTIONAL FORM AND INTERPRETS CONSTRAINTS

CHI
CALCULATES CHI**2 FOR N PEAKS N=1,10
PARAMETERS: I,J- PARAMETERS TO BE VARIED, DELTAI, DELTAJ - INCREMENT FOR PARAM(I) & PARAM(J)

CHIFST
A FAST VERSION OF CHI USED IN PARAMETER SEARCH ONLY.

LOWREJ
ROUTINE CHANGES LINE SHAPE TO LOW REJECTION.

CONVLT
ROUTINE TO CALCULATE CONVOLUTION INTEGRAL.

YSET
ROUTINE USED IN CONJUNCTION WITH THE CONVOLUTION INTEGRAL TO SPEED UP THE CALCULATION BY PROVIDING A TABLE OF THE PEAKS.

RDCORD
PARAMETER SEARCHING ROUTINE
PARAMETERS - PARAMETERS, MINIMUM AND MAXIMUM PARAMETER BOUNDS, NO OF PARAMETERS, NO OF RANDOM ROTATIONS, SHOULD BE AT LEAST NPARAM+1, ACRACY, THE ACCURACY TO WHICH THE PARAMETERS ARE DETERMINED ACRACY=(PMAX-PMIN), NREFS, NO OF REFERENCES TO RDCORD >100*NPARAM, AND IGOTO OUTPUT FLAG

PLOT
PLOTS DATA AND CALCULATED FIT
PARAMETERS: DATA, ERROR BARS, FIT, TITLE, STARTS END CHANNELS

INVT
MATRIX INVERSION
PARAMETERS: MATRIX, NO. PARAMETERS

ERROR
CALCULATES ERROR MATRIX
PARAMETERS: ACCURACY, NO. PARAMETERS, MATRIX, MIN CHI**2, PARAMETER LIMITS, INCREMENT, NTRY'S

SIGCAL
CONVERTS PARAMETER STANDARD DEVIATIONS TO STANDARD FORM FOR OUTPUT
CONVERSION IS THE SAME AS FOR P THE PARAMETER ARRAY

****
********** INPUT
****

INPUT: All input parameters (except the title) are in list directed format. As a result, any parameter not used or defaulted must be zero. What this means is that no parameter can be blank. If a default is desired use a zero. All list directed I/O is free format with blanks, commas and <returns> as delimiter.

LINE1: TITLE - A80 FORMAT

LINE2:
1. NPEAK - The number of peaks to be fit. I format.
2. IS - Starting channel of data in file. Defaulted to 1. I.
3. IE - Ending channel of data in file. Defaulted to 512. I.
4. NBACK - Background flag: 0 For no background. 1 Constant background. Put the value of the background in as the last parameter.

2 Background from the file. The background is given for every channel. See LINE8 for details. I

5. ILOW - The low rejection peak shape flag. If ILOW is nonzero the low rejection line shape is used. I

6. ILOR - The peak number of the gamma-ray to be convoluted into a Lorentzian line shape. Lines 7A-7e are required. I

7. NSUM - The number of areas summed. This allows the summation of any region of the spectrum. The output gives both the total area and net area = data - fit as well as the errors for both. For each sum an additional line (see LINE9) is required. I

8. LIN - The linear tail line shape is used if this parameter is nonzero. The linear tail begins 4 widths below the centroid of the peak and ends at IZEROCHAN.

LINE3A-LINE3e: This is a series of identical cards. Each peak requires three cards, the width, the centroid, and the height. The order of the cards is width, centroid, and height(WCH)!! Each card needs a control symbol and three numbers as given in the list below. If a constant background is used, it should be the last parameter. The fixed centroid peak separation constraint only works if the peak position that is referenced is before the constrained peak in the parameter list. If both PMIN and PMAX are zero then the limits are defaulted to +/- 50% for the height, +/- width/2 for centroid, and +/- 30% for the width. The peaks are numbered sequentially from the order of the data input.

1. PCHAR - Symbolic character identifying the parameter to follow. Each symbol must be in single quotes.
The following are all available options:

'W' - Width
'WF' - Width fixed. PMIN and PMAX ignored.
'C' - Centroid
'CF' - Centroid fixed. PMIN and PMAX are ignored.
'CFS'- Centroid fixed separation. PMIN is the peak number (< current peak number) and PMAX is the separation in energy (or channels if the energy calibration is not given) from this peak.
'H' - Height.
'B' - Background.
'BF' - Fixed background.

2. P - Initial parameter. Guesstimate of good value. F format

3. PMIN - Minimum value. Lower limit of search on parameter. F

4. PMAX - Maximum value. Upper limit of search on parameter. F

LINE4: 1. MINCHL - Lower bound of channels to which the peaks are fit. If zero MINCHL is defaulted to 10. I

2. MAXCHL - Upper bound of area to be fitted, note this is the area for which the fitting procedure actually calculates a CHI**2. The fit is calculated for all channels included in the input. By default, MAXCHL = IE. I

3. MINPLT - The minimum channel for the plot output. By default, MINPLT is six channels less than MINCHL. I

4. MAXPLT - The maximum channel for the plot output. By default, MAXPLT is six channels more than MAXCHL. I

5. IOBTRT - This is the lowest channel of a region to be ignored in the fitting search (ie. CHI**2 is not calculated for these channels). I

6. IOBTP - The highest channel of a region to be ignored in the fitting search. I

7. NRNDM - The number of random search rotations. This parameter is used in the parameter search to specify the maximum number of parameter rotations. NRNDM must be > # of parameters. It is defaulted to 3*NPEAK + 10. I

8. NREFS - The number of search references. This is the number of attempts the program makes at changing the parameters to find a fit. NREFS is defaulted to 300*NPEAK. It must be >100* the number of free parameters in the fit. I

LINE5: 1. ERGCAL - Energy calibration in keV or MeV per channel. Used in fixed width and centroid separation constraints. If used the fixed width and centroid parameters must be given in energy units. Width = W / ERGCAL. Defaulted to 1. F

2. XCUT - A lower limit of counts(y axis) to be included in the fitting procedure. Any channel which has fewer than XCUT counts is ignored in the fitting algorithm. Use to ignore tails that are nonstandard.
Note this discriminator reduces the number of channels considered in the CHI**2 fit. F

3. SUMFAC - A multiplicative summation factor. This specifies the number of full widths at half max below the peak that are summed in the calculation of peak area based on the line shape fits. A zero indicates whole spectrum down to the zero Energy CHANNEL is to be summed. For most work 2.0 should be used. See Russ Roberson for efficiency information. F

4. IZEROCHAN - The channel which corresponds to zero gamma-ray energy. Defaulted to 1. This is used for the linear tail line shape as well as a lower limit in integrating peak area. F

5. ACRACY - Accuracy of search. The search accuracy is the minimum step size for searching parameters. For a given parameter the step size is ACRACY*(PMIN - PMAX). Defaulted to .01. F.

6. ACRCY1 - The accuracy to which the errors in the errors in the parameters are determined. The errors should be accurate to 2**ACRCY1. Defaulted to 2**ACRACY. F.

7. DELTA1 - The error matrix calculation step size used for the minimum increment of the parameters. Defaulted to 3* ACRCY1. F.

8. NTRY - The number of convergence attempts in calculating the error matrix for the parameters. Defaulted to 20. I.

LINE6: 1. IWRITE - Optional long version of output. To use set to 1. I.

2. ISMOTH - Data smoothing option. This option uses the standard 3 point smoothing to minimize statistical fluctuation. To use set ISMOTH to 1. I.

3. IDISP - Optional display using the Tektronics terminal. If this option is used MULTI must be run interactive from the tektronics terminal. This option calls SUBLIB on early subroutine version of ZMVB DISP. I

4. IDUMP - Optional dump of fit on a file assigned to fortran unit 10. The fit for all SIZ channels is transferred in integer format. I.

5. ICOSM - Optional flag for cosmic ray background subtraction. If ICOSM = 1 then LINE10 is read. This option fits a horizontal line through the region given and subtracts the results from the data before fitting. This may be used to handle cosmic ray subtraction. I

6. IRESID - Option to plot the residuals = data - fit. I.

LINE7:

1. BCI - Beam current integration or a normalization factor. By default BCI=500.

2. BACKBCI - Background BCI. Used to normalize the background to the data. By default BACKBCI = 500. BCI/BACKBCI*BACKGROUND subtracted from the data.

3. DATACOR - Multiplicative normalization factor for the data

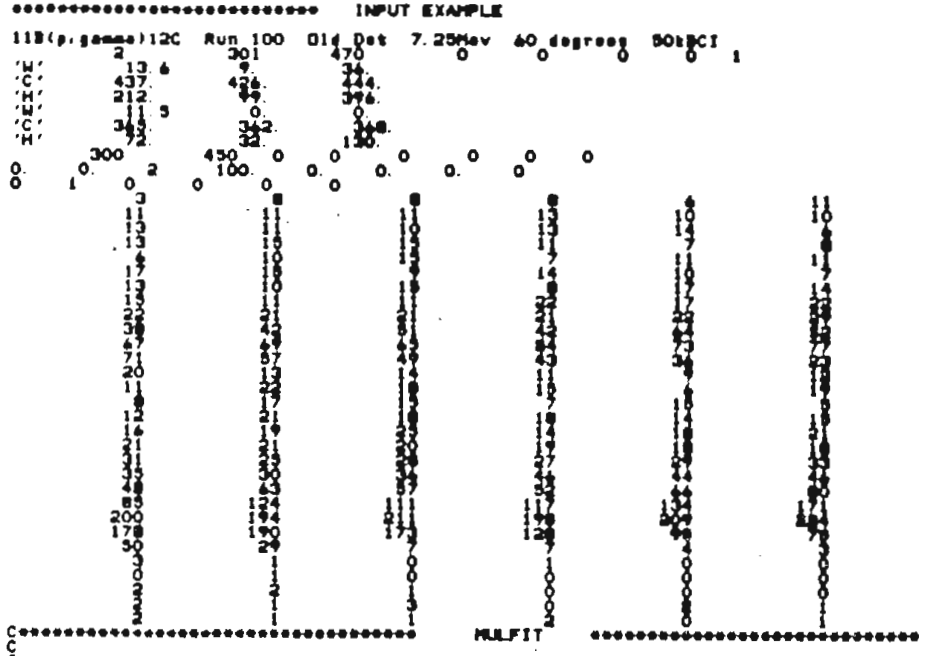

```
          4.   BACKCOR - Multiplicative normalization factor for the
               background

*
**********     OPTIONAL LINES - These lines are required only if the
*              appropriate options are chosen above.

   LINE7A:   Convolution Integral Option
             1. OAM - The width of level in energy/ or channels if EROCAL=1. F.

             2. STEP - The step size of the convolution integration in
                channels. F.

             3. NOAM - The number of penetrabilities given. Note the
                penetrabilities must be given in channel increments
                of energy starting with zero excitation energy. F

             4  IZRO - The zero excitation energy channel. I.

   LINE7*:      OMMA - The penetrabilities in channel steps. There should
                be NOAM number of penetrabilities on as many lines as needed.
                F.

   LINE8*:      BACK(I) - If NBACK=2 then the background is entered on a
                channel per channel basis.  The background must be supplied
                for channels IS through IE. F.

   LINE9*:      The summed area option with NSUM cards. Each card contains:

            1.  ISUMS - The start channel for area to be summed I

            2   ISUME - The end channel for area sum to be summed. I.

   LINE10:      The option to subtract a constant background given by
                the fit to a region of the spectrum specified by the following
                channels. ICOSM must be set to 1.  Used for cosmic
                ray subtraction

            1.  LCOSM - The start channel of the background area. I

            2.  IHCOSM - THE end channel for background area. I

******
*************************           FINALLY THE DATA
******

   LINE11*:     DATA IN REAL OR INTEGER FORMAT.

**************
*************************           OUTPUT
**************

  OUTPUT:

   1.  Input data

   2.  Initial and final parameters.

   3.  Record summary (long output option)

   4.  Plot of data(+), fit(*), and errors(---------)

   5.  Plot of residuals (IRESID=1)

   6.  ALPHA and ERROR matrices (ALPHA=ERROR**-1), (long output option)

   7.  DETERMINENT, CHI**2, and Energy calibration.

   8.  Table of integrated fit area, summed area, height, width, centroid
       and appropriate errors.  The error on the area is simply the square
       root of the area.  The summed area is calculated by subtracting the
       fit of all other peaks from the data and summing the net result over
       the same channels as the integrated fit area.  Both the summed and
       fit areas are integrated over the range from

                 Centroid-Sumfac*width to Centroid + 1.1*width.

   9.  Optional summed areas.
```

```
    10. Optional background subtraction.

    11. Optional cosmic ray subtraction information.

**************************    INPUT EXAMPLE

11B(p,gamma)12C  Run 100  Old Det  7.25Mev  60 degrees  50kECI
            2           301        470         0        0        0        0  1
'H'      13.6          9.        34.
'C'      437.        426.       444.
'H'      212.         99.       396.
'W'      11.5          0.         0.
'C'      345.        342.       348.
'H'       72.         32.       130.
         300         450    0      0     0     0    0    0
0.   0.    2       100.     0.     0.    0.    0
0    1     0     0     0     0
[illegible]
C*****************************     MULFIT     ***************************
C
C
C
C  MULFIT
C
C
C  STEVEN E KING
C  JUNE 20, 1980
C
C    MULFIT IS A FITTING ROUTINE DESIGNED TO FIT ONE TO TEN PEAKS
C      TO A BASIC LINE SHAPE.   IT IS POSSIBLE THROUGH THE USE OF POEN
C      TO SET ANY NUMBER OF CONSTRAINTS FOR THESE PEAKS.
C      LINE SHAPES USED WERE CALCULATED FROM Y(P,GAMMA) AT 5.0MEV FOR
C      BOTH HIGH AND LOW REJECTION
C
C       FOR DOCUMENTATION SEE MULFIT.HLP
C
C       TO COMPILE MULFIT THE FOLLOWING MUST BE LINKED
C                MULFIT.FOR
C                MULSUB1.FOR
C                MULSUB2.FOR
C                ROCORD.FOR
C                DECOM.FOR
C                DODIMP.FOR
C                [TUNL]ORZLIB.OLB/LIB
C
        IMPLICIT REAL*8(A-H,O-Z)
C
        INTEGER*4 TITLE, ONE
C
        CHARACTER*4 PCHAR(30)
C
        DIMENSION ALPHA(30,30), SIG1(30), DATARES(512), BACKAREA(10)
```

```
      DIMENSION ERRSUM(10), TERRSUM(10), AREASUM(10), NDATA(512)
      DIMENSION TITLE(20), DATA(512), FIT(512), P(30), PMIN(30)
      DIMENSION AREA(10), SIGMA(512), PARAM(30), SIG(30)
      DIMENSION PARLOR(3), IFIT(512), PINIT(30), PMAX(30)
      DIMENSION D(9), BACK(512), YTAB(1600)
      DIMENSION ERAREA(10), PARDEV(4), LFIT(512)
      DIMENSION GAMSQ(1024), OMGA(1024), BCKAREA1(10), BCKAREA2(10)
      DIMENSION IBUMS(10), IBUME(10), XNETSUM(10), TOTSUM(10), BCKAREA3(10)
C
      COMMON /BLK1/ PARMIN(30),PARMAX(30),PARAM,NPARAM,NCHL,IGSTRT,IGSTP
      COMMON /BLK2/ P, NP, NPEAK, PMIN, PMAX, NERO
      COMMON /BLK3/ MINCHL, MAXCHL, FIT, DATA, SIGMA, XCUT
      COMMON /BLK4/ D, UFAC, HFAC, STCEN, CUT
      COMMON /BLK5/ SIG, SIG1
      COMMON /BLK6/ EROCAL, IB, IE
      COMMON /BLK7/ GAM, STEP, GAMSQ, YTAB, OMGA, NGAM
      COMMON /BLK8/ PARLOR, LORFLG, ILOR, OMLMSQ(1024)
      COMMON /BLK9/ PCHAR
C
      DATA ZIP /0./, ONE /1./, COSM /0./, IWRT/0/, PARTCHAN/0./
      DATA BACK /512*0./, IBKIP/0/, BACKAREA/10*0./, AREA/10*0./
      DATA BCKAREA1/10*0./, BCKAREA2/10*0./, BCKAREA3/10*0./
C
C     READ DATA
C
C      CARD 1 - TITLE
C
      READ (1,10) TITLE
10    FORMAT (20A4)
C
C      CARD 2
C
      READ(1,*) NPEAK, IB, IE, NBACK, ILOM, ILOR, NBUM, LIN
C
C     DEFAULTS FOR IB AND IE
C
      IF (IB .EQ. 0) IB = 1
      IF (IE .EQ. 0) IE = 512
C
C     CALC NUMBER OF CHANNELS
C
C             NCHL - NUMBER OF CHANNELS
C
      NCHL = IE -IB +1
      IF (NCHL .GT. 512) THEN
              WRITE (3,18) 'ERROR  NUMBER OF CHANNELS EXCEEDS 512'
18            FORMAT ( II, A)
              GOTO 990
      ENDIF
C
C           READ PARAMETERS 3 PER PEAK PLUS BACKGROUND IF REQUESTED
C                NP - NUMBER OF VARIABLES
C
      NP = NPEAK*3
      IF (NBACK.EQ.1) NP = NP + 1
C                PARAMETER CARDS -CARD2?!
C                PINIT - INITIAL PARAMETERS
C
      DO 21 I=1,NP
C
      READ (1,*) PCHAR(I), P(I), PMIN(I), PMAX(I)
C
      PINIT(I) = P(I)
21    CONTINUE
C
      READ CARD4
C
      READ (1,*) MINCHL, MAXCHL, MINPLT, MAXPLT, IGSTRT, IGSTP, NRNDM, NREFS
C
      READ CARD5
C
      READ(1,*) EROCAL,XCUT, BUMFAC, ZEROCHAN, ACRACY, ACRCYI, DELTA1, NTRY
C
      READ CARD6 OPTIONS CARD
C
      READ (1,*) IWRITE, ISMOTH, IDISP, IDUMP, ICOSM, IRESID
C
      READ CARD7 DATA CORRECTION FACTOR AND BACKGROUND CORRECTION FACTOR
C
      READ (1,*) BCI, BACKBCI, DATACOR,BACKCOR
C
      IF (BCI .EQ. 0.) BCI = 500.
      IF (BACKBCI .EQ. 0.) BACKBCI = 500.
      IF (DATACOR .EQ. 0.) DATACOR = 1.
      IF (BACKCOR .EQ. 0.) BACKCOR = 1.
C
C     READ LORENTZIAN DATA - OPTIONAL
C
      IF (ILOR .NE. 0) THEN
C
              READ (1,*) GAM, STEP, NGAM, IZRO
C
              IZRO = IZRO -IB +1
              READ (1,*) (OMGA(IZRO-I+1), I=1,NGAM)
      ENDIF
C
C     READ BACKGROUND DATA CARD - OPTIONAL
C
      IF (NBACK .EQ. 2) THEN
C
              READ(1,*) (BACK(I),I=1,NCHL)
C
      ENDIF
C
C     READ AREA SUMS - OPTIONAL
C
      IF(NBUM .NE. 0) THEN
C
              DO 25 I=1,NBUM
C
              READ(1,*) IBUMS(I),IBUME(I)
C
              IBUMS(I) = IBUMS(I) - IB + 1
              IBUME(I) = IBUME(I) - IB + 1
25            CONTINUE
C
      ENDIF
C
C                              COSMIC RAY BACKGROUND SUBTRACTION OPTION
C
      IF(ICOSM .NE. 0) THEN
C
              READ(1,*) LCOSM,IHCOSM
C
      ENDIF
C
              READ DATA
C
      READ(1,*) (DATA(I),I=1,NCHL)
C
              CLOSE INPUT FILE
C
      CLOSE (UNIT=1)
C
              CORRECT DATA
C
      DO I= 1,NCHL
              DATA(I) = DATA(I)*DATACOR
              NDATA(I) = NINT(DATA(I))
      ENDDO
C
              SMOOTH DATA
C
      IF (ISMOTH .NE. 0) THEN
C
              DO 2710 I= 2, NCHL -1
              DATA(I) = (DATA(I-1)/2 + DATA(I) + DATA(I+1)/2) /2
2710          CONTINUE
C
      ENDIF
C
C     SUBTRACTION OF INPUTTED BACKGROUND FROM DATA
C
      IF (NBACK.EQ.2) THEN
              DO 2705 I= 1, NCHL
              BACK(I) = ((BCI/BACKBCI) * BACKCOR * BACK(I))
              DATA(I)= DATA(I) - BACK(I)
2705          CONTINUE
C
      ENDIF
C
C     FIT BACKGROUND RANGE AND SUBTRACT FROM DATA
C
      IF(ICOSM.NE.0) THEN
```

```
            COSM=0
            LCOSM=LCOSM- IB +1
            IHCOSM=IHCOSM- IB +1
C
            DO 290 I=LCOSM,IHCOSM
            COSM=DATA(I)+COSM
290         CONTINUE
C
            COSM= COSM / DFLOAT( IHCOSM - LCOSM + 1)
            IF(COSM .LT. 0.) COSM = 0.
C
            DO 291 I=1,NCHL
            DATA(I) = DATA(I) - COSM
291         CONTINUE
C     ENDIF
CCC
CCC         STATISTICAL ERROR CALCULATION
CCC
      B = 0.
      IF (NBACK .EQ. 1) B = P(NP)
      DO 27 I = 1, NCHL
      DX = DATA(I)
CCC                                     MINIMUM ERROR = 3
CCC
      IF (DATA(I) .LT. 9.) DX = 9.
      SIGMA(I) = DSQRT(DATACOR*DX + BACKCOR*(BCI/BACKBCI)*BACK(I)
     1          + DATACOR * (COSM +B))
27    CONTINUE
CCC
CCC   LOW REJECTION LINE SHAPE OPTION
CCC
      IF (ILOW.NE.0) CALL LOWREJ
CCC
CCC                                     DEFAULT SET UP
CCC
      IF (NRNDM.EQ.0) NRNDM= NP +10
      IF (NREFS.EQ.0) NREFS= NP +130
      IF (ACRACY.EQ.0.) ACRACY=.01
      IF (ACRCY1.EQ.0.) ACRCY1 = ACRACY * 2
      IF (DELTA1.EQ.0.) DELTA1= 3*ACRCY1
      IF (NTRY.EQ.0) NTRY=20
      IF (ZEROCHAN .EQ. 0.) ZEROCHAN = 1.
      IF (IWRITE .EQ. 2) THEN IWRT=1
      NERO = NINT(ZEROCHAN)
      IF (EROCAL .EQ. 0.) EROCAL = 1.
      IF (STEP .EQ. 0.) STEP = 1.
      IOSTRT= IOSTRT -IB +1
      IOSTP= IOSTP -IB +1
      IF (LIN.EQ.0) CUT=-1000.
      IF (MINCHL .EQ. 0) MINCHL = IB
      IF (MAXCHL .EQ. 0) MAXCHL = IE
      IF (MINPLT.EQ.0) MINPLT=MINCHL -6
      IF (MAXPLT.EQ.0) MAXPLT=MAXCHL +6
      IF (MINPLT .LT. IB) MINPLT = IB
      IF (MAXPLT .GT. IE) MAXPLT = IE
      MAXCHL = MAXCHL-IB+1
      MINCHL = MINCHL-IB+1
      MINPLT = MINPLT-IB+1
      MAXPLT = MAXPLT-IB+1
C
CCC                                   CALL PARAM SETUP ROUTINES
CCC
      CALL PARSET
CCC
CCC   SET UP LORENTZIAN WIDTH GIVEN PENETRABILITIES
CCC
      IF(ILOR .NE. 0) THEN
            KK= JIDINT(P(3*ILOR-1))
            GAM2I = GAM /GMMA(KK)
C
C     FOR CHANNELS WITH NO PENETRABILITIES THE LAST CHANNEL GIVEN IS USED
            IMIN = IZRO - NGAM + 1
            DO 257 I = IMIN, IZRO
            GMMA(I) = GMMA(I)*GAM2I
            GAMSQ(I) = (GMMA(I)/2.)**2
257         CONTINUE
C
            DO 2571 I = 1, IMIN-1
            GMMA(I) = GMMA(IMIN)
            GAMSQ(I) = (GMMA(I)/2.)**2
2571        CONTINUE
C
            II2 = IZRO-1
C
            DO 262 I=1,II2
            GMLMSQ(I) = GAMSQ(I)/FLOAT(IZRO-I)
262         CONTINUE
C
            GMLMSQ(IZRO) = GAMSQ(IZRO)
      ENDIF
C
C  WRITE INPUT
C
3715  WRITE (3,272) TITLE
272   FORMAT ('1',20A4)
C
      WRITE (3,273)
273   FORMAT ('0',///'***   MULFIT  WRITTEN BY STEVEN KING  --  TUNL **
     1   '///)
C
      WRITE (3,2721)' # OF PEAK  STRT CHAN  END CHAN   BACK OP
     1  LOW REJ   CONVO OP    # OF BUMS  LINE TAIL OP'
2721  FORMAT('0',A)
C
      WRITE(3,275) NPEAK, IB, IE, NBACK,ILOW,ILOR,NBUM,LIN
275   FORMAT(' ',8I10)
C
      WRITE(3,2721)' LOW & UPP FIT CHAN   MIN & MAX PLOT CHN
     1IGNOR START & STOP CHN  NRNDM    NREFS '
C
      WRITE(3,276) MINCHL+IB-1,MAXCHL+IB-1,MINPLT+IB-1, MAXPLT+IB-1,
     1 IOSTRT+IB-1, IOSTP+IB-1, NRNDM,NREFS
276   FORMAT(' ',8I10)
C
      WRITE(3,2721) ' ENERG CAL  LOW CUT  BUM WIDTH  ZERO ENG   ACRACY
     1ACRCY ERR  ERR INC     # TRYS'
C
      WRITE (3,277) EROCAL, XCUT, BUMFAC, ZEROCHAN, ACRACY,
     1       ACRCY1, DELTA1, NTRY
277   FORMAT(' ',7(F8.4,2X),I10)
C
      WRITE(3,2721)'   WRITE OP  SMOOTH OP   DISP OP  DUMP OP
     1  COSM BUM OP  RESID OP'
C
      WRITE (3,2775) IWRITE, ISMOTH, IDISP, IDUMP, ICOSM, IRESID
2775  FORMAT (' ', 6I10)
C
      WRITE (3,2721) '     BCI      BACKBCI  DATA CORR  BACK CORR '
C
      WRITE (3,2777) BCI, BACKBCI, DATACOR, BACKCOR
2777  FORMAT(' ', 4F10.4)
C
      IF (ILOR .NE. 0) THEN
            WRITE (3,2721) ' LORENTZIAN PEAK #   WIDTH       STEP SIZE
     1  # WIDTHS   ZERO CHAN'
            WRITE (3,2751) ILOR, GAM, STEP, NGAM, IZRO+IB-1
2751        FORMAT('0',I10,2F15.5,2I10)
      ENDIF
C
CCC   WRITE BUM INPUT
CCC
      IF (NBUM .NE. 0) THEN
            WRITE(3,2721)' PEAK #    START CHAN  END CHAN   FOR
     1 BUMMING REGIONS'
C
            DO 2781 I=1,NBUM
            WRITE (3,2782) I, IBUMB(I)+IB-1, IBUME(I)+IB-1
2782        FORMAT('0',3I10)
      ENDIF
C
CCC   WRITE COSMIC RAY SUBTRACTION INPUT
CCC
      IF(ICOSM.NE.0) THEN
            WRITE(3,2721)'LOWER AND UPPER CHAN FOR COSM RAY FIT.'
            WRITE(3,2776) LCOSM+IB-1 ,IHCOSM+IB-1
2776        FORMAT(1X,2I10)
      ENDIF
C
CCC   LONG OUTPUT VERSION
CC
      IF(IWRITE.EQ.0) GOTO 399
C
CCC   WRITE BACKGROUND
CCC
      IF (NBACK.EQ.2) THEN
```

```
                WRITE(3,2721) 'BACKGROUND INPUT'
                WRITE(3,279) (BACK(I),I=1,NCHL)
        ENDIF
C
CC      WRITE WEIGHTED LEVEL WIDTH
C
        IF (ILOR .NE. 0) THEN
                WRITE (3,2721) 'WEIGHTED WIDTHS'
                WRITE(3,2793) (GAMMA(I),I=1,NCHL)
2793            FORMAT('0',10E11.4,1X)
                WRITE (3,2793) (GAUSS4(I),I=1,NCHL)
        ENDIF
C
CC      WRITE DATA
C
        WRITE (3,2721) 'DATA'
        WRITE (3,279) (DATA(I),I=1,NCHL)
279     FORMAT(' ',10F11.4,1X)
C
C  SET NOCORD TO BEGIN SEARCH
C
399     CONTINUE
        IGOTO=1
C
C  FIT DATA
C
40      CONTINUE
C
CC      CALCULATE CHI**2 FOR FIT
C
        CALL FOEN
        CHI2 = CHIFST(ZIP)
C
        GOTO (420,420,65,60),IGOTO
C
CC      CALL NOCORD - PARAMETER SEARCHING SUBROUTINE
C
420     CALL NOCORD(PARAM,PARMIN,PARMAX,NPARAM,ACRACY,NREFS,NRNDM,
1       IWRT,   IGOTO,CHI2)
C
        GOTO 40
C
C  NUMBER OF REFERENCES EXCEEDED, GET CURRENT MINIMUM
C
60      CONTINUE
        WRITE (3,62)
62      FORMAT('0',31H  NUMBER OF REFERENCES EXCEEDED)
CC
CC      SEARCH COMPLETED MINIMUM FOUND
CC
65      CONTINUE
CC
C  CALCULATE MINIMUM CHI2
C
        PARLOR(1)=0.
        PARLOR(2)=0.
        PARLOR(3)=0.
        CALL FOEN
        CHI0 = CHIFST(ZIP)
C
CC      CALCULATE CHI**2 PER CHANNEL
C
        DO 655 I = MINCHL, MAXCHL
        IF (DATA(I) .LE. XCUT) IBKIP = IBKIP +1
655     CONTINUE
C
        CHI2 = CHI0 /DFLOAT(MAXCHL-MINCHL-NPARAM+1-IONCHL -IBKIP)
C
CC      CALCULATE FIT FOR ALL CHANNELS
C
        DO 66 I= 1, NCHL
        XI = DFLOAT(I)
        FIT(I) = 0.
C
        DO 64 J = 1, NPEAK
        FIT(I) = FIT(I) + CONVLT(J,XI)
64      CONTINUE
C
        IF(NP.NE.3*NPEAK) FIT(I) = FIT(I) + P(NP)
66      CONTINUE
CC
C  Plot data and fit & data and residual
C
C       WRITE OUT INITIAL AND FINAL PARAMETERS
C
        WRITE(3,2732) 'PTYPE', 'INIT PARAM', 'FINAL PARAM', 'MIN', 'MAX',
        1       'ORDER, WIDTH,
        1 CENTROID, AND HEIGHT)'
2732    FORMAT('0', A, 6X, A, 8X, A, 9X, A, 13X, A, 12X, A)
C
        DO 2736 I = 1, NP
        IF ((PCHAR(I).EQ.'C   ').OR.(PCHAR(I).EQ.'CF  ').OR.
        1       (PCHAR(I).EQ.'CFB ')) THEN
                WRITE (3,274) PCHAR(I), PINIT(I),P(I)+IB-1,
        1       PMIN(I)+IB-1,PMAX(I)+IB-1
        ELSE
                WRITE (3,274) PCHAR(I), PINIT(I),P(I),PMIN(I),PMAX(I)
274             FORMAT(' ',A4, 2X, 4(F13.3,3X))
        ENDIF
2736    CONTINUE
        DO I=1,NP
        IF ((((PMIN(I) .NE. 0.) .AND. (PMAX(I) .NE. 0.)).AND.
             (PMIN(I).NE.PMAX(I))) ) THEN
          IF  ( ( (ABS(P(I)-PMIN(I))/(PMAX(I)-PMIN(I))) .LT. .05).OR.
            ( (ABS(P(I)-PMAX(I))/(PMAX(I)-PMIN(I))) .LT. .05) ) THEN
            WRITE(3,2737) 'PARAMETER ',I,' CLOSE TO LIMIT'
2737        FORMAT(' ',A,I2,A)
          ENDIF
        ENDIF
        ENDDO
C
        CALL PLOT(DATA,SIGMA,FIT,NCHL,TITLE,MINPLT,MAXPLT)
C
CC      CONVERT FIT TO INTEGERS
C
        DO 6610 I=1, NCHL
6610    IFIT(I) = JIDNNT(FIT(I))
C
C Display data option
C
        IF(IDISP .NE. 0) THEN
C
                CALL BODISP(NDATA, TITLE, 1, NCHL, 0, 0, IFIT)
        ENDIF
C
CC              CALCULATE AND PLOT RESIDUAL (DATA - FIT)
C
        IF (IRESID .NE. 0) THEN
C
                DO 67 I=1,NCHL
                DATARES(I)=DATA(I)-FIT(I)
67              CONTINUE
C
                CALL  PLOT(DATA,SIGMA,DATARES,NCHL,TITLE,MINPLT,MAXPLT)
        ENDIF
C
C  Sum unfit regions
C
677     IF (NSUM .NE. 0) THEN
C
                DO 7540 I=1,NSUM
                TOTSUM(I) = 0.
                XNETSUM(I) = 0.
                IA = ISUMS(I)
                IB = ISUME(I)
C
                DO 7535 J=IA,IB
                TOTSUM(I) = TOTSUM(I) + DATA(J)
                XNETSUM(I) = XNETSUM(I) + DATA(J) - FIT(J)
7535            CONTINUE
C
                TERRSUM(I) = DSQRT(TOTSUM(I))
                ERRSUM(I) = DSQRT( TOTSUM(I) + DABS(XNETSUM(I)) )
7540            CONTINUE
        ENDIF
C
CC  ERROR ANALYSIS
CCC
CC      CALCULATE ERROR MATRIX
C
        LORFLG=0
        CALL ERROR(ACRCY1,NPARAM,ALPHA,CHI0,PARMIN,PARMAX,DELTA1,NTRY,
        1       IERR)
        IF (IERR .NE. 0) THEN
                WRITE (3,2721) 'ERROR FROM ERROR MATRIX CALCULATION -
        1 PARAMETER ERRORS BAD'
                GOTO 8555
        ENDIF
```

```
C
      IF(IWRITE.EQ.0) GOTO 852
C
      WRITE (3,272) TITLE
C
      WRITE (3,843)
843   FORMAT('0ALPHA')
C
      WRITE (3,87)
C
      DO 845 I=1,NPARAM
845   WRITE (3,85) (ALPHA(I,J),J=1,NPARAM)
85    FORMAT('0',12E10.3/9X,8E10.3)
C
C     INVERT ERROR MATRIX
C
852   CALL INVT(ALPHA,NPARAM,DET)
C
      IF(IWRITE.EQ.0) GOTO 8558
C
      WRITE (3,853)
853   FORMAT('0ERROR')
C
      WRITE (3,87)
      DO 859 I=1,NPARAM
855   WRITE (3,85) (ALPHA(I,J),J=1,NPARAM)
      WRITE (3,87)
87    FORMAT('0 ')
CC
CC    STANDARD OUTPUT SUMMARY
CC
8555  WRITE (3,272) TITLE
C
      WRITE (3,875) DET
875   FORMAT('0DETERMINANT= ',F11.4)
C
      WRITE (3,878) EROCAL
878   FORMAT('0ENERGY CALIBRATION =',F10.3,' KEV/CHL')
C
      DO 88 I=1,NPARAM
      IF(ALPHA(I,I).LT.0.) WRITE (3,882) I
882   FORMAT('0*** ERROR - NEGATIVE VARIANCE FOR FREE PARAMETER',I2)
88    BIG1(I)=DSQRT(DABS(ALPHA(I,I)))
C
C     CALL STANDARD DEVIATION PARAMETER CONVERSION PROGRAM
C
      CALL BIGCAL
C
      WRITE (3,77) CHI2
77    FORMAT ('0','CHI**2', 2X, F11.5)
CC
CC  AREA CALCULATION
CC
      DO 81 I=1,NPEAK
      LORFLG=0
      J=3*(I-1)+1
      PARTCHAN = 0.
C
CCC   SET MINIMUM SUMMING POINT TO EITHER ZERO ENERGY CHANNEL
CCC   OR IF SUMFAC IS NOT ZERO TO SUMFAC WIDTHS BELOW THE CENTROID
C
      MINSUM= ZEROCHAN  - IS
      IF (SUMFAC  .NE.  0.) THEN
            MINSUM= INT(P(J+1) -SUMFAC*P(J))
            PARTCHAN = P(J+1)- SUMFAC*P(J) - DFLOAT(MINSUM)
      ENDIF
      NEROPRIM = NERO - IS +1
      MINSUM = MAX(MINSUM, NEROPRIM)
      LIMUPP = IDNINT (P(J+1) + 1.1*P(J))
      LHI =  MIN (NCHL, LIMUPP)
C
      DO 78 K= MINSUM,LHI
      XK=DFLOAT(K)
      AREA(I) = AREA(I) + CONVLT(I,XK)
      IF (NBACK  .EQ.  1) THEN
            BCKAREA1(I) = BCKAREA1(I) + P(NP)
      ENDIF
      IF (NBACK  .EQ.  2) THEN
            BCKAREA2(I) = BCKAREA2(I) + BACK(K)
      ENDIF
      IF (ICOSM  .NE.  0) THEN
            BCKAREA3(I) = BCKAREA3(I) + COSM
      ENDIF
78    CONTINUE
C
CC    SUBTRACT PARTIAL CHANNEL
CC
      XK=DFLOAT(MINSUM)
      AREA(I) = AREA(I) - PARTCHAN*CONVLT(I,XK)
      IF (NBACK  .EQ.  1) THEN
            BCKAREA1(I) = BCKAREA1(I) - PARTCHAN*P(NP)
      ENDIF
      IF (NBACK  .EQ.  2) THEN
            BCKAREA2(I) = BCKAREA2(I) - PARTCHAN*BACK(MINSUM)
      ENDIF
      IF (ICOSM  .NE.  0) THEN
            BCKAREA3(I) = BCKAREA3(I) - PARTCHAN*COSM
      ENDIF
      BACKAREA(I) = BCKAREA1(I) + BCKAREA2(I) + BCKAREA3(I)
C
81    CONTINUE
CCCCC
CCCCC SUM PEAK AREA
CCCCC
CCCCC       THE AREA UNDER EACH PEAK IS SUMMED.  NOTE THIS IS DONE BY
CCCCC       FIRST SUBTRACTING THE FIT FROM ALL OTHER PEAKS AND THEN
CCCCC       SUMMING THE AREA DOWN THE PRESCRIBED NUMBER OF CHANNELS
CCCCC       AND UP ONE WIDTH.  IF THE MINIMUM OR MAXIMUM OF THE REGION
CCCCC       TO BE SUMMED EXTENDS BEYOND THE DATA GIVEN IT IS TRUNCATED.
CCCCC
CCCCC SUBTRACT OTHER PEAKS - IF FIT IS GREATER THAN DATA NEGATIVE VALUES
CCCCC RESULT
CC
      DO 811 I =1,NPEAK
      AREASUM(I) = 0.
      PARTCHAN=0.
C
      DO 805 K = 1, NCHL
      DATARES(K) = DATA(K)
805   CONTINUE
C
      DO 812 K = 1, NPEAK
      IF (K .NE.  I) THEN
            DO 813 L=1,NCHL
            XL = DFLOAT(L)
            DATARES(L) = DATARES(L) - CONVLT(K,XL)
813         CONTINUE
      ENDIF
C
812   CONTINUE
CC
CC                      SUBTRACT BACKGROUND
CC
      IF (NP .NE. NPEAK*3) THEN
C
      DO 8111 L = 1,NCHL
      DATARES(L) = DATARES(L) - P(NP)
8111  CONTINUE
C
      ENDIF
CCC
CCC   SET UPPER AND LOWER LIMITS OF SUM
CC
      J = 3*(I-1) + 1
      MINSUM= ZEROCHAN  - IS
      IF (SUMFAC  .NE.  0.) THEN
            MINSUM= IDNINT(P(J+1) -SUMFAC*P(J))
            PARTCHAN = P(J+1) - SUMFAC*P(J) - DFLOAT(MINSUM)
      ENDIF
      LIMUPP = IDNINT (P(J+1) + P(J))
      LLOW = MAX (1, MINSUM)
      LHI =  MIN (NCHL, LIMUPP)
C
CCC   SUM AREA FOR PEAK I
CC
      DO 814 K = LLOW, LHI
      AREASUM(I) = AREASUM(I) + DATARES(K)
814   CONTINUE
C
      AREASUM(I) = AREASUM(I) - DATARES(LLOW)*PARTCHAN
811   CONTINUE
CCCCC
CCCCC  AREA ERROR CALCULATION
CCCCC
C**************** ERR = SQRT ( AREA-BACKGROUND ) ****************
C
```

```
C       NOTE AREA IS ALREADY CORRECTED ONCE BY DATACOR
C
        DO 826 I=1,NPEAK
        ERPEAK2 = AREA(I) * DATACOR
        ERBACK12 = 2 * DATACOR * BCKAREA1(I)
        ERBACK22 = (DATACOR+BACKCOR*BCI/BACKBCI)*BCKAREA2(I)
        ERBACK32 = 2*DATACOR* BCKAREA3(I)
        ERAREA(I)=DSQRT(DABS(ERPEAK2 + ERBACK12 + ERBACK22 + ERBACK32))
826     CONTINUE
C
C  Output Peak Summary
C
        WRITE (3,815)
815     FORMAT('0', 13X, 'AREA', 13X, 'AREA SUMMED', 2X,'BACKGROUND',8X
        1 , 'WIDTH', 21X,
        1       'CENTROID', 20X, 'HEIGHT')
C
        DO 83 I=1,NPEAK
        J=3*(I-1)+1
        PPRI = P(J+1)+IB-1
C
        WRITE (3,82) (I,AREA(I),ERAREA(I),AREASUM(I),BACKAREA(I),P(J),BIG(J),
        1       PPRI,BIG(J+1), P(J+2),BIG(J+2))
82      FORMAT('0',I2,1X,F10.2,' +/-' ,F8.2,3X,F10.2,1X,F10.2,1X,3(F11.2,
        1 ' +/-', F9.2,3X))
83      CONTINUE
C
        IF ( NBUM .NE. 0) THEN
        DO 8560 I=1,NBUM
        IBPRI = IBUMB(I)+IB-1
        IEPRI = IBUME(I)+IB-1
        WRITE(3,8550) I, TOTSUM(I), TERRSUM(I), XNETSUM(I), ERRSUM(I),
        1       IBPRI,IEPRI
8550    FORMAT('0','TOTAL SUMMED AREA(',I2,')  ', F10.2,' +/- ', F8.2,
        1 '  NET SUMMED AREA = ',F10.2,' +/- ',F8.2,' START & END
        1 CHLS ',2I8)
8560    CONTINUE
        ENDIF
C
        IF(ICOSM.NE.0) WRITE(3,8622) COSM,LCOSM+IB-1,IHCOSM+IB-1
8622    FORMAT('0', 'COSMIC SUBTRACTION = ',F8.2,'  FROM CHANNELS ',I5,
        1       3X,I5)
C
        IF (LIN .NE. 0) WRITE(3,8633) 'LINEAR TAIL USED'
8633    FORMAT ('0',A)
C
C*****  DUMP DATA AND FIT ON UNIT = 10 IF IDUMP SET
C
9001    CONTINUE
C
        IF(IDUMP.NE. 0) THEN
C
                OPEN(UNIT=10,TYPE='NEW',ERR=9006)
C
                DO 9002 I = 1, 512
                IF (I .LT. IB) THEN
                        LFIT(I) = 0
                ELSE
                IF (I .GT. IE) THEN
                        LFIT(I) = 0
                ELSE
                LFIT(I) = IFIT(I - IB +1)
                ENDIF
C
                ENDIF
C
9002            CONTINUE
C
                WRITE(10,9003) (LFIT(I),I=1,512)
9003            FORMAT (8I10)
C
                CLOSE(UNIT=10)
                GOTO 990
9006            CONTINUE
C
                WRITE(3,2721) 'ERROR IN DUMP FILE OPEN'
        ENDIF
C
990     CONTINUE
C
        STOP
        END
C
C       BLOCK DATA STRUCTURE CONTAINING THE HIGH RESOLUTION LINE SHAPE
C
C               PARAMETERS
C
        BLOCK DATA
C
        IMPLICIT REAL*8(A-H,O-Z)
C
        DIMENSION D(9)
C
        COMMON /BLK4/ D,HFAC,HFAC,BTCEN,CUT
        COMMON /BLK7/ GAM, BTEP, GAMBG(1024), YTAB(1400), GMMA(1024), NGAM
        COMMON /BLK8/ PARLOR(3), LOWPL0, ILOW, GMLMBG(1024)
C
        DATA BTCEN,HFAC,HFAC/316.94,0.015077,0.0433681/
C
        DATA CUT/178./
C
        DATA D/-9.789650973, 1.547997401,-0.7821982062D-3,
        1 -.1351031478D-5,1.304.765153,-14.47939301,.5373043408D-1,
        2 -.4430620399D-4,312.3738175/
C
        DATA GMMA /1024*0./
C
        DATA GMLMBG /1024*0./
C
        DATA GAMBG /1024*0./
C
        DATA PARLOR /3*0./
        END
      SUBROUTINE INVT(BRR,NX,D)
      IMPLICIT REAL*8(A-H,O-Z)
      DIMENSION BRR(30,30),A(900),AA(30)
      DIMENSION L(30),M(30)
      N=NX
      DO 11 I=1,NX
   11 AA(I)=BRR(I,I)
      DO 22 I=1,NX
      DO 22 J=1,NX
      K=(J-1)*N+I
   22 A(K)=     (BRR(I,J))/DSQRT(AA(I)*AA(J))
C
C
C       SEARCH FOR LARGEST ELEMENT
C
      D=1.DO
      NK=-N
      DO 80 K=1,N
      NK=NK+N
      L(K)=K
      M(K)=K
      KK=NK+K
      BIGA=A(KK)
      DO 20 J=K,N
      IZ=N*(J-1)
      DO 20 I=K,N
      IJ=IZ+I
   10 IF(DABS(BIGA)-DABS(A(IJ))) 15,20,20
   15 BIGA=A(IJ)
      L(K)=I
      M(K)=J
   20 CONTINUE
C
C       INTERCHANGE ROWS
C
      J=L(K)
      IF(J-K) 35,35,25
   25 KI=K-N
      DO 30 I=1,N
      KI=KI+N
      HOLD=-A(KI)
      JI=KI-K+J
      A(KI)=A(JI)
   30 A(JI) =HOLD
C
C       INTERCHANGE COLUMNS
C
   35 I=M(K)
      IF(I-K) 45,45,38
   38 JP=N*(I-1)
      DO 40 J=1,N
      JK=NK+J
      JI=JP+J
      HOLD=-A(JK)
      A(JK)=A(JI)
   40 A(JI) =HOLD
```

```
C
C        DIVIDE COLUMN BY MINUS PIVOT (VALUE OF PIVOT ELEMENT IS
C        CONTAINED IN BIGA)
C
   45 IF(BIGA) 48,46,48
   46 D=0.DO
      DET=D
      RETURN
   48 DO 55 I=1,N
      IF(I-K) 50,55,50
   50 IK=NK+I
      A(IK)=A(IK)/(-BIGA)
   55 CONTINUE
C
C        REDUCE MATRIX
C
      DO 65 I=1,N
      IK=NK+I
      HOLD=A(IK)
      IJ=I-N
      DO 65 J=1,N
      IJ=IJ+N
      IF(I-K) 60,65,60
   60 IF(J-K) 62,65,62
   62 KJ=IJ-I+K
      A(IJ)=HOLD*A(KJ)+A(IJ)
   65 CONTINUE
C
C        DIVIDE ROW BY PIVOT
C
      KJ=K-N
      DO 75 J=1,N
      KJ=KJ+N
      IF(J-K) 70,75,70
   70 A(KJ)=A(KJ)/BIGA
   75 CONTINUE
C
C        PRODUCT OF PIVOTS
C
      D=D*BIGA
C
C        REPLACE PIVOT BY RECIPROCAL
C
      A(KK)=1.DO/BIGA
   80 CONTINUE
C
C        FINAL ROW AND COLUMN INTERCHANGE
C
      K=N
  100 K=(K-1)
      IF(K) 150,150,105
  105 I=L(K)
      IF(I-K) 120,120,108
  108 JQ=N*(K-1)
      JR=N*(I-1)
      DO 110 J=1,N
      JK=JQ+J
      HOLD=A(JK)
      JI=JR+J
      A(JK)=-A(JI)
  110 A(JI) =HOLD
  120 J=M(K)
      IF(J-K) 100,100,125
  125 KI=K-N
      DO 130 I=1,N
      KI=KI+N
      HOLD=A(KI)
      JI=KI-K+J
      A(KI)=-A(JI)
  130 A(JI) =HOLD
      GO TO 100
  150 CONTINUE
      DO 3 I=1,NX
      DO 3 J=1,NX
      K=(J-1)*N+I
    3 A(K)=A(K)/DSQRT(AA(I)*AA(J))
      DO 4 I=1,NX
      DO 4 J=1,NX
      TEST=0.DO
      DO 5 K=1,NX
      KI=(J-1)*N+K
    5 TEST=TEST+     (BRR(I,K))*A(KI)
      IF(I.EQ.J) TEST=TEST-1.DO
      TEST=DABS(TEST)
      IF(TEST.LT.1.D-7)  GO TO 4
      WRITE(3,8) TEST,I,J
    8 FORMAT(1H ,'****ERROR IN MATRIX INVERSION VALUE, AND INDEX
        1***',D20.9,2I5)
    4 CONTINUE
      DO 7 I=1,NX
      DO 7 J=1,NX
      K=(J-1)*N+I
    7 BRR(I,J)=     (A(K))
      DET=D
      RETURN
      END
      SUBROUTINE ERROR(ACRACY,  NDF,ALPHA,CHIO,XMIN,XMAX,DELTA1,
        1NTRY,IERR)
      IMPLICIT REAL*8(A-H,O-Z)
      DIMENSION DELTAO(30),XMIN(30),XMAX(30),ALPHA(30,30)
      DATA ZIP/0./
        DO 9 I=1,NDF
    9 DELTAO(I)=(XMAX(I)-XMIN(I))*ACRACY
      DO 1 I=1,NDF
      DO 1 J=1,NDF
      IFLAG=0
      XDELTA=DELTA1
    4 DELTAI=DELTAO(I)*XDELTA
      DELTAJ=DELTAO(J)*XDELTA
      IF(I.EQ.J) GO TO 2
      CHI1=CHI(I,DELTAI,J,DELTAJ)
      CHI2=CHI(I,DELTAI,J,ZIP)
      CHI3=CHI(I,ZIP,J,DELTAJ)
      TEST=(CHI1-CHI2-CHI3+CHIO)/(DELTAI*DELTAJ)
      GO TO 5
    2 CHI1=CHI(I,DELTAI,J,ZIP)
      CHI2=CHI(I,-DELTAI,J,ZIP)
      CHI3=0.DO
      TEST=(CHI1+CHI2-2.DO*CHIO)/(DELTAI*DELTAI)
    5 IFLAG=IFLAG+1
      IF(IFLAG.EQ.NTRY) GO TO 98
      IF(IFLAG.EQ.1) GO TO 3
      TEMP=DABS(ALPHA(I,J)-TEST)
      IF(TEMP.LT.ACRACY*DABS(TEST)) GO TO 15
    3 ALPHA(I,J)=TEST
      XDELTA=XDELTA*.5DO
      GO TO 4
   98 WRITE(3,444)'ERROR CALCULATING PART DERIVATIVES FOR ERRORS. PARAME
     1ARE FIRST TWO 0.   ALL ERRORS ARE SUSPECT'
  444 FORMAT('0',A)
      WRITE(3,7)I,J,TEST,ALPHA(I,J)
    7 FORMAT(2I10,2D20.10)
        IERR = 1
        RETURN
   15 ALPHA(I,J)=TEST*.5DO
    1 CONTINUE
      DO 6 I=1,NDF
      DO 6 J=1,NDF
    6 ALPHA(J,I)=ALPHA(I,J)
      RETURN
      END
      SUBROUTINE PLOT(A,B,C,N,TITLE,ISTRT,IEND)
      IMPLICIT REAL*8(A-H,O-Z)
      INTEGER TITLE,PL
      INTEGER PLUS,STAR,DASH,BLANK,QUOTE
      DIMENSION TITLE(20),PL(101)
      DIMENSION A(512),B(512),C(512)
      COMMON /BLK6/ EROCAL,  IB,  IE
      DATA PLUS/'+'/,STAR/'*'/,DASH/'-'/,BLANK/' '/,QUOTE/''''/
      WRITE(3,1)(TITLE(I),I=1,20),N,ISTRT+IB-1,IEND+IB-1
    1 FORMAT(1H1,20A4,3I5)
      DO 5 I=1,100
    5 PL(I)=BLANK
      XMAX=-1.D30
      XMIN=1.D30
      DO 2 I=ISTRT,IEND
      AHI=A(I)+DABS(B(I))
      ALO=A(I)-DABS(B(I))
      IF(AHI.GT.XMAX) XMAX=AHI
      IF(ALO.LT.XMIN) XMIN=ALO
      IF(C(I).GT.XMAX) XMAX=C(I)
      IF(C(I).LT.XMIN) XMIN=C(I)
    2 CONTINUE
      IF(XMIN .GT. 0.) XMIN=0.
      SCALE=99./(XMAX-XMIN)
      IZRO=IFIX(SNGL((0.-XMIN)*SCALE))+1
      DO 3 I=ISTRT,IEND
      IA=IFIX(SNGL((A(I)-XMIN)*SCALE))+1
```

```
      IC=IFIX(SNGL((C(I)-XMIN)*SCALE))+1
      IBH=IFIX(SNGL((A(I)+DABS(B(I))-XMIN)*SCALE))+1
      IBL=IFIX(SNGL((A(I)-DABS(B(I))-XMIN)*SCALE))+1
      PL(IZRO)=QUOTE
      IF(IBL.EQ.IBH) GO TO 8
      DO 4 J=IBL,IBH
    4 PL(J)=DASH
    8 PL(IA)=PLUS
      PL(IC)=STAR
      WRITE(3,6) A(I), I+IB-1,(PL(J),J=1,100)
    6 FORMAT(F10.4,I8,100A1)
      DO 7 J=1,100
    7 PL(J)=BLANK
    3 CONTINUE
      RETURN
      END
C
      FUNCTION CONVLT(J,XJ)
C  PEAK FITTING CURVE EVALUATION
C
C  ROUTINE TO CALCULATE THE CONVOLUTION OF THE NATURAL LINE SHAPE AND
C    A LORENTZIAN
C
      IMPLICIT REAL*8 (A-H,O-Z)
      CHARACTER*4 PCHAR(30)
      DIMENSION PARLOR(3),FUNC(1000)
      DIMENSION P(30), PARMAX(30),PARMIN(30),PARAM(30)
      DIMENSION GAMSQ(1024),YTAB(1600),GMLMSQ(1024),PMIN(30)
      DIMENSION PMAX(30)
      COMMON /BLK1/ PARMIN, PARMAX, PARAM, NPARAM, NCHL
      COMMON /BLK2/ P, NP,NPEAK, PMIN, PMAX
      COMMON/BLK4/ ERGCAL, IB, IE
      COMMON /BLK7/GAM,STEP,GAMSQ,YTAB,GMLMSQ,NGAM
      COMMON /BLK8/ PARLOR,LORFLG,ILOR,GMLMSQ(1024)
      COMMON /BLK9/ PCHAR
      DATA PI2 /6.2831853/
      DATA A /0.0576/
      IF(J .NE. ILOR) GOTO 90
      XJ1=XJ
      IF(LORFLG.EQ.1) GOTO 60
      N = IDINT(FLOAT(NCHL)/STEP)
      CONVLT = 0.D0
C
      DO 30 I=1,N
      XI = FLOAT(I)*STEP
      XK = XJ-XI
      IX1 = IDINT(P(3*ILOR-1)+XK)
      IF (IX1.LT.1) IX1=1
      CONVLT = CONVLT + YTAB(I)*GMLMSQ(IX1)/(XK*XK + GAMSQ(IX1))
30    CONTINUE
C
      CONVLT = CONVLT*STEP/(PI2*A)
      FUNC(J1+IB-1)=CONVLT
      RETURN
C
60    CONVLT = FUNC(J1+IB-1)
      RETURN
C
90    CONVLT = YFIT(J,XJ)
C
99    RETURN
      END
C
C
      SUBROUTINE LOWREJ
C
C  SUBROUTINE TO CHANGE PARAMETERS TO THOSE FOR LOW REJECTION DATA
C
      IMPLICIT REAL*8(A-H,O-Z)
      DIMENSION D(9)
      COMMON /BLK4/ D,WFAC,HFAC,BTCEN,CUT
      CUT=161.9
      D(1) = -6.73035379
      D(2) =  .9620299494D-1
      D(3) = -.4518347029D-3
      D(4) =  .8100237177D-6
      D(5) = 1307.141397
      D(6) = -14.66984629
      D(7) =  .5369144931D-1
      D(8) = -.6429714999D-4
      D(9) = 312.4382714
      BTCEN = 316.15
      HFAC = .0179413
      WFAC = .03891
      RETURN
      END
C
      SUBROUTINE BIOCAL
      IMPLICIT REAL*8(A-H,O-Z)
      CHARACTER*4 PCHAR(30)
      DIMENSION BIO(30),BIO1(30)
      DIMENSION PARAM(30), PMIN(30), PMAX(30), PARMAX(30), PARMIN(30)
      DIMENSION P(30)
      COMMON /BLK1/ PARMIN, PARMAX, PARAM, NPARAM, NCHL
      COMMON /BLK2/ P, NP, NPEAK, PMIN, PMAX
      COMMON /BLK5/BIO,BIO1
      COMMON /BLK9/ PCHAR
C
      J = 1
      DO 100 I= 1,NP
      IF ((PCHAR(I) .EQ. 'B   ').OR.(PCHAR(I) .EQ. 'W   ') .OR. (PCHAR(I)
     1      .EQ. 'C   ').OR. (PCHAR(I) .EQ. 'H   ')) THEN
            BIO(I)= BIO1(J)
            J= J +1
      ELSE
C
      BIO(I) = 0.
      ENDIF
100   CONTINUE
RETURN
END
C
      SUBROUTINE PARSET
C
C  SUBROUTINE TO GENERATE THE STANDARD PARAMETER ARRAY FROM ANY SET OF
C  PARAMETERS AND CONSTRAINTS
C
      IMPLICIT REAL*8(A-H,O-Z)
      CHARACTER*4 PCHAR(30)
      DIMENSION PARAM(30),PMIN(30),PMAX(30),P(30)
      DIMENSION PARMIN(30), PARMAX(30)
      COMMON /BLK1/ PARMIN, PARMAX, PARAM, NPARAM, NCHL
      COMMON /BLK2/ P, NP, NPEAK, PMIN, PMAX
      COMMON /BLK4/ ERGCAL, IB, IE
      COMMON /BLK9/ PCHAR
C
C                   IDENTIFY PARAMETERS ACCORDING TO PCHAR
C                         W  - WIDTH
C                         WF - WIDTH FIXED
C                         C  - CENTROID
C                         CF - CENTROID FIXED
C                         CFS- CENTROID FIXED SEPARATION
C                         H - HEIGHT
C                         B  - BACKGROUND
C                         BF - BACKGROUND FIXED
C
      DO 100 I=1,NP
      IF ( PCHAR(I) .EQ. 'H   ') THEN
            IF((PMIN(I) .EQ. 0.) .AND. (PMAX(I) .EQ. 0.)) THEN
                  PMIN(I) = P(I)/2
                  PMAX(I) = P(I) * 1.5
            ENDIF
            GOTO 90
      ELSE
C
      IF ( PCHAR(I) .EQ. 'C   ') THEN
            IF((PMIN(I) .EQ. 0.) .AND. (PMAX(I) .EQ. 0.)) THEN
                  PMIN(I) = P(I) - P(I-1)/2
                  PMAX(I) = P(I) + P(I-1)/2
            ENDIF
            P(I) = P(I) - IB + 1
            PMIN(I) = PMIN(I) -IB + 1
            PMAX(I) = PMAX(I) - IB + 1
            GOTO 90
      ELSE
C
      IF ( PCHAR(I) .EQ. 'CF  ') THEN
            P(I) = P(I) - IB + 1
            PMIN(I) = PMIN(I) -IB +1
            PMAX(I) = PMAX(I) -IB +1
            GOTO 100
      ELSE
C
      IF ( PCHAR(I) .EQ. 'CFS ') THEN
            NDEX = IDINT( PMIN(I)+2 -1)
            P(I) = P(NDEX) - PMAX(I)/ERGCAL
            GOTO 100
```

```
C
      ELSE
C
      IF ( PCHAR(I) .EQ. 'M   ') THEN
           IF((PMIN(I) .EQ. 0.) .AND. (PMAX(I) .EQ. 0.)) THEN
                PMIN(I) = P(I) * .65
                PMAX(I) = P(I) * 1.35
           ENDIF
           GOTO 90
      ELSE
C
      IF ( PCHAR(I) .EQ. 'MF  ') THEN
           P(I) = P(I)/EROCAL
           GOTO 100
      ELSE
C
      IF ( PCHAR(I) .EQ. 'B   ') THEN
           IF((PMIN(I) .EQ. 0.) .AND. (PMAX(I) .EQ. 0.)) THEN
                PMIN(I) = P(I) * .8
                PMAX(I) = P(I) * 1.2
           ENDIF
           GOTO 90
      ELSE
C
      IF ( PCHAR(I) .EQ. 'BF  ') THEN
           GOTO 100
      ELSE
C
      WRITE (3,50) 'ERROR IN PARAMATER LIST OPTIONS PARAMETER #', I
50    FORMAT ('0', A, 1X, I2)
      RETURN
      ENDIF
      ENDIF
      ENDIF
      ENDIF
      ENDIF
      ENDIF
      ENDIF
      ENDIF
C
90    CONTINUE
      NPARAM = NPARAM +1
      PARAM(NPARAM) = P(I)
      PARMIN(NPARAM) = PMIN(I)
      PARMAX(NPARAM) = PMAX(I)
C
100   CONTINUE
      RETURN
      END
CCC
CCC             SUBROUTINE TO CALCULATE THE P'S BASED ON THE PARAM ARRAY
      SUBROUTINE POEN
      IMPLICIT REAL*8(A-H,O-Z)
        CHARACTER*4 PCHAR(30)
      DIMENSION PARAM(30), PMIN(30), PMAX(30), PARMAX(30), PARMIN(30)
        DIMENSION P(30)
      COMMON /BLK1/ PARMIN, PARMAX, PARAM, NPARAM, NCHL
        COMMON /BLK2/ P, NP, NPEAK, PMIN, PMAX
      COMMON/BLK6/EROCAL, IB, IE
        COMMON /BLK9/ PCHAR
C
        J = 1
        DO 100 I= 1,NP
        IF ((PCHAR(I) .EQ. 'B   ') .OR. (PCHAR(I) .EQ. 'M   ') .OR. (PCHAR(I)
     1        .EQ. 'C   ') .OR. (PCHAR(I) .EQ. 'H   ')) THEN
              P(I)= PARAM(J)
              J= J +1
        ELSE
C
        IF (PCHAR(I) .EQ. 'CFB ') THEN
              NDEX = IDINT (PMIN(I)+3 -1)
              P(I) = P(NDEX) - PMAX(I)/ EROCAL
        ENDIF
        ENDIF
100     CONTINUE
      RETURN
      END
CCCCCCC
        FUNCTION SUBROUTINE TO CALCULATE THE LINE SHAPE GIVE THE
        PARAMETERS P,  COEFFICIENTS D, ECT.  THE LINE SHAPE IS IN THREE
        PARTS - TWO EXPONENTIAL AND A LINEAR TAIL.  THE LINEAR TAIL
        BEGINS 6 WIDTHS DOWN FROM THE CENTROID.  IF THE LINEAR TAIL IS NOT
        TO BE USED SET CUT TO A LARGE NEGATIVE NUMBER.
CCCCCCC
      FUNCTION YFIT(N,XI)
      IMPLICIT REAL*8(A-H,O-Z)
C
      DIMENSION P(30), D(9)
      COMMON /BLK2/ P, NP, NPEAK, PMIN(30), PMAX(30), NDR0
      COMMON /BLK4/ D, HFAC, HFAC, BTCEN, CUT
      COMMON /BLK6/ EROCAL, IB, IE
C
      J = 3*N-2
      XFIT = (XI-P(J+1))/(P(J)*HFAC)+BTCEN
CCC
CCC   LINEAR TAIL CALCULATION TO MATCH UP TO EXPONENTIAL TAIL
CCC
      IF(XFIT.LE.CUT) THEN
            ALPH=(-6*P(J))/(P(J)*HFAC) + BTCEN
            AR0 = D(1) + D(2)*ALPH + D(3)*(ALPH*ALPH) +
     1      D(4)*((ALPH*ALPH)*ALPH)
            IF(DABS(AR0).LT.75.) DE=DEXP(AR0)
            CONVB = IB -1 -NDR0
            X = XI +CONVB
            XPT = P(J+1) -6*P(J) +CONVB
            YFIT = (X * P(J+2) * HFAC *DE)/ XPT
      ELSE
C
      L = 0
      IF (XFIT.GT.D(9)) L=L+4
      AR0 =D(L+1) +D(L+2)*XFIT +D(L+3)*(XFIT*XFIT) +D(L+4)*((XFIT*XFIT)*XFIT)
      DE = 0.D0
      IF (DABS(AR0).LT.75.D0) DE=DEXP(AR0)
      YFIT = P(J+2)*HFAC*DE
      ENDIF
C
      RETURN
      END
CCC
CCC   CHIFBT - IS A SORT VERSION OF CHI USED IN RODORD SEARCH
CCC   NOTE IT CAN NOT BE USED IN ERROR ANALYSIS
CCC
      FUNCTION CHIFBT(DUMMY)
C
      IMPLICIT REAL*8(A-H,O-Z)
CC
CC  SUBROUTINE TO CALCULATE CHI**2 GIVEN A FUNCTION YFIT
CC
      DIMENSION FIT(512),DATA(512),SIGMA(512),P(30)
      DIMENSION PARLOR(3), PARMIN(30), PARMAX(30)
      DIMENSION PMIN(30),PMAX(30),PARAM(30)
C
      COMMON /BLK1/ PARMIN, PARMAX, PARAM, NPARAM, NCHL, IGSTRT, IGSTP
      COMMON /BLK2/P, NP, NPEAK
      COMMON /BLK3/MINCHL,MAXCHL,FIT,DATA,SIGMA,XCUT
      COMMON /BLK8/ PARLOR,LORFLG,ILOR,GHLM64(1024)
C
40    CHIFBT = 0.D0
CCC
CC    IS CONVOLUTION INTEGRAL OF LORENTZIAN TO BE DONE
C
      LORFLG=0
      IF (ILOR.EQ.0) GOTO 48
      X1 = (PARLOR(1)-P(3*ILOR-2))
      IF(X1 .NE. 0.)          GOTO 44
      X2 = (PARLOR(2)-P(3*ILOR-1))
      IF(X2 .NE. 0.)          GOTO 44
      X3 = (PARLOR(3)-P(3*ILOR))
      IF(X3 .NE. 0.)          GOTO 44
      LORFLG=1
      GOTO 48
44    PARLOR(1)=P(3*ILOR-2)
      PARLOR(2)=P(3*ILOR-1)
      PARLOR(3)=P(3*ILOR)
C
      CALL YSET
C
      DO 45 I= MINCHL, MAXCHL
      XI = DFLOAT(I)
      FIT(I) = 0.
C
      DO 450 J=1,NPEAK
450   FIT(I) = FIT(I) + CONVLT(J,XI)
C
      IF(NP.NE.3*NPEAK) FIT(I)=FIT(I)+P(NP)
      IF (DATA(I).LE.XCUT) GOTO 45
      IF ((I .GT. IGSTRT) .AND. (I .LE. IGSTP)) GOTO 45
      IF (CHIFBT .GT. 1.D31) GOTO 46
```

```
      CHIFST = CHIFST + (FIT(I)-DATA(I))**2 / (SIGMA(I))**2
45    CONTINUE
46    CONTINUE
      GOTO 90
C
48    DO 55 I= MINCHL, MAXCHL
      XI = DFLOAT(I)
      FIT(I) = 0.
C
      DO 50 J=1,NPEAK
50    FIT(I) = FIT(I) + YFIT(J,XI)
C
      IF(NP.NE.3*NPEAK) FIT(I)=FIT(I)+P(NP)
      IF (DATA(I).LE.XCUT) GOTO 55
      IF ((I .GE. IOSTRT) .AND. (I .LE. IOSTP)) GOTO 55
      CHIFST = CHIFST + (FIT(I)-DATA(I))**2 / (SIGMA(I))**2
      IF (CHIFST .GT. 5.D29) GOTO 56
55    CONTINUE
56    CONTINUE
90    CONTINUE
C
      RETURN
      END
C
C
C
      FUNCTION CHI(K,DELTAK,L,DELTAL)
      IMPLICIT REAL*8(A-H,O-Z)
C
C  SUBROUTINE TO CALCULATE CHI**2 GIVEN A FUNCTION YFIT
C *** NOTE IF K=L THE INCREMENT IS DELTAK
      DIMENSION FIT(512),DATA(512),SIGMA(512),P(30)
      DIMENSION PARLOR(3), PARMIN(30), PARMAX(30)
      DIMENSION PMIN(30),PMAX(30),PARAM(30)
      COMMON /BLK1/ PARMIN, PARMAX, PARAM, NPARAM, NCHL, IOSTRT, IOSTP
      COMMON /BLK2/P, NP, NPEAK
      COMMON /BLK3/MINCHL,MAXCHL,FIT,DATA,SIGMA,XCUT
      COMMON /BLK8/ PARLOR,LORFLG,ILOR,GMLMBO(1024)
40    CHI = 0.DO
      XK=PARAM(K)
      XL=PARAM(L)
      PARAM(K)=XK+DELTAK
      IF(K.EQ.L) GO TO 405
      PARAM(L)=XL+DELTAL
405   CALL PGEN
      LORFLG=0
      IF (ILOR.EQ.0) GOTO 48
      X1 = (PARLOR(1)-P(3*ILOR-2))
      IF(X1 .NE.0.)        GOTO 44
      X2 = (PARLOR(2)-P(3*ILOR-1))
      IF(X2 .NE.0.)        GOTO 44
      X3 = (PARLOR(3)-P(3*ILOR))
      IF(X3 .NE.0.)        GOTO 44
      LORFLG=1
      GOTO 48
44    PARLOR(1)=P(3*ILOR-2)
      PARLOR(2)=P(3*ILOR-1)
      PARLOR(3)=P(3*ILOR)
C
      CALL YSET
C
      DO 45 I= MINCHL, MAXCHL
      XI = DFLOAT(I)
      FIT(I) = 0.
C
      DO 450 J=1,NPEAK
450   FIT(I) = FIT(I) + CONVLT(J,XI)
C
      IF(NP.NE.3*NPEAK) FIT(I)=FIT(I)+P(NP)
      IF (DATA(I).LE.XCUT) GOTO 45
      IF ((I .GE. IOSTRT) .AND. (I .LE. IOSTP)) GOTO 48
      IF (CHI2.GT.1.D31) GOTO 46
      CHI = CHI + (FIT(I)-DATA(I))**2 / (SIGMA(I))**2
45    CONTINUE
46    CONTINUE
      GOTO 90
C
48    DO 55 I= MINCHL, MAXCHL
      XI = DFLOAT(I)
      FIT(I) = 0.
C
      DO 50 J=1,NPEAK
50    FIT(I) = FIT(I) + YFIT(J,XI)
C
      IF(NP.NE.3*NPEAK) FIT(I)=FIT(I)+P(NP)
      IF (DATA(I).LE.XCUT) GOTO 55
      IF ((I .GE. IOSTRT) .AND. (I .LE. IOSTP)) GOTO 55
      IF (CHI2.GT.1.D31) GOTO 56
      CHI = CHI + (FIT(I)-DATA(I))**2 / (SIGMA(I))**2
55    CONTINUE
56    CONTINUE
90    CONTINUE
      PARAM(L)=XL
      PARAM(K) = XK
C
40    CALL PGEN
C
      RETURN
      END
C
C
C
      SUBROUTINE YSET
      IMPLICIT REAL*8(A-H,O-Z)
      DIMENSION YTAB(1600), GAMSQ(1024)
      DIMENSION PARMIN(30), PARMAX(30), PARAM(30)
      COMMON /BLK1/ PARMIN, PARMAX, PARAM, NPARAM, NCHL
      COMMON /BLK7/GAM,STEP,GAMSQ,YTAB,GMLA(1024),NGAM
      COMMON /BLK8/ PARLOR(3), LORFLG, ILOR, GMLMBO(1024)
      IF (ILOR .EQ. 0) GOTO 40
      N = IDINT(FLOAT(NCHL)/STEP)
      DO 30 J= 1,N
      XJ = J*STEP
      YTAB(J) = YFIT(ILOR,XJ)
30    CONTINUE
40    CONTINUE
      RETURN
      END
      SUBROUTINE ROCORD(P,GL,GU,N,SS,MAX,NRS,IWRITE,IGOTO,F1)
C
C        P---------PARAMETER VECTOR
C        GL--------LOWER BOUNDS
C        GU--------UPPER BOUNDS
C        N---------NUMBER OF PARAMETERS, LENGTH OF P
C        SS--------STEP SIZE, GIVING FINAL ACCURACY OF PARAMETERS
CAS A FRACTION OF ALLOWED PHASE SPACE
C        MAX-------MAXIMUM NUMBER OF FUNCTION REFERENCES
C        NRS-------NUMBER OF RANDOM STEPS TAKEN TO IMPROVE MINIMUM
C        IWRITE----WRITE FLAG  =0 NO OUTPUT, =1 BRIEF, =2 EXTENSIVE
C        IGOTO-----MULTIPLE ENTRY FLAG
C=1  INITIALIZE, =2 SEARCHING, =3 ROCORD FINISHED,
C=4 ABEND  (CHANGED BY ROCORD SO THAT CALLING PROGRAM
CCAN MONITOR PROGRESS)
C        F1--------CURRENT VALUE OF FUNCTION TO BE MINIMIZED
C
      DOUBLE PRECISION P(30),GL(30),GU(30),A(30,30),B(30,30),GH(30),
     C  D(30),Q(30)
      DOUBLE PRECISION F1,F2,F3,D1,D2,D3,SD1,SD2,DBS,SS,BIGSTP,DELTA,
     C  ZERO,DX1,DX2,DY1,DY2,D0,D0,XYX
      DATA DELTA, ZERO / 0.D00, 0.D00 /
      DATA IW /3/
      XSQRT(XXX)=DSQRT(XXX)
      XABS(XXX)=DABS(XXX)
C
C        BRANCH TO ENTRY POINT
C
      GO TO (100,300,800,900), IGOTO
C
C        INITIALIZATION
C
  100 CONTINUE
      DO 120 I=1,N
      Q(I)=P(I)
      GH(I)=GU(I)-GL(I)
      B(I,I)=SS*GH(I)
      DO 110 J=1,N
  110 A(I,J)=ZERO
  120 A(I,I)=1.D00
      BIGSTP=.05D0
      SD1=1.01D0+BIGSTP/SS
      SD2=1.5D0
      DBS=(15.D0*SS)**2
      ITR=1
      IRS=-1
      KOUNT=1
      IGOTO=2
      IF (IWRITE.EQ.0) GO TO 150
      WRITE(IW,130) (Q(I),I=1,N)
```

```
      WRITE(IW,132) F1
      WRITE(IW,134) (GL(I),I=1,N)
      WRITE(IW,136) (GU(I),I=1,N)
      WRITE(IW,138) (B(I,1),I=1,N)
      WRITE(IW,140)
  130 FORMAT(/ 5X,16H***** RECORD ****//25H INITIAL PARAMETER VALUES /
     C   (5D15.6))
  132 FORMAT(24H INITIAL FUNCTION VALUE=,D13.6)
  134 FORMAT(17H LOWER BOUNDS--GL / (5D15.6))
  136 FORMAT(17H UPPER BOUNDS--GU / (5D15.6))
  138 FORMAT(37H FINAL ACCURACY OF PARAMETERS WILL BE /(5D15.6))
  140 FORMAT(1H ,20(1H-))
      DO 160 I=1,N
      IF ((P(I).LT.GL(I)).OR.(P(I).GT.GU(I))) GO TO 190
  160 CONTINUE
      GO TO 200
  190 IF (IWRITE.EQ.0) GO TO 198
      WRITE(IW,195)
  195 FORMAT(32H INITIAL PARAMETER OUT OF BOUNDS)
  198 IGOTO=4
      RETURN

C
C         BASIC ITERATION BEGINS HERE
C         THIS IS A DO 400 J=1,N
C
  200 J=1
  201 CONTINUE
      D1=BB
      IGAIN=0
      F2=F1
      D2=ZERO
      IPARA=0
  210 DO 220 I=1,N
  220 P(I)=Q(I)+A(I,J)*D1*GH(I)
C         CHECK UPPER AND LOWER BOUNDS
      DO 240 I=1,N
      IF ((P(I).LT.GL(I)).OR.(P(I).GT.GU(I))) GO TO 280
  240 CONTINUE
      KOUNT=KOUNT+1
      IF (KOUNT.GT.MAX) IGOTO=4
C         EXECUTION WILL CONTINUE AT 300
      RETURN
  280 IF (IWRITE.LT.1) GO TO 290
      WRITE(IW,282) KOUNT,F1,(P(I),I=1,N)
  282 FORMAT(I5,4H  F=,D13.6 / (5D15.6))
      WRITE(IW,284)
  284 FORMAT(28H PREVIOUS STEP OUT OF BOUNDS)
  290 IF (IGAIN) 390,330,360
  300 IF (IPARA.EQ.1) GO TO 340
      IF (XABS(F1-F2).LT.DX(J)) GO TO 310
      IF (F1.GT.F2) GO TO 320
      IGAIN=1
      F3=F2
      D3=D2
      F2=F1
      D2=D1
  310 IF (XABS(D1).LT.BIGSTP) GO TO 315
      D1=D1+SD1
      GO TO 210
  315 D1=D1+SD2
      GO TO 210
C         FUNCTION IS NOW INCREASING
  320 IF (IGAIN) 390,330,340
  330 D1=-BB
      IGAIN=-1
      GO TO 210
C         USE PARABOLA TO FIND MINIMUM
  340 DX1=D1-D3
      DX2=D2-D3
      DY1=DX2*(F1-F3)
      DY2=DX1*(F2-F3)
      D0=(DX2*DY1-DX1*DY2)/(2.*(DY1-DY2))+D3
      XD0=XABS(D0)
      IF ((XD0.LT.XABS(D3)).OR.(XD0.GT.XABS(D1))) GO TO 380
      DO 350 I=1,N
  350 P(I)=Q(I)+A(I,J)*D0*GH(I)
      IPARA=1
      KOUNT=KOUNT+1
      IF (KOUNT.GT.MAX) IGOTO=4
C         EXECUTION WILL CONTINUE AT 340
      RETURN
  360 IF (F1.GT.F2) GO TO 380
      DO 365 I=1,N
  365 Q(I)=P(I)
      D(J)=D0
      GO TO 395
  380 DO 385 I=1,N
  385 Q(I)=Q(I)+A(I,J)*D2*GH(I)
      D(J)=D2
      GO TO 392
  390 D(J)=ZERO
  392 F1=F2
  395 J=J+1
      IF (J.LE.N) GO TO 201
  400 CONTINUE
      DD=ZERO
      DO 410 I=1,N
  410 DD=DD+D(I)*D(I)
      IF (DD.LE.ZERO) GO TO 600
      IRS=-1
      IF (DD.GE.DBB) GO TO 420
      SD1=3.D0
      SD2=1.5D0
      BIGSTP=.001*DD
      GO TO 430
  420 SD1=15.D0
      SD2=5.D0
      BIGSTP=.01*DD
  430 IF (N.EQ.1) GO TO 580
C         LOAD COLUMNS OF -A- INTO -B- ACCORDING TO MAGNITUDE OF -D-
  500 CONTINUE
      DO 510 J=1,N
  510 P(J)=XABS(D(J))
      K=N
      DO 520 J=1,N
      IF (P(J).GT.ZERO) GO TO 520
      DO 515 I=1,N
  515 B(I,K)=A(I,J)
      K=K-1
  520 CONTINUE
C         NOW K=NUMBER OF NON-ZERO ELEMENTS
      DO 530 L=1,K
      J=1
      DO 525 I=1,N
  525 IF (P(J).LT.P(I)) J=I
      P(J)=ZERO
      DO 530 I=1,N
  530 B(I,L)=A(I,J)*D(J)
C         GENERATE NEW VECTORS IN DIRECTIONS OF GREATEST PROGRESS
      IF (K.LE.1) GO TO 550
      DO 540 L=2,K
      J=K+2-L
      DO 540 I=1,N
  540 B(I,J-1)=B(I,J-1)+B(I,J)
C         PERFORM A GRAM-SCHMIDT ORTHONORMALIZATION
  550 CONTINUE
      DO 560 K=2,N
      KK=K-1
      DO 552 I=1,N
  552 P(KK)=P(KK)+B(I,KK)*B(I,KK)
      DO 560 J=1,KK
      BB=ZERO
      DO 554 I=1,N
  554 BB=BB+B(I,J)*B(I,K)
      DO 560 I=1,N
  560 B(I,K)=B(I,K)-BB*B(I,J)/P(J)
      DO 562 J=2,N
      P(J)=ZERO
      DO 562 I=1,N
  562 P(J)=P(J)+B(I,J)*B(I,J)
      DO 566 J=1,N
      P(J)=DSQRT(P(J))
      DO 566 I=1,N
  566 A(I,J)=B(I,J)/P(J)
C         THE ITERATION IS NOW COMPLETE
  580 ITR=ITR+1
      IF (IWRITE-1) 200,590,595
  590 WRITE(IW,592) ITR,F1
  592 FORMAT(5H ITR=,I3,4H  F=,D13.6)
      GO TO 200
  595 WRITE(IW,592) ITR,F1
      WRITE(IW,598) (Q(I),I=1,N)
  598 FORMAT(5D15.6)
      WRITE(IW,140)
      GO TO 200
C
C         PROCEDURE COMES HERE WHEN NO PROGRESS IS MADE
```

```
C
  600 IF (N.EQ.1) GO TO 690
      IF (IRS.GE.NRS) GO TO 690
      IRS=IRS+1
      IF (IRS.GE.1) GO TO 620
      DO 615 J=1,N
      DO 610 I=1,N
  610 A(I,J)=ZERO
  615 A(J,J)=1.0D0
      WRITE(IW,618)
  618 FORMAT(1H1H AXIS RESET)
      GO TO 500
  620 DO 625 I=1,N
  625 D(I)=DBLE(RAN(idum))
      IF (IWRITE.LE.0) GO TO 500
      WRITE(IW,630) IRS
  630 FORMAT(14H RANDOM ROTATION,I3)
      GO TO 500
C        RECORD IS NOW FINISHED
  690 IGOTO=3
      DO 692 I=1,N
  692 P(I)=Q(I)
      IF (IWRITE.LT.1) RETURN
      WRITE(IW,140)
      WRITE(IW,695) KOUNT,F1,(Q(I),I=1,N)
  695 FORMAT(28H RECORD FINISHED, THERE WERE ,I4,34H FUNCTION REFERENCES
     C  FINAL VALUE=,D13.6/20H FINAL PARAMETERS.../(5D15.6))
      RETURN
C
CC       DUMMY ROUTINE
C
  800 CONTINUE
      RETURN
C
CC       ERROR ENTRY
C
  900 CONTINUE
      IGOTO=3
      IF (KOUNT.GT.1) GO TO 950
      WRITE(IW,195)
      RETURN
  950 IF (KOUNT.LT.MAX) GO TO 990
      WRITE(IW,960)
  960 FORMAT(30H FUNCTION REFERENCES EXHAUSTED)
      RETURN
  990 CONTINUE
      RETURN
      END
```

BIOGRAPHY

Steven Eugene King

PERSONAL: Born in Gettysburg, PA, June 22, 1956

EDUCATION: B.S. summa cum laude and with distinction
Duke University, 1978

POSITIONS: Research Assistant, Triangle Universities Nuclear Laboratory, 1979-1983

Graduate Research Associate, Los Alamos National Laboratory, Los Alamos, NM, 1979

Shell Teaching Fellow, Duke University, 1978-1979

Research Assistant, National Bureau of Standards, Gaithersburg, MD, 1977, 1978

Systems Development Programmer, Digital Systems Corp., Walkersville, MD, 1977

SOCIETY MEMBERSHIPS:

American Physical Society
Southeastern Section of the American Physical Society
Phi Eta Sigma (Freshman Honor Society)
Phi Beta Kappa
Sigma Xi

PUBLICATIONS AND ABSTRACTS:

"Vector Analyzing Powers of $^{2}H(p,\gamma)^{3}He$ and $^{1}H(d,\gamma)^{3}He$ Reactions at E_x=6 MeV" with N.R. Roberson, D.R. Tilley, H.R. Weller, H.P. Engelbert, W. Arnold, H. Berg, E. Huttel, and G. Clausnitzer (to be published, 1983)

"D-State Effects in the $^{2}H(p,\gamma)^{3}He$ Reaction" with H.R. Weller, N.R. Roberson and D.R. Tilley, Phys. Rev. Lett. 51 (1983) 877.

"Polarized Capture Studies of Three Body Systems" with H.R. Weller, N.R. Roberson, D.R. Tilley, and G. Mitev, to be published in International Conference on Nuclear Physics Proceedings, Florence, Italy, August, 1983.

"Radiative Capture of Protons by ^{2}H" with N.R. Roberson, H.R. Weller, and D.R. Tilley, Bull. Am. Phys. Soc. 27, (1982) 700

"Radiative Capture of Neutrons by ^{208}Pb" with M. Potokar, N.R. Roberson, H.R. Weller and D.R. Tilley, Nucl. Phys. A384, (1982) 129

"The XSYS Data Acquisition System At Triangle Universities Nuclear Laboratory" with C.R. Gould, L.G. Holzsweig, Y.C. Lau, R.V. Poore, N.R. Roberson, and S.A. Wender, IEEE Trans. on Nucl. Sci. NS28, (1981) 3708

"Data Acquisition with a VAX 11/780 and MBD Branch Driver" with C.R. Gould and Y.C. Lau, IEEE Trans. on Nucl. Sci. NS28, (1981) 3822

"Radiative Capture of Neutrons by ^{208}Pb" with M. Potokar, N.R. Roberson, H.R. Weller, S.A. Wender, and D.R. Tilley, Bull. Am. Phys. Soc. 26, (1981) 590

"Absolute Neutron Flux Measurement Using a Proton Recoil Telescope" with N.R. Roberson, and S.A. Wender, Bull. Am. Phys. Soc. 26, (1981) 90

"Laser Spectrometer for Precise Energy Measurement of 10-120 KeV D^- and T^- Ions" with G.G. Ohlsen, Ronald E. Brown, Nelson Jarmie, R.A. Hardekopf, F.D. Correll, and D.A. Clark, Bull. Am. Phys. Soc. 24, (1979) 822

"Charge Exchange in Low Energy D and T Beams" with Nelson Jarmie, LA-7999-MS report, 1979.